Investigations of the Magnetic Fields from Ships due to Corrosion and its Countermeasures.

Thesis submitted to the University of Glasgow

for the degree

of Doctor of Philosophy.

Peter J. Allan

Department of Physics and Astronomy

University of Glasgow

August 2004

ProQuest Number: 10753960

ProQuest 10753960

Abstract

Corrosion is one of the main concerns for the shipping industry. The enormous cost associated with the corrosion of ships means that operators are more than ever seeking methods to provide optimal protection. Another problem which results from the corrosion of ships is that the electric currents produced give rise to a corrosion related magnetic field which adds to the ships overall electromagnetic field which can trigger underwater mines. Hence for the Admiralty to protect their fleet, they need to understand, predict and reduce these electromagnetic signatures. This will also be a concern for operators of merchant ships if, as recently suggested, terrorists begin to target them.

There are a number of factors contributing to the electromagnetic signature of a ship. The work presented in this study is concerned with the magnetic field arising due to corrosion and the countermeasures employed against it (namely Impressed Current Cathodic Protection (ICCP) systems). This field is called the Corrosion Related Magnetic (CRM) field. Since this field is directly related to the rate of corrosion of a ship, it may also be used as an indicator as to the efficiency of the corrosion protection measures. This work presents a range of techniques which may be used to model the CRM field.

Simple dipole models are used to investigate the general behaviour of a corroding ship in sea water. These investigations result in an expression for an approximation of the CRM field from a dipole-wire configuration which can be used to estimate the CRM field from a corroding ship with an active ICCP system.

A second, more detailed, method was then developed using the Boundary Element Method (BEM) to model a ship corroding in a tank of sea water. The BEM uses a large set of simultaneous equations, the coefficients of which are calculated by numerical integration using a new method based around the moments of triangular surface elements which discretise the boundary of the domain.

i

By using a Point Successive Over-relaxation Method (PSOM) to solve the BEM equations, the electric potential and its flux are calculated for each discrete element on the boundary. These potentials are then used to evaluate the CRM field within the domain. Rather than use the Biot-Savart Law for this purpose, a new method is presented which removes the requirement for an internal volume mesh of the domain, allowing the CRM field to be calculated directly from the electric potentials of the surface elements.

To test this method, results are presented for a tank of sea water with a hull located on the top surface and an appropriately placed propeller. Calculations were performed for an unprotected propeller and the hull with various degrees of protection from corrosion offered by paint coatings and an ICCP system. Results from the "exact" method are in good agreement with those from the simple dipole model and although there were no published results of the kind produced by this research available for comparison, published results from similar studies of related topics appear to further support the results presented. These results indicate that the method developed is capable of modelling all the key characteristics required for a detailed analysis of an actual corroding ship, with protective paint coatings and ICCP system, in a physical environment.

Acknowledgements

I would like to thank sincerely my supervisors, Dr. A. Watt and Prof. C. Davies of the Department of Physics and Astronomy, University of Glasgow, for their help, continuous support, and unbelievable patience throughout the duration of this work. My thanks are also due to Dr. A. Jennings, Dr. I. McKenna, and Dr. J. Shepherd of BAE Systems, Glasgow, for their invaluable advice on the work presented in this thesis.

Additionally, I would like to thank my fellow students (Jack, Grieg, Alan, Ian, Dave C, Dave T, Joe, and Alessandro) for all their assistance and friendship over the past few years.

Also it goes without saying that I offer my biggest thanks to my family and friends for their unfailing support without which this research would never have been completed.

I feel obliged to express my gratitude to Mr. R. Glen, who inspired my interest in physics many years ago. I would now have to agree with him when he warned me that while I may never be the best, hard work can get you a long way.

Finally I wish to acknowledge that this work was funded by a CASE Research Studentship from the Particle Physics and Astronomy Research Council (PPARC), sponsored by BAE Systems.

Declaration

Except where specific references are given, the work in this thesis has been performed by myself, with guidance from my supervisor Dr. A. Watt.

Table of Contents

List of Figures

List of Tables

Chapter 1

Corrosion and Corrosion Protection

1.1 Introduction

Damage caused by corrosion is something with which we are all familiar. Whether it be a rusty spade lying in the garden or the damage to the body work of an old car, we are reminded constantly of the damage that corrosion can cause. It would be slightly unfair though to not mention the good side to corrosion. One of the most famous landmarks in the world is the Statue of Liberty in New York, the massive green icon of the free world. If it was not for corrosion she would not be her familiar green colour as her coating (or 'patina') is the product of the corrosion of the copper material that she is constructed from [1]. In saying this it still remains the case that the disadvantages of corrosion far outweigh the advantages and it is these disadvantages which we all tend to associate with corrosion. However, not many of us have stopped and actually thought about the cost associated with corrosion.

The U.S. shipping industry approximated that the financial cost of corrosion to their business is $2.7 billion [2], whilst other sources believe the cost to be as much as 4% of the Gross National Product [3].

Add to this the fact that around 80% of all around us is delivered, at some stage, via shipping and we can begin to get a good idea as to the significance corrosion plays in our everyday lives [2]. Almost all of us own a car or at least travel in one several times a week, but do we ever stop and consider how we get the fuel for the engines? The majority of the fuels are farmed overseas and shipped into this country so if the corrosion problem was not addressed by these

oil tankers, it would be quite possible that we would experience a fuel shortage which could bring the country to a standstill.

These consequences can be regarded as mere inconveniences when compared to the true irreparable damage which can occur due to corrosion. When ships corrode, their structure weakens often to the extent that the ship will sink. When this happens costs are incurred and vital cargo is lost but most importantly lives and the environment are put at serous risk. In December 1999, the oil tanker Erika sank $70km$ off the French cost spilling its cargo of over 12500 tonnes of oil. This devastated 250 miles of coast line and maimed or killed in excess of 300,000 birds [2, 4]. The investigation into the tragedy cited corrosion as being one of the main factors in the accident.

The question that now springs to mind is why do materials which are resistant to corrosion such as fibreglass or stainless steel not get used to build ships? Well, the answer to this question is that they do in specific circumstances where there is a need for absolute minimal corrosion such as in the construction of minesweepers [5] where, in addition to the induced magnetism, the corrosion of metal would result in underwater electromagnetic signatures which may trigger mines. The problem is that to construct ships using these materials is very expensive and in an industry striving to be as economical as possible, this cost is simply not acceptable. So ships continue to be made from strong, inexpensive materials (i.e. steel) which need to be protected against corrosion [2].

Before describing the various protective measures taken against corrosion by the shipping industry, it is necessary to provide a brief overview of the electro-chemical process which we call corrosion. Since this research is concerned with ships, the majority of which have hulls made from steel, this will be the material that will be considered as corroding [6] (the term 'corroding' is preferred to 'rusting' as it is more widely applicable, only steel and iron can rust [7]). When steel corrodes, the iron combines with oxygen and water to form a weaker material that is a mixture of iron oxides and hydroxides. At the iron surface, iron ions are taken into the solution leaving negatively charged electrons on the metal surface. This is the anodic reaction, it produces electrons. This negative surface attracts back the positive iron ions and they can recombine with the electrons to reform the iron atoms. Hence an equilibrium is possible where by the number of divisions is equal to the number of reformations and no corrosion occurs. Unfortunately

it is often the case that this equilibrium is disturbed so that there is a shortage of electrons on the surface to attract the iron ions back. This happens when the electrons flow to a site of another reaction. This other reaction is called the cathodic reaction, it consumes electrons. The anodic and cathodic reactions feed off each other and the corrosion continues [2, 8, 9].

There are various types of corrosion common to ships but the one with which we are concerned is 'galvanic corrosion' [9] in which one metal (the steel hull) corrodes quickly and another metal (the Nickel-Aluminium-Bronze propeller) more slowly [6, 8, 10]. In this corrosion, which is a type of aqueous corrosion [3], the electrons flow through the sea water which, due to its sodium chloride content, acts as a good electrolyte. This electron flow results in a 'corrosion current' [8]. Because these currents of a few hundred amps [11] flow for long distances ($\approx 100m$) through the water and through the fabric of the ship, they generate appreciable magnetic fields well away from the ship. Other sources of corrosion such as particles of carbon on the surface of the iron generate very localised currents with no extended magnetic fields.

In general, there are five methods [3] for controlling the corrosion of metals in sea water. Three of these

- the use of corrosion inhibitors to make the metal passive

- chemical dosing to change the pH of the local environment

- use of corrosion resistant materials

are not practical solutions for ships moving in a vast expanse of sea water and hence are not considered here.

The most common defence mechanism is the painting of the hull with a protective coating [12] which provides a physical barrier to the sea water and hence impedes the ion and electron movement. This is an ancient solution proposed by the Romans (circa 100BC). Indeed around this time, the first corrosion prevention device was proposed by Phing who suggested that the corrosion of metals such as copper and iron could be prevented by applying coatings to the metal, these coatings being either tar or oil [13]. Indeed since the Romans often constructed some parts of their ships using metallic iron, it is more than likely that they were the first to coat the metal components of their vessels in these protective coatings.

This is a principle that is still heavily relied upon today although modern day coatings serve three purposes [2]:

1. to protect the hull from corrosion

2. to prevent the build up of marine life on the hull which may create an environment that will aggravate any corrosive attack

3. to provide a smooth finish to the hull which will reduce drag.

The coatings used in the modern era to prevent corrosion of vessels have obviously advanced with expensive, purpose designed paints now employed, but the principle still remains the same. Until recently the general practise was to only coat the hull [14] as the turbulence of the sea water around the propeller and rudder made it extremely difficult to apply a coating to these which would be able to stay in place for a feasible time period. To replace coatings on the propeller would require the ship coming out of service into dry dock costing the operator further expense [15]. However, recent developments in the adhesive properties of the coatings has meant that several trials are currently underway testing new propeller coatings [16]. Damage also occurs to the paint coating on the hull in the areas where there is turbulent flow, such as the bow and the stern, and although these areas should be repaired periodically, the final method of protection is employed to prevent corrosion in these damaged areas.

Cathodic Protection (CP) systems work on the principle that if a metal is introduced to the system which is more anodic (i.e. likely to corrode) [17] than the metal being protected then this metal will corrode with the electrons flowing to the protected metal which becomes cathodic [2]. There are two forms of CP systems used today.

The sacrificial anode cathodic protection (SACP) system was the original one to use the CP principle. It was in 1824 that Sir Humphrey Davy made his initial presentation to the Royal Society of London on his investigations, commissioned by the Admiralty, into the corrosion of the copper sheathing on 'His Majesty's ships of war' [13]. In it he said

> I have ascertained many facts...to illustrate some obscure parts of the electrochemical science...seem to offer important applications.

In short Davy had succeeded in protecting copper against corrosion from seawater by the use of iron anodes. This work, aided by Micheal Faraday, was the cornerstone of modern SACP systems whereby zinc anodes are attached to strategic locations on the hull which protect those areas most susceptible to paint damage.

The drawbacks of these SACP methods are that the anodes have a finite life and need to be replaced [17]. This is done in one of two ways, the ship can be brought into dry dock; or they can be replaced in-situ. Both of these methods cost the operators large sums of money so another method was developed working from the CP principle.

The Impressed Current Cathodic Protection (ICCP) system protects a metal by coupling it to the negative pole of a DC source while the positive pole is coupled to an auxiliary anode. This system pushes currents via the sea to parts of the hull which are requiring protection thus preventing corrosion [17]. The use of reference electrodes on the hull [17] can ensure that the correct amount of current is supplied to ensure that the potential of the hull remains in a safe range [9]. If too little current is supplied then corrosion occurs while too much current can damage the coatings on the hull. One pioneer of this method was Charles Edison but he had no real success due to inadequacies in the materials and techniques that were available at the time [13].

In this research, an ICCP system will be coupled with paint coatings to form a defence mechanism against corrosion.

There is another aspect to the corrosion of ships which has not yet been mentioned. During World War One, the Royal Navy developed the mine which was activated by the magnetic field from a ship [18]. Since then the sensitivity of these devices have improved to such a level that a variation in the magnitude of the magnetic field from a ship of a mere 1nT is enough to trigger one. There are many sources of magnetic (and electric) field from a ship, one of which is the corrosion currents.

1.2 Naval Electromagnetic Theory

There are several reasons why knowledge of a ship's electromagnetic signature is of great importance. From a defence point of view, the electromagnetic signature allows a ship to be identified and classed [15]. There exist many ways of identify-

ing a ship with the electromagnetic signature being regarded as the second most important indicator behind the infrared signature, and ahead of the audio and visual indicators [11]. Such a great importance is placed on the electromagnetic signature as it can activate mines which severely compromises survivability of the ship[19]. Hence it is crucial that when a ship is designed, it is done so with the electromagnetic signature in mind, with careful consideration also taken over how this signature will be effected over time and service.

1.3   Origins of Electromagnetic Signatures

There are various components which contribute to producing the total electromagnetic signature around a ship in sea water. These include fields from

- Induced Magnetisation

- Permanent Magnetisation

- Machinery (on board the ship)

- Eddy Currents

- Extremely Low Frequency Electromagnetic (ELFE) signatures

- Corrosion Related Fields.

When a ship is constructed, its hull and other steel components will be held in a fixed position relative to the earth's magnetic field for a long period of time. Due to the ferromagnetic nature of steel and the construction work on this material, this results in it becoming magnetised [18]. It is this magnetisation which is referred to as the permanent magnetisation. Whenever the ship is exposed to different magnetic fields for extended periods this magnetisation will be affected but will remain present. The permanent magnetisation will be present when there is no external field, and in the presence of such a field, it will behave non-linearly with it. One can almost regard the permanent magnetisation of a ship as a record of the magnetic history of the vessel.

The presence of an external field will also induce a magnetic field in the metal work of the vessel due to its induced magnetisation [18]. This field, being a direct consequence of the external magnetic field, will vary in direct proportion to this

field and would disappear if the external field were zero (which is unlikely since although the earth's magnetic field will vary in orientation to the vessel, it will always be present).

Since each ship has its own unique design and hence metal structure, this field will be unique to each class of ship [20]. The advances on magnetic sensitive ordnance means that mines and similar devices can class a passing ship by its unique electromagnetic signature and hence decide whether to target the ship and if so when is the optimal point at which to detonate. To prevent this, it is desirable for a ship to be able to 'hide' its electromagnetic signature, and there are various approaches to achieving this.

Incorporated in the design of modern ships are cables known as degaussing coils [18]. Current is supplied to these coils to produce magnetic fields which act to 'counter' the effect of the Earth's magnetic field. Since the Earth's magnetic field will be dependent on the location of the vessel, this involves the constant monitoring of the currents supplied to the degaussing coils. The degaussing coils are also capable of eliminating the fields due to permanent magnetisation to a certain extent, but not completely. However it is possible to remove the permanent magnetisation using other methods.

Consider an iron paper clip brought into contact with a magnet. The paper clip will become magnetised, and will remain so while the magnetic moments of its atoms remain aligned. However, by dropping the paper clip onto the floor or perhaps by heating the paper clip, the energy added can throw the atom's magnetic moments out of alignment hence removing the permanent magnetisation. The process which removes the permanent magnetisation of a ship is known as 'deperming' and should be done on a regular basis to any vessel where these signatures are of utmost importance. This process involves wrapping the vessel in a long copper cable and berthing it inside a special enclosure where the effects of the earth's magnetic field has been negated. Pulses of current are then sent through the copper cable in alternating directions resulting in alternating magnetic fields which shakes up the orientation of the magnetic moments of the atoms resulting in the permanent magnetisation being removed.

As mentioned previously another option is to construct the hull from a non-magnetic material, an approach which is often used with minesweepers. However the expense involved means that this is an impractical solution to the problem

for all vessels. An associated problem to this solution is that the fields that are generated by equipment on board the vessel then become significant [18]. These fields can generally be tackled by applying degaussing coils to individual items of equipment or to rooms which house several items of equipment.

Eddy currents arise from the movement of the ship. Although a ship may be travelling on a fixed bearing and hence in a fixed direction with reference to the earth's magnetic field, the roll of the sea will mean that it is in a changing magnetic field. Since the vessel is constructed from conducting materials, these changes in magnetic field will induce circulating currents known as eddy currents. These eddy currents will also give rise to magnetic fields which can be detected, although they are small. It is very difficult to deal with these fields but they have been modelled previously [18] so their effect is known and can be accounted for.

The ELFE signatures from a ship are produced due to the various propulsion and power systems on a ship. They are time dependent (AC) electromagnetic fields. The sources of these signature can be both electric and magnetic, and may produce signatures at various frequencies [19]. These signatures have been investigated heavily over the years with many approaches to their modelling producing several papers [14, 19]. However they do not concern this research.

As mentioned above, this research does not consider these sources but instead focuses on evaluating the magnetic field which arises from the corrosion of the hull and the protective measures (paint and ICCP systems) employed against this corrosion. The field that arises from these sources is commonly referred to as the Corrosion Related Magnetic (CRM) field.

1.4 Corrosion Related Magnetic Field

In simple terms this field arises due to the flow of corrosion currents through the sea water. This current density has many sources with one of the most prominent being the currents that arise due to the corrosion of the metal work of the ship. Various corrosion countermeasures (ICCP systems) also directly effect the current density and hence an accurate model of the electromagnetic signatures can provide crucial information about the level of corrosion on the ship. The signature therefore acts as an indicator to the efficiency of the corrosion protection devices employed. Consider the case where the only protection offered

is from a paint coating. The current in this situation can be explained as follows. The anodic reaction sees the emission of electrons from the propeller which can travel through the sea water to the hull where the steel has become positively charged. Here the electrons are absorbed by the iron ions. However at the same time the iron on the hull has emitted some of its electrons into the structure of the ship. Since the propeller and the hull are electrically connected via the propeller shaft, these electrons can travel through the ship and back to the propeller as depicted in figure 1.1.
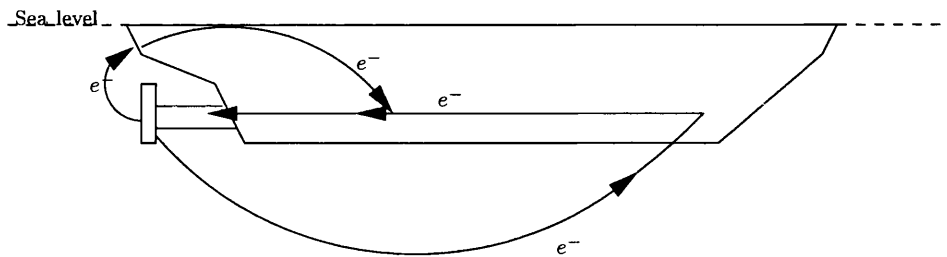
Figure 1.1: The flow of electrons due to corrosion.

The combined result of these reactions is that there is now a complete circuit by which the electrons can flow creating a current loop. Due to these sea currents, a magnetic field occurs as a consequence of the Biot-Savart Law. These charge separations also create an electric potential field in the sea, and consequently an electric field in the sea. Thus if the only counter-corrosion measure was a coating of the hull, the damage to it which would increase over time and use will seriously compromise its efficiency meaning the electromagnetic signatures would become more prominent which is why the ICCP system is introduced [21].

The mechanisms of the ICCP system are described above. Without doubt these Cathodic Protection devices enhance the protection of the vessel from corrosion which is their primary objective. However, it should be recognised that they do this by supplying the hull with current, so there are new sources of current on the ship. These contribute to the electromagnetic signatures which can be so damaging to a ship's detectability. With SACP systems, there can be little control exerted over the amount of current supplied but this is one of the main benefits with the ICCP systems. The current in these systems can be controlled to maximise the protection provided whilst also attempting to minimise the CRM signature of the ship.

1.5 The Aim of this Research

The preceding sections should highlight exactly why corrosion, and the counter-measures against it, are of such importance to the shipping industry. Whether it be for commercial or military ships, it is crucial for ship operators to be able to gauge exactly how badly their vessels are corroding so that they can be maintained to a safe standard. The added military desire to be able to minimise the magnetic fields further complicates matters.

The aim of the research was to develop tools which, for a ship in sea water, model the corrosion related magnetic (CRM) field in a variety of environments and for a range of hull conditions. The main objective was to be able to have tools which could calculate the CRM field with a variety of ICCP configurations so that an educated choice could be made as to which configuration best suited the operators requirements, whether it be maximum protection or minimal detection.

To achieve this objective, various areas were researched. Firstly, simple dipole models were used to represent a ship corroding in seawater. These allowed the basic principles of the corrosion process to be investigated and lead to a method by which the return currents through the hull could be accurately modelled.

It was then necessary to model a real situation of a hull corroding in sea water. The complex geometries involved meant that mathematical models had to be used with the best modelling method deemed to be the boundary element method. To use this method it was necessary to perform many numerical integrations, and to perform these a new, unique method was developed.

This modelling method provided values for the potential on the ship so the next stage was to calculate the magnetic fields from these values. Again, a new method was developed to perform this task which effectively side stepped the need to use the Biot-Savart Law.

The final stage was to then apply these methods for situations which represented real-life situations as closely as possible. This leads to a series of test calculations presented in chapter 7.

Chapter 2

Dipole Models

2.1　Introduction

The problem of evaluating the corrosion related magnetic (CRM) fields from marine vessels in seawater is extremely complicated, with the level of complexity increased in this work by the use of techniques which have been developed from first principles. It is therefore necessary to develop simplified models which can serve as test calculations and checks of the results.

One of the most common ways of modelling systems like that of a corroding ship is to use electric multi-poles to represent the vessel [5], with the multi-poles providing electric potentials on the surface of the ship which are equal to those that arise from the corrosion [22]. With this done, the ship can then be removed from the calculation and the fields from the poles used to estimate the electromagnetic fields at points in space. This idea shall be stripped back to the simplest case with a single point source of current in an infinite, uniformly conducting medium being considered. This model will then be developed to incorporate the fields from feed lines, and then the fields from a model consisting of a wire between a sink and a source will be calculated. This represents a simplified model of a submarine totally immersed in seawater. Finally, the effect of a boundary being introduced will be considered (i.e. a semi-infinite medium). When a boundary is introduced to a model of a wire connecting a sink and a source, the situation can be thought of as that of a simple submarine, or part of the hull of a ship corroding near the surface of the sea.

The term "electrode" in the following work means a small spherical conducting

sphere emitting current uniformly in all directions.

In section 2.3, we obtain a formula for the magnetic field arising from a submarine just below the surface of the sea. It is represented by an electrode emitting current fed by a horizontal wire from a second electrode absorbing an equal current from the sea. A number of steps is necessary to obtain the formula.

2.2 Fields in an Infinite, Uniformly Conducting Medium

2.2.1 Fields from a Submerged Electrode.

Consider a positive electrode in an infinite uniformly conducting medium as shown in figure 2.1. This is rather unphysical since the electrode would need to be supplied by a current source, such as a wire from infinity, but for the moment this technicality will be ignored. We will prove that the magnetic field from such a current distribution is zero.
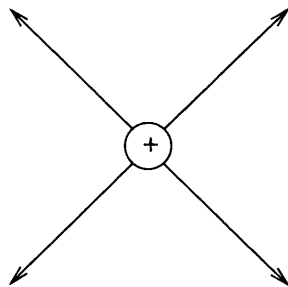
Figure 2.1: Current emitted from a positive electrode (source) in an infinite sea.

With the current being emitted uniformly in all directions, it is straight forward to calculate the electric field **E** at some arbitrary point within the medium from the inverse square law. Then

$$\mathbf{J} = \sigma\mathbf{E} = \frac{J_0 \hat{\mathbf{r}}}{4\pi r^2} \qquad (2.2.1)$$

where **J** is the current density at **r** from the electrode, σ is the conductivity of the medium and J_0 is the total current emitted by the electrode.

The interesting field here, and in all the subsequent cases, is the magnetic

field. Basic electromagnetic theory says that the magnetic field arises due to the movement of charged particles (currents). Indeed the governing rules of electromagnetism, Maxwell's equations, state that in the situation considered here, when the electric field is not time dependent, when there is no time-dependent electric polarization, and no magnetisation, a magnetic field should result from the current density

$$\nabla \times \mathbf{B} = \mu_0 \mathbf{J}. \tag{2.2.2}$$

This equation can be inverted to calculate $\mathbf{B}$ from $\mathbf{J}$, which gives the Biot-Savart Law.

To clarify the various properties required to implement the Biot-Savart Law consider figure 2.2. With the current being emitted uniformly into the medium,
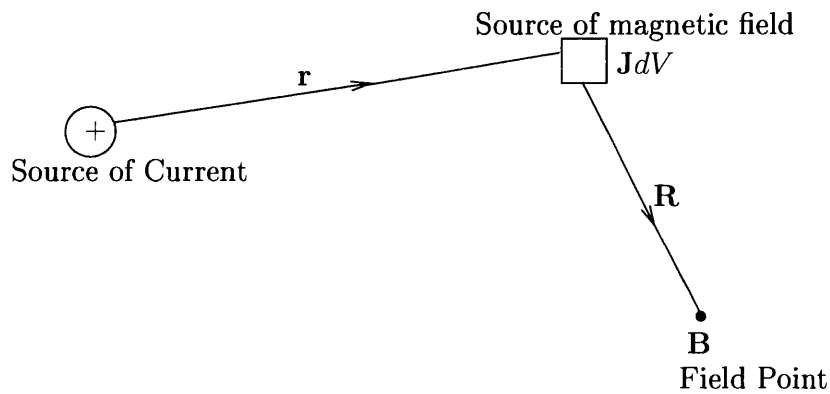
Figure 2.2: A current source produces a current density $\mathbf{J}$ at $\mathbf{r}$, which in turn results in a magnetic field $\mathbf{B}$ at $\mathbf{R}$

the most convenient form of the law is

$$\mathbf{B} = \frac{\mu_0}{4\pi} \int_V \frac{\mathbf{J} \times \mathbf{R}}{R^3} dV \tag{2.2.3}$$

where V is the volume of the media, and $\mathbf{R}$ is a vector pointing from the position of the current elements to the field point. With the medium infinitely big, it is symmetric about all straight lines which pass through the source. Hence choose an axis of symmetry which passes through the field point and the source point as shown in figure 2.3.

At some point along the axis of symmetry, consider a toroid. This toroid, whose cross-section is square and small compared with its radius, is equidistant at all points from the source electrode, and as a result the current density in the
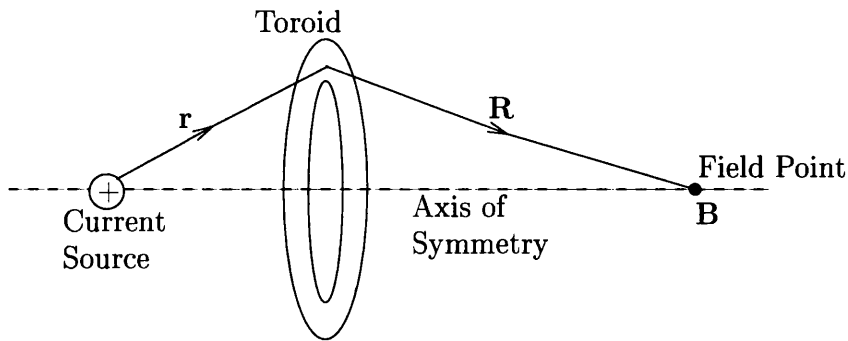
Figure 2.3: Axis of symmetry through the field point and the source with a toroid shown used for evaluating **B**.

toroid will be constant. Further the distance from the toroid to the field point is also constant, hence the contribution to the magnetic field from each section of the toroid

$$\frac{\mathbf{J} \times \mathbf{R} dV}{R^3}$$

will have the same magnitude. By the right-hand screw rule, the contributions will be such that they all act in the plane perpendicular to the axis of symmetry. Hence as the contributions are evaluated as the toroid is circumnavigated, they all have an equal but opposite contributions resulting in a complete cancellation (see figure 2.4). Hence the field from the current density in the arbitrary toroid is zero. By filling the entire space with toroids, it follows that the magnetic field contributions from each is zero. It is now possible to conclude that the magnetic field from an electrode in an infinite, uniformly conducting media is in fact zero!
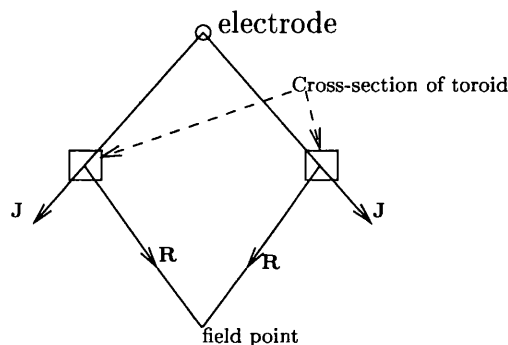
Figure 2.4: Cross-section of the toroid indicating the equal magnitudes but opposite directions of **B** (in and out of the page).

This result can be confirmed by considering Ampére's Circuital Theorem, although it is necessary to consider a more detailed form than the simple one considered in the remaining discussions. The full form of Ampére's Circuital Theorem corresponding to Maxwell's Equation

$$\nabla \times \mathbf{H} = \mathbf{J} + \frac{\partial \mathbf{D}}{\partial t}$$

(recall there is no magnetic material within the domain) ought to have $\mathbf{J}$ replaced by $\mathbf{J} + \frac{\partial \mathbf{D}}{\partial t}$ [23] referring to the case where the point source has a time dependent charge $Q(t)$ such that

$$\frac{\partial Q(t)}{\partial t} = -I$$

where I is the total current emitted from the electrode into the medium at any given instant. In this case,

$$\frac{\partial \mathbf{D}}{\partial t} = \frac{1}{4\pi r^2}\frac{\partial Q}{\partial t} = -\frac{I}{4\pi r^2} = -\mathbf{J}$$

and Ampére's Circuital Theorem applied to the loop as shown in figure 2.5 gives $H = 0$. All subsequent calculations deal with complete circuits so there is no
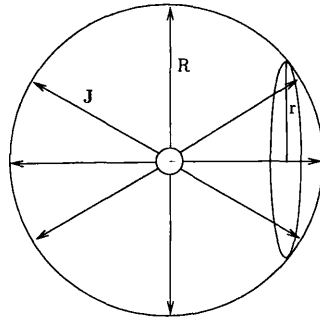
Figure 2.5: Current source of charge Q emitting current uniformly into the domain. Applying Ampére's Circuital Theorem on the circle of radius r requires the inclusion of the time dependent displacement current.

build up of free charge and therefore no time dependent displacement currents.

Consider the practical case of the electrode being supplied by a feeder wire carrying current I from infinity. In this scenario the magnetic field can be evaluated by separating the problem into two parts, the field due to the electrode and the field due to the feeder wire. As shown above, for an infinite, uniformly

conducting medium, the magnetic field from the source is zero. Hence any field will be due to the wire. This is a standard electromagnetic problem which can be found in many texts [24, 25]. The field from such a semi-infinite wire can be shown to be, using the Biot-Savart Law,

$$B = \frac{\mu_0 I}{4\pi\rho}(1 + \cos\phi) \qquad (2.2.4)$$

$$= \frac{\mu_0 I}{4\pi\rho}\left(1 + \frac{z}{\sqrt{z^2 + \rho^2}}\right) \qquad (2.2.5)$$

where ϕ is the appropriate angle made by a vector from the near end of the feed to the field point, as shown in figure 2.6. To further convince the reader, the same
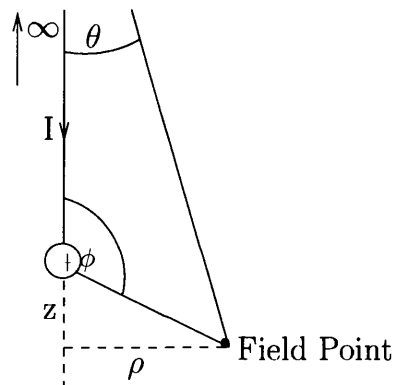
Figure 2.6: Schematic of the semi-infinite source wire.

result can be obtained from Ampere's Law where the current emanating from the electrode has to be included, and it is easy to verify that the appropriate Maxwell equation $\nabla \times \mathbf{B} = \mu_0 \mathbf{J}$ is satisfied.

2.2.2 Magnetic Field from a Straight Wire.

Consider a straight wire of finite length in an infinite, uniformly conducting medium as depicted in figure 2.7.

The wire is of length L between points $\mathbf{r}_1$ and $\mathbf{r}_2$, and carries a current of I. The field point is located at $\mathbf{r}$. By applying the Biot-Savart Law in the form

$$\mathbf{B} = \frac{\mu_0 I}{4\pi}\int_L \frac{d\mathbf{L} \times \mathbf{r}}{r^3}. \qquad (2.2.6)$$
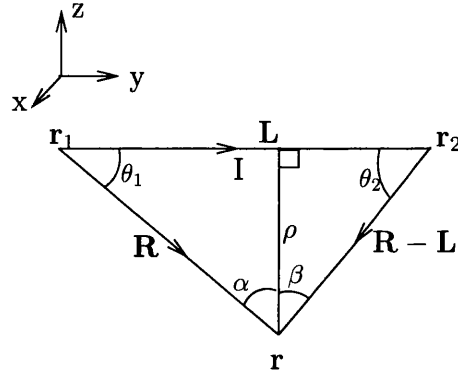
Figure 2.7: Schematic for the calculation of the magnetic field from a finite wire at an arbitrary point in space.

the magnetic field can evaluated to be [24]

$$\mathbf{B} = \frac{\mu_0 I}{4\pi} \frac{1}{\rho} \left(\cos\theta_1 + \cos\theta_2\right) \left(-\left(z - c\right)\mathbf{i} + \left(x - a\right)\mathbf{k}\right) \qquad (2.2.7)$$

where $\mathbf{r}_1 = (a_1, b_1, c_1)$, $\mathbf{r}_2 = (a_2, b_2, c_2)$, and $\mathbf{r} = (x, y, z)$ Further, it is possible to replace the trigonometric functions with equivalent vector expressions which allows eqn (2.2.7) to be expressed as

$$\mathbf{B} = \frac{\mu_0 I}{4\pi} \frac{\mathbf{L} \times \mathbf{R}}{|\mathbf{L} \times \mathbf{R}|^2} \left[\frac{\mathbf{R} \cdot \mathbf{L}}{R} + \frac{\mathbf{L} \cdot (\mathbf{L} - \mathbf{R})}{|\mathbf{L} - \mathbf{R}|}\right] \qquad (2.2.8)$$

2.2.3 Model of a 'Simple Submarine'

Suppose that there is a source and a sink in an infinite, uniformly conducting domain, linked by a length of wire, as shown in figure 2.8. This can be thought to
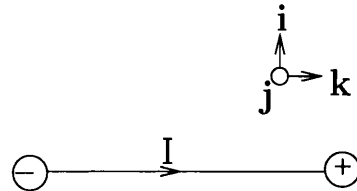
Figure 2.8: Simple model of a corroding submarine.

represent a basic submarine corroding in the sense that the propeller will corrode to an electrochemical potential significantly more negative than the main body

of the submarine. This results in the galvanic corrosion with which this research is concerned. Using the discussions above for an electrode and a finite wire, the magnetic field can be calculated for each individual component. However, it is also possible to apply Ampére's Circuital Theorem to this model which will provide an expression for the total magnetic field. This result can therefore be used as a check of the results used from the previous discussions.

Begin by considering the discussions above. These stated that in an infinite, uniformly conducting medium, the magnetic field from an electrode would be zero. Hence at any point within the domain, the magnetic field must be produced only by the wire connecting the two electrodes. Choose the origin O to be the midpoint of the line joining the two electrodes, the z-axis to be the axis of symmetry directed from O to the positive electrode, and the x and y axes to be mutually orthogonal to the axis of symmetry with the y-axis out of the plane of the paper. To evaluate the magnetic field, begin with the Biot-Savart Law of the form shown in eqn (2.2.6). In this situation $d\mathbf{L}$, an infinitesimal element of the wire in the direction of the current, is simply dz' which is located at $(0, 0, z')$, and $\mathbf{r}$ is the vector from the element to the field point $\mathbf{P} = (x, y, z)$ in the medium. With this arrangement the expression for $\mathbf{B}$ becomes

$$\mathbf{B} = \frac{-\mu_0 I}{4\pi} \int_L \frac{dz'}{(x^2 + y^2 + (z - z')^2)^{\frac{3}{2}}} y\mathbf{i} + \frac{\mu_0 I}{4\pi} \int_L \frac{dz'}{(x^2 + y^2 + (z - z')^2)^{\frac{3}{2}}} x\mathbf{j} \quad (2.2.9)$$

Making the substitution $z - z' = (x^2 + y^2)^{\frac{1}{2}} \sinh\theta$ to perform the integration, eqn (2.2.9) becomes

$$\mathbf{B} = \frac{\mu_0 I}{4\pi(x^2 + y^2)} \left[\frac{z - z'}{(x^2 + y^2 + (z - z')^2)^{\frac{1}{2}}} \right]_{z_-}^{z_+} (y\mathbf{i} - x\mathbf{j}) \quad (2.2.10)$$

Using the distances and notation shown in figure 2.9 this expression may be expressed as

$$\mathbf{B} = \frac{\mu_0 I}{4\pi(x^2 + y^2)} \left[\cos\phi + \cos\theta \right] (y\mathbf{i} - x\mathbf{j}) \quad (2.2.11)$$

$$= \frac{\mu_0 I}{2\pi(x^2 + y^2)} \left[\cos\left(\frac{\phi + \theta}{2}\right) \cos\left(\frac{\phi - \theta}{2}\right) \right] (y\mathbf{i} - x\mathbf{j}) \quad (2.2.12)$$

This calculation, along with all those previously performed in this section, has
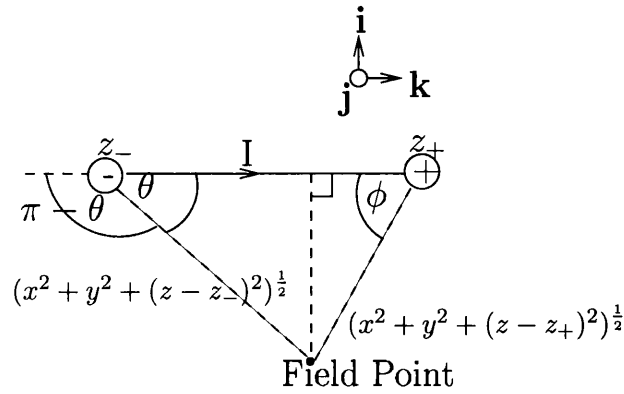
Figure 2.9: Detailed description of the simple model of a corroding submarine.

been based on the various forms of the Biot-Savart Law. To act as a check of these calculations, the magnetic field will be recalculated only this time the theorem which will be used is the Ampére's Circuital Theorem [26]. The outcome for this calculation and that from the previous calculation should provide equivalent expressions for the *total* magnetic field. To make use of Ampére's Circuital Theorem, consider figure 2.10. The shaded disk has radius of $(x^2 + y^2)^{\frac{1}{2}}$ and Ampére's
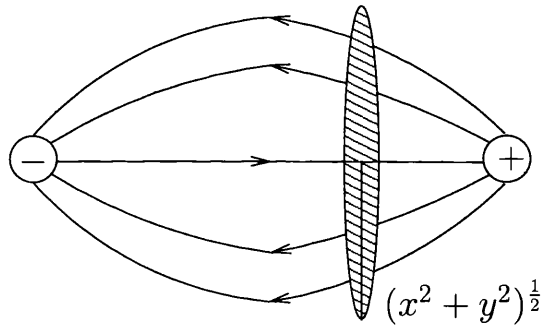
Figure 2.10: Simple model of a corroding submarine for use with Ampére's Circuital Theorem.

Circuital Theorem states that the magnetic field round this disk is given by

$$\mathbf{B} = \frac{\mu_0 I_{tot}}{2\pi (x^2 + y^2)^{\frac{1}{2}}}$$

(2.2.13)

where $I_{tot} = I - I_{sea}$ is the total current flowing through the disk. For the ease of calculation, the field point will be chosen to be located on the plane of the page, so $y = 0$. Hence equating eqn (2.2.12) with eqn (2.2.13) and also neglecting the

directions for the moment,

$$B = \frac{\mu_0 I}{2\pi x} \left[\cos\left(\frac{\phi + \theta}{2}\right) \cos\left(\frac{\phi - \theta}{2}\right) \right] = \frac{\mu_0(I - I_{sea})}{2\pi x} \qquad (2.2.14)$$

which provides the following expression for the currents flowing from the positive electrode to the negative through the sea as

$$I_{sea} = -I \left[1 - \cos\left(\frac{\phi + \theta}{2}\right) \cos\left(\frac{\phi - \theta}{2}\right) \right]. \qquad (2.2.15)$$

A simple analysis indicates that this seems to be correct. When positioned close to the wire, $\phi \approx \theta \approx 0$ which forces $I_{sea} = 0$ as expected. Whilst if far from the wire, $\phi \approx \theta \approx \frac{\pi}{2}$ which would force $I_{sea} = -I$ and $\mathbf{B} = 0$ again as expected. However, the field point could be at any point on the plane previously mentioned so the current at an arbitrary point on the plane is required so that the field at the arbitrary point can be evaluated. To do this, consider figure 2.11, which depicts a positive electrode, surrounded by a sphere, emitting current uniformly. To be able to calculate the current that will flow back through the sea passing through the disk shown in figure 2.10, it is necessary to be able to calculate the current that will pass out of any section of the sphere in figure 2.11.
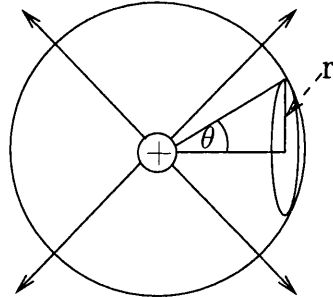
Figure 2.11: A source uniformly emitting current surrounded by a sphere. A circle of radius r is shown whose circumference lies on the surface of the sphere.

The current density at some distance R from the source will be

$$J = \frac{I}{4\pi R^2} \qquad \text{units:} \quad \frac{A}{m^2} \qquad (2.2.16)$$

so the current through the circle marked with radius r on figure 2.11 is

$$
\begin{aligned}
I_{circle} &= J \times (\text{area of sphere of radius R cut off by circle}) & (2.2.17) \\
&= J \times R^2 \times \Omega \text{ where } \Omega \text{ is the solid angle subtended} & (2.2.18) \\
&\qquad\qquad\qquad\qquad\qquad \text{by the circle.} \\
&= JR^2 2\pi(1 - \cos\theta) & (2.2.19) \\
&= \frac{I}{2}(1 - \cos\theta). & (2.2.20)
\end{aligned}
$$

Consider figure 2.12. It can be said that the total current flowing to the right
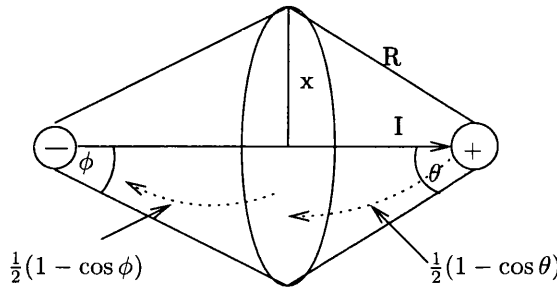
Figure 2.12: Currents returning from source to sink via the sea passing through a circle of evaluation.

is

$$
I_{total} = I - \frac{I}{2}\left(1 - \cos\theta\right) - \frac{I}{2}\left(1 - \cos\phi\right) \tag{2.2.21}
$$

$$
I_{total} = \frac{I}{2}(\cos\theta + \cos\phi) \tag{2.2.22}
$$

When eqn (2.2.22) is entered into eqn (2.2.13), the expression for the magnetic field magnitude at a distance x from the wire on the plane of the page is

$$
B = \frac{\mu_0 I}{4\pi x}(\cos\theta + \cos\phi) \tag{2.2.23}
$$

which is the same result obtained using Biot-Savart analysis.

This calculation therefore verifies the previous analysis carried out for an electrode and a wire in an infinite, uniformly conducting medium. This however is a very idealised scenario, and the effect of a boundary to represent the sea surface must be considered to deem these calculations useful.

2.3 Fields in a Semi-infinite Domain

The discussions so far have focused on the idealised case of an infinite domain. This could possibly be considered valid for a corroding submarine where it is reasonable to approximate the sea surface and the sea bed as being far enough away from the vessel to have negligible effects. However, this is not the situation which is being analysed. For a ship corroding in the sea, the sea bed could be deemed distant enough so as to be neglected but the sea surface plays a very prominent role. Indeed, one of the easiest ways to picture the discussion is to consider the model of the simple submarine (of section 2.2.3) submerged just below the sea surface.

As before, the first case which will be considered is that of an electrode, supplied by a wire from infinitely far below.

2.3.1 Submerged Electrode - Magnetic Field in Air

To begin with the magnetic field in the air will be calculated. Consider figure 2.13. The domain $z > 0$ is filled with air, which is non-conducting, while $z < 0$
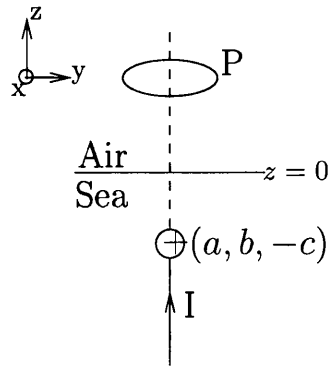
Figure 2.13: Electrode submerged just below sea surface fed by a wire from $-\infty$.

is filled with conducting sea water. The electrode is located at $(a, b, -c)$ where $c > 0$, and is fed by a current I from $-\infty$ along the z-axis.

The current distribution has cylindrical symmetry about the z-axis. We will now show that lines of $\mathbf{B}$ are circles centred on a line parallel to the z-axis passing through the electrode at $x = a, y = b$ in planes parallel to the xy plane.

Consider a field point P which lies on the yz plane. Let $P = \mathbf{R}_{yz}$ to emphasise that it has no x-component. Ignore the wire for the moment and consider the

current at point $\mathbf{x}_1 = x\mathbf{i} + \mathbf{x}_{yz}$. Let it be $\mathbf{J}_1 = J\mathbf{i} + \mathbf{J}_{yz}$. Also consider point $\mathbf{x}_2$: the reflection of $\mathbf{x}_1$ in the yz plane, $\mathbf{x}_2 = -x\mathbf{i} + \mathbf{x}_{yz}$ and because of symmetry, $\mathbf{J}_2 = -J\mathbf{i} + \mathbf{J}_{yz}$.

The field at P from equal volumes, dV, at $\mathbf{x}_1$ and $\mathbf{x}_2$ is by the Biot-Savart Law (eqn (2.2.3))

$$d\mathbf{B} = \frac{\mu_0 dV}{4\pi} \left[\frac{\mathbf{J}_1 \times (\mathbf{R} - \mathbf{x}_1)}{|\mathbf{R} - \mathbf{x}_1|^3} + \frac{\mathbf{J}_2 \times (\mathbf{R} - \mathbf{x}_2)}{|\mathbf{R} - \mathbf{x}_2|^3} \right]. \tag{2.3.1}$$

However,

$$|\mathbf{R} - \mathbf{x}_1| = \sqrt{x^2 + |\mathbf{R}_{yz} - \mathbf{x}_{yz}|^2} = |\mathbf{R} - \mathbf{x}_2| \tag{2.3.2}$$

so the denominators are equivalent. Investigating the numerators,

$$
\begin{aligned}
\mathbf{J}_1 \times (\mathbf{R} - \mathbf{x}_1) + \mathbf{J}_2 \times (\mathbf{R} - \mathbf{x}_2) &= (J\mathbf{i} + \mathbf{J}_{yz}) \times (-x\mathbf{i} + (\mathbf{R}_{yz} - \mathbf{x}_{yz})) \\
&\quad + [(-J\mathbf{i} + \mathbf{J}_{yz}) \times \\
&\qquad (x\mathbf{i} + (\mathbf{R}_{yz} - \mathbf{x}_{yz}))] \tag{2.3.3} \\
&= (J - J)\mathbf{i} \times (\mathbf{R}_{yz} - \mathbf{x}_{yz}) \\
&\quad + 2\mathbf{J}_{yz} \times (\mathbf{R}_{yz} - \mathbf{x}_{yz}) \tag{2.3.4}
\end{aligned}
$$

The first term is 0 and the second, being the cross-product of two vectors in the yz-plane, is in the x-direction. Therefore all contributions to $\mathbf{B}$ on the yz-plane are perpendicular to the yz-plane. By rotating about the z-axis, the axis of symmetry, the lines of $\mathbf{B}$ are circles.

We also know, from the Biot-Savart Law, that the magnetic field from the wire forms circles around the z-axis.

To utilise this result, consider the circular loop in figure 2.13. By the previous result, $\mathbf{B}$ is constant on the loop by symmetry and tangential to it. Also since this loop is in the non-conducting air, no current can pass through it. Hence by Ampére's Circuital Theorem eqn (2.2.13),

$$\int \mathbf{B} \cdot d\mathbf{l} = 0 \Rightarrow \mathbf{B} = 0 \tag{2.3.5}$$

where $d\mathbf{l}$ is a infinitesimal segment of the circular path in the direction of $\mathbf{B}$. But field must be equal to the sum of the fields calculated from the Biot-Savart Law for the wire and the electrode. If $\mathbf{B}_w$ denotes the field from the wire and $\mathbf{B}_{sea}$

denotes the field from the electrode, it follows that

$$\mathbf{B}_w + \mathbf{B}_{sea} = 0 \Rightarrow \mathbf{B}_{sea} = -\mathbf{B}_w. \tag{2.3.6}$$

To evaluate the magnetic field due to the wire, use the version of the Biot-Savart Law in eqn (2.2.6). This provides an expression for the magnetic field as

$$\mathbf{B} = \frac{\mu_0 I}{4\pi\rho^2} \left[1 + \frac{z+c}{(\rho^2 + (z+c)^2)^{\frac{1}{2}}} \right] ((y-b)\mathbf{i} - (x-a)\mathbf{j}) \tag{2.3.7}$$

where $\rho^2 = ((x-a)^2 + (y-b)^2)$ which from eqn (2.3.6) gives

$$\mathbf{B}_{sea} = \frac{\mu_0 I}{4\pi\rho^2} \left[1 + \frac{z+c}{(\rho^2 + (z+c)^2)^{\frac{1}{2}}} \right] (-(y-b)\mathbf{i} + (x-a)\mathbf{j}) \tag{2.3.8}$$

The important point to garner from this example is that the introduction of a boundary has effectively allowed the electrode to produce a magnetic field due to the non-symmetric emission of currents. This calculation could be treated as an aside as it is in the sea that the main area of interest lies.

2.3.2 Submerged Electrode - Magnetic Field in the Sea

Consider the two diagrams shown in figure 2.14. To calculate the fields (both electric and magnetic) in the sea due to the symmetry being broken, it is necessary to model the new current density patterns in a fashion which allows their calculation and hence enable the calculation of the electromagnetic fields at points within the sea. This can be done using the method of images. The diagram (a) shows the general shape of the current distribution from the electrode due to the effect of the boundary with air. Diagram (b) suggests that by introducing an image circuit (symmetric about the non-conducting boundary) and replacing the air with sea water will have the effect of producing the same current distribution in the real sea.

In the image situation (b), the boundary between the sea and the air has been removed and the whole domain filled with sea water. It is necessary to ensure that the current distribution in the region of sea water, $z < 0$, is still the same as for the real case, 2.14(a). To satisfy this a second electrode, or image
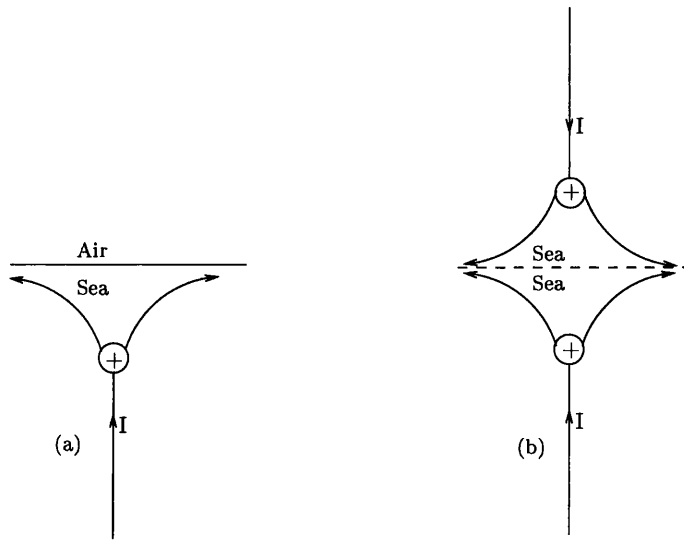
Figure 2.14: (a) Shows the current density distribution due to the boundary. (b) Shows that the same distribution in the sea can be achieved by introducing an image source.

electrode, is located exactly the same distance above the boundary as the original electrode is below it. This image must be supplied by a feeder wire which should come from infinitely far above, as shown. Thus on the boundary, the currents in the sea from either electrode are identical in magnitude with opposite normal components resulting in no net sea currents across the boundary.

Consider the region of the real sea, $z < 0$. The boundary conditions for the current distribution from both electrode arrangements must be identical: zero normal component at the surface of the sea ($z = 0$) and $\mathbf{J} \propto R^{-2}$ at large R. As discussed in section 2.3.1, there is a magnetic field from the currents emitted from the electrode as the boundary has destroyed the spherical symmetry of the current emission. Also as a consequence of $\mathbf{J}_n = 0$ at the boundary, $\mathbf{E}_n = \frac{\mathbf{J}_n}{\sigma} = 0$ at $z = 0$ as required. Imagine now that there is a hemisphere with base centred at $(a, b, -c)$ facing downward with large radius R. The current density on this hemisphere will be

$$J = \frac{I}{2\pi R^2} \qquad (2.3.9)$$

$$\propto \frac{1}{R^2} \qquad (2.3.10)$$

since no current crosses the boundary from the image electrode. Therefore in the sea ($z < 0$) for the image case, the boundary conditions are the same as for the real situation. The uniqueness theorem then forces the current distribution in $z < 0$ to be the same in the image case as the real case, which implies the same electromagnetic fields. We are now in a position to calculate the magnetic field in the sea using figure 2.14(b)

By the results shown in section 2.3.1, the wire and current in $z < 0$ give $\mathbf{B} = \mathbf{0}$ above the xy-plane. So for $z < 0$, $\mathbf{B}$ is not affected by these extra current sources above the plane. To calculate the magnetic fields within the $z < 0$ region, there are two regions of interest. Both are shown by loops in figure 2.15. Consider loop
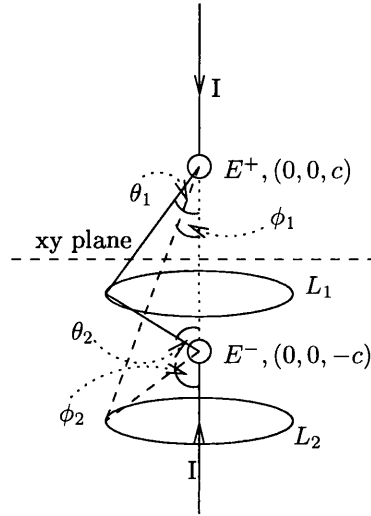
Figure 2.15: The two main areas of interest for calculating the $\mathbf{B}$ fields in the region $z < 0$ shown by loops L_1 and L_2.

L_1 which lies in the region $0 > z > -c$. To evaluate the magnetic field, Ampére's Circuital Theorem will be used since the total magnetic field is required. The current that passes through the loop in the positive z direction from E^+ is

$$I_1^+ = -\frac{I}{4\pi}2\pi(1 - \cos\theta_1) \qquad (2.3.11)$$

whilst the current passing through in the positive z direction from E^- is

$$I_1^- = +\frac{I}{4\pi}2\pi(1 - \cos\theta_2) \qquad (2.3.12)$$

Using these values for the current, Ampére's Circuital Theorem says

$$2\pi\rho\mathbf{B} \;=\; \frac{\mu_0 I}{2}(\cos\theta_1 - \cos\theta_2)\frac{1}{\rho}(-y\mathbf{i} + x\mathbf{j}) \tag{2.3.13}$$

$$\mathbf{B} \;=\; \frac{\mu_0 I}{4\pi\rho^2}(\cos\theta_1 - \cos\theta_2)(-y\mathbf{i} + x\mathbf{j}) \tag{2.3.14}$$

$$=\; \frac{\mu_0 I}{4\pi\rho^2}\left(\frac{c-z}{\sqrt{\rho^2 + (c-z)^2}} - \frac{c+z}{\sqrt{\rho^2 + (c+z)^2}}\right)(-y\mathbf{i} + x\mathbf{j}) \tag{2.3.15}$$

where $\rho^2 = x^2 + y^2$.

Consider loop L_2 which lies in the region $z < -c$. Running a similar argument to the preceding one, but including also the current I from the wire, the current passing through the loop in the positive z direction is

$$I_2 = I_2^+ + I_2^- = I - \frac{I}{2}(1 - \cos\phi_1) - \frac{I}{2}(1 - \cos\phi_2) \tag{2.3.16}$$

which, using Ampére's Circuital Theorem gives the magnetic field to be

$$\mathbf{B} \;=\; \frac{\mu_0 I}{4\pi\rho^2}(\cos\phi_1 + \cos\phi_2)(-y\mathbf{i} + x\mathbf{j}) \tag{2.3.17}$$

$$=\; \frac{\mu_0 I}{4\pi\rho^2}\left(\frac{c-z}{\sqrt{\rho^2 + (c-z)^2}} - \frac{(z+c)}{\sqrt{\rho^2 + (c+z)^2}}\right)(-y\mathbf{i} + x\mathbf{j}). \tag{2.3.18}$$

These results for the two regions are exactly the same, so in general for $z < 0$

$$\mathbf{B} = \frac{\mu_0 I}{4\pi\rho^2}\left(\frac{c-z}{\sqrt{\rho^2 + (c-z)^2}} - \frac{z+c}{\sqrt{\rho^2 + (c+z)^2}}\right)(-y\mathbf{i} + x\mathbf{j}) \quad (z < 0). \tag{2.3.19}$$

In the original sea region, $z < 0$, the field from the wire is

$$\mathbf{B}_w = \frac{\mu_0 I}{4\pi\rho^2}\left(1 - \frac{z+c}{\sqrt{\rho^2 + (z+c)^2}}\right)(-y\mathbf{i} + x\mathbf{j}) \tag{2.3.20}$$

so as before the field in the sea from the sea currents emitted by the electrode is

$$\mathbf{B}_{sea} \;=\; \mathbf{B} - \mathbf{B}_w \tag{2.3.21}$$

$$=\; \frac{\mu_0 I}{4\pi\rho^2}\left(1 - \frac{c-z}{\sqrt{\rho^2 + (c-z)^2}}\right)(y\mathbf{i} - x\mathbf{j}) \tag{2.3.22}$$

This is the same answer as for a wire down the z-axis from $+\infty$ to the image point $(0, 0, +c)$ carrying current downward! This gives a simple way of calculating the magnetic field from the currents in the sea: ignore them, and introduce a fictitious wire from $+\infty$ to $(0, 0, +c)$.

2.3.3 Submerged Simple Submarine - Method of Images.

The previous section has shown that to account for a boundary close to an electrode in the sea, the method of images can be used to calculate the fields that arise, with the magnetic field that results from the introduction of the boundary being equivalent to that from the feeder wire to the image electrode. For a model of a simple submarine as shown in figure 2.8, when situated in the vicinity of a boundary the resultant fields can again be calculated using images. However, only images of the electrodes are required and not of the connecting wire. It may seem incorrect to not have an image of the wire but the reason lies in how the fields are calculated. At any point in the medium, the electric field can be calculated from the current density

$$\mathbf{E} = \frac{\mathbf{J}}{\sigma} \tag{2.3.23}$$

and the magnetic field from the Biot-Savart Law. For the Biot-Savart Law, the magnetic field contribution from each individual component of the circuit can be calculated. This requires using eqn (2.2.3) for the field due to the current density in the sea emitted by the electrodes and eqn (2.2.6) for the field due to the current flowing down the wire. The important facts are that the field is due to the current density in the sea *emitted* by the electrodes and the current *in* the wire. By introducing the boundary, the currents emitted from the electrodes are perturbed, but the current in the wire remains unaltered, hence there is no requirement to add an image of the wire to get the correct representation of the current. Therefore, the method of images for this situation is shown in figure 2.16

From this arrangement it is apparent that to calculate the magnetic fields from a simple submarine model requires the evaluation of the fields from the three wires as shown. This can be done for each individual wire using the Biot-Savart Law eqn (2.2.6). The location of the electrodes are $(a, -b, c)$ and $(a, +b, c)$
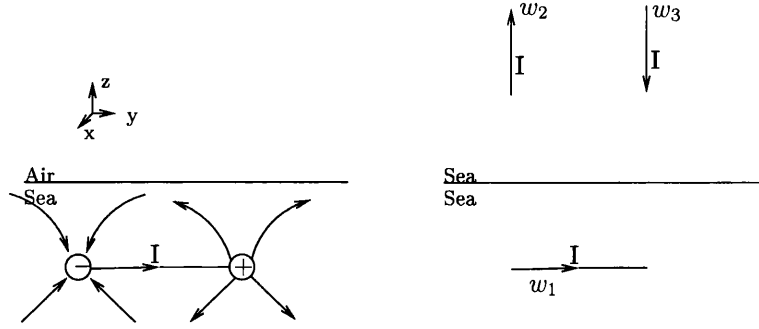
Figure 2.16: The left hand diagram shows the effect of the sea level on the emitted currents whilst the right hand diagram shows the equivalent situation modelled using images.

for the negative and positive ones respectively, with the wire running between these two coordinates. The field from wire w_3 representing that from the positive electrode is

$$\mathbf{B}_{w_3} = \frac{\mu_0 I}{4\pi \rho_+^2} \left(1 + \frac{c - |z|}{\sqrt{\rho_+^2 + (c - |z|)^2}} \right) ((y - b)\mathbf{i} - (x - a)\mathbf{j}) \qquad (2.3.24)$$

where $\rho_+^2 = (x - a)^2 + (y - b)^2$. Similarly, the field from wire w_2 representing that from the negative electrode is

$$\mathbf{B}_{w_2} = \frac{\mu_0 I}{4\pi \rho_-^2} \left(1 + \frac{c - |z|}{\sqrt{\rho_-^2 + (c - |z|)^2}} \right) ((y + b)\mathbf{i} - (x - a)\mathbf{j}) \qquad (2.3.25)$$

where $\rho_-^2 = (x - a)^2 + (y + b)^2$. Finally the field from the wire w_1 which is the original one in the configuration is

$$\mathbf{B}_{w_1} = \frac{\mu_0 I}{4\pi \rho^2} \left(\frac{y - b}{\sqrt{(x - a)^2 + (y - b)^2 + (z - c)^2}} + \right.$$
$$\left. \frac{y + b}{\sqrt{(x - a)^2 + (y + b)^2 + (z - c)^2}} \right) ((z - c)\mathbf{i} - (x - a)\mathbf{k}), (2.3.26)$$

where $\rho^2 = (x - a)^2 + (z - c)^2$. By adding these three fields, the total field for a simple submarine model near the surface of the sea can be calculated.

2.4 Applying the result for the Simple Submarine Model

This result from section 2.3.3 is crucial to the calculation of CRM fields from a corroding ship.

Consider a ship in the sea which is corroding, the sea surface will provide an upper boundary to the area which is corroding. From the hull corrosion currents will be emitted and flow through the sea to, in most cases, the propeller. If the hull is discretized and the density of the current emitted from each element known, then these elements may be thought of as positive electrodes with the propeller being regarded as a negative electrode. Since no net current can escape from the ship, a current loop must be formed with the current absorbed at the propeller flowing back through the ship (via the propeller shaft) to the hull, or more specifically, back to the element from which it was originally emitted. This situation is identical to that of the simple submarine in a semi-infinite domain.

This allows the CRM field to be calculated. Take several points of interest within the sea domain and calculate the current at these points due to the emitted corrosion currents from the hull. Later this process will be described in more detail. From these currents, contributions to the CRM may be obtained using the Biot-Savart Law. The contributions from the return currents through the ship need to be calculated and this is done by considering the emitting hull element to be a positive electrode, the absorbing propeller to be a negative electrode, and joining the two via a simple wire (thus completing a current loop). This is exactly the set up described in section 2.3.3 and hence the result from here may be used to calculate the contribution to the magnetic field at the field points within the domain. By summing all the contributions from all the hull elements to that obtained for the current in the sea, the total CRM field for a point within the sea can be estimated.

This indicates how useful this result is but it depends on knowing what current is emitted from different parts of the hull. To model these currents it is necessary to use a numerical modelling method called the Boundary Element Method.

Chapter 3

The Boundary Element Method

3.1 Introduction

The geometry of a ship is too complicated to be modelled analytically, which makes it necessary to use a numerical model to describe the physical interaction between the sea water and the ship, and this requires the domain or its boundary to be meshed into discrete elements. The type of mesh required, either a volume mesh of the domain or a surface mesh of the boundary, depends on the numerical method used to model the system.

The situation considered here is a volume of sea water bounded by rectangular faces, the top face coinciding with the surface of the sea. The ship's hull intersects the top surface. The boundary consists of the hull, propeller, and the surface of the 'box' of sea water. For the moment, we assume that either the electric potential or its outward normal derivative (flux) are known everywhere on the surface. These two variables are actually related on the ship via a polarization relationship but this will be considered in more detail in later chapters. Currently, the aim is to develop a modelling technique which will determine the values for the potential and its outward normal derivative so that the magnetic fields may be calculated within the domain.

There are many numerical modelling methods used today, but for this problem the choice reduces to two, the Boundary Element Method (BEM) which requires a surface mesh, and the Finite Element Method (FEM) which requires a volume mesh. The FEM is the older method of the two and as a result is probably still the most widely applied method but it is now clear that the BEM is far more

suitable for specific types of problem and is being employed more widely with each passing year [27].

In this section, a brief historical account will be given for the development of the FEM, and this will be continued into the development of the BEM by indicating the problems encountered by FEM and why BEM manages to avoid these, justifying itself as the preferred choice for tackling the type of problem encountered in this research.

3.2 Development of the Finite Element Method - An Historical Account

The FEM is a numerical technique which is used to solve problems in which the governing equations over the domain can be described by a partial differential equation or can be formed by a functional minimisation. A definition of the FEM may be

> a computer-aided mathematical technique for obtaining approximate
> numerical solutions to the abstract equations of calculus that predict
> the response of physical systems subjected to external influences.[28]

This definition is accurate but slightly misleading. While it is most definitely a 'computer-aided' technique, this suggests that it has only been developed since the advent of high-power digital computing which is not the case. More detailed acounts of the historical development of the FEM can be found in the texts of Burnett [28] and Tony & Rossettos [29].

There is no single person who could claim credit for developing the FEM, the founding ideas being laid down by a collection of physicists, mathematicians, and engineers. The most popular point in the literature to begin tracking the development of FEM is the 1940's, with a paper in 1943 by Courant [30] being of great significance. In this paper, Courant tackled the torsion problem in elasticity by defining piecewise linear polynomials over a triangularized region.

In 1946, Schoenberg [31] developed his ideas on splines and recommended the use of piecewise polynomials in approximation and interpolation. A significant step was made in 1959 by Greenstadt [32] who divided a domain into 'cells', assigned different functions to each cell, and then applied a variational principle.

White [33] and Friedrichs [34] (in 1962) then used triangular elements and were able to develop difference equations from these variational principles.

While these developments were occurring within the mathematics fraternity, similar work was being done by physicists and engineers. One piece of work of particular relevance to this research presented here was that of McMahon [35], who successfully dealt with a three-dimensional electrostatic problem by using tetrahedral elements and linear trial functions.

In the 1950's, researchers in the field gained access to high-speed stored-program digital computers. By reformulating the existing well established framework of analysis procedures into equivalent matrix equations, the computers were used to perform efficient automatic computations.

In 1956, the modelling of odd shaped wing panels of aircrafts using smaller, triangular-shaped panels by Turner, Clough, Martin and Topp [36] was the first reported instance of a complicated two or three dimensional structure being represented by a collection of simpler two or three dimensional pieces. This was a major development since it is essentially the principle that is used by the majority of modern numerical techniques. It was this final development which sparked the actual development of the FEM.

In a paper by Clough [37] in 1960, the name 'finite elements' was finally born. Between the mid-1950's and the late-1970's, the FEM was applied to various problems. Initially only large scale structural applications were considered since it was mainly engineers that were involved with the conception of the method, but by the end of the period, mathematicians had taken a greater interest and developed the method so that it was built on a more mathematically solid foundation. These mathematicians looked beyond the variational methods and incorporated weighted-residuals and global energy balance principles. The development and incorporation of automatic mesh generators, interactive graphics and various other pre and post processing tools lead to the software packages available today for application of the FEM [28].

3.3 FEM - How does it work?

The preceding section accounts for the historical background of how the method was developed but to determine why an alternative method was developed, it is

necessary to look at how the FEM works and what problems may arise.

The FEM is a typical example of what is known as a 'domain type solution' in which the domain of the problem is discretized into a number of three dimensional elements. The governing equations are then approximated over the region by functions which will satisfy the boundary conditions between each element. In all numerical techniques applied to solving differential equations, the goal is to seek approximate solutions of the equations by reducing the problem to a series of additions and multiplications [38]. This requires the problem to be approximated in a fashion which results in a loss of accuracy. The two options are either to approximate the differential operator, or the analytic solution (or a combination of them both). The FEM uses an approximation of the solution by representing it as a finite rather than infinite series [38].

The FEM is at its most powerful when tackling boundary value problems concerning finite domains in which the properties of the med ium vary throughout its volume and as a result it is common that in problems where some of the variables are subject to boundary value problems but others to initial value problems, only those of boundary value type are discretized using finite elements. When the finite elements are used to carry out the discretisation, the 'nodes' or 'solution locations' may be located on either the sides or vertices of the elements, as well as within the elements themselves [38].

The approximation of the solution is then made by using basis functions as interpolation polynomials. These basis functions are piecewise continuous interpolation polynomials and are defined over the discretizing elements. It is also possible to define the basis functions so as they have continuous derivatives over the boundaries of the finite elements. There is a common practise to only have the basis functions as being non-zero over a limited portion of the grid which allows for greater economy when applying the method. Generally a basis function will be associated directly with a node and will only be non-zero for elements which use this node.

The need for greater economy in storing the details of the basis functions indicates the main drawback of the FEM. To apply a FEM and obtain accurate solutions requires a colossal amount of information to be stored by the computer. The matrices that are used to describe the system are extremely large although they are sparse allowing them to be condensed which helps save on memory

requirements. The main expense in terms of memory is the storing of the mesh. For a problem with a complicated irregular domain and perhaps varying physical properties such as conductivities, the amount of data required to describe the finite element discretisation of the domain is colossal, with every node, vertex and side of the elements required along with the definition of the basis functions, physical properties of each element and the boundary conditions of the finite elements. This puts an enormous strain on the memory capacity of even the most advanced modern day computers. Of course, fewer elements could be used but this would reduce the accuracy of the obtained solution. Another problem occurs when the method is applied to an open boundary problem (which, for example, could be a ship corroding in an infinite sea) as there is a difficulty in specifing the external boundary of the mesh [20].

3.4 The Boundary Element Method

This method presents a conceptually different approach to solving a set of differential equations describing a practical problem. The first step with the BEM is to perform some sort of integration before discretisation or approximation, i.e. the differential equations are initially transformed to equivalent integral equations. As a result, the new set of integral equations only involve values of the variables at the extremes of the integration range, i.e. at the boundaries. Therefore, any discretisation would only involve the division of the boundary and not the actual volume of the domain. A direct consequence of this being that the solution variables will then vary continuously throughout the region, which is not the case with the FEM [27].

The mathematical subject of integral equations is a relatively new field with the first rigorous investigation on the classical kinds of integral equation not published until 1905 by Fredholm [27]. However from this point forth, they have been researched intensively with particular interest to field theory applications. The majority of this research was performed by mathematicians and was presented within the rigorous mathematical framework, which excluded many applied scientists from the area. Indeed it appears that it was only when the high-speed digital computer was made commercially available that the key players in the field started to consider using their integral equation research as a solution tool

for practical problems, considerations which produced the BEM.

To speak of 'the' BEM is somewhat misguiding, as there are different formulations of BEM's but they all can be grouped into three categories which, although extremely closely related, are fundamentally different as discribed by Banerjee and Brebbia. [27, 39, 40].

The first category is known as the 'direct formulation of BEM' in which the unknown functions are the physical variables of the problem. The second is the 'semi-direct formulation of BEM' where the integral equations are formulated using unknown functions which are analogous to physically meaningful functions. With these methods, the solution can be differentiated to produce internal distributions of the physically meaningful variable. The final category is the 'indirect formulation of BEM' where the integral equations are expressed in terms of a unit singular solution of the original differential equations distributed at a specific density over the boundaries of the region of interest. Once these physically meaningless density functions are obtained from a numerical solution of the integral equations, they can be integrated to provide values of the solution parameters at any point within the domain. The type of formulation used to tackle a problem depends on the equations which dictate how the variables behave, i.e. the governing equations. For a ship corroding in the sea, which is free from external sources of current, the governing equation is simply Laplace's Equation. For this governing equation, any of the three classes could be used as it is linear [27]. However since the objective of the model is to calculate the magnetic field within the domain, the most suitable formulation is the indirect one.

In general, any problem which involves a system which is either linear or incrementally linear (or approximated as such) can be tackled by the BEM. Indeed there are very few problems for which the FEM can be used whilst the BEM cannot, these being problems in which either there is a spatial dimension which is dis-proportionally small in relation to the others or when each individual material element has different properties [27]. However for a ship in sea water, neither of these scenarios are of concern so the problem can be tackled by either method.

So why is BEM chosen ahead of FEM? One reason is that the dimensionality of the mesh is reduced by one for the BEM as a result of the initial integration [27]. So when considering a three dimensional domain of seawater, the BEM only requires a two dimensional mesh of the boundary while FEM required a three

dimensional volume mesh which requires more memory allocation [41].

Also in the sea domain, there are no sources and it is therefore homogeneous which means that the BEM can tackle the problem with little or no subdivision. If the domain was inhomogeneous then the required subdivision of the whole body to allow the application of the BEM would just be equivalent to a FEM scheme [27].

The effect of the reduced mesh is that the BEM requires a smaller set of simultaneous equations than the FEM (or any other method requiring whole-body discretisation). These matrices are however heavily populated whilst those of the FEM are sparsely populated. To evaluate the matrix elements in the BEM also takes slightly more computational time than those of the FEM due to the more arithmetic nature of the calculation. This means that for small problems (i.e. few elements) the difference in computational time between the two is not significant. As the magnitude of the problems increase, significant saving can be made in computation time using the BEM. Studies have shown that for three dimensional problems tackled with BEM rather than FEM, the speed of the calculation to provide answers of similar precision has been improved by somewhere in the region of four to ten to one [27]. Alternatively, BEM can solve larger problems than FEM can for the same cost of computing resources.

For the specific research presented here another consideration is the size of the domain. It is perfectly feasible to approximate the domain as having some boundaries at infinity (i.e. a semi-infinite domain). With the BEM, the admissible boundary conditions at infinity are automatically satisfied and no subdivision of these boundaries is required. For the FEM, this situation would require the infinite boundaries to be approximated by the mesh stopping at some distant elements which is going to have effect on the accuracy of the calculation [27, 41].

Another advantage of the BEM alluded to before is that once the solutions on the boundary are known then the solution variables can be calculated at interior points with the solutions being continuous throughout the interior of the body. Thus after the 'problem' has been solved, the values of the solution variables at any interior point which subsequently become of interest can be calculated directly as a post-process calculation. With the FEM, if a point within the domain became of interest which was not the location of a node in the initial calculation, then the whole calculation may need to be performed which is very

time consuming as it would also involve the re-meshing of the domain.

As far as the accuracy of the two methods are concerned the BEM is again fundamentally superior [41]. Any errors and numerical approximations occur only at the boundary [6] and these can be minimised by using suitably sophisticated boundary elements or a greater density of simple elements, the approach adopted in this work. Also, numerical integration is a more stable and precise process than numerical differentiation, making the BEM more stable and precise than the FEM since it avoids using this process [27].

For these reasons, the BEM was felt to be the more suitable modelling method for this specific problem although it should be noted that for every person who shares this opinion [6, 17, 41, 42], there will be another who will support the FEM instead.

3.5 Formulation of the Boundary Element Method.

As mentioned above, the formulation of the boundary element method most suitable to the problem being considered here is that of the 'indirect formulation' and may also be interpreted as a weighted residual technique. The following is based on the formulation by Brebbia [39, 43].

3.5.1 Deriving the Boundary Element Method.

Begin by considering the following example which although depicted in two dimensions should be considered as being in three dimensions.
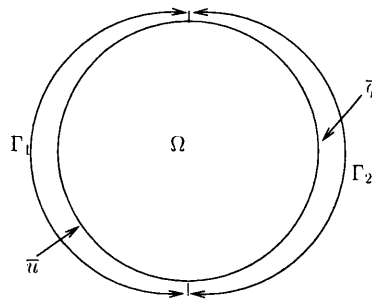
Figure 3.1: Outline of Basic BEM Problem

It is given that:

- $\nabla^2 u = 0$ in Ω (which is a volume),

- $u = \bar{u}$ on Γ_1 (which is a surface),

- $q = \frac{du}{dn} = \bar{q}$ on Γ_2 (which is a surface).

where n is an outward normal vector to the surface, $\bar{u}$ and $\bar{q}$ are functions and $\Gamma_1 + \Gamma_2$ is a closed surface surrounding Ω. For the physical example of a ship corroding, u can be thought of as the electric potential whilst q can be thought of as the negative of the outward normal component of electric field, or the flux of u passing out from the domain. In this work, it is assumed that unless otherwise stated that the units of the electric potential, u, are Volts (V), while the units of the outward flux, q, are Volts per metre $\left(\frac{V}{m}\right)$.

To begin with, consider an approximate function to the actual potential (just call it u) such that the above conditions are not exactly satisfied. The aim is to get this approximation of the potential u to be as close to the actual potential as possible which requires the minimising any discrepancies between the two. Let the sum of these discrepancies be M given by

$$M = \int_{\Omega} \nabla^2 u d\Omega + \int_{\Gamma_1} (\bar{u} - u) d\Gamma + \int_{\Gamma_2} (q - \bar{q}) d\Gamma. \tag{3.5.1}$$

By weighting these integrals with a weighting function w so that each error has the required significance, and then setting M to be zero, the following can be obtained

$$\int_{\Omega} \left(\nabla^2 u\right) w d\Omega - \int_{\Gamma_1} (\bar{u} - u) \frac{dw}{dn} d\Gamma - \int_{\Gamma_2} (q - \bar{q}) w d\Gamma = 0$$

(note that in the second integrand, the weighting function has been differentiated to ensure that each integrand has the same dimensions). This can be rewritten as

$$\int_{\Omega} \left(\nabla^2 u\right) w d\Omega = \int_{\Gamma_2} q w d\Gamma - \int_{\Gamma_2} \bar{q} w d\Gamma + \int_{\Gamma_1} \bar{u} \frac{dw}{dn} d\Gamma - \int_{\Gamma_1} u \frac{dw}{dn} d\Gamma. \tag{3.5.2}$$

Continue by integrating the left-hand side by parts. Assume that Ω is a volume hence $d\Omega = dxdydz$, which means that the boundaries Γ are actually surfaces. For a small element of surface, the x axis can be rotated into the outward normal

direction to the surface. If integration is carried out in the x direction and the rotational invariance of the Laplacian exploited, the following is obtained

$$\int_\Omega \left(\frac{d^2u}{dx^2}\right) w d\Omega = \int_{\Gamma_1+\Gamma_2} q w dy dz - \int_\Omega \frac{du}{dx}\frac{dw}{dx} d\Omega$$

which allows 3.5.2 to be written as

$$-\int_\Omega \frac{du}{dx}\frac{dw}{dx} d\Omega = -\int_{\Gamma_1} q w d\Gamma - \int_{\Gamma_2} \bar{q} w d\Gamma + \int_{\Gamma_1} \bar{u}\frac{dw}{dx} d\Gamma - \int_{\Gamma_1} u\frac{dw}{dx} d\Gamma \quad (3.5.3)$$

where $d\Gamma = dydz$. Again integrate the left-hand side by parts with respect to x to give

$$\int_\Omega u\frac{d^2w}{dx^2} d\Omega - \int_{\Gamma_1+\Gamma_2} u\frac{dw}{dx} d\Gamma = -\int_{\Gamma_1} q w d\Gamma - \int_{\Gamma_2} \bar{q} w d\Gamma +$$
$$\int_{\Gamma_1} \bar{u}\frac{dw}{dx} d\Gamma - \int_{\Gamma_1} u\frac{dw}{dx} d\Gamma. \quad (3.5.4)$$

As a consequence of the rotational invariance of the Laplacian, similar integrations can be performed in the y and z directions. Hence generalising the above integration to three dimensions, the equation obtained is

$$\int_\Omega u\nabla^2 w d\Omega = -\int_{\Gamma_1} q w d\Gamma - \int_{\Gamma_2} \bar{q} w d\Gamma + \int_{\Gamma_1} \bar{u}\frac{dw}{dn} d\Gamma + \int_{\Gamma_2} u\frac{dw}{dn} d\Gamma. \quad (3.5.5)$$

This equation is regarded as the starting point for the boundary element method.

The derivation of the method continues by addressing the issue of the weighting function. This function must be such that it provides the correct emphasis on each of the contributions to the total discrepancy in eqn (3.5.1). One method of choosing a good weighting function is to use the distributive properties of a solution to a more fundamental problem which shares the same characteristics to the one considered here. This solution is referred to as the fundamental solution. One example of a fundamental problem with the same characteristics is that of there being a concentrated charge acting at a point i within the domain. In this problem the governing equation is

$$\nabla^2 w + \delta^i = 0 \quad (3.5.6)$$

where δ^i is a Dirac Delta function with the property that

$$\int_\Omega u \left(\nabla^2 w + \delta^i\right) d\Omega = \int_\Omega u\nabla^2 w d\Omega + u^i$$

and u^i represents the value of the unknown function u at the point of application of the charge. With eqn (3.5.6) satisfied by the fundamental solution which is the weighting function in the main problem, then eqn (3.5.5) becomes

$$u^i + \int_{\Gamma_2} u\frac{dw}{dn}d\Gamma + \int_{\Gamma_1} \bar{u}\frac{dw}{dn}d\Gamma = \int_{\Gamma_1} qwd\Gamma + \int_{\Gamma_2} \bar{q}wd\Gamma \qquad (3.5.7)$$

or

$$u^i + \int_{\Gamma_2} uq^*d\Gamma + \int_{\Gamma_1} \bar{u}q^*d\Gamma = \int_{\Gamma_1} qwd\Gamma + \int_{\Gamma_2} \bar{q}wd\Gamma \qquad (3.5.8)$$

where $q^* = \frac{dw}{dn}$.

It can be shown that for an isotropic, three dimensional medium, the fundamental solution of eqn (3.5.6) is [43, 44]

$$w = \frac{1}{4\pi R}.$$

For details on this choice, see appendix B

The problem with eqn (3.5.8) is that whilst it is valid for any point in the domain, it can not qualify as a boundary element method as it does not depend on values at the boundary alone since u^i is a potential at an interior point. Hence this equation needs to be modified so that it has no dependence on interior points and this is done by taking the potential at an interior point to the boundary.

Consider the following hemisphere on the boundary of the three dimensional domain. The boundary point is assumed to be at the centre of the sphere placing
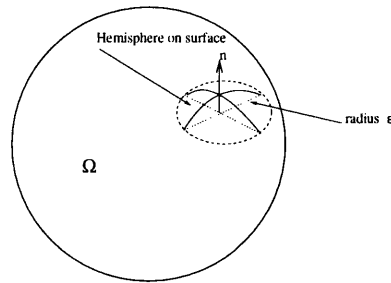
Figure 3.2: Hemisphere on the boundary of a three dimensional domain

it in a volume which will be reduced back down to the boundary by letting the radius of the sphere ϵ tend to zero. For the sake of the following argument, let the boundary be smooth and the point be on the boundary Γ_2 (note that a similar argument exists for Γ_1). Consider that the Γ_2 boundary is split into two parts, one which is excluded from the hemisphere $\Gamma_{2-\epsilon}$ and one which is the hemisphere Γ_ϵ, so

$$\int_{\Gamma_2} u \frac{dw}{dn} d\Gamma = \int_{\Gamma_{2-\epsilon}} u \frac{dw}{dn} d\Gamma + \int_{\Gamma_\epsilon} u \frac{dw}{dn} d\Gamma. \tag{3.5.9}$$

Now substitute the weighting function into the second integral on the right-hand side of the equation and take the limit as ϵ tends to zero

$$\lim_{\epsilon \to 0} \left\{ \int_{\Gamma_\epsilon} u \frac{dw}{dn} d\Gamma \right\} = \lim_{\epsilon \to 0} \left\{ -\int_{\Gamma_\epsilon} u \frac{1}{4\pi\epsilon^2} d\Gamma \right\}$$
$$= -\frac{1}{2} u \tag{3.5.10}$$

Note that as ϵ is now zero, the boundary $\Gamma_{2-\epsilon}$ again becomes Γ_2. This argument can be introduced on the right-hand side of eqn (3.5.8) but for this case, the limit takes the values to zero leading to no new terms. Substituting 3.5.10 into 3.5.8

$$\frac{1}{2} u^i + \int_{\Gamma_2} u q^* d\Gamma + \int_{\Gamma_1} \bar{u} q^* d\Gamma = \int_{\Gamma_1} q w d\Gamma + \int_{\Gamma_2} \bar{q} w d\Gamma \tag{3.5.11}$$

which can be written as

$$\frac{1}{2} u^i + \int_\Gamma u q^* d\Gamma = \int_\Gamma q w d\Gamma \tag{3.5.12}$$

where $\Gamma = \Gamma_1 + \Gamma_2$ and it is assumed that $u = \bar{u}$ on Γ_1 and $q = \bar{q}$ on Γ_2.

This equation now applies on the boundary and hence it is time to consider how the boundary will be discretized. To simplify matters, only the two dimensional case is considered and each element of the boundary is thought of as being a straight line between successive points on the boundary and has the constant value of the function u or q evaluated at a node in the centre of the element, see figure 3.3 (this is known as constant elements). There are other types of elements which could be used such as linear elements and quadratic elements where the unknown variable varies linearly and quadratically respectively [6, 39, 43]. These other choices of elements have been shown to improve accuracy but it was felt

that these improvements in accuracy could be matched using the simpler constant elements by refining the mesh. As explained later in chapter 4, for a three dimensional domain the discretising elements will be constant triangular ones.
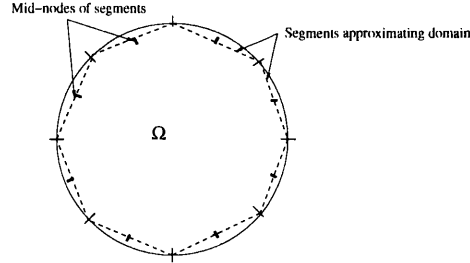
Figure 3.3: Discretisation of the domain

Eqn 3.5.12 will now be applied on the boundary of this domain. Suppose that the boundary has been discretized into n elements, where n_1 belong to Γ_1 and n_2 belong to Γ_2. Hence equation 3.5.12 can be written in discretized form as

$$\frac{1}{2}u^i + \sum_{j=1}^{n} u_j \int_{\Gamma_j} q^* d\Gamma = \sum_{j=1}^{n} q_j \int_{\Gamma_j} w d\Gamma \qquad (3.5.13)$$

where this equation applies for a particular node at the centre of element i.

The terms

$$\int_{\Gamma_j} q^* d\Gamma \qquad (3.5.14)$$

relate the node i with the element j over which the integral is carried out. These integrals will be denote $\hat{H}_{ij}$ whilst the integral on the right-hand side shall be denoted G_{ij}. So the equation becomes

$$\frac{1}{2}u^i + \sum_{j=1}^{n} u_j \hat{H}_{ij} = \sum_{j=1}^{n} q_j G_{ij}. \qquad (3.5.15)$$

This equation relates the value of u at a mid-node i with the value of u and q at all nodes on the boundary including i.

Although the choice of constant elements makes the required integrals easier to calculate, they still need to be calculated numerically and the method used is covered in the following chapter. However, the integrals over the loaded elements which are those integrals over elements which are also the source elements, i.e.

$\hat{H}_{ii}$, may be evaluated analytically but again this will be covered in the following chapter.

It is clear from eqn (3.5.15), that if the equation for each i node is written out in full, there will be n equations. Introducing the new notation

$$H_{ij} = \begin{cases} \hat{H}_{ij}, & \text{when } i \neq j, \\ \hat{H}_{ij} + \frac{1}{2}, & \text{when } i = j \end{cases} \tag{3.5.16}$$

eqn (3.5.15) may be written as

$$\sum_{j=1}^{n} H_{ij} u_j = \sum_{j=1}^{n} G_{ij} q_j \tag{3.5.17}$$

or in matrix notation

$$H\mathbf{u} = G\mathbf{q}. \tag{3.5.18}$$

It should be noted that n_1 values of u and n_2 values of q are known hence leaving a set of n unknowns in 3.5.18. This equation can thus be reordered so as all the unknowns are on the left-hand side, giving

$$A\mathbf{x} = \mathbf{b} \tag{3.5.19}$$

where $\mathbf{x}$ is the vector of unknown u and q values.

Solving either eqn (3.5.18) or eqn (3.5.19) (depending on the solving algorithm used, see chapter 5) the values of u and q will be known on the whole boundary, thus enabling the value of u to be calculated at any interior point using equation 3.5.8 which after discretisation becomes

$$u_i = \sum_{j=1}^{n} q_j G_{ij} - \sum_{j=1}^{n} u_j \hat{H}_{ij}. \tag{3.5.20}$$

Similarly the internal fluxes $q_x = \frac{\partial u}{\partial x}$ and $q_y = \frac{\partial u}{\partial y}$ can be calculated by differentiating 3.5.8 giving

$$(q_x)_i = \int_{\Gamma} q \frac{\partial w}{\partial x} d\Gamma - \int_{\Gamma} u \frac{\partial q^*}{\partial x} d\Gamma \tag{3.5.21}$$

$$(q_y)_i = \int_{\Gamma} q \frac{\partial w}{\partial y} d\Gamma - \int_{\Gamma} u \frac{\partial q^*}{\partial y} d\Gamma. \tag{3.5.22}$$

This has outlined how the boundary element method models the physical system but to form the equations which will model that of a corroding ship it is necessary to perform numerous numerical integrations of the type shown in eqn (3.5.14), which once the weighting function has been introduced become

$$G_{ij} = \int_{\Gamma_j} \frac{1}{4\pi R_{ij}} d\Gamma \text{ and } \hat{H}_{ij} = \int_{\Gamma_j} \frac{\partial}{\partial \mathbf{n}} \frac{1}{4\pi R_{ij}} \cdot d\Gamma. \tag{3.5.23}$$

The vast number of such integrations required means that the method used to perform them will have a critical role to play in the speed at which the overall method operates. There are many existing numerical methods available for performing such integrations but as shown in the following chapter, using constant triangular elements to discretise the boundary made it possible to use a new method which has some advantages over existing ones.

Chapter 4

Numerical Integration - A New Method.

4.1 Introduction

As shown in the proceeding chapter, the formation of the boundary element matrices which are required to describe the physical system require the evaluation of the integrals 4.1.1 and 4.1.2.

$$\int_{S_j} \frac{1}{4\pi} \frac{1}{R_{ij}} dS \tag{4.1.1}$$

$$\int_{S_j} \frac{\partial}{\partial \mathbf{n}} \left(\frac{1}{4\pi} \frac{1}{R_{ij}} \right) \cdot d\mathbf{S}. \tag{4.1.2}$$

where the integrals are over the surface of element j, $d\mathbf{S}$ is a infinitesimal surface element pointing normally out of the domain, and $\mathbf{R}_{ij}$ points from the source point i to the field element j. Removing the coefficients reduces these integrals to

$$\int_{S_j} \frac{1}{R_{ij}} dS \tag{4.1.3}$$

and

$$\int_{S_j} \frac{\partial}{\partial \mathbf{n}} \left(\frac{1}{R_{ij}} \right) \cdot d\mathbf{S}. \tag{4.1.4}$$

There are many existing methods used to numerically evaluate these integrals such as Gaussian Quadrature (Press et al.[45]) with the majority following similar

algorithms.

With most numerical methods, the accuracy is determined by the number of sub-domains into which the domain is separated (over each sub-domain, the integral is evaluated approximately and the resultant values summed for the whole domain) and obviously if more sub-domains are used then a higher level of accuracy is obtained but this costs more time. Hence a balance needs to be struck between the precision of the numerical integration and the time invested. This is an extremely important consideration for the BEM where there are a great number of integrals to be evaluated, meaning that a small compromise in the precision of the integrals can seriously damage the accuracy of the final solutions.

Therefore an alternative method for calculating the integrals was developed for which the accuracy does not depend on the number of sub-domains into which the domain is separated. This method was developed for triangular elements and is based round the formation of a polynomial from pre-calculated coefficients and the moments of the triangle, along with the subsequent differentiation of this polynomial. This new method was then implemented for a very simple test calculation and its accuracy compared to other more conventional methods.

4.2   Method of Moments

Consider the situation depicted in figure 4.2, which is the general case for all the non-diagonal elements of the boundary element matrices.
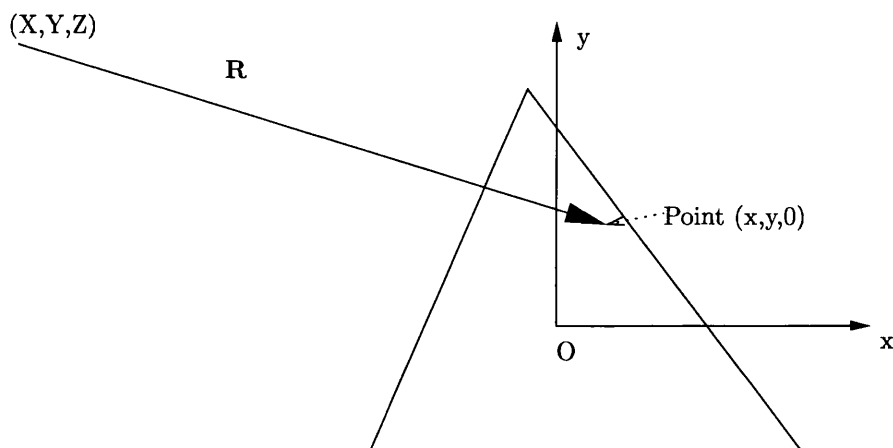
Figure 4.1: Shows the vector **R** pointing from a source point (X, Y, Z) to a field element with centroid at origin of a localised coordinate system.

A local coordinate system is implemented such that the triangular element lies on the xy plane, with the origin at its centroid and its base parallel to the x axis. The positive z direction is out from the volume contained within the boundary surface.

R denotes the distance from the point (X, Y, Z) on the boundary of the domain to $(x, y, 0)$ in the triangular element, i.e. $R = R(XYZ, xy)$. The point (X, Y, Z) is the centroid of one of the other surface elements where the potential is known and constant over the whole of that element. Thus the expression for $\frac{1}{R}$ can be written as a two dimensional Taylor Series expanded about the origin (i.e. a Maclaurin Series)

$$\frac{1}{R(XYZ, xy)} = \sum_{i=0}^{\infty} \frac{1}{i!} \left(x\frac{\partial}{\partial x_1} + y\frac{\partial}{\partial y_1} \right)^i \left(\frac{1}{R(XYZ, x_1 y_1)} \right) \qquad (4.2.1)$$

with the derivatives evaluated at $x_1 = y_1 = 0$.

It is possible to expand the differential operator further using the Binomial Theorem which allows eqn (4.2.1) to be written as

$$\frac{1}{R} = \sum_{i=0}^{\infty} \frac{1}{i!} \left(\sum_{r=0}^{i} \binom{i}{r} x^r y^{i-r} \frac{\partial^i}{\partial x_1^r \partial y_1^{i-r}} \right) \left(\frac{1}{R} \right) \qquad (4.2.2)$$

where the combinatorial number $\binom{i}{r}$ is the binomial coefficient, and can be thought of as the number of ways of picking 'r' unordered outcomes from 'i' possibilities. It should be noted that these coefficients can be calculated from

$$\binom{i}{r} = \frac{i!}{(i-r)!r!} \qquad (4.2.3)$$

At this point a simple, yet discrete, change of tack can result in greatly reducing the work required to form the matrices. Consider the matrix element G_{ij}, the element is evaluated using the integral

$$\int \frac{1}{R_{ij}} dS \qquad (4.2.4)$$

where 'i' is the source point $((X, Y, Z)$ above) and 'j' refers to the field element over which the integral is performed. At present the integrand depends on the field point and the source point. This means that for every element in the matrix,

the integral calculation needs to be performed in its entirety. If it was possible to separate the integrand into two functions, one which depends on the source point and one which depends on the field element, then calculating either a complete row or column would mean that for each matrix element, part of the integral would already be calculated which would save computation time.

To achieve this separation of variables, first notice that

$$\frac{\partial^{m+n}}{\partial x^m \partial y^n}\left(\frac{1}{R}\right) = (-1)^{m+n}\frac{\partial^{m+n}}{\partial X^m \partial Y^n}\left(\frac{1}{R}\right) \qquad (4.2.5)$$

so by including a factor -1^{m+n} into equation eqn (4.2.2), the differentiation can be performed with respect to X and Y rather than x and y.

Eqn (4.2.5) allows eqn (4.2.2) to be written as (see Appendix D for outline)

$$\frac{1}{R} = \sum_{m=0}^{\infty}\sum_{n=0}^{\infty} x^m y^n \underbrace{\sum_{p=m\,mod2}^{m}\sum_{q=n\,mod2}^{n}}_{\text{Steps of 2}} A_{pq}^{mn}\left(\frac{X}{R}\right)^p\left(\frac{Y}{R}\right)^q\frac{1}{R^{m+n+1}}. \qquad (4.2.6)$$

The coefficients A_{pq}^{mn} contain all the signs, binomials, etc. for ease of computation, and are just constants.

A closer look at eqn (4.2.6) shows its variables have been separated as desired so that the second pair of summations effect only the coordinates of the source point (X, Y, Z) while the first pair of summations concern the variables of the element (x, y). The coefficients A_{pq}^{mn} are dependent on the m, n, p, and q only and hence can be calculated in advance and referred to for each individual calculation. If the matrices are calculated column-wise the source point changes but the field element remains constant. Writing eqn (4.2.6) as

$$\frac{1}{R} = \sum_{m=0}^{\infty}\sum_{n=0}^{\infty} x^m y^n \mathcal{R}^{mn} \qquad (4.2.7)$$

this means that for each element in the column, only the $\mathcal{R}^{mn}$ factor changes (since R goes from (X, Y, Z) to the origin). Hence the integral becomes

$$\int \frac{1}{R}dS = \sum_{m=0}^{\infty}\sum_{n=0}^{\infty}\left(\int x^m y^n dS\right)\mathcal{R}^{mn} \qquad (4.2.8)$$

where $\int x^m y^n dS$ is the m, n^{th} moment and may be written as

$$\int x^m y^n dS = X^{m+1} Y^{n+1} M_{mn}(\alpha) \qquad (4.2.9)$$

where X and Y have been redefined to denote half the base and $\frac{2}{3}$ of the height from the base to the highest vertex respectively. $M_{mn}(\alpha)$ is a number with a dependence on the shape of the element denoted by the unique shape parameter α and is called the m, n^{th} normalised moment.

Therefore, for a column, the required m, n^{th} moments can be calculated for all elements in the column and then simply referred to for all the elements to form the required polynomials to evaluate the integrals (the $\mathcal{R}^{mn}$ factor is the variable since for a column the field element remains the same, i.e. the x and y variables apply to the same surface for each column element).

4.3 Properties of the Coefficients

As stated above, it is known that

$$\frac{\partial^{m+n}}{\partial x^m \partial y^n}\left(\frac{1}{R}\right) = (-1)^{m+n} \frac{\partial^{m+n}}{\partial X^m \partial Y^n}\left(\frac{1}{R}\right) \qquad (4.3.1)$$

whilst appendix D shows that the effect of the partial differentiation on the $\frac{1}{R}$ function is to alter its power in steps of two. If the order of the differentiation is '$m+n$' (i.e. m partial derivatives with respect to X and n partial derivatives with respect to Y), then the highest power of $\frac{1}{R}$ will be '$m+n+1$' whilst the smallest will be either 0 or 1, depending on the values of $m mod 2$ and $n mod 2$.

Adopting the following notation for these partial derivatives

$$D(m,n) = \frac{\partial^{m+n}}{\partial X^m \partial Y^n}\left(\frac{1}{R}\right) \tag{4.3.2}$$

$$= \underbrace{\sum_{p=0,1}^{m}\sum_{q=0,1}^{n}}_{\text{Steps of 2}} A_{pq}^{mn}\frac{X^p Y^q}{R^{m+n+1+p+q}} \tag{4.3.3}$$

$$= \frac{1}{R^{m+n+1}}\underbrace{\sum_{p=0,1}^{m}\sum_{q=0,1}^{n}}_{\text{Steps of 2}} A_{pq}^{mn}\left(\frac{X}{R}\right)^p\left(\frac{Y}{R}\right)^q \tag{4.3.4}$$

it can be shown that

$$D(m+1,n) = \frac{\partial}{\partial X}\left(\underbrace{\sum_{p=0,1}^{m}\sum_{q=0,1}^{n}}_{\text{Steps of 2}} A_{pq}^{mn}\frac{X^p Y^q}{R^{m+n+1+p+q}}\right) \tag{4.3.5}$$

$$= \underbrace{\sum_{p=0,1}^{m}\sum_{q=0,1}^{n}}_{\text{Steps of 2}} A_{pq}^{mn}\left(\frac{pX^{p-1}Y^q}{R^{m+n+1+p+q}}\right) \tag{4.3.6}$$

$$-(m+n+p+q+1)\frac{X^{p+1}Y^q}{R^{m+n+1+p+q+2}}\bigg)$$

$$D(m+1,n) = \frac{1}{R^{m+n+2}} \underbrace{\sum_{p=0,1}^{m} \sum_{q=0,1}^{n}}_{\text{Steps of 2}} A_{pq}^{mn} \left[p \left(\frac{X}{R}\right)^{p-1} \left(\frac{Y}{R}\right)^{q} \right. \tag{4.3.7}$$

$$\left. -(m+n+p+q+1) \left(\frac{X}{R}\right)^{p+1} \left(\frac{Y}{R}\right)^{q} \right]$$

$$= \frac{1}{R^{m+n+2}} \underbrace{\sum_{p=0,1}^{m} \sum_{q=0,1}^{n}}_{\text{Steps of 2}} A_{p-1q}^{m+1n} \left(\frac{X}{R}\right)^{p-1} \left(\frac{Y}{R}\right)^{q} \tag{4.3.8}$$

$$-A_{p+1q}^{m+1n} \left(\frac{X}{R}\right)^{p+1} \left(\frac{Y}{R}\right)^{q}.$$

Although this does not actually provide the values of the coefficients it does indicate one of the key properties that they must have, namely that differentiation by a variable results in two terms, one of which has the power of the variable over R term increased by 1, whilst the other has the power reduced by one. Again this agrees with the stepping increment of 2.

4.4 Derivative of $\frac{1}{R}$ with Respect to n.

For the elements of the H matrix, it is necessary to perform the integration of the function

$$\frac{\partial}{\partial \mathbf{n}} \left(\frac{1}{R}\right). \tag{4.4.1}$$

By adopting the notation for the $\frac{1}{R}$ shown in eqn (4.2.6), this differentiation will only effect the terms after the p and q summations.

Further, having adopted the local coordinate system described above, the outward normal to the element $\mathbf{n}$ has become the vector in the positive z direction, i.e.

$$\frac{\partial}{\partial \mathbf{n}} \left(\frac{1}{R}\right)_{z=0} = \frac{\partial}{\partial z} \left(\frac{1}{R}\right)_{z=0} = -\frac{\partial}{\partial Z} \left(\frac{1}{R}\right)_{z=0}. \tag{4.4.2}$$

Applying this to the partial derivatives of $\frac{1}{R}$ required to form the matrices

$$-\frac{\partial}{\partial Z}\left[\frac{\partial^{m+n}}{\partial X^m \partial Y^n}\left(\frac{1}{R}\right)\right] = -\frac{\partial}{\partial Z}\left(\sum_p \sum_q A_{pq}^{mn}\frac{X^p Y^q}{R^{m+n+p+q+1}}\right) \quad (4.4.3)$$

$$= \sum_p \sum_q A_{pq}^{mn}\frac{X^p Y^q z}{R^{m+n+p+q+3}} \times$$

$$(m+n+p+q+1) \quad (4.4.4)$$

$$= \frac{z}{R^{m+n+3}}\sum_p \sum_q (m+n+p+q+1) \times$$

$$A_{pq}^{mn}\left(\frac{X}{R}\right)^p \left(\frac{Y}{R}\right)^q \quad (4.4.5)$$

There is no effect on the $\frac{X}{R}$ and $\frac{Y}{R}$ terms, and hence the constant coefficient A_{pq}^{mn} need not be recalculated, only multiplied by a number. By acknowledging this, the rest of the discussion will focus on the integral of $\frac{1}{R}$ with the integral for $\frac{\partial}{\partial n}\left(\frac{1}{R}\right)$ being calculated by the multiplication by the factors indicated above.

4.5   Normalised Moments

4.5.1   Construction of a General Element

Before the calculation of the normalised moments are considered, it is first necessary to determine all the useful information about a general element in the model.

Consider the element shown in figure 4.2 whose construction was as follows. The origin was taken to be at the centroid and the base parallel to the x axis.
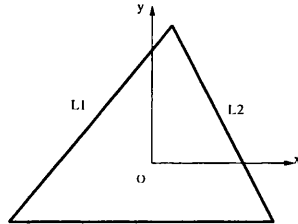
Figure 4.2: A basic triangular element

The top vertex has $y = Y$ whilst the base is at $y = -\frac{Y}{2}$. The length of the base was taken as $2X$ so that the sides L1 and L2 cut the x axis at $x = \pm\frac{2}{3}X$. Using

these values it is possible to say that the equation of line L1 is $x = py - \frac{2}{3}X$ where p is the tangent of the angle L1 makes with the y axis.

With reference to figure 4.3, the following can now be deduced about the vertexes and equations of the sides.
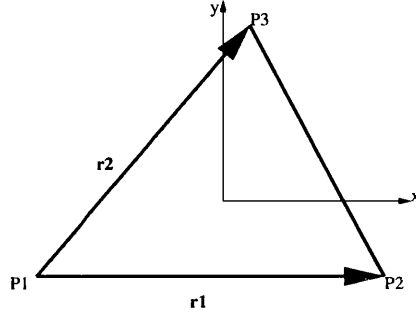
Figure 4.3: A more detailed description of the element

For vertex P3, $y_3 = Y$ whilst it follows that $x_3 = pY - \frac{2}{3}X$. As for P1, $y_1 = -\frac{Y}{2}$ while $x_1 = -p\frac{Y}{2} - \frac{2}{3}X$. To calculate the coordinates for P2, it is necessary to first obtain an equation for the line L2 in figure 4.2. By using the common point of P3 and the known intercept with the x axis, the equation for L2 can be shown to be $x = \left(p - \frac{4}{3}\frac{X}{Y}\right)y + \frac{2}{3}X$. Thus it is possible to say that $y_2 = -\frac{Y}{2}$ while $x_2 = \frac{4}{3}X - p\frac{Y}{2}$.

So in summary, $X = \frac{1}{2}(x_2 - x_1)$, $Y = y_3$, and $p = \frac{x_3 - x_1}{\frac{(3Y)}{2}}$. This means that a variable α, which describes the shape of the triangle, can be expressed as

$$\alpha = \frac{pY}{X} = \frac{4}{3}\frac{\mathbf{r1} \cdot \mathbf{r3}}{\mathbf{r1}^2}.$$

It is also possible to write the equations for the lines L1 and L2 in dimensionless form

$$L1 : x = py - \frac{2}{3}X \implies \frac{x}{X} = \left(p\frac{Y}{X}\right)\frac{y}{Y} - \frac{2}{3}$$

$$L2 : x = \left(p - \frac{4}{3}\frac{X}{Y}\right) + \frac{2}{3}X \implies \frac{x}{X} = \left(p\frac{Y}{X} - \frac{4}{3}\right)\frac{y}{Y} + \frac{2}{3}.$$

By defining the dimensionless variables $\zeta = \frac{x}{X}$ and $\eta = \frac{y}{Y}$ these equations can be expressed as

$$L1 : \zeta = \alpha\eta - \frac{2}{3} \tag{4.5.1}$$

$$L2 : \zeta = \left(\alpha - \frac{4}{3}\right)\eta + \frac{2}{3}. \qquad (4.5.2)$$

4.6 Properties of the Moments

4.6.1 Calculation of $M_{mn}(\alpha)$ Recursively

Employing the information obtained from figures 4.2 and 4.3, the calculation of the m, n^{th} moment of a triangle can now be attempted. If eqn (4.5.1) and eqn (4.5.2) are used to describe L1 and L2, the calculation of the moments become

$$\int x^m y^n ds = X^{m+1} Y^{n+1} \int_{-\frac{1}{2}}^{1} \eta^n d\eta \int_{L1}^{L2} \zeta^m d\zeta \qquad (4.6.1)$$

$$= X^{m+1} Y^{n+1} \int_{-\frac{1}{2}}^{1} \eta^n \left[\left(\left(\alpha - \frac{4}{3}\right)\eta + \frac{2}{3}\right)^{m+1} \qquad (4.6.2)\right.$$

$$\left. - \left(\alpha\eta - \frac{2}{3}\right)^{m+1}\right] \frac{1}{(m+1)} d\eta$$

$$= X^{m+1} Y^{n+1} M_{m,n}(\alpha) \qquad (4.6.3)$$

where again it should be noted that $M_{m,n}(\alpha)$ depends only on the shape of the triangle, i.e

$$M_{mn}(\alpha) = \frac{1}{m+1} \int_{-\frac{1}{2}}^{1} \eta^n \left[\left(\left(\alpha - \frac{4}{3}\right)\eta + \frac{2}{3}\right)^{m+1} - \left(\alpha\eta - \frac{2}{3}\right)^{m+1}\right] d\eta \quad (4.6.4)$$

By adopting the notation that

$$J_{mn}(\beta) = \int_{-\frac{1}{2}}^{1} \eta^n \left(\beta\eta + \frac{2}{3}\right)^m d\eta$$

the expression for the normalised moment M_{mn} may be written as

$$M_{mn}(\alpha) = \frac{1}{m+1}\left[J_{m+1n}\left(\alpha - \frac{4}{3}\right) + (-1)^m J_{m+1n}(-\alpha)\right] \qquad (4.6.5)$$

The reason behind introducing this new function J is that it can be calculated

recursively, as shown below

$$J_{mn}(\beta) = \int_{-\frac{1}{2}}^{1} \eta^n \left(\beta\eta + \frac{2}{3}\right)^{m-1} \left(\beta\eta + \frac{2}{3}\right) d\eta \qquad (4.6.6)$$

$$= \beta J_{m-1n+1}(\beta) + \frac{2}{3} J_{m-1n}(\beta) \qquad (4.6.7)$$

$$J_{0n}(\beta) = \frac{1}{n+1}\left[1 - \left(-\frac{1}{2}\right)^{n+1}\right]. \qquad (4.6.8)$$

This indicates that it will be possible to calculate J_{mn} without performing an integral explicitly if J_{m-1n+1} and J_{m-1n} are known. Hence if J_{0n} is calculated up to a large enough 'n' value, it is possible to calculate all J_{mn} without performing a single integration.

Leaving the J_{mn} notation for a moment, there are various other properties that can be predicted about the normalised moments of an element.

4.6.2 $M_{mn}(\alpha)$ when m and n are Zero

Firstly, it is possible to calculate the $0,0^{th}$ normalised moment since the $0,0^{th}$ moment is equal to $XYM_{00}(\alpha)$ and is by definition the area of the element, i.e.

$$Area = \frac{1}{2} base \times height \qquad (4.6.9)$$

$$= \frac{1}{2}(2X) \times \left(\frac{3}{2}Y\right) \qquad (4.6.10)$$

$$= \frac{3}{2}XY \qquad (4.6.11)$$

$$Therefore\ M_{00}(\alpha) = \frac{3}{2}. \qquad (4.6.12)$$

Following on from this, because the origin is at the centre of mass, the first moments in m and n are given by

$$M_{01} = 0 \qquad (4.6.13)$$

$$M_{10} = 0. \qquad (4.6.14)$$

These values are shown in appendix E to be true.

By setting $m = 0$ in eqn (4.6.4), an expression for $M_{0n}(\alpha)$ may be obtained.

As indicated by eqn (4.6.7), it should be possible to compute all the required moments from this expression.

$$M_{0n}(\alpha) = \int_{-\frac{1}{2}}^{1} \eta^n d\eta \left[\left(\left(\alpha - \frac{4}{3} \right) \eta + \frac{2}{3} \right) - \left(\alpha\eta - \frac{2}{3} \right) \right] \quad (4.6.15)$$

$$= \frac{4}{3} \int_{-\frac{2}{3}}^{1} \eta^n (1 - \eta) \, d\eta \quad (4.6.16)$$

$$= \frac{4}{3(n+1)(n+2)} \left[1 + (3n+5) \left(-\frac{1}{2} \right)^{n+2} \right] \quad (4.6.17)$$

Note that this is independent of the shape parameter of the element α. In physical terms, the distribution of mass is similarly distributed about the x-axis whatever the shape of the triangle.

Having obtained an expression for $M_{0n}(\alpha)$ it would seem logical to try and obtain and expression for $M_{m0}(\alpha)$. Beginning from eqn (4.6.4),

$$M_{m0}(\alpha) = \frac{1}{m+1} \int_{-\frac{1}{2}}^{1} \left[\left(\left(\alpha - \frac{4}{3} \right) \eta + \frac{2}{3} \right)^{m+1} \right.$$
$$\left. - \left(\alpha\eta - \frac{2}{3} \right)^{m+1} \right] d\eta \quad (4.6.18)$$

$$= \frac{1}{(m+1)(m+2)} \left[\frac{4 \left(\alpha - \frac{2}{3} \right)^{m+2}}{3\alpha \left(\alpha - \frac{4}{3} \right)} \right.$$
$$\left. + \left(-\frac{1}{2} \right)^{m+2} \left[-\frac{\left(\alpha - \frac{8}{3} \right)^{m+2}}{\alpha - \frac{4}{3}} + \frac{\left(\alpha + \frac{4}{3} \right)^{m+2}}{\alpha} \right] \right] \quad (4.6.19)$$

$$= \frac{1}{(m+1)(m+2)\alpha \left(\alpha - \frac{4}{3} \right)} \left[\frac{4}{3} \left(\alpha - \frac{2}{3} \right)^{m+2} + \left(-\frac{1}{2} \right)^{m+2} \times \right.$$
$$\left. \left[\left(\alpha - \frac{4}{3} \right) \left(\alpha + \frac{4}{3} \right)^{m+2} - \alpha \left(\alpha - \frac{8}{3} \right)^{m+2} \right] \right] . \quad (4.6.20)$$

4.6.3 Differentiating the Normalised Moments

Consider the effect of differentiating the m, n^{th} normalised moment with respect to α, using eqn (4.6.4)

$$\frac{d}{d\alpha} M_{mn}(\alpha) = \int_{-\frac{1}{2}}^{1} \eta^{n+1} \left[\left[\left(\alpha - \frac{4}{3} \right) \eta + \frac{2}{3} \right]^{m} - \left[\alpha\eta - \frac{2}{3} \right]^{m} \right] d\eta \quad (4.6.21)$$

$$= m M_{m-1n+1}. \quad (4.6.22)$$

In particular this means

$$\frac{d^n}{d\alpha^n} M_{m+n0} = \frac{(m+n)!}{m!} M_{mn} \quad (4.6.23)$$

so that it is possible to calculate the m, n^{th} normalised moment by differentiating the $m + n, 0^{th}$ normalised moment, i.e.

$$M_{mn} = \frac{m!}{(m+n)!} \frac{d^n}{d\alpha^n} M_{m+n0}. \quad (4.6.24)$$

Further this result indicates the form of M_{m0}. Since M_{0m} is independent of the shape parameter α, and is also non zero, this result says

$$M_{0m} = \frac{m!}{m!} \frac{d^m}{d\alpha^m} M_{m0} \quad (4.6.25)$$

from which it follows that M_{m0} is a polynomial in α of degree m.

4.6.4 Changing the Variable

By changing the variable $\alpha \to \beta = \frac{4}{3} - \alpha$, the effect on the normalised moments is that

$$M_{mn}(\beta) = (-1)^{m} M_{mn}(\alpha). \quad (4.6.26)$$

Also if a variable β is introduced such that $\beta = \frac{3}{4}\alpha$, or $\beta = p\frac{height}{base}$, the $m,0^{th}$ moment of β from eqn (4.6.20) is

$$
\begin{aligned}
M_{m0}\left(\beta\right) & = \frac{1}{\left(m+1\right)\left(m+2\right)\frac{4}{3}\beta\frac{4}{3}\left(\beta-1\right)}\left[\frac{4}{3}\left(\frac{2}{3}\right)^{m+2}\left(2\beta-1\right)^{m+2}\right. \\
& \quad + \left(-\frac{1}{2}\right)^{m+2}\left(\frac{4}{3}\right)^{m+3}\left[\left(\beta-1\right)\left(\beta+1\right)^{m+2}\right. \\
& \quad \left.\left.-\beta\left(\beta-2\right)^{m+2}\right]\right] \hspace{2cm} (4.6.27) \\
& = \frac{1}{\left(m+1\right)\left(m+2\right)\beta\left(\beta-1\right)}\frac{\left(\frac{3}{4}\right)^{2}}{}\left(\frac{2}{3}\right)^{m+3}\left[2\left(2\beta-1\right)^{m+2}+\right. \\
& \quad \left. + \left(-1\right)^{m+2}2\left(\left(\beta-1\right)\left(\beta+1\right)^{m+2}-\beta\left(\beta-2\right)^{m+2}\right)\right]. \hspace{0.5cm} (4.6.28)
\end{aligned}
$$

Alternatively using the integral notation from eqn (4.6.18)

$$
\begin{aligned}
M_{m0}\left(\beta\right) & = \frac{1}{m+1}\int_{-\frac{1}{2}}^{1}\left[\left(\left(\frac{4}{3}\beta-\frac{4}{3}\right)\eta+\frac{2}{3}\right)^{m+1}\right. \\
& \quad \left.-\left(\frac{4}{3}\beta-\frac{2}{3}\right)^{m+1}\right]d\eta \hspace{2cm} (4.6.29) \\
& = \frac{1}{m+1}\left(\frac{2}{3}\right)^{m+1}\sum_{r=0}^{m+1}\binom{m+1}{r}\left[\left(2\left(\beta-1\right)\right)^{r}-\left(-1\right)^{m+1-r}\left(2\beta\right)^{r}\right] \\
& \quad \times \int_{-\frac{1}{2}}^{1}\eta^{r}d\eta \hspace{3cm} (4.6.30) \\
& = \frac{1}{m+1}\left(\frac{2}{3}\right)^{m+1}\sum_{r=0}^{m+1}\binom{m+1}{r}2^{r}\left[\left(\beta-1\right)^{r}-\left(-1\right)^{m+1-r}\beta^{r}\right] \\
& \quad \times \frac{1}{r+1}\left(1-\left(-\frac{1}{2}\right)^{r+1}\right). \hspace{2cm} (4.6.31)
\end{aligned}
$$

This is an explicit non-recursive constructive algorithm for calculating the M_{m0}.

4.6.5 Normalised Moments of an Isosceles Triangle

Consider the special case of an isosceles triangle as depicted in figure 4.4. Using the notation and set up as described in section 4.5.1, the variable values for this isosceles triangle of height 'h' are
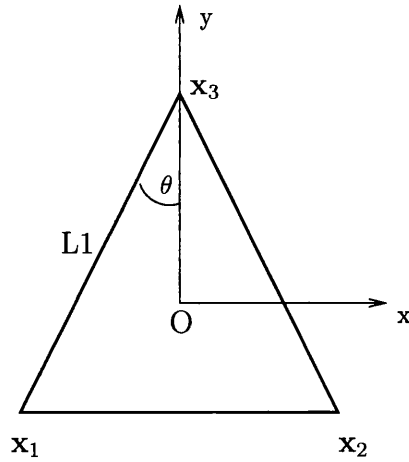
Figure 4.4: The special case of an isosceles triangle.

- $p = \tan\theta$,

- $Y = \frac{2}{3}h$,

- $X = h\tan\theta$,

- $\alpha = p\frac{Y}{X} = \frac{2}{3}$.

Note that the value for α is *independent* of θ. So one set of normalised moments $M_{mn}(\alpha)$ is enough for *all* isosceles triangles.

Reverting back to the notation for M_{mn} involving the J_{mn} functions (eqn (4.6.5)), for an isosceles triangle

$$M_{mn}\left(\frac{2}{3}\right) = \frac{1}{m+1}\left[J_{m+1n}\left(-\frac{2}{3}\right) + (-1)^m J_{m+1n}\left(-\frac{2}{3}\right)\right] \qquad (4.6.32)$$

Clearly $M_{mn}\left(\frac{2}{3}\right) = 0$ if m is odd.

Assuming that m is even,

$$M_{m0}\left(\frac{2}{3}\right) = \frac{2}{m+1}\int_{-\frac{1}{2}}^{1}\left[\left(-\frac{2}{3}\right)\eta + \frac{2}{3}\right]^{m+1} d\eta \qquad (4.6.33)$$

$$= \frac{2}{(m+1)(m+2)}\left(-\frac{3}{2}\right)\left[\left(-\frac{2}{3}\eta + \frac{2}{3}\right)^{m+2}\right]_{-\frac{1}{2}}^{1} \qquad (4.6.34)$$

$$= \frac{-3}{(m+1)(m+2)}\left[-(1)^{m+2}\right] \qquad (4.6.35)$$

$$M_{m0}\left(\frac{2}{3}\right) = \frac{3}{(m+1)(m+2)} \text{ (m even).} \qquad (4.6.36)$$

Using the integral notation of eqn (4.6.15), the $0, n^{th}$ normalised moment is given by

$$M_{0n}\left(\frac{2}{3}\right) = \int_{-\frac{2}{3}}^{1}\eta^{n}\left[\left(-\frac{2}{3}\eta + \frac{2}{3}\right) - \left(\frac{2}{3}\eta - \frac{2}{3}\right)\right] d\eta \qquad (4.6.37)$$

$$= 2\int_{-\frac{2}{3}}^{1}\eta^{n}\left(-\frac{2}{3}\eta + \frac{2}{3}\right) d\eta \qquad (4.6.38)$$

$$= \frac{4}{3}\int_{-\frac{2}{3}}^{1}\left(\eta^{n} - \eta^{n-1}\right) d\eta \qquad (4.6.39)$$

$$M_{0n}\left(\frac{2}{3}\right) = \frac{4}{3(n+1)(n+2)}\left[1 + (3n+5)\left(-\frac{1}{2}\right)^{n+2}\right] \qquad (4.6.40)$$

which holds true for n even or odd.

4.7 The Problem of Convergence

The expression which has been derived for the integral may be written as

$$\int \frac{1}{R} dS = \frac{1}{R_0}\sum_{m,n}\left(\frac{X}{R_0}\right)^{m+1}\left(\frac{Y}{R_0}\right)^{n+1} M_{mn}(\alpha) D_{mn}(\mathbf{R}_0) \qquad (4.7.1)$$

where

- $\mathbf{R}_0$ is the vector from the origin O to the point P (see figure 4.5),

- X is half the base,

- Y is two-thirds of the height,

- D_{mn} ($\mathbf{R}_0$) are the derivative factors required,

- M_{mn} (α) are the normalised moments which are independent of scale.
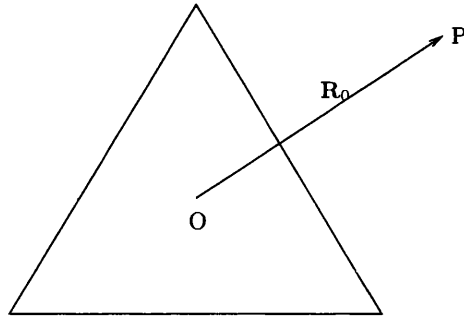
Figure 4.5: Outline of the convergence problem.

The series shown in eqn (4.7.1) will not be convergent if

$$\left|\frac{X}{R_0}\right| > 1 \text{ or } \left|\frac{Y}{R_0}\right| > 1. \tag{4.7.2}$$

When this is the case the problem is easily addressed. The triangular element is divided into 4 similar triangles by joining the midpoints of the sides. By similar it is meant that the corresponding angles are congruent while the lengths of corresponding sides are proportional [46]. This is shown in figure 4.6.
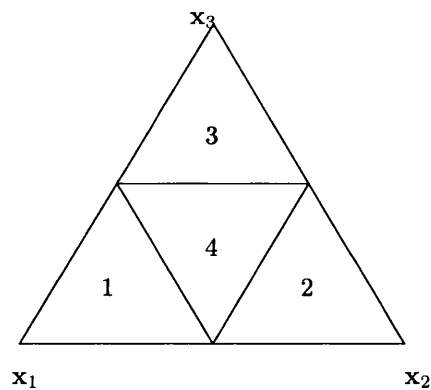
Figure 4.6: Subdivision of an element to satisfy convergence criteria.

For each of the sub-triangles, they are scaled version of the original element with

- $X \to \frac{X}{2}$,

- $Y \to \frac{Y}{2}$.

They have the same shape as the original and therefore have the same moments, except for sub-element 4, where due to the rotation through π radians

$$M_{mn}(\alpha) \to (-1)^{m+n} M_{mn}(\alpha). \tag{4.7.3}$$

If these sub-elements still do not satisfy the convergence criteria 4.7.2, they can again be sub-divided further using the same process. When this is programmed a simple recursive function can perform this task until convergence is assured.

4.8 Calculating $\int \frac{1}{R} dS$ for Diagonal Elements.

For the diagonal elements, it is possible to use a closed formula to calculate the integrals analytically. An arbitrary element is chosen with the potential being calculated at the centroid of the element (which is always located inside the element) and held constant over the entire element. This setup is commonly referred to as the element being loaded.

Consider the triangle shown on figure 4.7. Note that the origin has been positioned at a vertex which is *not* right-angled, the reason for this will be explained shortly. When performing the necessary surface integrals, the r integration will
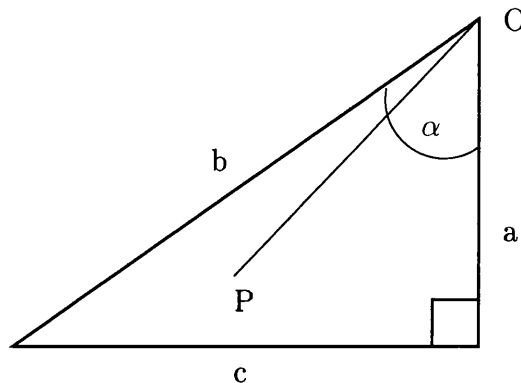
Figure 4.7: Integration over a right-angled, loaded element.

run from 0 to R where

$$R = \frac{a}{\cos \theta} \tag{4.8.1}$$

and the θ integration will be from 0 to α. Hence the required integral over the right-angled triangle may be written as

$$I = \int_\Delta \frac{1}{r} dS \;\; = \;\; \int_\Delta \frac{1}{r} r \, d\theta dr \qquad (4.8.2)$$

$$= \;\; \int_{\theta=0}^{\alpha} d\theta \int_{0}^{R} dr \qquad (4.8.3)$$

$$= \;\; a \int_{0}^{\alpha} \sec\theta d\theta \qquad (4.8.4)$$

$$= \;\; a \ln(\sec\alpha + \tan\alpha) \qquad (4.8.5)$$

$$= \;\; a \ln\left(\frac{1 + \sin\alpha}{\cos\alpha}\right) \qquad (4.8.6)$$

$$= \;\; a \ln\left(\frac{1 + \frac{c}{b}}{\frac{a}{b}}\right) \qquad (4.8.7)$$

Consider the variable of the logarithmic function

$$\frac{1 + \frac{c}{b}}{\frac{a}{b}} \;\; = \;\; \left(\frac{b+c}{a}\right)\frac{(a+b-c)}{(a+b-c)} \qquad (4.8.8)$$

$$= \;\; \frac{a(a+b+c)}{a(a+b-c)} \qquad (4.8.9)$$

$$= \;\; \frac{a+b+c}{a+b-c}. \qquad (4.8.10)$$

Therefore for a right-angled triangle

$$\int \frac{1}{r} dS = a \ln\left(\frac{a+b+c}{a+b-c}\right) \qquad (4.8.11)$$

Due to the sophisticated geometries of the hull and propeller it is unlikely that the elements will be right-angled hence it is necessary to have such a formula which may be applied to non-right-angled triangles. Consider figure 4.8, which depicts a non-right-angled triangle. The integration will be performed by dividing it into two right-angled triangles as shown.

The eqn (4.8.11) for a right-angled triangle can not be directly applied to the right-angled triangles in figure 4.8 since the lengths of the sides which add to give 'l' are unknown, although they are straightforward to calculate. Similarly, 'h' is not immediately known and will need to be evaluated. To avoid these computations, eqn (4.8.11) will be adapted to work directly on the triangle in
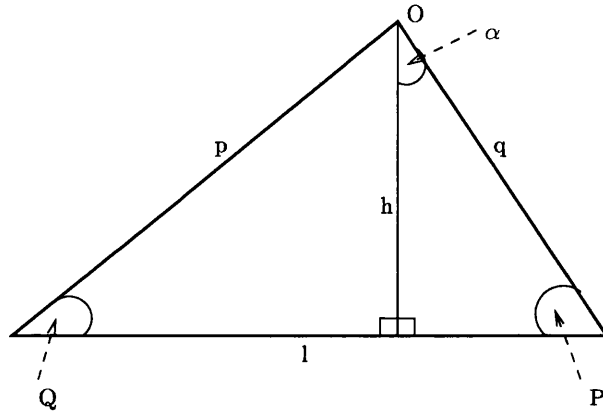
Figure 4.8: A non-right-angled triangle is divided into two right-angled triangles for the necessary integration.

figure 4.8 without the need for the separation into two right-angled triangles. Begin with equation 4.8.5, with reference to figure 4.8 it is possible to say

$$\sec \alpha + \tan \alpha \;=\; \frac{1 + \cos P}{\sin P} \tag{4.8.12}$$

$$=\; \frac{2 \cos^2 \frac{P}{2}}{2 \sin \frac{P}{2} \cos \frac{P}{2}} \tag{4.8.13}$$

$$=\; \cot \frac{P}{2}. \tag{4.8.14}$$

If a variable s is defined such that $s = \frac{1}{2}\left(p + q + l\right)$, then

$$\cot \frac{P}{2} = (s - p)\sqrt{\frac{s}{(s-p)(s-q)(s-l)}}. \tag{4.8.15}$$

A similar expression can be obtained for the other triangle in figure 4.8, i.e.

$$\cot \frac{Q}{2} = (s - q)\sqrt{\frac{s}{(s-p)(s-q)(s-l)}}. \tag{4.8.16}$$

These equations, 4.8.15 and 4.8.16, provide values to which the logarithmic function can be applied in the process of calculating the integrations over the two right-angled triangles in figure 4.8. These values are calculated directly from the known lengths of the sides. To complete the calculation of the integrals over either right-angled triangle, the side 'h' must be known. If the area of the whole triangle in figure 4.8 is 'A', then $h = \frac{2A}{l}$. Hence integration over the complete

triangle gives

$$\int \frac{1}{r_0} dS = h \ln \left(\cot \frac{P}{2} \right) + h \ln \left(\cot \frac{Q}{2} \right) \tag{4.8.17}$$

$$= h \ln \left(\cot \frac{P}{2} \cot \frac{Q}{2} \right) \tag{4.8.18}$$

$$= h \ln \left((s-p)(s-q) \frac{s}{(s-p)(s-q)(s-l)} \right) \tag{4.8.19}$$

$$= h \ln \left(\frac{s}{(s-l)} \right) \tag{4.8.20}$$

$$= \frac{2A}{l} \ln \left(\frac{p+q+l}{p+q-l} \right) \tag{4.8.21}$$

This formula can now be used to extend the required integration over any shape of triangle. However, the formula eqn (4.8.21) can not be applied immediately to an element. This formula relies on the origin being located at a vertex of the triangular element. In the calculation of the matrix elements, the coordinate system is transformed to a local system with the origin located at the centroid of the triangular element. Therefore to apply formula eqn (4.8.21), the element must be divided into three sub-elements as shown in figure 4.9, and the formula applied to each individual sub-element before summing the results to obtain a value for the integration over the main element.
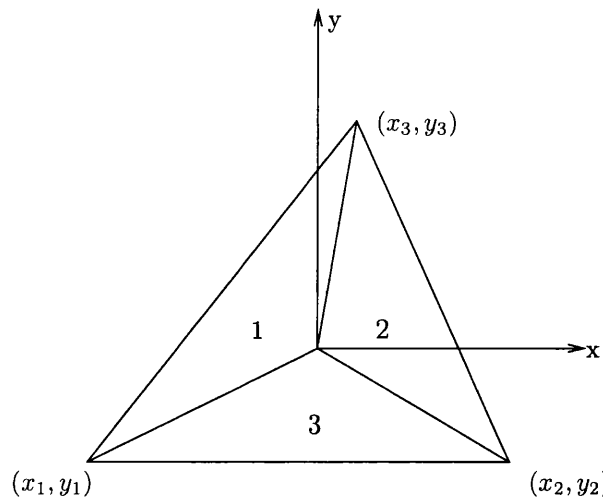
Figure 4.9: Division of a loaded element into three sub-elements to allow the integration to be performed.

4.9 Summary: Method of Moments

It is sensible to collect all that has been discussed previously into a short summary of how the method of moments can be used to calculate the required integrals before proceeding onto a test calculation.

In subsection 4.6.3, eqn (4.6.24) was discovered which meant that if the polynomial expression for $M_{m,0}(\alpha)$ is known for all values of m, simple differentiation will generate the required $M_{m-n,n}(\alpha)$ values.

Using eqn (4.6.18), the expression for $M_{m,0}(\alpha)$ may be written as

$$M_{m,0}(\alpha) = \int_{-\frac{1}{2}}^{1} \sum_{r=0}^{m} C_r^{(m)}(\eta)\, \alpha^r \, d\eta \qquad (4.9.1)$$

where the polynomial coefficients $C_r^{(m)}(\eta)$ depends on m, r, and η. The integration only effects these coefficients so eqn (4.9.1) may be written as

$$M_{m,0}(\alpha) = \sum_{r=0}^{m} \alpha^r d_r^{(m)} \text{ where } d_r^{(m)} = \int_{-\frac{1}{2}}^{1} C_r^{(m)}(\eta)\, d\eta. \qquad (4.9.2)$$

Writing this in a compact form produces

$$M_{m,0}(\alpha) = \frac{1}{(m+1)(m+2)} \frac{1}{\alpha\left(\alpha - \frac{4}{3}\right)} \left[\frac{4}{3}\left(\alpha - \frac{2}{3}\right)^{m+2} + \left(-\frac{1}{2}\right)^{m+2} \times \right.$$
$$\left. \left\{ \left(\alpha - \frac{4}{3}\right)\left(\alpha + \frac{4}{3}\right)^{m+2} - \alpha\left(\alpha - \frac{8}{3}\right)^{m+2} \right\} \right]. \quad (4.9.3)$$

It should be stressed that this form appears to have singularities, but is actually a finite polynomial of degree $m+1$. The coefficients of α, $d_r^{(m)}$, do not depend on the size nor shape of the triangular elements, therefore they may be calculated once and then referred to whenever an integration is required. Because $M_{m,0}(\alpha)$ is a finite polynomial, it is defined by the coefficients $d_r^{(m)}$ which may be stored in an array and used to obtain exact derivatives of any order for any value of α. This eliminates the requirement to perform time-consuming numerical integrations each time a matrix element is calculated. The required integrations can now be

calculated simply by forming a polynomial and then differentiating, i.e.

$$\int \frac{1}{R} ds = \sum_{m,n} \left\{ X^{m+1} Y^{n+1} \frac{m!}{(m+n)!} \frac{d^n}{d\alpha^n} \sum_{r=0}^{m+n} d_r^{(m+n)} \alpha^r \right\} \mathcal{R}^{m,n}. \qquad (4.9.4)$$

Differentiation with respect to the outward normal of the element, the positive z-direction in figure 4.2, will produce the other required integral for the H matrix.

4.10 Test Calculations

The method described above for calculating the necessary integrals to form the coefficient matrices of the BEM is quite unique and different from the more established methods on performing numerical integrations such as Gaussian Quadrature and Clenshaw-Curtis Method, therefore it was tested for accuracy against these methods.

The following problem was used to carry out the accuracy tests. Two tetrahedral of identical size were located inside an infinite domain. In the context of the overall problem of evaluating the electromagnetic signatures due to corrosion and its countermeasures on a ship, the tetrahedrons can be thought to represent the propeller and the hull in an infinite tank of sea water. A schematic of the problem is shown in figure 4.10.
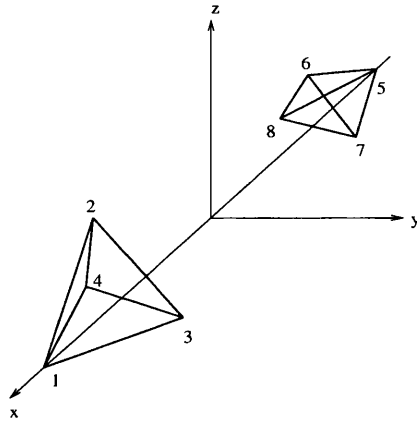
Figure 4.10: Outline of the tetrahedral example.

For tetrahedral of side one unit, the coordinates of the points and the formation of the triangular elements are shown in the following tables:

Vertex	x coord	y coord	z coord
1	A	0	0
2	$A-\sqrt{\frac{2}{3}}$	0	$\frac{1}{\sqrt{3}}$
3	$A-\sqrt{\frac{2}{3}}$	$\frac{1}{2}$	$-\frac{1}{2\sqrt{3}}$
4	$A-\sqrt{\frac{2}{3}}$	$-\frac{1}{2}$	$-\frac{1}{2\sqrt{3}}$
5	$-A$	0	0
6	$-\left(A-\sqrt{\frac{2}{3}}\right)$	0	$\frac{1}{\sqrt{3}}$
7	$-\left(A-\sqrt{\frac{2}{3}}\right)$	$\frac{1}{2}$	$-\frac{1}{2\sqrt{3}}$
8	$-\left(A-\sqrt{\frac{2}{3}}\right)$	$-\frac{1}{2}$	$-\frac{1}{2\sqrt{3}}$

Element	Vertex 1	Vertex 2	Vertex 3
1	1	2	3
2	1	3	4
3	1	4	2
4	2	3	4
5	5	7	6
6	5	8	7
7	5	6	8
8	6	7	8

It should be noted that the value of A in the x-coordinate specifies how far apart the tetrahedral are. This example has a very simple symmetry which can provide a quick indication on validity of the matrix elements that were produced by the method previously described. To simplify matters the integrals will only be calculated for the G matrix and constant factors will be neglected. In other words the integrals being examined are simply

$$\int_{\Gamma_j} \frac{1}{R_{i,j}} d\Gamma. \tag{4.10.1}$$

For the diagonal elements the integrals can be calculated via the analytic formula eqn (4.8.21) which is described above in section 4.8. Since this is an analytic formula, there should be no numerical discrepancy associated with these elements.

For the off-diagonal elements, it is possible to predict elements which should

have identical values using the symmetry. Since the values of integral 4.10.1 depend on the distance R between the field elements and the source points, all matrix elements which result from the relation between a source point and field element on the same tetrahedral should have the same value, thus

$$
\begin{aligned}
G_{1,2} &= G_{1,3} \\
&= G_{1,4} \\
&= G_{2,1} \\
&= \text{all pairs in left hand tetrahedral} \\
&= \text{all pairs in right hand tetrahedral.}
\end{aligned}
$$

For the same reason, the following equalities are also expected:

$$
\begin{aligned}
G_{1,5} &= G_{2,6} = G_{3,7} \\
G_{1,6} &= G_{1,7} = G_{2,5} = G_{2,7} = G_{3,5} = G_{3,6} \\
G_{1,8} &= G_{2,8} = G_{3,8} \\
G_{4,5} &= G_{4,6} = G_{4,7}
\end{aligned}
$$

whilst $G_{4,8} = G_{8,4}$ will have their own distinct value. In general, it can be said that

$$
G_{i+4,j-4} = G_{i,j}.
$$

which basically says that $G_{i,j} = G_{j,i}$.

Also it is possible to predict some inequalities, for example considering the relations between elements 1, 3, 4, 8, 5, and 6, the following inequalities can be predicted.

$$
G_{4,8} > G_{4,5} = G_{4,5} = G_{1,8} = G_{3,8} > G_{1,5} = G_{3,6} = G_{1,6} = G_{3,5}.
$$

To check these equalities and inequalities, the values for the integrals for the off-diagonal elements were calculated. As well as the method of moments which is being tested, the mathematical package Maple and the accepted numerical method of Gaussian Quadrature were used. The Gaussian Quadrature was performed by a simple ten point Gauss-Legendre integration, which was sufficient for these simple

elements to indicate whether the new method was providing satisfactory values. It is generally accepted that when the functions being integrated are known analytically, the Gaussian Quadrature methods are the best methods of integration since the sub-domains may be chosen so that the most accurate approximation is given. The method used by Maple was the Clenshaw-Curtis method which requires a n-th order Chebyschev polynomial approximation to the integral being integrated to give an approximation to the integral.

The following pages contain tables of results that were obtained for the integrals. Recall that matrix element $G_{i,j}$ refers to the ith element's centroid (the source point), labelled Pt in the table, and the jth element (the field element), labelled Elt. Therefore to check the value of the integral for $G_{1,2}$ the entry in the table is $Elt = 2$, $Pt = 1$.

Elt(j)	Pt(i)	Gaussian	Clenshaw	Moments
1	2	1.077816	1.07268	1.07268
1	3	1.077892	1.07268	1.07268
1	4	1.077767	1.07268	1.07268
1	5	0.022908	0.02289	0.02289
1	6	0.022904	0.02289	0.02289
1	7	0.022904	0.02289	0.02289
1	8	0.023241	0.02323	0.02323
2	1	1.077891	1.07268	1.07268
2	3	1.077816	1.07268	1.07268
2	4	1.077767	1.07268	1.07268
2	5	0.022904	0.02289	0.02289
2	6	0.022908	0.02289	0.02289
2	7	0.022904	0.02289	0.02289
2	8	0.023241	0.02323	0.02323
3	1	1.077818	1.07268	1.07268
3	2	1.077893	1.07268	1.07268
3	4	1.077769	1.07268	1.07268
3	5	0.022904	0.02289	0.02289
3	6	0.022904	0.02289	0.02289
3	7	0.022908	0.02289	0.02289
3	8	0.023241	0.02323	0.02323
4	1	1.077767	1.07268	1.07268
4	2	1.077891	1.07268	1.07268
4	3	1.077816	1.07268	1.07268
4	5	0.023237	0.02323	0.02323
4	6	0.023237	0.02323	0.02323
4	7	0.023237	0.02323	0.02323
4	8	0.023583	0.02357	0.02357

Elt (j)	Pt (i)	Gaussian	Maple	New
5	1	0.022906	0.02289	0.02289
5	2	0.022904	0.02289	0.02289
5	3	0.022904	0.02289	0.02289
5	4	0.023241	0.02323	0.02323
5	6	1.077891	1.07268	1.07268
5	7	1.077816	1.07268	1.07268
5	8	1.077767	1.07268	1.07268
6	1	0.022904	0.02289	0.02289
6	2	0.022908	0.02289	0.02289
6	3	0.022904	0.02289	0.02289
6	4	0.023241	0.02323	0.02323
6	5	1.077816	1.07268	1.07268
6	7	1.077891	1.07268	1.07268
6	8	1.077767	1.07268	1.07268
7	1	0.022904	0.02289	0.02289
7	2	0.022904	0.02289	0.02289
7	3	0.022908	0.02289	0.02289
7	4	0.023241	0.02323	0.02323
7	5	1.077893	1.07268	1.07268
7	6	1.077818	1.07268	1.07268
7	8	1.077769	1.07268	1.07268
8	1	0.023237	0.02323	0.02323
8	2	0.023237	0.02323	0.02323
8	3	0.023237	0.02323	0.02323
8	4	0.023583	0.02357	0.02357
8	5	1.077767	1.07268	1.07268
8	6	1.077816	1.07268	1.07268
8	7	1.077891	1.07268	1.07268

The first thing to note is the fact that all three methods do not provide exactly the same values. This is to be expected however since they are all different numerical calculations, and the accuracy of each was different. The Gaussian

Quadrature method had a relatively small number of sub-domains whilst the Clenshaw-Curtis method used by Maple aimed to achieve a relative error tolerance of approximately 5×10^{-9}, obviously making it the more accurate method of the two. As can be seen from the table, the values of the new method were identical to those provided from Maple (Clenshaw-Curtis) to five decimal places. The Gaussian Quadrature method may not match these values for more than two decimal places, but its clearly supports the magnitudes of the other two methods. Also the equalities and the inequalities predicted earlier also hold true which further supports the proposed method of moments.

This test calculation clearly indicates that in terms of accuracy of the numerical integrations, the proposed method of moments is comparable to other more accepted methods. The relative speeds of the methods have not been compared due to there being various algorithms for implementing the methods which meant that the most efficient one may not have been used which could have lead to unjustified conclusions. Hence this test calculation has shown the proposed method of moments to be a viable alternative to existing methods.

Using this new 'method of moments' to calculate the necessary integrals to form the BEM matrices used to model the problem, it is then necessary to solve the BEM matrix equation. This is again crucial to the efficiency of the method overall as a quick solving algorithm could save large amounts of computation time. However, as will be explained, for the calculations which will be carried out in this research it is not enough to pick the quickest method as there are a number of other properties which the solving algorithm must have.

Chapter 5

Solving the BEM System of Equations

5.1 Introduction

Chapter 3, which described the BEM, indicated that to use the BEM to model a ship corroding in sea water requires the formation of large, dense, coefficient matrices for the physical variables of the problem. This basically means that, as with most numerical modelling techniques, the boundary element method produces a large set of simultaneous equations which describe the physical system being considered with the added complication that in this case these equations are non-linear. As stated previously, the dimensions of the equations for BEM are less than those for FEM, but with the matrices being densely populated whilst those in FEM are sparsely populated.

The solving algorithm will therefore play an important role in creating an efficient modelling tool. Several solving algorithms of both direct and iterative types were investigated to explore the most suitable for the calculations required for this research. Linear equations were used for this purpose. These methods were:-

- LU Decomposition

- Singular Value Decomposition

- Lanczos Method

- Conjugate Gradient Method

- Point Successive Over-relaxation Method.

In the following, each of these methods will be briefly explained, and an outline of the algorithm implemented provided (for further details, see [45, 46],[48]-[51]). The advantages and disadvantages of each method will then be discussed. To conclude the chapter, the methods will be compared against each other and against a set of pre-requisite criteria to determine the most suitable method.

Before beginning, it should be made clear that the algorithms implemented and tested may not be the most advanced forms of the methods, however they were able to solve the matrix equation and allowed the key properties of each method to be investigated.

5.2 Criteria for the Solving Algorithm.

In the following investigations of possible solving algorithms, the general linear system

$$A\mathbf{x} = \mathbf{b} \qquad (5.2.1)$$

shall be used to explain the workings of the methods, where $\mathbf{x}$ is a vector of unknowns and $\mathbf{b}$ is a vector of knowns. However, the BEM equations which describe the problem of the corroding ship has the form

$$H\mathbf{u} = G\mathbf{q} \qquad (5.2.2)$$

where $\mathbf{q}$ (or $\mathbf{u}$) may not be known fully over all the elements. This can cause some difficulties when trying to apply the general algorithms to this specific physical problem.

Firstly, there may be strict conditions on the form of A in eqn (5.2.1) which must be satisfied for a specific algorithm to work. While it may be known whether H and G satisfy these conditions, if neither of the full vectors of $\mathbf{u}$ or $\mathbf{q}$ are known, the pre-conditioning involved in writing eqn (5.2.2) in the form eqn (5.2.1) may mean that the new coefficient matrix does not satisfy these conditions so the algorithm may not be applied.

Suppose for now that the potentials on all the elements are known, i.e.

$$A = G \qquad (5.2.3)$$

$$\mathbf{x} = \mathbf{q} \qquad (5.2.4)$$

$$\text{and } \mathbf{b} = H\mathbf{u}. \qquad (5.2.5)$$

This situation would enable the proposed algorithms to be applied with relative ease. In actual fact, the values of the potential, **u**, and its flux, **q**, on the elements of the ship are related by a non-linear 'polarization relation' [6, 7, 8, 47] which is usually represented by a curve of plotted experimental data [17]. Using this relation for the elements on the ship would mean that the **q** values could be obtained without solving a system of equations. On the elements which form the boundary of the sea box, there are two possible situations if it is assumed that the air and the sea bed are non-conducting. For those elements on the sea box, either $u = 0$ or $q = 0$ but not both together. With $u = 0$, these boundary elements are considered as being conductive, which is a valid situation for those elements on the boundary separating the sea in the domain from the rest of the sea. On the boundaries of the sea level and the sea bed, $q = 0$ is a sensible condition to enforce since q may be regarded as the negative of the outward normal component of **E** which is proportional to the current density crossing the surface, and this condition forces the boundaries to be non-conducting. In these situations, where the polarization data is used on the ship, and sensible conditions are enforced on the other boundaries, applying the algorithm once should result in **u** and **q** being determined in full.

Unfortunately the problems tackled by this research were not as simple as this. To begin with, the theoretical nature of this research meant that for the calculations performed, neither **u** nor **q** were known fully. Indeed the only values that were known were the values on the various boundaries of the sea box as described above, no values were known for either variable on the ship despite the fact that a value for either **u** or **q** must be known on an element for a solution to be attainable (i.e. restrict the system to n unknowns). Thus an initial guess was made at the potentials on the ship, a polarization relation was then used to calculate the respective **q** values and then eqn (5.2.2) was used to check the guess. If eqn (5.2.2) was not satisfied to suitable accuracy then a new, improved

estimate at the solution potentials would be made using the discrepancy for each row i of eqn (5.2.2) known as the residual r_i, where

$$r_i = |G\mathbf{q} - H\mathbf{u}|_i = \left[\sum_j G_{ij}q_j - H_{ij}u_j\right]^{\frac{1}{2}}. \qquad (5.2.6)$$

Another factor which should be accounted for is that although the values of the potentials on the ship may not be known precisely, consideration of the materials and the environment involved makes it possible to deduce a sensible range of acceptable potentials. Therefore it would be desirable to be able to control the values taken by $\mathbf{u}$ on the ship elements when the residual is used to make an improved guess, i.e. forces limits on $\mathbf{u}$.

One condition which the eventual solution should satisfy is that there should be no stray corrosion currents from the ship (conservation of charge), i.e. all the currents that flow from the ship due to corrosion are absorbed by another area of the ship otherwise the ship would become increasingly charged [17]. This condition can be enforced by incorporating the potential of the metal structure of the ship into the polarization relation. This concept will be explained in detail in chapter 7 but in the meantime it is important to note that to satisfy this condition, the solving algorithm should allow the polarization relation to be modified every time a new estimate at the solution has produced an updated value for $\mathbf{q}$ on the ship.

Actually, currents from other sources are important when the ship is in dock and electrically connected to equipment on shore, when welding is being done on the ship in dock, or when in contact with another ship. However we do not consider these situations here.

Finally if, after a few runs, the algorithm appears to be oscillating and not heading toward a sensible solution, the process could be helped by being able to scale the residual eqn (5.2.6) used to obtain the next estimate thus allowing the algorithm to be caressed toward a feasible solution.

All these points can be pulled together to form the following list of criteria which the solving algorithm should meet:-

- allow direct manipulation of $\mathbf{u}$

- allow the calculation of a new $\mathbf{q}$ from the new $\mathbf{u}$ via a polarization relation

- allows potential of the ships metal structure to be altered in the polarization relation to remove stray currents.

- allows control over the direction in which the solution is sought.

As stated previously, the algorithms tested were all checked against these criteria, and each other, before the most suitable one was selected. To begin with, direct methods of solving eqn (5.2.1) were considered.

5.3 LU Decomposition

5.3.1 Background Theory

This method is also known as 'LU factorization' and is closely related to 'Gaussian Elimination'. Consider the general problem of solving a general linear system eqn (5.2.1) where A is a n-by-n non-singular matrix, and x and b are vectors of length n containing unknowns and knowns respectively. One of the simplest tactics employed to solve eqn (5.2.1) is to transform this system into one whose solution is the same as the original but is easier to solve [48]. One of the easiest linear systems to solve is that where the coefficient matrix A is either upper or lower triangular, in which case the system may be solve by forward or backward substitution respectively. Algorithms for forward and backward substitution can be found in appendix A.

The obstacle in trying to implement this strategy is how to transform the system so A is triangular but the solution is unaffected. This can be achieved by pre-multiplying the left hand side and the right hand side by a series of elementary elimination matrices, or transformations. The generation of these matrices is widely covered in many texts [45, 48] and shall not be covered in detail, however a quick and simple example of such matrices and their effect is demonstrated in the following example [48]. Let M_k denoted the transform which will zero all

elements in a vector, e.g. one column of A, after the kth.

$$
\cdot \begin{bmatrix} 1 & \cdots & 0 & 0 & \cdots & 0 \\ \vdots & \ddots & \vdots & \vdots & \ddots & \vdots \\ 0 & \cdots & 1 & 0 & \cdots & 0 \\ 0 & \cdots & -m_{k+1} & 1 & \cdots & 0 \\ \vdots & \ddots & \vdots & \vdots & \ddots & \vdots \\ 0 & \cdots & -m_n & 0 & \cdots & 1 \end{bmatrix} \begin{bmatrix} a_1 \\ \vdots \\ a_k \\ a_{k+1} \\ \vdots \\ a_n \end{bmatrix} = \begin{bmatrix} a_1 \\ \vdots \\ a_k \\ 0 \\ \vdots \\ 0 \end{bmatrix} \qquad (5.3.1)
$$

where $m_i = \frac{a_i}{a_k}$, $(i = k+1, \ldots, n)$. The element on the denominator is referred to as the pivot. Utilizing this general transform, it is possible to generate a series of transforms which when applied in turn to eqn (5.2.1) produce on the right-hand side an new vector of knowns, whilst on the left

$$MA = U \qquad (5.3.2)$$

where $M = M_{n-1}M_{n-2}\ldots M_1$ is the series of transformations which has reduced A to an upper triangular form. For a system of equations to correspond to eqn (5.2.1), it is necessary to have the matrix A expressed as a product of two matrices, and this is accomplished by pre-multiplying both sides of eqn (5.3.2) by M^{-1} so that $A = M^{-1}U$. From the general form of a transformation, it is known that all the transforms M_k are matrices with zeros everywhere except on the main diagonal where the values are one, and also on the kth column where the values are as in eqn (5.3.1). Hence M_k is a unit lower triangular matrix which will have an inverse. Also it is known that the product of two unit lower triangular matrices L_kL_j, where $k < j$, is also a unit lower triangular matrix, so that

$$M^{-1} = (M_{n-1}\ldots M_1)^{-1} = M_1^{-1}\ldots M_{n-1}^{-1} = L_1 \ldots L_{n-1} = L.$$

where each L is a unit lower triangular matrix. Hence A can be written as the product LU so eqn (5.2.1) may be equivalently written as

$$LU\mathbf{x} = \mathbf{b}. \qquad (5.3.3)$$

If $U\mathbf{x} = \mathbf{y}$, then the forward substitution algorithm may be used to solve $L\mathbf{y} = \mathbf{b}$ for $\mathbf{y}$ which in turn can be used with the backward substitution algorithm to solve

for x, which is the solution of eqn (5.2.1).

The algorithm in table 5.1 describes how the LU decomposition was performed using Gauss transformations. Note that when there is a restriction on the

for $k = 1$ to $n - 1$	(looping over the columns)
if $a_{kk} = 0$ then stop	(stop if a zero pivot is encountered)
$l_{kk} = 1$	(diagonal element of L set to 1)
for $i = k + 1$ to n	
$m_{ik} = \frac{a_{ik}}{a_{kk}}$	(compute the multipliers for current column)
$l_{ik} = m_{ik}$	(assigns the multiplier to the L element)
end	
$u_{kk} = a_{kk}$	(setting diagonal element of U to be that of A)
for $j = k + 1$ to n	
for $i = k + 1$ to n	(apply transformation to the remaining sub-matrix)
$u_{ij} = a_{ij} - m_{ik}a_{kj}$	(assigning the elements of U)
end	
$b_j = b_j - m_{ik}b_k$	(applying the multiplier to b vector)
end	

Table 5.1: LU Decomposition using Transformations

memory capacity available, L and U can be stored in A to economise with l_{ii} not specifically stored but it is known that these values are unity.

Thus the LU Decomposition is a very efficient, direct method for solving eqn (5.2.1) but it has some disadvantages when faced with the task of solving the BEM system eqn (5.2.2) and satisfying the desired criteria.

5.3.2 Suitability Discussion.

There can be no doubt the LU Decomposition is a very powerful method for solving systems expressed as eqn (5.2.1), however questions remain over how well it matches the key criteria required of an algorithm to solve eqn (5.2.2) efficiently.

A problem could easily arise over the requirement that A must be non-singular. In a calculation based on the physical problem such as that being considered here, it is impossible to guarantee that the method will not be applied to a geometry

which will give rise to a singular, or nearly singular, A matrix. However, as most of the methods discussed will have a similar constraint on A, it would be unreasonable to dismiss this method on these grounds.

The main problem with this method is that it must be applied to a system which is expressed in the general form eqn (5.2.1) which seriously hinders its application to the BEM system. The necessity to express eqn (5.2.2) as eqn (5.2.1) means that it is very difficult to control the values of u and q during the solution seeking process, with neither being accessible until a complete decomposition has been performed. Also a complete LU Decomposition must be performed before the accuracy of solution provided by the current estimates can be assessed. Then while it may be easy enough to amend the potentials, amending the values of q and the reforming eqn (5.2.1) would require expensive matrix-vector calculations. However, one advantage of this is that the polarization relation may be altered before the new estimates are made so there should be no difficulties ensuring that there are no stray currents.

Another disadvantage is that the search direction which is controlled by the residual eqn (5.2.6) also cannot be altered until after a full decomposition has been completed. This will mean that while the solution is been sought, there will be long periods when it will be impossible to check the progress being made and during these periods it will be impossible to help the process in its search.

These disadvantages are something which all direct methods will share, so the clear indication is that iterative methods would be more suitable. However, before considering algorithms of this type, one further direct method will be considered which has the distinct advantage in that it will always provide a solution to a system, even though one may not actually exist!

5.4 Singular Value Decomposition

5.4.1 Background Theory

With the LU Decomposition, one of the key conditions was that in eqn (5.2.1), A had to be non-singular but with the practical nature of the problem being considered here this can not be guaranteed. Furthermore, there must be a solution to the physical problem but not necessarily to our model of it. Hence it is necessary to have a method which is able to deal with a singular system of equations.

Another eventuality is that since the system is calculated numerically it is also possible it could be numerically very close to singular, making it very unstable to small perturbations. Again this must be dealt with.

The most popular and robust method used to handle these troublesome situations is the Singular Value Decomposition (SVD). When trying to solve a singular system of equations, or a system which is numerically very close to being singular, the SVD will diagnose the problem (i.e. highlight the troublesome singular value) and then enable this value to be altered if required so that a solution to the system can be obtained. It should be noted however that this solution may not be the expected one [45].

The SVD is based on the following theorem whose proof can be found in [45]

Theorem 1 (The Singular Value Decomposition). *Any M-by-N matrix A (M $\geq$ N) can be written as the product of an M-by-N column orthogonal matrix U, an N-by-N diagonal matrix Σ with positive or zero elements (i.e. $\sigma_{ij} \geq 0 \iff i = j$), and the transpose of an N-by-N orthogonal matrix V*

$$A = U \Sigma V^T.$$ (5.4.1)

This decomposition will be unique unless the same permutations are made to the columns of U, the elements of Σ, and the columns of V. The values of the diagonal elements and the vectors which form the columns of U and V are closely related to the eigenpairs of $A^T A$ and $A A^T$ respectively. However these properties have no immediate relevance to this work and will not be considered. Further information may be found in [48]. It is a very stable method with the version implemented here being based in the reduction of A to bidiagonal form using a Householder reduction, followed by diagonalization by a QR procedure with shifts. These 'black-box' algorithms can be found in appendix A. When these two procedures are combined, the SVD produced uses a step known as the *Golub-Kahan SVD step* [49]. The outline of the algorithm for this is given below

Basically the system of equations originating from the boundary element

Any n-by-n matrix A can be written as the product of an n-by-n column orthogonal matrix U, an n-by-n diagonal matrix Σ with positive or zero elements (i.e. $\sigma_{ij} \geq 0 \iff i = j$), and the transpose of an n-by-n orthogonal matrix V $A = U\Sigma V^T$ so that eqn (5.2.1) may be solved by eqn (5.4.2) by the following (where the singular values σ_j must be greater than σ_{lim})

> Perform a Householder reduction on A to reduce it to bidiagonal form
> Accumulate the right-hand transformation in matrix V
> Accumulate the left-hand transformation in matrix U
> Diagonalize the bidiagonal form using a QR iteration with shifts to zero off-diagonal entries
> Now have $U\Sigma V^T \mathbf{x} = \mathbf{b}$
> Calculate $\mathbf{b}' = U^T \mathbf{b}$
> Calculate $b''_j = \frac{b'_j}{\sigma_j}$
> If $\sigma_j < \sigma_{lim}$, $b''_j = 0$.
> Solve by $\mathbf{x} = V\mathbf{b}''$.

Table 5.2: Outline of SVD Algorithm.

method eqn (5.2.2) which have square matrices are being eqn (5.2.1) solved by

$$\mathbf{x} = A^{-1}\mathbf{b} \tag{5.4.2}$$

$$= V \cdot diag\left(\frac{1}{\sigma_i}\right) \cdot U^T \mathbf{b} \tag{5.4.3}$$

This clearly shows that the problems will arise when at least one of the σ_i singular values are zero (or numerically small enough to be indistinguishable from the roundoff error). Hence the SVD will give a clear diagnosis of an ill-conditioned problem.

One of the consequences of the SVD is that the columns of U and V provide bases for the range and the nullspace of the transform corresponding to the matrix A. The columns of U which have non-zero corresponding singular values form an orthonormal basis of the range of A while the columns of V which have zero corresponding singular values form a basis of the nullspace of A. These concepts play a key role in demonstrating the strength of the SVD [45].

Suppose that A is singular. If $\mathbf{b} \in Range(A)$ then the singular set of equations will have a solution, which may be found by replacing the problematic $\frac{1}{\sigma_i}$ by zero in eqn (5.4.2) and then solving. Consider now the situation where $\mathbf{b} \notin Range(A)$, then no solution exists to the system. However, the SVD is still able to produce

a vector $\mathbf{x}$ which will minimise the residual $r = |A\mathbf{x} - \mathbf{b}|$ in the least squares sense by zeroing the singular $\frac{1}{\sigma}$. This is all very clear cut in theory but there needs to be a degree of discretion used when rather than being singular, A is only ill-conditioned. For an ill-conditioned matrix, other methods will provide solution vectors but these solutions will have been found via processes which were unstable with the consequence that they will not be feasible solutions to eqn (5.2.1) (i.e. $A\mathbf{x} \neq \mathbf{b}$). If SVD is used, then the extremely small singular values can, at the user's discretion, be used to zero the elements $\frac{1}{\sigma}$ causing the instability which results in an invalid solution vector being removed producing a solution with a very small residual indicating a good approximation to the actual solution. This is a difficult concept to grasp since it is counter-intuitive. By zeroing an element in $diag\left(\frac{1}{\sigma}\right)$, information which is known about the physical system is being thrown away. In most cases this would reduce the accuracy of the obtained solution but in this algorithm it actually improves the accuracy because unreliable information is being thrown away. However the process is actually removing an equation from the system which is forcing the solution vector away from the actual solution and toward infinity in some direction which is almost, but not quite, in the null-space. The removal of this equation removes this search direction and the solution is free to head toward the most accurate available solution.

5.4.2 Suitability Discussion.

So obviously the SVD has some extremely important and powerful features, but again its application to this research is hampered by many of the same problems as encountered with the application of the LU Decomposition.

Like the LU Decomposition, the problem is that a full SVD must be calculated before the accuracy of the estimate to the actual solution can be checked. Whilst this is being done, no control can be exerted over the $\mathbf{u}$ and $\mathbf{q}$ values that form the current estimate, so there will be lengthy periods during which the method can not be aided in its search for a solution. However like the LU Decomposition, after each complete decomposition, the polarization relation can be altered so there should be no problem in ensuring that there are no stray currents. Hence this method may not be the most suitable for the calculations performed here but since it is possible that a singular system of equations could be obtained from the boundary element method, the SVD should not be completely dismissed but

instead should be held in reserve in case this situation arises.

Two direct methods have now been considered and both were deemed unsuitable since they did not allow enough access to modify the estimate of the solution. To have an algorithm which allows close control and frequent access to the estimated solution means being able to alter the $\mathbf{u}$ and $\mathbf{q}$ values in eqn (5.2.2) continuously throughout the calculation. This can be done by iterative methods which will now be considered.

5.5 Iterative Methods

5.5.1 The Lanczos Method and the Conjugate Gradient Method

To begin the investigation into iterative methods for solving large systems of equations, consider the Lanczos Method. This method is very popular as it is extremely powerful and has remarkable convergence properties making it possibly the best method for obtaining the extremal eigenvalues of a system. Initially, the Lanczos method was applied to large sparse matrices but it can be used to solve systems with densely populated matrices, although it still operates best on the former. One key requirement is that the matrix A in eqn (5.2.1) must be symmetric, with dimensions n-by-n.

The method involves the tridiagonalization of A by a method that produces no intermediate sub-matrices. It is a method which seeks out a solution by using an orthonormal set of basis vectors which span a *Krylov Subspace*. This means that the set of basis vectors is built up incrementally from an arbitrary starting vector, say $\mathbf{x}_0$, by the repeated pre-multiplication by the matrix A so that $\mathbf{x}_k = A\mathbf{x}_{k-1}$. The outcome of this is that for each $k = 1, \ldots, n$, a new n-by-k Krylov matrix is defined by

$$K_k = [\mathbf{x}_0 \quad \mathbf{x}_1 \quad \ldots \quad \mathbf{x}_{k-1}] \tag{5.5.1}$$

$$= [\mathbf{x}_0 \quad A\mathbf{x}_0 \quad \ldots \quad A^{k-1}\mathbf{x}_0]. \tag{5.5.2}$$

There are many ways in which to derive the Lanczos method but the one which highlights its impressive convergence properties can be found in the text by Golub

& Van Loan [49]. The following is a brief overview of their derivation.

Begin by considering the Rayleigh Quotient

$$r(\mathbf{x}) = \frac{\mathbf{x}^T A \mathbf{x}}{\mathbf{x}^T \mathbf{x}}, \qquad \mathbf{x} \neq \mathbf{0}. \tag{5.5.3}$$

The Courant-Fischer Minimax Characterization says that the maximum and minimum values of $r(x)$ are the maximum and minimum eigenvalues of A, $\lambda_1(A)$ and $\lambda_n(A)$ respectively [49]. Define a matrix $Q_j = [\mathbf{q}_1, \ldots, \mathbf{q}_j]$ (where the vectors $\mathbf{q}_j$ are real and orthonormal) and also scalars

$$
\begin{aligned}
M_j = \lambda_1(Q_j^T A Q_j) &= max_{\mathbf{y}} \frac{\mathbf{y}^T (Q_j^T A Q_j) \mathbf{y}}{\mathbf{y}^T \mathbf{y}} \\
&= max_{\mathbf{y}} \, r(Q_j y) \leq \lambda_1(A) \tag{5.5.4} \\
m_j = \lambda_n(Q_j^T A Q_j) &= min_{\mathbf{y}} \frac{\mathbf{y}^T (Q_j^T A Q_j) \mathbf{y}}{\mathbf{y}^T \mathbf{y}} \\
&= min_{\mathbf{y}} \, r(Q_j \mathbf{y}) \geq \lambda_n(A). \tag{5.5.5}
\end{aligned}
$$

The key to deriving the Lanczos method is to try and generate the orthonormal vectors $\mathbf{q}_j$ so that the M_j and m_j become better estimates of $\lambda_1(A)$ and $\lambda_n(A)$. Let $\mathbf{u}_j \in span\{\mathbf{q}_1, \ldots, \mathbf{q}_j\}$ be such that $M_j = r(\mathbf{u}_j)$. Consider the gradient of r

$$\nabla r(\mathbf{x}) = \frac{2}{\mathbf{x}^T \mathbf{x}} [A\mathbf{x} - r(\mathbf{x})\mathbf{x}] \tag{5.5.6}$$

which gives the direction in which r is most rapidly changing. To get M_{j+1} to become a better estimate to $\lambda_1(A)$ than M_j, it is necessary to determine a new orthonormal vector $\mathbf{q}_{j+1}$ such that when the vector $\mathbf{u}_{j+1} \in span\{\mathbf{q}_1, \ldots, \mathbf{q}_{j+1}\}$ is formed, $r(\mathbf{u}_{j+1}) > r(\mathbf{u}_j)$. This requires that $r(\mathbf{u}_{j+1}) = r(\mathbf{u}_j) + b$ where $b > 0$. To maximise the increase, b should be in the direction of steepest ascent, i.e. $\nabla r(\mathbf{u}_j)$. With $\mathbf{u}_{j+1}$ formed by a linear combination of $\mathbf{q}_1, \ldots, \mathbf{q}_{j+1}$, it makes sense that the new vector $\mathbf{q}_{j+1}$ should point in this direction and therefore should be chosen so that

$$\nabla r(\mathbf{u}_j) \in span\{\mathbf{q}_1, \ldots, \mathbf{q}_{j+1}\} \tag{5.5.7}$$

An analogous argument holds for the search of the new $\mathbf{q}_{j+1}$ that will make $m_{j+1} < m_j$ since the negative direction of the gradient is the direction of steepest descent. From eqn (5.5.6), $\nabla r(\mathbf{x}) \in span\{\mathbf{x}, A\mathbf{x}\}$ which indicates that the

orthonormal vectors can in fact be generated by a Krylov sequence meaning that the space spanned by $q_1 \ldots q_j$ is just a Krylov subspace so the problem can be viewed as trying to compute an orthonormal bases for the Krylov subspaces $K(A, q_1, j)$ (i.e. $[q_1, Aq_1, \ldots, A^{j-1}q_1]$).

Suppose that a QR factorization (see Appendix A) has been done on $K(A, q_1, n)$ and has produced a matrix Q with $Qe_1 = q_1$ such that $Q^T A Q = T$, where T is a tridiagonal matrix. Then it is straightforward to show that

$$[q_1, Aq_1, \ldots, A^{n-1}q_1] = Q[e_1, Te_1, \ldots, T^{n-1}e_1] \qquad (5.5.8)$$

which means that the q_j can effectively be generated by tridiagonalizing A with an orthogonal matrix whose first column is q_1.

The elements of the T are generated directly. With $Q = [q_1, \ldots, q_n]$, and

$$T = \begin{bmatrix} \alpha_1 & \beta_1 & 0 & 0 & \ldots & 0 \\ \beta_1 & \alpha_2 & \beta_2 & 0 & \ldots & 0 \\ 0 & \ddots & \ddots & \ddots & \ddots & \beta_{n-1} \\ 0 & 0 & \ldots & 0 & \beta_{n-1} & \alpha_n \end{bmatrix} \qquad (5.5.9)$$

the fact that $AQ = QT$ says

$$Aq_j = \beta_{j-i}q_{j-1} + \alpha_j q_j + \beta_j q_{j+1} \qquad (\beta_0 q_0 \equiv 0) \qquad (5.5.10)$$

for $j = 1, \ldots, n - 1$. Because the q_j are orthogonal, $\alpha_j = q_j^T A q_j$ and if $r_j = (A - \alpha_j I)q_j - \beta_{j-1}q_{j-1}$ is nonzero, then $q_{j+1} = \frac{r_j}{\|r_j\|_2}$.

Thus the Lanczos algorithm shown in table 5.3 can be formed [49].

The key benefit of this method is that in a situation when only the extreme eigenvalues are required, the Lanczos method will only take a few iterations ($j \ll n$) to produce a tridiagonal matrix T_j which will have eigenvalues matching the extremal ones of A. Thus the process could be thought of as condensing the physics contained in A into a smaller matrix T.

One thing about this process is that there appears to be no benefits to the problem investigated here. The method may have its main benefits in solving for the extremal eigenvalues but to solve the complete system, it is necessary to fully generate the complete tridiagonal matrix T, store all the eigenvectors in the

Given a symmetric matrix $A \in \Re^{n \times n}$, the following computes a j-by-j symmetric tridiagonal matrix T_j with the property that $\lambda(T_j) \subset \lambda(A)$.

Assign initial values

$\mathbf{r}_0 = \mathbf{q}_1$, $\beta_0 = 1$, $\mathbf{q}_0 = 0$, $j = 0$.

While $\beta_j \neq 0$

$\mathbf{q}_{j+1} = \frac{\mathbf{r}_j}{\beta_j}$

$j = j + 1$

$\alpha_j = \mathbf{q}_j^T A \mathbf{q}_j$

$\mathbf{r}_j = (A - \alpha_j I)\mathbf{q}_j - \beta_{j-1}\mathbf{q}_{j-1}$

$\beta_j = \|\mathbf{r}_j\|_2$

end.

Table 5.3: The Lanczos Algorithm

matrix Q and then solve the resultant tridiagonal system of equations.

However there is another iterative process which will now be considered which is intimately linked to the Lanczos method, the Conjugate Gradient method. Indeed both methods are so closely linked that they can almost be viewed as two ways of expressing the same process, only while the Lanczos method looks for the eigenvalues, the conjugate gradient method looks directly to solve the system

As with the Lanczos method, the Conjugate Gradient (CG) method uses A to generate a Krylov subspace for which an orthogonal basis is sought by means of a three-term recurrence relation. Again, the CG method works best for sparse linear systems but can be applied to densely populated ones. The conditions on A for the CG method to work is that it is square, symmetric and positive definite (i.e. for all $\mathbf{x} \in \Re^n$ which are non-zero, $\mathbf{x}^T A \mathbf{x} > 0$, assuming $A \in \Re^{n \times n}$).

It is difficult to explain the CG method without first investigating two other methods, those of steepest descent and conjugate directions. The following will briefly introduce these methods, highlighting their advantages and disadvantages, and how they lead to the derivation of the CG method. This discription is based on that of Shewchuk [50].

The fundamental concept to these solution methods is that of the quadratic form of eqn (5.2.1), which is the scalar, quadratic function of a vector shown in eqn (5.5.11)

$$f(\mathbf{x}) = \frac{1}{2}\mathbf{x}^T A \mathbf{x} - \mathbf{b}^T \mathbf{x} + c. \tag{5.5.11}$$

With A symmetric and positive-definite, eqn (5.2.1) has its solution located at

the minimum of $f(\mathbf{x})$. To see this consider the gradient of eqn (5.5.11)

$$\nabla f(\mathbf{x}) = \begin{bmatrix} \frac{\partial}{\partial x_1} f(\mathbf{x}) \\ \frac{\partial}{\partial x_2} f(\mathbf{x}) \\ \vdots \\ \frac{\partial}{\partial x_n} f(\mathbf{x}) \end{bmatrix} \qquad (5.5.12)$$

At the minimum of $f(\mathbf{x})$, $\mathbf{x}$ will be such that the gradient will be zero in which case

$$\frac{1}{2}A^T\mathbf{x} + \frac{1}{2}A\mathbf{x} - \mathbf{b} = 0 \qquad (5.5.13)$$

$$\Longrightarrow \ A\mathbf{x} - \mathbf{b} = 0 \quad \text{since } A \text{ is symmetric} \qquad (5.5.14)$$

$$\Longrightarrow \ A\mathbf{x} = \mathbf{b} \qquad (5.5.15)$$

as required. Hence the best way to gain an understanding of CG method is to consider it as being a minimization problem. To this end consider the situation where $n = 2$, then a contour plot of a generic system is shown in figure 5.1. In
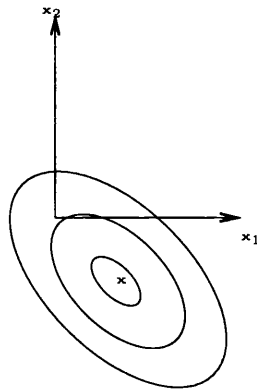
Figure 5.1: Contour plot for the quadratic function for a generic n=2 system

this situation the challenge is to vary x_1 and x_2 until the solution $\mathbf{x}$ is found.

The first method that will be considered is that of Steepest Descent. The gradient of the quadratic form at any point will give the direction of steepest ascent, so the negative will give the direction of steepest descent and this is the direction in which this method alters $\mathbf{x}$ is an attempt to get closer to the solution. However the problem with steepest descent is that it is unable to produce orthogonal search directions, so to obtain a solution it is necessary to repeat steps

in directions which have already been used. A basic outline of the process is as follows.

An initial guess $\mathbf{x}_0$ is made at the solution $\mathbf{x}$. Let the error between the guess and the solution be given by $\mathbf{e}_0 = \mathbf{x}_0 - \mathbf{x}$. If $\mathbf{e}_0 \neq 0$ then make an improved guess $\mathbf{x}_1 = \mathbf{x}_0 + \alpha_0 \mathbf{r}_0$ where α_0 is the step length in direction of the residual $\mathbf{r}_0 = \mathbf{b} - A\mathbf{x}_0 = A\mathbf{e}_0$. By setting the directional derivative to be zero,

$$\frac{\partial f(\mathbf{x}_1)}{\partial \alpha} = 0 \tag{5.5.16}$$

it can be shown that α_0 should be chosen so that the residual and the gradient of the quadratic function at $\mathbf{x}_0$ are orthogonal. By using the fact that $f'(\mathbf{x}_1) = -\mathbf{r}_1$, analysing $\mathbf{r}_1^T \mathbf{r}_0 = 0$ can show that

$$\alpha = \frac{\mathbf{r}_0^T \mathbf{r}_0}{\mathbf{r}_0^T A \mathbf{r}_0}.$$

The complete method can be summarised by the following three equations

$$\mathbf{r}_i = \mathbf{b} - A\mathbf{x}_i \tag{5.5.17}$$

$$\alpha_i = \frac{\mathbf{r}_i^T \mathbf{r}_i}{\mathbf{r}_i^T A \mathbf{r}_i} \tag{5.5.18}$$

$$\mathbf{x}_{i+1} = \mathbf{x}_i + \alpha_i \mathbf{r}_i. \tag{5.5.19}$$

As mentioned above, the problem with steepest descent is that it often finds itself seeking the solution in directions which it has already search along due to the non-orthogonality of the search directions. This is improved on by the next method, named the conjugate direction method, which uses a set of orthogonal search directions $\mathbf{d}_i$ $(i = 0, \ldots, n - 1)$.

In this method, $\mathbf{x}_{i+1} = \mathbf{x}_i + \alpha_i \mathbf{d}_i$, and it can be shown that the direction $\mathbf{d}_i$ is in fact orthogonal to the error $\mathbf{e}_{i+1}$ which suggests the step length to be calculated from

$$\alpha_i = -\frac{\mathbf{d}_i^T \mathbf{e}_i}{\mathbf{d}_i^T \mathbf{d}_i}. \tag{5.5.20}$$

Unfortunately this cannot be calculated since it requires prior knowledge of the solution (need to know $\mathbf{x}$ to calculate $\mathbf{e}_i$). To avoid this problem, it is necessary to abandon the notion of having orthogonal search directions and replace it with the notion of having A-orthogonal search directions. This means that $\mathbf{d}_i^T A \mathbf{d}_j = 0$

(for $i \neq j$). The new requirement is for the error $\mathbf{e}_{i+1}$ to be A-orthogonal to $\mathbf{d}_i$, which means that the step length can be calculated from

$$\alpha_i = -\frac{\mathbf{d}_i^T A \mathbf{e}_i}{\mathbf{d}_i^T A \mathbf{d}_i} = \frac{\mathbf{d}_i^T \mathbf{r}_i}{\mathbf{d}_i^T A \mathbf{d}_i}. \tag{5.5.21}$$

The convergence of this method is very impressive with the solution being obtained after exactly n iterations. The only problem appears to be the need for a set of A-orthogonal search directions, but these can be generated using a *conjugate Gram-Schmidt process*. This process requires a set of n linearly independent vectors, and proceeds to produce a set of A-orthogonal vectors by taking each of these vectors and subtracting out any component which is not A-orthogonal to previously calculate A-orthogonal vectors. This is straight forward but it does require that all search vectors are kept in memory for use when calculating the next A-orthogonal vector which puts strain on the memory of the computer. The process of generating a full set of search directions is also computationally expensive. These problems seriously hamper an otherwise elegant method, but fortunately the method of conjugate gradients tackles these problems and provides a more efficient method.

The conjugate gradient method is simply that of conjugate directions only the search directions are found by conjugation of the residuals. In this sense the method is similar to steepest descent which used the residuals as search directions, and an added benefit is that the residuals can be shown to be orthogonal to the previous search directions which means a new linearly independent search direction is produced every-time except if the residual is zero in which case the problem has been solved.

Consider the consequence of this choice for the search directions. Define $\mathcal{D}_i$ as the i-dimensional subspace spanned by the i search directions to this point in the calculation. Since the search directions are based on the residuals, $\mathcal{D}_i = span\{\mathbf{d}_0, A\mathbf{d}_0, \ldots, A^{n-1}\mathbf{d}_0\}$ is equivalent to $span\{\mathbf{r}_0, \ldots, \mathbf{r}_{i-1}\}$. It is known that a residual will be orthogonal to the previous search directions so this equivalence highlights that the residuals will be orthogonal to each other.

Recall that the residual can be found from the error by $\mathbf{r}_i = -A\mathbf{e}_i$, this means that each subsequent residual may be found from

$$\mathbf{r}_{i+1} = \mathbf{r}_i - \alpha_i A \mathbf{d}_i \tag{5.5.22}$$

which indicates that the subspaces $\mathcal{D}_{i+1}$ are just Krylov subspaces with the original residual $\mathbf{r}_0$ being the source vector, i.e. $\mathcal{D}_i = span\{\mathbf{r}_0, \ldots, A^{i-1}\mathbf{r}_0\}$. It should be noted that the although the search directions are constructed from the residuals, the fact that a conjugate Gram-Schmidt process is used means that the ith search direction, $\mathbf{d}_i$, is $A^{i-1}\mathbf{r}_0$ and not $\mathbf{r}_{i-1}$. The fact that Krylov subspaces are being dealt with makes applying the conjugate Gram-Schmidt process easier as it intrinsically forces the new residual $\mathbf{r}_{i+1}$ to be A-orthogonal to all the previous search directions except the most recent, $\mathbf{d}_i$. This becomes more obvious if it is remembered that $\mathcal{D}_i$ will include $A\mathcal{D}_{i-1}$. Each new $\mathbf{x}_i$ is the linear combination of $\mathbf{x}_{i-1}$ and the new search direction $A\mathbf{d}_{i-1}$, and recalling that the aim is to minimise the quadratic form eqn (5.5.11), setting the directional derivative to zero gives

$$\mathbf{r}_i^T A \mathbf{d}_{i-1} = 0. \tag{5.5.23}$$

This combined with the A-orthogonality of the search directions forces the residual $\mathbf{r}_i$ to be orthogonal to $\mathcal{D}_i$ which implies immediately that $\mathbf{r}_i$ must be A-orthogonal to $\mathcal{D}_{i-1}$. Hence as required the only search direction to which $\mathbf{r}_{i+1}$ is not A-orthogonal is $\mathbf{d}_i$.

When the conjugate Gram-Schmidt process is used to calculate the necessary coefficient in the calculation of new search direction from the current residual and the previous search directions, it can be shown that

$$\beta_{ij} = \begin{cases} \frac{1}{\alpha_{i-1}} \frac{\mathbf{r}_i^T \mathbf{r}_i}{\mathbf{d}_{i-1}^T A \mathbf{d}_{i-1}} & i = j+1 \\ 0 & i \neq j+1 \end{cases} \tag{5.5.24}$$

where

$$\mathbf{d}_i = \mathbf{r}_i + \sum_{k=0}^{i-1} \beta_{ik}\mathbf{d}_k. \tag{5.5.25}$$

Therefore

$$\mathbf{d}_i = \mathbf{r}_i + \beta_{ii-1}\mathbf{d}_{i-1} \tag{5.5.26}$$

which means only the previous search direction must be stored, unlike the conjugate direction method which required all the previous search directions stored. Using eqn (5.5.21) along with the orthogonality of residuals and eqn (5.5.26), the

expression for β may be written as

$$\beta_i = \frac{\mathbf{r}_i^T \mathbf{r}_i}{\mathbf{r}_{i-1}^T \mathbf{r}_{i-1}}. \tag{5.5.27}$$

This can now be pulled together in table 5.4 to form the algorithm for the conjugate gradient method which should converge in at most n steps [50]

> Given a symmetric, positive definite matrix $A \in \Re^{n \times n}$ and vector $\mathbf{b} \in \Re^n$ such that an unknown vector $\mathbf{x}$ exists satisfying $A\mathbf{x} = \mathbf{b}$, the following searches for $\mathbf{x}$ along n A-orthogonal search directions.
>
> Make an initial guess at the solution $\mathbf{x}_0$.
>
> $\mathbf{d}_0 = \mathbf{r}_0 = \mathbf{b} - A\mathbf{x}_0$
> for $i = 1, \ldots, n$
> $\qquad \alpha_i = \frac{\mathbf{r}_i^T \mathbf{r}_i}{\mathbf{d}_i^T A \mathbf{d}_i}$
> $\qquad \mathbf{x}_{i+1} = \mathbf{x}_i + \alpha_i \mathbf{d}_i$
> $\qquad \mathbf{r}_{i+1} = \mathbf{r}_i - \alpha_i A \mathbf{d}_i$
> $\qquad \beta_{i+1} = \frac{\mathbf{r}_{i+1}^T \mathbf{r}_{i+1}}{\mathbf{r}_i^T \mathbf{r}_i}$
> $\qquad \mathbf{d}_{i+1} = \mathbf{r}_{i+1} + \beta_{i+1} \mathbf{d}_i.$

Table 5.4: Algorithm for the Conjugate Gradient Method

There is one problem with this method, and that is the A-orthogonality condition on the search directions. When implemented, the limited numerical accuracy of the computer will mean that the residuals will begin to lose their accuracy and the search vectors their A-orthogonality. However it is possible to avoid these problems and confidently apply this method.

5.5.2 Suitability Discussion.

Both the Lanczos and the Conjugate Gradient methods match the key criteria extremely well which was expected due to their iterative nature. As stated above, the two methods are very closely related with the main strength of the Lanczos method being in the search of the eigenpairs of a system while the CG method specifically targets the solution of eqn (5.2.1). For this reason, if the choice had to be made between these two, the CG method would be chosen and it will be this method which will now be compared against the key criteria.

Suppose that an initial guess has been made for $\mathbf{u}$, and the polarization relation has calculated the corresponding $\mathbf{q}$ values. The method can be modified to

be applied to eqn (5.2.2) rather than the general case eqn (5.2.1) by calculating the residuals r from eqn (5.2.6) and searching for the potentials.

It is apparent that access is readily available to the values of u and q after each iterative step has been calculated so there is ability in this method to constrain these variables that is far superior to that offered by the direct methods. Also the polarization relation can be accessed after every iteration so the ability to modify this to ensure that there are no stray currents is again present.

So far, the CG method seems to be perfect for the task at hand, and especially since the method should, for $A \in \Re^{n \times n}$, converge in n steps [50]. However, this is only the case when b (or Gq) is known and fixed which in eqn (5.2.2) is not the case. The values of q are dependent on u which is being altered to try and find values for the two vector of variables which satisfy eqn (5.2.2) and the various conditions imposed on the system, i.e. no stray currents and values within realistic constraints. Therefore it is unknown how many steps will be required to obtain a solution. This problem of effectively varying the two vectors means that it would be desirable to be able to try and help the method find a solution by altering the search directions, something which the CG method does not specifically allow.

Another draw back is that A must be symmetric and positive-definite. These conditions can not be guaranteed for either of the matrices in eqn (5.2.2) and any pre-conditioning done to the matrices to satisfy these conditions adds computational expense to the process which is undesirable.

So, while the Conjugate Gradient method is superior for solving the types of problems faced in this work than the previously discussed direct methods, it still does not satisfy all the key criteria to a high enough standard. Hence another iterative process was considered.

5.5.3   The Point Successive Over-relaxation Method

The Point Successive Over-relaxation Method (PSOM) is not a method that is favoured for the solving of linear systems such as eqn (5.2.1) with its main application lying in other fields such as the deconvolution of images which is where the algorithm implemented in this research can be found originally [51].

The PSOM is without doubt the simplest of all the algorithms that have been discussed but it remains a very powerful method for solving systems of equations such as eqn (5.2.1) or eqn (5.2.2), and being an iterative method it is possible

for the user to exert control over the iterated solution to prevent unphysical or spurious solutions being obtained. To derive the PSOM, like the conjugate gradient method, it is necessary to first derive an intermediate method which is not quite as powerful as the full PSOM.

Consider eqn (5.2.1). An iterative solution will be obtainable if A is diagonally dominant by which it is meant that

$$a_{ii} > \sum_{j \neq i} |a_{ij}|.$$ (5.5.28)

In practise, this constraint is not strictly necessary and can be relaxed so that all that is required is that the diagonal element of a row is larger than its neighbours in that row. This does to a certain extent decrease the importance of each row in the matrix since, for each row, the greater the ratio

$$\frac{a_{ii}}{\sum_{j \neq i} |a_{ij}|}$$ (5.5.29)

then the more independent information that row brings to the system. However this is a necessary trade-off to ensure that the method can be applied to a wide range of systems.

Begin by considering eqn (5.2.1) in component form, and remove the diagonal term from the summation

$$b_i = a_{ii} x_i + \sum_{i \neq j} a_{ij} x_j$$ (5.5.30)

from which it is possible to solve for the unknown

$$x_i = \frac{1}{a_{ii}} \left\{ b_i - \sum_{i \neq j} a_{ij} x_j \right\}.$$ (5.5.31)

Hence, if all x_j are known exactly such that $i \neq j$, eqn (5.5.31) can be used to calculate x_i. The reason for solving for x_i and not one of its neighbours is that because a_{ii} is the largest element in the ith row, x_i will be the element most heavily effected by this row.

As discussed in section 5.2, this situation is not going to arise with the values of x_j originating from a guess at the true solution with repeated application of

this method moving the guess toward an accurate estimate of the true solution. Label the estimate of x_j after k iterations have been performed on the original guess as x_j^k. Then the next round of the iteration will produce new estimates from

$$x_i^{k+1} = \frac{1}{a_{ii}} \left\{ b_i - \sum_{i \neq j} a_{ij} x_j^k \right\} \tag{5.5.32}$$

where i will run through the full n elements of $\mathbf{x}$ in order.

From a programming prospective, the summation is slightly awkward as an element has to be missed out. However this can be avoided by including the $i = j$ situation in the summation and simple add on x_i^k outside the parenthesis, as shown

$$x_i^{k+1} = x_i^k + \frac{1}{a_{ii}} \left\{ b_i - \sum_{j} a_{ij} x_j^k \right\}. \tag{5.5.33}$$

In words, the new estimate of x_i equals the old one plus a correction. In this form the algorithm is known under a variety of names such as the Point Simultaneous Relaxation Method, the Point Jacobi Method and the Method of Simultaneous Displacements.

One problem associated with any algorithm based on eqn (5.5.33) is that there is no control over the size of the correction term. If the original estimate at the solution, $\mathbf{x}^0$, is not accurate then the size of the steps taken by the correction term will be so large that the method may well fail to converge to the actual solution. The solution to this is the introduction of a relaxation factor, κ, on the correction term which will ensure that this situation will not arise. Hence the governing equation of the algorithm becomes

$$x_i^{k+1} = x_i^k + \frac{\kappa}{a_{ii}} \left\{ b_i - \sum_{j} a_{ij} x_j^k \right\}. \tag{5.5.34}$$

The method based on eqn (5.5.34) is called the Point Simultaneous Over-relaxation Method. In favourable circumstances, κ may be greater than one, but κ is usually much less than one to obtain slow but reliable convergence.

Another improvement can be made if the fact that the improved estimates of x_i^k are made in order of increasing i. Hence to increase the rate of convergence, the most recent approximation of the solution can be used by incorporating the

values of x_j^{k+1} in to the summation in eqn (5.5.34) for all $j < i$, which gives

$$x_i^{k+1} = x_i^k + \frac{\kappa}{a_{ii}} \left\{ b_i - \sum_{j<i} a_{ij} x_j^{k+1} - \sum_{j\geq i} a_{ij} x_j^k \right\}. \qquad (5.5.35)$$

The algorithm based on eqn (5.5.35) is known as the Point Successive Over-relaxation Method (PSOM), the method used by this research. If the relaxation factor κ is set to one, then the method is also known as the Method of Successive Displacements, the Point Successive Relaxation Method, and the Gauss-Seidel Method.

It should be noted that this method is intrinsically asymmetrical and as a result will produce slightly asymmetric solutions [51]. Also it should be noted that by using the most recent solution approximations where available, it is possible to store $\mathbf{x}^k$ and $\mathbf{x}^{k+1}$ in the same array which reduces the memory demand on the running computer.

The speed with which the PSOM will converge depends on the values of the starting guess and the relaxation factor. For a starting estimate of the solution, the only real guideline is the users' own personal experience which should be utilised as much as possible. The solution vector should have similar traits to the vector of knowns so a reasonable guess would be to try starting the iterative process off with $\mathbf{x} = \mathbf{b}$. As indicated previously, it is possible to force convergence by using a small enough relaxation factor, but it is not desirable to have a method which will always take very small, tentative steps toward a solution as this would cause the runtime to make the method unfeasible. It is possible to obtain an optimum value for κ from the largest eigenvalue of A, which in turn can be approximated by the relative magnitudes of $\mathbf{x}^k$ and $\mathbf{x}^{k+1}$ but this adds more computation time to the calculation. Therefore the most common approach to deciding on a relaxation factor is through trial and error[51].

5.5.4   Suitability Discussion.

As stated above, this is by far the simplest method considered but it still allows all the necessary control outlined in section 5.2.

As an iterative process, it allows access to the values of $\mathbf{u}$ and $\mathbf{q}$ after every iteration so these values can be keep within the constraints that are set in the

problem. Also there is easy access to the polarization relation, which gets applied after every iteration, which will allow the stray currents to be removed from the model.

Thus the PSOM shares all the benefits of the Conjugate Gradient method but it also has some very important other benefits. The inclusion of the relaxation factor κ in eqn (5.5.34) means that the directions in which the solutions are sought can easily be modified, which makes the PSOM unique out of all the methods considered in satisfying this key criteria. Also the requirements on A in eqn (5.2.1) are very simple. In eqn (5.2.2), this condition translates to the diagonal elements of H being larger that its neighbours in the row. In the derivation of the BEM method, it is shown that the diagonal elements have $\frac{1}{2}$ added to the values of the integrals performed to calculate the matrix entries. It follows that the diagonal elements of H should be larger than its neighbours satisfying the condition so the PSOM can be applied without any pre-conditioning.

5.6   Conclusion

To conclude, various methods have been considered of both direct and iterative type. The direct methods were very robust but did not allow enough access to the calculated values of **u** and **q** to be considered as first choice solution methods. However, the SVD was the only method considered which would offer a solution when the matrix A was singular so this method should be kept as a backup for when this situation arises.

To get good access to the values of the variables, iterative methods were considered to be more appropriate. The first methods of the type considered were the Lanczos and the Conjugate Gradient methods which satisfied all the key criteria except the ability to control the search directions which is necessary to help caress the estimate of the solution toward the actual solution. The only method which allowed this property was the PSOM which also satisfied the other criteria and hence it is this method which is used as the first choice method for finding the solution to eqn (5.2.2).

Using the PSOM, eqn (5.2.2) can be solved to find the values of the potential, u, and its flux, q, on the boundary of the domain. These results however are not the end point of the calculation as it is necessary to use them to calculate

the corrosion related magnetic field within the domain. The standard method for doing this uses the Biot-Savart Law, but this method has some significant drawbacks, so an alternative method was developed.

Chapter 6

Calculation of the Magnetic Field

6.1   Introduction

Once the boundary element method (BEM) has been applied to the ship and sea domain, the results will provide known values for the electric potential, u, and the outward normal derivative of the potential, q, on the boundary. The objective of this work is to evaluate the corrosion related magnetic signature of the ship, hence it is necessary to use these values to calculate the resultant magnetic field at points on the interior of the domain, i.e. in the sea.

This is relatively straightforward to achieve using classical methods, and it is these methods which are commonly applied by those working in this area [52]. However, these 'classical' methods have a counterintuitive element about them which indicates the existence of a more direct approach. Investigation of these suspicions have indeed led to a new method being proposed which is shown below.

However before this proposed method is described, the classical approach will be explained and questioned.

6.2   The Accepted Method

Assume that the interior of the domain has been discretized into an array of points labelled (i, j, k). With the values of u and q known for all elements on the boundary, it is possible to use eqn (3.5.20) from the derivation of the BEM to calculate the potential at any of these interior points. To recap and update the notation, this equation says

$$u_{i,j,k} = \sum_{p=1}^{n} q_p G_{ijk,p} - \sum_{p=1}^{n} u_p H_{ijk,p} \qquad (6.2.1)$$

where as before

$$G_{ijk,p} = \int_{\Gamma_p} w d\Gamma \text{ and } H_{ijk,p} = \int_{\Gamma_p} \frac{dw}{d\mathbf{n}} d\Gamma$$

(w is the weighting function and p denotes an element on the surface).

With these potentials known at all interior points, it is then possible to calculate the electric field at an interior point from

$$\mathbf{E}_{ijk} = -\nabla V_{ijk}.$$

Since there is no analytic form of V, this differentiation will have to be carried out numerically using finite differences. The current density at a point can now be calculated since

$$\mathbf{J} = \sigma \mathbf{E}$$

where σ is the conductivity of the medium which fills the domain at the point (i, j, k) i.e. the sea water. Finally the magnetic flux density can be calculated from the discretized version of the Biot-Savart Law

$$\mathbf{B} = \frac{\mu_0}{4\pi} \int_{v'} \frac{\mathbf{J} \times \mathbf{R}}{R^3} dv' = \frac{\mu_0}{4\pi} \sum_{v'} \frac{\mathbf{J} \times \mathbf{R}}{R^3} dv'$$

which leads to the magnetic field strength at (i, j, k).

This method is relatively straightforward and hence commonly applied. However it has the major drawback that the interior of the domain needs to be discretized to calculate the fields via a series of time-consuming computations providing intermediate values at the interior points, many of which may be of no interest. Since each set of variables depend linearly on the previous set (e.g. $\mathbf{B}$ on $\mathbf{J}$), the $\mathbf{B}$ values depend linearly on the variables of the system, i.e. the u and q values on the boundary, although the relation appears to be very tortuous.

The numerical evaluation of the magnetic field at an arbitrary point within the domain using standard finite difference techniques is presented in appendix C, and the result indicates total cancellation of the contribution of internal points. This supports the proposal that the magnetic field can be calculated directly from

the u and q values on the boundary.

6.3 The Proposed Method

6.3.1 Introduction

It has been shown in appendix C that it appears unnecessary to perform the intermediate calculation of the electric potential, the electric field, and the current density at interior points within the domain before obtaining a value for the magnetic field at some other point. For this claim to be substantiated there must be a full analytical proof of a theorem which states that the magnetic field within a domain where the electric potential and its outward normal derivative are known on the boundary, depends solely on these known values.

Before such a proof is attempted, it is necessary to revise some basic vector identities which will be used in the proof.

6.3.2 Vector Identities

The following vector identities and theorems can be found in most textbooks that cover vector calculus [26]. Nonetheless, since they play a crucial role in the development of an attempted proof of the proposed theorem, they have been quoted below, along with proofs for the theorems.

Identity 1. *Let f be a scalar function and $\mathbf{A}$ a vector function, then*

$$\nabla \cdot (f\mathbf{A}) = (\nabla f) \cdot \mathbf{A} + f (\nabla \cdot \mathbf{A}).$$

Identity 2. *Let a and b be scalar functions, then*

$$\nabla (ab) = a\nabla b + b\nabla a.$$

Identity 3. *Let f be a scalar function, then*

$$\nabla \times (\nabla f) = 0.$$

Identity 4. *Let f be a scalar function and* $\mathbf{A}$ *a vector function, then*

$$\nabla \times (f\mathbf{A}) = (\nabla f) \times \mathbf{A} + f\,(\nabla \times \mathbf{A}) .$$

Identity 5. *Let* $\mathbf{A}$ *be a vector function and let v be a volume enclosed by the surface s, with d$\mathbf{s}$ pointing in the direction of the unit normal out of the volume, then*

$$\int_s \mathbf{A} \times d\mathbf{s} = -\int_v (\nabla \times \mathbf{A})\,dv$$

In addition to these identities, the following theorems are required.

Theorem 2. *For any function f,*

$$\int_v \nabla f\,dv = \int_s f\,d\mathbf{s} \tag{6.3.1}$$

where v is a volume bounded by the surface s, and d$\mathbf{s}$ points in the direction of the unit normal out of the volume.

Proof. Let $\mathbf{a}$ be any constant vector. Using vector identity 1

$$
\begin{aligned}
\mathbf{a} \cdot \int_v \nabla f\,dv &= \int_v \nabla \cdot (f\mathbf{a})dv - \int_v f\,(\nabla \cdot \mathbf{a})\,dv \\
&= \int_s f\mathbf{a} \cdot d\mathbf{s} - 0 \text{ (from the divergence theorem and } \nabla \cdot \mathbf{a} = 0) \\
&= \mathbf{a} \cdot \int_s f\,d\mathbf{s}.
\end{aligned}
$$

Since $\mathbf{a}$ is an arbitrary vector,

$$\int_v \nabla f\,dv = \int_s f\,d\mathbf{s}.$$

$\square$

Theorem 3. *Consider a vector* $\mathbf{R}$ *such that* $\mathbf{R} = \mathbf{r} - \mathbf{r}'$ *(where* $\mathbf{r} = (x, y, z)$ *and* $\mathbf{r}' = (x', y', z')$*). If* ∇ *and* ∇' *are the gradient operators associated with* $\mathbf{r}$ *and* $\mathbf{r}'$ *respectively, then*

$$\nabla' \frac{1}{R} = -\nabla \frac{1}{R}.$$

Where

$$\nabla = \mathbf{i}\frac{\partial}{\partial x} + \mathbf{j}\frac{\partial}{\partial y} + \mathbf{k}\frac{\partial}{\partial z}$$

and

$$\nabla' = \mathbf{i}\frac{\partial}{\partial x'} + \mathbf{j}\frac{\partial}{\partial y'} + \mathbf{k}\frac{\partial}{\partial z'}.$$

Proof. It is known that

$$\frac{1}{R} = \frac{1}{\sqrt{(x-x')^2 + (y-y')^2 + (z-z')^2}},$$

therefore

$$
\begin{aligned}
\nabla'\frac{1}{R} &= \mathbf{i}\frac{\partial}{\partial x'}\frac{1}{R} + \mathbf{j}\frac{\partial}{\partial y'}\frac{1}{R} + \mathbf{k}\frac{\partial}{\partial z'}\frac{1}{R} \\
&= \mathbf{i}\frac{x-x'}{R^3} + \mathbf{j}\frac{y-y'}{R^3} + \mathbf{k}\frac{z-z'}{R^3} \\
&= \frac{\mathbf{R}}{R^3} \\
&= -\nabla\frac{1}{R}.
\end{aligned}
$$

$\square$

6.3.3 Proof of the Proposed Theorem.

Let there be a current source with density $\mathbf{J}'$ in a volume dv' at $\mathbf{r}'$, then the magnetic flux density at $\mathbf{r}$ is

$$
\begin{aligned}
d\mathbf{B} &= \frac{\mu_0}{4\pi}\frac{\mathbf{J}' \times \mathbf{R}}{R^3}dv' \text{ (where } \mathbf{R} = \mathbf{r} - \mathbf{r}') \\
&= \frac{\mu_0}{4\pi}\mathbf{J}' \times \left(-\nabla\frac{1}{R}\right) dv' \text{ (from theorem 3)} \\
&= \frac{\mu_0}{4\pi}\nabla\frac{1}{R} \times \mathbf{J}'dv' \\
&= \frac{\mu_0}{4\pi}\left[\nabla \times \left(\frac{\mathbf{J}'}{R}\right) - \frac{1}{R}(\nabla \times \mathbf{J}')\right] dv' \text{ (using vector identity 4)} \\
&= \nabla \times \left[\frac{\mu_0}{4\pi}\frac{\mathbf{J}'}{R}\right] dv' \\
&= \nabla \times d\mathbf{A} \text{ where } \mathbf{A} \text{ is the vector potential.}
\end{aligned}
$$

Notice that $\nabla \times \mathbf{J}' = 0$ because $\mathbf{J}'$ exists only at the source point $\mathbf{r}'$ whilst $\nabla\times$ only effects variables which are at the point of evaluation $\mathbf{r}$, whilst $\nabla \times \frac{\mathbf{J}'}{R} \neq 0$ because R is dependent on $\mathbf{r}$ as well as on the source point $\mathbf{r}'$.

To find $\mathbf{A}$ it is necessary to integrate over the entire volume v',

$$\mathbf{A} = \frac{\mu_0}{4\pi} \int_{v'} \frac{\mathbf{J}'}{R} dv'.$$

So far, this is just the usual derivation of the formula for the vector potential, but in our case the current is of a very specific nature with $\mathbf{J}' = \sigma'\mathbf{E}' = -\sigma'\nabla'u'$ (u' being the electric potential at $\mathbf{r}'$). Therefore

$$
\begin{aligned}
\mathbf{A} &= -\frac{\mu_0}{4\pi} \int_{v'} \left(\frac{\sigma'}{R}\right) \nabla'u' dv' \\
&= -\frac{\mu_0}{4\pi} \int_{v'} \left[\nabla'\left(\frac{\sigma'u'}{R}\right) - u'\nabla'\left(\frac{\sigma'}{R}\right)\right] dv' \quad \text{(using vector identity 2)} \\
&= -\frac{\mu_0}{4\pi} \int_{s} \frac{\sigma'u'}{R} d\mathbf{s} + \frac{\mu_0}{4\pi} \int_{v'} u'\nabla'\left(\frac{\sigma'}{R}\right) dv' \quad \text{(using theorem 2)} \\
&= -\frac{\mu_0}{4\pi} \int_{s} \frac{\sigma'u'}{R} d\mathbf{s} + \frac{\mu_0}{4\pi} \int_{v'} u'\left\{\frac{1}{R}\nabla'\sigma' + \sigma'\nabla'\left(\frac{1}{R}\right)\right\} dv'
\end{aligned}
$$

$$\text{(using vector identity 2).}$$

This last term may be written as

$$\frac{\mu_0}{4\pi} \int_{v'} \sigma'u'\nabla'\left(\frac{1}{R}\right) dv' = -\nabla\left(\frac{\mu_0}{4\pi} \int_{v'} \sigma'u'\left(\frac{1}{R}\right) dv'\right).$$

which uses the fact that ∇' acts only on the point $\mathbf{r}'$ whilst ∇ acts only on the point $\mathbf{r}$. Thus theorem 3 can be used to perform the change

$$\nabla'\left(\frac{1}{R}\right) \rightarrow -\nabla\left(\frac{1}{R}\right)$$

and since ∇ has no effect on any factor other than the $\frac{1}{R}$, the gradient function can be taken out the front as shown.

Since the curl of a gradient is zero, this last term does not contribute to $\mathbf{B} = \nabla \times \mathbf{A}$ which leaves

$$\mathbf{A} = -\frac{\mu_0}{4\pi} \int_{s'} \frac{\sigma'u'}{R} d\mathbf{s}' + \frac{\mu_0}{4\pi} \int_{v'} \frac{u'}{R} \left(\nabla'\sigma'\right) dv'. \tag{6.3.2}$$

as the only contributing factors to $\mathbf{A}$. If σ' is constant, then $\nabla'\sigma' = 0$ yielding

$$\mathbf{A} = -\frac{\mu_0}{4\pi}\sigma' \int_{s'} \frac{u'}{R} d\mathbf{s}'. \tag{6.3.3}$$

This is the vector potential at $\mathbf{r}$. Therefore the magnetic flux density at $\mathbf{r}$ is given by $\mathbf{B} = \nabla \times \mathbf{A}$. Observe that

$$\frac{\partial}{\partial x}\frac{1}{R} = -\frac{(x-x')}{R^3} \ , \ \frac{\partial}{\partial y}\frac{1}{R} = -\frac{(y-y')}{R^3} \ , \ \frac{\partial}{\partial z}\frac{1}{R} = -\frac{(z-z')}{R^3}$$

which basically says that

$$\nabla \times \frac{d\mathbf{s}'}{R} = \frac{1}{R^3} d\mathbf{s}' \times \mathbf{R}$$

using vector identity 4

Hence the expression for the magnetic flux density becomes

$$\mathbf{B} = -\frac{\mu_0}{4\pi}\sigma' \int_{s'} \frac{u'}{R^3} d\mathbf{s}' \times \mathbf{R} \tag{6.3.4}$$

so the magnetic field can be calculated from

$$\mathbf{H} = -\frac{1}{4\pi}\sigma' \int_{s'} \frac{u'}{R^3} d\mathbf{s}' \times \mathbf{R} \tag{6.3.5}$$

i.e. a surface integral.

In the calculation performed as part of the research, it was actually the magnetic flux density which was calculated using eqn (6.3.4), and not the actual magnetic field. The key point is that this formula can calculate the magnetic field from the potentials u' on the surface boundary s' which are the u values from the BEM calculation.

6.3.4 Non-Constant Conductivity

The proposed method claimed that the magnetic field at any point could be calculated directly from the values of u and q on the boundary of the domain. The proof above proves this to be the case for constant conductivity within the domain. However it can be shown that the proposed method also holds true when

this is not the case, although further terms need to be included. Return to eqn (6.3.2) but now assume that the conductivity within the volume is not constant. In this case the term

$$\int_{v'} \frac{u'}{R} \left(\nabla' \sigma' \right) dv'$$

must also be calculated.

Suppose a surface s separates two volumes in the domain with constant conductivities σ_1' and σ_2' respectively. If dv' is entirely within one of these volumes, $\nabla' \sigma' = 0$ and there is no contribution to the integral. If dv' is a small cylinder of
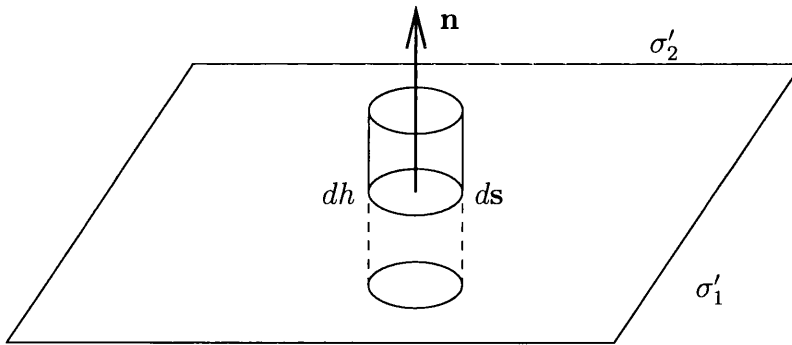
Figure 6.1: Surface element separating two different conductivities.

height dh that crosses the surface as shown in figure 6.1, then

$$\nabla' \sigma' dv' = \left(\frac{\sigma_2' - \sigma_1'}{dh} \right) dh ds \mathbf{n} \qquad (6.3.6)$$

$$= (\sigma_2' - \sigma_1') ds \mathbf{n} \qquad (6.3.7)$$

where $\mathbf{n}$ is a unit normal directed from σ_1' to σ_2'. Then

$$\int_{v'} \frac{u'}{R} \left(\nabla' \sigma' \right) dv' = \int_{s} \frac{u'}{R} \left(\sigma_2' - \sigma_1' \right) d\mathbf{s}$$

where $d\mathbf{s}$ is directed from σ_1' to σ_2'. This is another surface integral over a surface which does *not* lie on the boundary, hence the potentials u' must be calculated on this surface using equation 6.2.1.

6.3.5 Dependence on the Potential?

One problem that appears to have arisen is the dependence of the magnetic field on the absolute magnitude of the potential, u'. In theory $\mathbf{B} \propto \nabla u'$ so if the potential u' was increased by 100V everywhere, the magnetic field $\mathbf{B}$ should stay the same. However the eqn (6.3.4) gives $\mathbf{B} \propto u'$ which indicates that $\mathbf{B}$ would change if u' was increased everywhere. In response to this apparent problem consider the following.

If $u' \to u' + \delta u$, the change in $\mathbf{B}$ is

$$
\begin{aligned}
\delta \mathbf{B} \quad \propto \quad & \int \delta u \frac{ds' \times \mathbf{R}}{R^3} \\
= \quad & -\delta u \int \nabla' \left(\frac{1}{R} \right) \times ds' \text{ (from proof of theorem 3)} \\
= \quad & +\delta u \int \left[\nabla' \times \nabla' \left(\frac{1}{R} \right) \right] dv \text{ (using vector identity 5)} \\
= \quad & 0 \text{ (curl of a gradient is 0).}
\end{aligned}
$$

Therefore adding a constant to u' does not change the magnetic field, as required.

6.4 Test Calculations.

The most reliable method of verifying the validity of this new formula eqn (6.3.4) is to calculate the magnetic fields produced in some classical cases, namely those of:

1 . the field from a circular coil

2 . the field from an infinite wire

3 . the field from a finite wire

6.4.1 The Field from a Circular Coil

This is a common problem that can be found in most general physics textbooks [53]. To apply our method, consider the following problem:

The magnetic field will be evaluated at the centre of the coil. Suppose the cross-section of the coil is square with side a, where $a \ll R$. The coil has a small
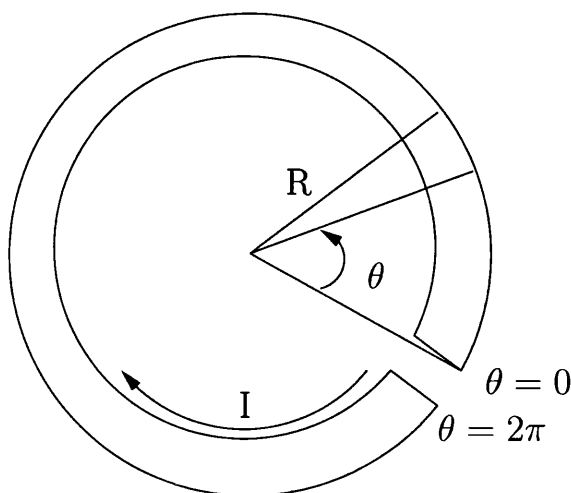
Figure 6.2: Diagram for calculation of the magnetic field at the centre of a circular coil

break at $\theta = 0$, $\theta = 2\pi$. If the resistivity of the coil is ρ then the resistance of the coil is given by

$$R_0 = \frac{\rho L}{A} = \frac{1}{\sigma}\frac{2\pi R}{a^2} \tag{6.4.1}$$

where σ is the conductivity of the wire.

If the current flowing round the loop is I, and the electric potential is set at one side of the break to be zero, i.e. $u_{\theta=0} = 0$, then

$$u_{\theta=2\pi} = IR_0 \tag{6.4.2}$$
$$= \frac{I2\pi R}{\sigma a^2}. \tag{6.4.3}$$

To use the new formula eqn (6.3.4) requires integration over the surfaces of the coil. Firstly consider the integration over the inner and outer surfaces of the coil, denoted A and B in figure 6.3. Here $d\mathbf{S}$ is parallel and anti-parallel to $\mathbf{R}$, so $d\mathbf{S} \times \mathbf{R} = 0$, i.e. these make no contribution to the magnetic field at $\mathbf{R}$.
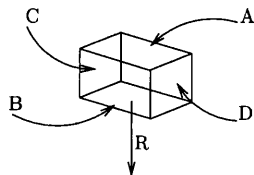
Figure 6.3: A segment of the circular coil

Secondly consider the front and back surfaces denoted C and D in figure 6.3. In this case the dS for either face is exactly opposite so the contributions to the field at **R** cancel each other (see figure 6.4).
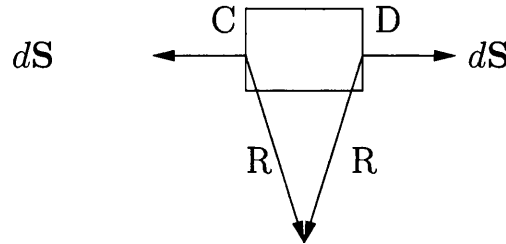
Figure 6.4: Cancellation of the contribution from the front and back faces of the circular coil

This means that the only source of field can come from the ends, either side of the small break. The integral for $\theta = 0$ is 0 since at this point $u = 0$. For $\theta = 2\pi$,

$$\mathbf{B} = -\frac{\mu_0}{4\pi}\sigma'\left(\frac{I2\pi R}{\sigma a^2}\right)\frac{a^2}{R^2} \text{ (out of page)},\qquad(6.4.4)$$

$$= \frac{\mu_0 I}{2R} \text{ (into page)}.\qquad(6.4.5)$$

where σ' is the conductivity at the boundary of the medium in which the field is evaluated. In this case the only boundary is the wire so $\sigma' = \sigma$. Hence the cancellation to leave this answer which matches that obtained by classical methods.

6.4.2   Field from a Long Straight Wire of Rectangular Cross-section.

Again this is a standard physics example which can be found in most general physics textbooks [54]. To apply the postulated method, consider the wire shown in figure 6.5. Its height is $2a$ whilst its width is w.

The field will be calculated at some distance Z below the wire, which should be thin, i.e. $a << Z$ and $w << Z$. From the previous example, it is known that the integrals over the front and rear faces will cancel. So consider the top face shown in figure 6.6.
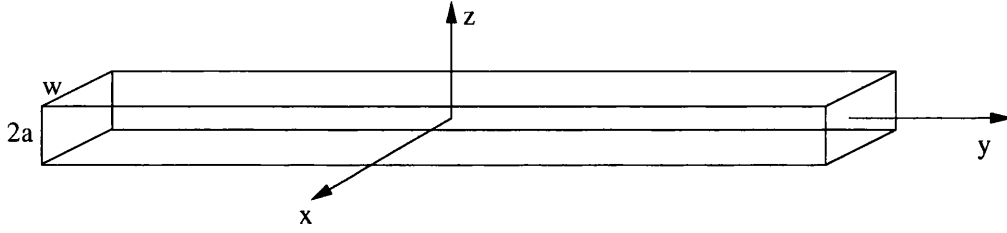
Figure 6.5: An effectively infinitely long straight wire.
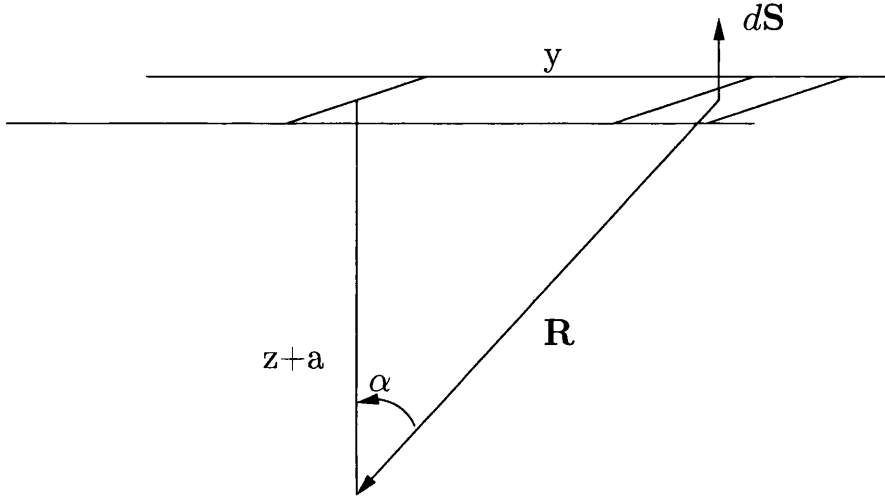
Figure 6.6: Contribution of the magnetic field at $\mathbf{R}$ from the top face.

Let ν denoted the voltage change per metre, so at a point along the top face the electric potential will be $u = \nu y$. Further, the small element of surface area is $d\mathbf{S} = wdy\mathbf{k}$, whilst $\mathbf{R} = -y\mathbf{j} - (z + a)\mathbf{k}$. Therefore

$$d\mathbf{S} \times \mathbf{R} = +wydy\mathbf{i}, \tag{6.4.6}$$

so, with σ the conductivity of the wire, eqn (6.3.4) says

$$\mathbf{B}_{top} = -\frac{\mu_0 \sigma}{4\pi} \int_{-\infty}^{\infty} \frac{ud\mathbf{S} \times \mathbf{R}}{R^3} \tag{6.4.7}$$

$$= -\frac{\mu_0 \sigma w}{4\pi}\mathbf{i} \int_{-\infty}^{\infty} \frac{\nu y y dy}{\left(y^2 + (z + a)^2\right)^{\frac{3}{2}}} \tag{6.4.8}$$

$$= -\frac{\mu_0 \sigma w \nu}{4\pi}\mathbf{i} \int_{-\infty}^{\infty} \frac{y^2 dy}{\left(y^2 + (z + a)^2\right)^{\frac{3}{2}}}. \tag{6.4.9}$$

This integral is divergent. The contribution from the bottom face can be found by the same calculation only it is necessary to make the substitution $a \rightarrow -a$. Having done this, it is then necessary to take the difference between the two since the $d\mathbf{S}$ vectors point in opposite directions. However since the aim is to compare this solution obtained here for that for the field from a long thin wire, the a values will have to be made extremely small so the effect of calculating this difference is actually to perform the derivative $2a\frac{d}{dz}$. So

$$
\begin{aligned}
\mathbf{B} &= \mathbf{B}_{top} - \mathbf{B}_{bottom} & (6.4.10) \\
&= -\frac{\mu_0 \sigma w \nu}{4\pi} \mathbf{i} 2a \int_{-\infty}^{\infty} y^2 dy \, (-3z) \frac{1}{(y^2 + z^2)^{\frac{5}{2}}} & (6.4.11) \\
&= \frac{3\mu_0 \sigma 2a w \nu z}{4\pi} \mathbf{i} \int_{-\infty}^{\infty} \frac{y^2 dy}{(y^2 + z^2)^{\frac{5}{2}}}. & (6.4.12)
\end{aligned}
$$

To perform this integral requires the standard substitution

$$
y = z \tan \alpha \tag{6.4.13}
$$

so that

$$
\begin{aligned}
y^2 + z^2 &= z^2 \left(1 + \tan^2 \alpha\right) & (6.4.14) \\
&= z^2 \sec^2 \alpha, & (6.4.15)
\end{aligned}
$$

and

$$
dy = z \sec^2 \alpha d\alpha. \tag{6.4.16}
$$

The integral in 6.4.12 now becomes

$$
\begin{aligned}
\int_{-\frac{\pi}{2}}^{\frac{\pi}{2}} \frac{z^2 \tan^2 \alpha}{z^5 \sec^5 \alpha} z \sec^2 \alpha d\alpha &= \frac{1}{z^2} \int_{-\frac{\pi}{2}}^{\frac{\pi}{2}} \sin^2 \alpha \cos \alpha d\alpha & (6.4.17) \\
&= \frac{1}{z^2} \frac{2}{3}. & (6.4.18)
\end{aligned}
$$

If the resistance of 1 metre is $\frac{1}{\sigma 2aw}$, the current in the wire is

$$
\begin{aligned}
I &= \frac{V}{R} & (6.4.19) \\
&= \nu \sigma 2aw. & (6.4.20)
\end{aligned}
$$

Now substituting eqn (6.4.18) and eqn (6.4.19) into eqn (6.4.12) gives

$$\mathbf{B} = \mu_0 I \frac{1}{z} \frac{2}{4\pi} \mathbf{i} \qquad (6.4.21)$$

$$= \mu_0 \frac{I}{2\pi z} \mathbf{i} \qquad (6.4.22)$$

which is the solution provided by classical methods.

6.4.3 Field for a Finite Straight Wire

This problem follows on from the previous example, and sample solutions using classical physics techniques can be found in [55, 56]. To apply the proposed method, use the wire described in the previous case, only this time it has a finite length as indicated in figure 6.7.
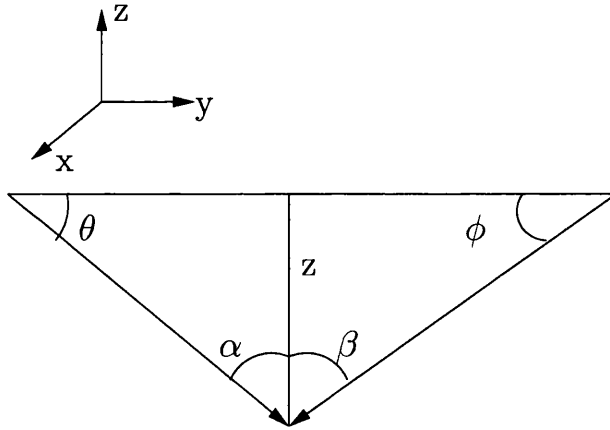
Figure 6.7: Magnetic field from a finite wire

In this situation the integral in eqn (6.4.12) may be written (using the same substitution as eqn (6.4.13)) as

$$\int_{-\alpha}^{\beta} \frac{1}{z^2} \sin^2 \alpha \cos \alpha \, d\alpha \qquad (6.4.23)$$

which when substituted into eqn (6.4.12) gives the following expression for the

contribution from the wire, excluding end faces, to the magnetic field

$$\mathbf{B} = \frac{3\sigma 2aw\nu z\mu_0}{4\pi} \int_{-\alpha}^{\beta} \frac{1}{z^2} \sin^2\alpha\cos\alpha\, d\alpha \tag{6.4.24}$$

$$= 2aw\nu\sigma\frac{3\mu_0}{4\pi z}\frac{1}{3}\left[\sin^3\beta + \sin^3\alpha\right] \tag{6.4.25}$$

$$\mathbf{B} = \frac{\mu_0 I}{4\pi z}\left[\sin^3\beta + \sin^3\alpha\right]. \tag{6.4.26}$$

Now the ends need to be considered (see figure 6.8).
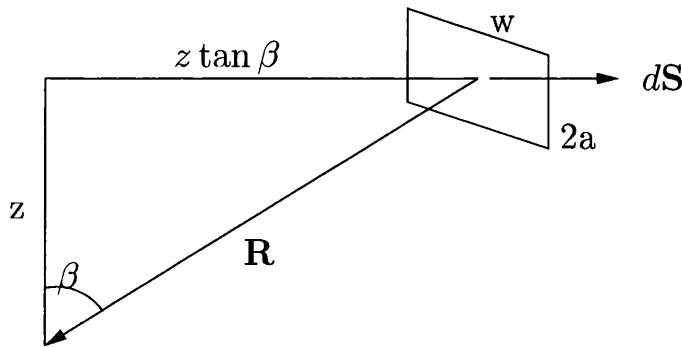
Figure 6.8: The contribution from the end of a finite wire

Again using ν is the voltage change per metre, the potential at the end shown is

$$u = \nu z\tan\beta. \tag{6.4.27}$$

The cross product in eqn (6.3.4) may be written as

$$d\mathbf{S} \times \mathbf{R} = 2aw\mathbf{j} \times (z\tan\beta(-\mathbf{j}) + z(-\mathbf{k})) \tag{6.4.28}$$

$$= zd\mathbf{S}(-\mathbf{i}) \text{ i.e. into the plane.} \tag{6.4.29}$$

Since $R = z\sec\beta$, the contribution from this end to the magnetic field may be written as

$$\mathbf{B} = -\frac{\sigma\mu_0}{4\pi}u\frac{d\mathbf{S} \times \mathbf{R}}{R^3} \tag{6.4.30}$$

$$= \mathbf{i}\frac{\mu_0\sigma\nu 2aw}{4\pi}\frac{z}{z^3\sec^3\beta}z\tan\beta \tag{6.4.31}$$

$$\mathbf{B} = \mathbf{i}\frac{\mu_0 I}{4\pi z}\sin\beta\cos^2\beta. \tag{6.4.32}$$

A similar calculation shows that the contribution from the other end is

$$\mathbf{B} = \mathbf{i}\frac{\mu_0 I}{4\pi z} \sin\alpha \cos^2\alpha. \tag{6.4.33}$$

To get an expression for the total magnetic field, equations 6.4.32 and 6.4.33 are combined with equation 6.4.26 to give

$$
\begin{aligned}
\mathbf{B}_{total} &= \mathbf{i}\frac{\mu_0 I}{4\pi z}\left[\sin^3\beta + \sin\beta\cos^2\beta + \sin^3\alpha + \sin\alpha\cos^2\alpha\right] & (6.4.34) \\
&= \mathbf{i}\frac{\mu_0 I}{4\pi z}\left[\sin\alpha + \sin\beta\right] & (6.4.35) \\
\mathbf{B}_{total} &= \mathbf{i}\frac{\mu_0 I}{4\pi z}\left[\cos\theta + \cos\phi\right]. & (6.4.36)
\end{aligned}
$$

which is the expected solution from the classical calculation.

6.5 Conclusion

These three calculations in the previous section show that the formula proposed for calculating the magnetic fields from the values of the potential on the boundary of a domain appears correct. This means that once the BEM equations have been solved providing values for the potentials on the discretized boundary of a ship in a finite box of sea water, the magnetic field at any point inside the sea water domain may be calculated directly from these potentials.

Chapter 7

Analysis of Linear Test Calculations

7.1 Introduction

The preceding chapters have covered various technical aspects of the method which has been developed to calculate the corrosion related magnetic field (or signature) from a ship corroding in sea water. It now remains to combine all of these into one method and then test the method by evaluating the CRM field from a ship in various situations.

Chapter 2, concerning calculations of magnetic field from simple dipole models, provided a method in section 2.3.3 for calculating the field contribution from a straight wire between a current absorbing sink and a current emitting source near a non-conducting boundary which represented the sea surface. This result can be used to model the return currents through the ship. As previously mentioned, when the corrosion currents leave the corroding parts of the ship (the source), most likely to be areas of the hull, they flow through the sea water to another area of the ship which is at a lower potential (the sink), most likely the propeller. To prevent a build up of charge at the sink, the current must then flow back along the internal structure of the ship to the source thus completing the current loop. By assuming that this return current is along a straight wire, the equation 2.3.26 can be used to calculate the contribution from the return current to the CRM field.

Chapters 3 and 4 introduced the BEM which will be used to model the ship corroding in a finite tank of sea water, and showed that by discretising the boundary of the domain using constant triangular elements, a new method of calculating

numerical integrations could be used based around the moments of the triangles. Using this new method, the BEM coefficient matrices will be calculated.

Chapter 5 then investigated the most suitable solving algorithm for the resulting large, dense matrix equation which arises from the BEM description of the system. The method chosen was the PSOM which uses eqn (5.5.35) to iterate an estimate at the solution closer to the actual solution. The reason this method was chosen over the others was because it best satisfied a list of key criteria. Depending on the type of boundary on the sea box, values for u or q would be known [17]. For the non-conducting sea bed and sea surface, $q = 0$, while the other faces are assumed to represent conducting boundaries, so $u = 0$ on them. There were no known values for the potential u or its outward flux q on any of the elements on the ship. However using the electrochemical series it was possible to estimate a range of suitable potentials for the various materials on the ship which were exposed to the sea water. The PSOM allowed access to the variables at all times so that they could be kept within these constraints.

Since there are no knowns in the model on the ship elements it is necessary to make an initial guess at one set of variables, in these calculations the potentials u, and then use a relation called the polarization relation to calculate the corresponding q values. This is covered in more detail in section 7.2. Therefore for each estimate at the solution, both u and q are known and the accuracy to the actual solution can be checked using the BEM equation (eqn (5.2.2)). The PSOM and the polarization relation also enables the range of acceptable potentials to be amended to ensure that the currents that are flowing in the sea are of magnitudes that would be expected from analysis of real ships in sea water.

The discrepancy of the actual solution can then be used by the PSOM to move the estimate at the solution closer to an acceptable one. Since the final solution could lie anywhere within the acceptable range of potentials, the PSOM must search for the most accurate solution and this search may be aided in the PSOM by the user who can modify the search directions which is obviously beneficial as it prevents the PSOM looking in completely the wrong place for a solution.

To further complicate the calculations, it is necessary that all currents that result from the corrosion of the ship flow to other regions of the ship and are not permitted to escape the model (the 'no stray currents' condition). This is a difficult condition to compensate for but may be satisfied by using the discrepancy

between the emitted and absorbed corrosion currents to alter the potential V of the internal structure of the ship. As the potentials obtained by the BEM are located on the interface between the sea and the ship, this has the effect of altering the values of q which is dependant on the values of u and V. To ensure that this alteration effects the model in the correct manner it is therefore necessary to make the polarization relation a function of $V - u$, which in turn means that the PSOM must allow access to the polarization relation after every new estimate is completed. An intelligent choice of the relaxation factor in the PSOM is made to maximise the rate of convergence of the method. For the following test calculations, each iteration of the PSOM which produced a new estimate at the solution took between one and two seconds on a PC with a 1.8 GHz AMD Athlon processor with 512 MB RAM.

Once this stray current condition has been satisfied, and the BEM equation is accurately solved with values of q giving rise to sea currents which are reasonable from real life experience, the problem can be considered solved. The values of the potentials can then be used with eqn (6.3.4) to calculate the related magnetic field at points within the domain.

Before commencing with the test calculations, the issue of the polarization relation will be addressed in some further detail.

7.2 Polarization Behaviour

The electric potential across the interface between the steel of the hull and the neighbouring sea water determines the surface current density, which is proportional to the variable q. It is crucial to have a realistic relation between V, the potential of the steel, u the potential of the neighbouring sea water and q. The relation depends on electro-potentials e_i, resistance of paint and any other material or organisms covering the surface. This relation is known as the polarization relation, and the relationship chosen obviously plays a significant role in obtaining the solution to the problem.

To test the method described, calculations were carried out using two differing polarization relationships for the hull. In real calculations used in industry, rather than using relationships to represent the polarization, massive tables of data are used which are accumulated from experimental results [6]. The tables exist for

various types of metals and are also dependent on external factors such as the temperature of the sea water, the salinity, the level of calcareous deposits on the surface, the levels of turbulence and flow of the water, and the length of time the test metal has been in the given climate [6, 7]. This data is a closely guarded industrial secret and is very difficult to obtain which meant that it was not available for these test calculations. As a consequence the results that are presented in the following are not wholly realistic, but are intended to show that the methods presented are able to perform the calculations required and would, if real polarization were available, be perfectly capable of providing a detailed analysis of a physical situation.

As mentioned two different polarization relations were used. In chapter 8, the analysis of test calculations which were performed using a non-linear polarization relation is carried out. This relation does complicate the calculation of a solution to the BEM equations and hence was not regarded as being a good starting point for testing the method presented by this research. For a starting point, initial calculations were preformed using a simple linear relation.

7.2.1   Linear Polarization.

The first polarization relation used was one which dealt with the simplest case, where the q and u values were related by a linear relation. The relation used was developed in house and aimed to take into consideration the electrochemical potentials of the metals which could come into contact with the sea water, namely the nickel-aluminium-bronze (NAB) propeller [12], and the steel hull [17]. Also since the model would have to incorporate some level of paint protection (see chapter 1) the relation would also have to be able to include this. The current density normal to the surface J_i is related to the potential across the surface $(V + e_i - u_i)$ via an effective resistance: $\frac{t}{\sigma_{paint}}$ per unit area where t is the thickness of the coating on the element. But $J_i = -\sigma_{sea} q_i$ so

$$q_i = k_i \left(V + e_i - u_i \right) \qquad (7.2.1)$$

where i varies over all elements on the ship (the hull and the propeller). In eqn (7.2.1), V represents the voltage of the metal work on the interior of the ship, e_i represents the electrochemical potential in sea water for the material of

the element being considered, and u_i is the calculated potential from the BEM calculation, which may be thought of as the potential just at the interface between the element and the sea, i.e. just on the outside of any coating on the element [6, 42]. As required, the coefficient k_i can vary for the individual elements and is dependant on both the conductivity of the paint coating and the sea water, as well as the thickness of the paint coating,

$$k_i = \frac{\sigma_{paint}}{\sigma_{sea} t} \tag{7.2.2}$$

where t is the thickness of the coating on the element (whether it be a paint coating or due to some calcareous deposits) and σ denotes the conductivity of the medium indicated by the subscript. For all the calculations performed, the value of k_i for a propeller element was 100 whilst its value on the hull varied depending on the paint coating.

For these calculations, the propeller and the hull were constructed from the metals indicated above which meant that their respective electrochemical potential values in sea water for these calculations were taken as being

$$e_i = -0.4V \quad \forall i \in prop \tag{7.2.3}$$

$$e_i = 0.3V \quad \forall i \in hull \tag{7.2.4}$$

with the values being relative to a saturated hydrogen electrode (SHE). All the potentials mentioned in this work are relative to a SHE. In an attempt to model the real polarization behaviour of the materials as closely as possible within the constraints of a linear relation, these values were obtained from real polarization curves [47]. However further research has indicated that these values may not have been as suitable as originally thought [9, 10, 57]. The propeller and the hull are linked electrically and physically via the propeller shaft which means that their potentials on the inside of any coatings, V, should be the same since the resistance of the shaft, if considered stationary, is minimal. If the transient case was being modelled, the shaft would be rotating which would result in a modulation in the D.C. current flowing through the ship caused by the rotating contact made with the brushes. This topic is considered in more detail on the web-page of Davis Engineering [14, 58] and is not considered here. In this work, the shaft has been removed from the model for simplicity. If it was included, its

corrosion would also have to be considered which would complicate the simple model which is being used. However, the effect of it providing an electrical link between the propeller and the hull is still included and is a vital requirement of the model.

The beauty of this polarization relation is that whilst it may be very simple, it allows the key factors to be modelled.

Firstly, varying degrees of damage to the paint on the hull can be modelled by altering the value of k_i on the required elements. In a physical case, this could correspond to a change in the conductivity of the paint or its thickness. The only condition which should be enforced on the k values is that the propeller should never be less conductive than any painted area of the hull. Also, as mentioned before, the value of V allows the u and q values calculated to be altered to ensure that there are no stray currents in the model, which means that all the currents flowing through the sea due to corrosion return to the ship.

Whilst this relation allows all the physical characteristics of the model to be considered, the linear nature is very unrealistic. Real polarization data is extremely non-linear [6, 17] and to test whether these methods could handle this scenario another relation was required but this is considered later in section 8.2. For now, this linear relation will be used to test the method.

7.3 The Model

The model which was used for these calculations was based on data provided by BAE Systems. It consisted of a box of sea water which had length $500m$ ($-250m \leq x \leq 250m$), breadth $300m$ ($-150m \leq y \leq 150m$), and depth $50m$ ($0m \leq z \leq 50m$). Inserted into the sea surface was the ship. This consisted of a hull and a propeller, with the propeller shaft and the rudder removed to allow the calculation to be as basic as possible. Remember that the aim is to prove that the method developed works, not provide a detailed numerical analysis. The propeller was modelled as a cylinder which had the same surface area as a real propeller. The hull was that of a cruise liner which had roughly the same shape as the majority of ships of similar size. The hull was inserted centrally in the sea surface and was located between $-100m \leq x \leq 175m$, $-19.5m \leq y \leq 19.5m$, with depth in the range $40m \leq z \leq 50m$. The propeller was located a short distance behind

the stern with centre at $(-82m, 0m, 41m)$. As mentioned previously, the u and q values on the ship were related by a polarization relation, while on the sea box boundary the sea surface and sea bed were non-conducting with $q = 0$ and the other faces conducting with $u = 0$. This is also necessary since the physics of the problem so far has contained no reference to a zero of potential. Without this, any constant value can be added to all the potentials without altering the validity of the solution. It turns out that the sum of each row of the H matrix in the BEM is exactly zero, which is consistent with this. It is therefore necessary to choose a value of the electric potential somewhere and this boundary condition does just that. The conductivity of the sea water was taken to be uniform [59] at $5\Omega^{-1}m^{-1}$ [12] and although this is within the acceptable range [13] it is now recognised that this may be a slight over-estimation [8].

7.4 Perfect Paint Coating - Analysis.

This calculation was for the situation where the hull is coated with a highly protective coating, i.e. a coating which has low conductivity. The linear polarization relation (eqn (7.2.1)) was used.

7.4.1 Predicted Behaviour

Before looking at the results obtained from the calculation, it is possible to make some predictions as to the behaviour of the system. It is first necessary to recap the physical meanings and implications of the quantities used to describe the system. q is the normal derivative of the potential u out of the volume of sea water, and so can be regarded as a measure of the negative normal component of E, which will be in the direction of J. So if an element has $q > 0$, this corresponds to the emission of a corrosion current, i.e. the element is corroding.

If the system is considered as a whole, there is a large surface area, namely the hull, which has been coated in a anti-corrosive paint coating. This surface will not corrode significantly and therefore its elements should have values of q that are extremely small in magnitude. Since this paint coating is uniform over the entire hull it is equally possible that it may absorb current as emit it. This means that positive and negative values for q are possible but they will remain extremely small in magnitude. Close to the rear, or stern, of this large well protected hull is

the small cylinder representing the propeller which is unprotected from the effects of the sea water. On the propeller, the values of q will therefore be non-zero. Since no net corrosion currents may stray from the ship, any current emitted from the corroding propeller must be absorbed by some other area of the ship. With the hull being almost non-conductive and unwilling to emit or absorb the currents, it follows that the most probable location for the absorption of the current are the elements on the propeller with the lowest potential. It is known from practise that when the paint on the hull has been damaged, then the corrosion currents will flow from the hull to the propeller which will therefore have a lower potential than the hull. Applying this knowledge here, it follows that the elements on the propeller which are closest to the hull, i.e. those on the 'inward' face, should be less inclined to accept current than those on the outer face. This is because these elements, due to their close proximity to the hull, will be at higher potentials than those elements further from the hull. Hence the elements on the inward region should have positive q values while those on the outward face should have negative q values. Due to the close proximity of the propeller to the stern, it is also possible that the stern may have some elements on it which behave differently from the rest of the hull and have values for q more akin to the behaviour of the closest elements of the propeller.

The potentials of the various elements are difficult to predict because one of the key requirements to having solved the BEM equations is that there are no stray currents. This is obtained by altering V in eqn (7.2.1) which means that the final values obtained for V, $\mathbf{u}$ and $\mathbf{q}$ are all intertwined in a complex optimisation loop. However there should be a smooth distribution of the potential over the ship to avoid the occurrence of unwanted poles. As indicated above, it follows that the potentials on the elements of the propeller nearest the hull should be closer to the hull potentials (i.e. higher) than those further away. With the majority of corrosion activity being focused around the propeller and the stern, it follows that over the majority of the hull, especially toward the bow, the potentials should be fairly constant.

In this calculation, the hull is taken to have $k_i = 1 \times 10^{-6}$ while the propeller has $k_i = 100$. From eqn (7.2.1) it is clear that these values will result in extremely small q_i values on the hull compared with those on the propeller. Since q_i can be though of as the negative of the inward normal component of the electric field,

and

$$\mathbf{J} = \sigma\mathbf{E} \qquad (7.4.1)$$

this will force the currents emitted from the hull due to corrosion to be very low, i.e. very small sea currents, which will correspond to a CRM field of small magnitude. Hence when the CRM field is calculated it should be very small everywhere with a peak in the vicinity of the propeller.

7.4.2 Calculated Behaviour

The results from the BEM calculation are shown on figures 7.1 - 7.4. For the propellers, there are two figures each for the u and the q values to highlight the differences that occur on the inner and outer faces.

Consider first the values of q that occur on the propeller, figure 7.1. On the outer rim of the propeller, the q values are more negative than at any other point which implies that more current is absorbed by the rim than any other area. The negative values of q were predicted but the reasons why the values should be more negative than elsewhere on the propeller are not obvious. This clearly indicates that the corrosion currents, which will always follow the path of least resistance, find it easier to reach the rim and be absorbed. This will be due to the fact that the elements on the propeller which are closest to the hull are the most likely to corrode. Hence the outer face of the propeller will be absorbing current, but for the corrosion currents to pass from the inward face to the outer would involve a longer path through the resistive sea water so the currents finds it easier to be absorbed by the rim. Hence these values on the rim seem acceptable.

On the furthest face from the hull where the corrosion currents were expected to be absorbed, the q values are negative as predicted and for the reasons given above, these elements have a smaller magnitude than those on the rim. On the inner face, where the potentials of the elements are expected to be most similar to the hull and hence emit corrosion currents, the values of q are positive as required. The variation of the q values over the elements on the propeller is encouraging since it follows a logical pattern. For an element that shares a side with another element of greater q magnitude, this element has a larger q magnitude than an element which only shares a point with the original element. This pattern is most apparent on either of the faces. Following on from this, the elements on the rim

which share a side with elements in the inward corroding face have more negative q values than those elements which only share a point. This is encouraging since as mentioned above, the corrosion currents will flow by the path of least resistance so that they will look to be absorbed by the first rim element they encounter which are those which share sides with the corroding elements.

It is also noticeable that there is a slight change in the values of q toward the top of the propeller. This is due to the over-hang found at the rear of modern hulls, which brings the hull in a closer proximity to the upper section of the rim of the propeller than the other areas of the rim. This results in the behaviour of these propeller elements being altered to be more like that of the hull. As a consequence these elements are not able to absorb as much of the corrosion current as other elements in the rim and outer face.

Consider the values for q on the hull as shown in figure 7.3. As mentioned, the only area of activity is around the stern where the elements have positive q values indicating corrosion and current emission. This implies that the areas of the ship which are corroding are those hull elements closest to the propeller and the inward face of the propeller. However, if the magnitude of these q values are considered, it is clear that although these is some current emission by elements on the stern, it is negligible. The magnitude of the q values being emitted from the propeller are approximately 10^{-3} while those emitted by the stern elements are only of the order 10^{-7}. Hence it is clear that the protective paint is successfully preventing any current flow to or from the hull.

Consider briefly the potentials on the model. In a calculation where the aim was to provide a high level of protection to the hull, these potential values would be used to discern whether an the element was protected or not [60, 61]. However this calculation is not concerned with these issues and is instead focusing on the magnetic field which arises from corrosion and its countermeasures which means that the flux values q are of more interest since the field is a result of the current flow through the sea. Despite this, analysing the potentials remains a worthwhile exercise as they can help identify the validity of the result. As mentioned above, these potentials are directly linked to the flux values by the polarization relation of eqn (7.2.1). Since one of the main conditions in deciding whether the solving algorithm had solved the system to a valid solution was that the total current emitted from the ship was zero, these values for u will have been

a direct consequence of the q values which satisfied this condition. In eqn (7.2.1), the value of V is varied to ensure there are no stray currents, while the other values are predetermined. For this perfect paint situation the value of V required to ensure that there were no stray currents was $0.399913V$. To recap, the values of k_i and e_i in eqn (7.2.1) are

$$k_i = 1 \times 10^{-6} \text{ and } e_i = 0.3 \qquad \forall i \in hull \qquad (7.4.2)$$
$$k_i = 100 \text{ and } e_i = -0.4 \qquad \forall i \in propeller. \qquad (7.4.3)$$

Using these values in eqn (7.2.1), it is apparent that the values of u and q obtained over the ship are consistent with those provided by the polarization relation. As a consequence of this, the pleasing pattern in the potential distribution which was mentioned for the q values is again evident for u. The smooth distribution of the potentials over the hull and the propeller in which an element which shares a side with another element has a potential more closer to this original potential than one which shares only a point means that there is no singularities on the potential plots which further supports these solutions as being valid.

Further these potentials make sense when their physical significance is analysed. With a perfect paint coating in the hull, there should be almost no current from the hull. This means that there should also be almost no net current into the propeller which when the magnitudes of the q values on the propeller are analysed indicates this to be the case. The consequence of this is that there should be almost no current in the sea from the hull which means that the potential on the outside of the hull should be approximately zero (a condition which allows the currents to stay focused around the propeller). As mention in section 7.2.1, there is a $-0.4V$ electrochemical potential associated with the propeller which can be thought of as a 'battery' in the propeller which itself has very little internal resistance, and as noted above there is only a small current flowing through the propeller. Therefore the potential of the metal structure of the ship, V, should be almost $0.4V$ (the value calculated is $0.399913V$). On the hull, there is an electrochemical potential of $0.3V$ and a very high resistance due to the paint, whilst again there is very little current flow. This means that across the paint there is a potential drop of approximately -0.7V. This is precisely the behaviour portrayed by the calculated results.
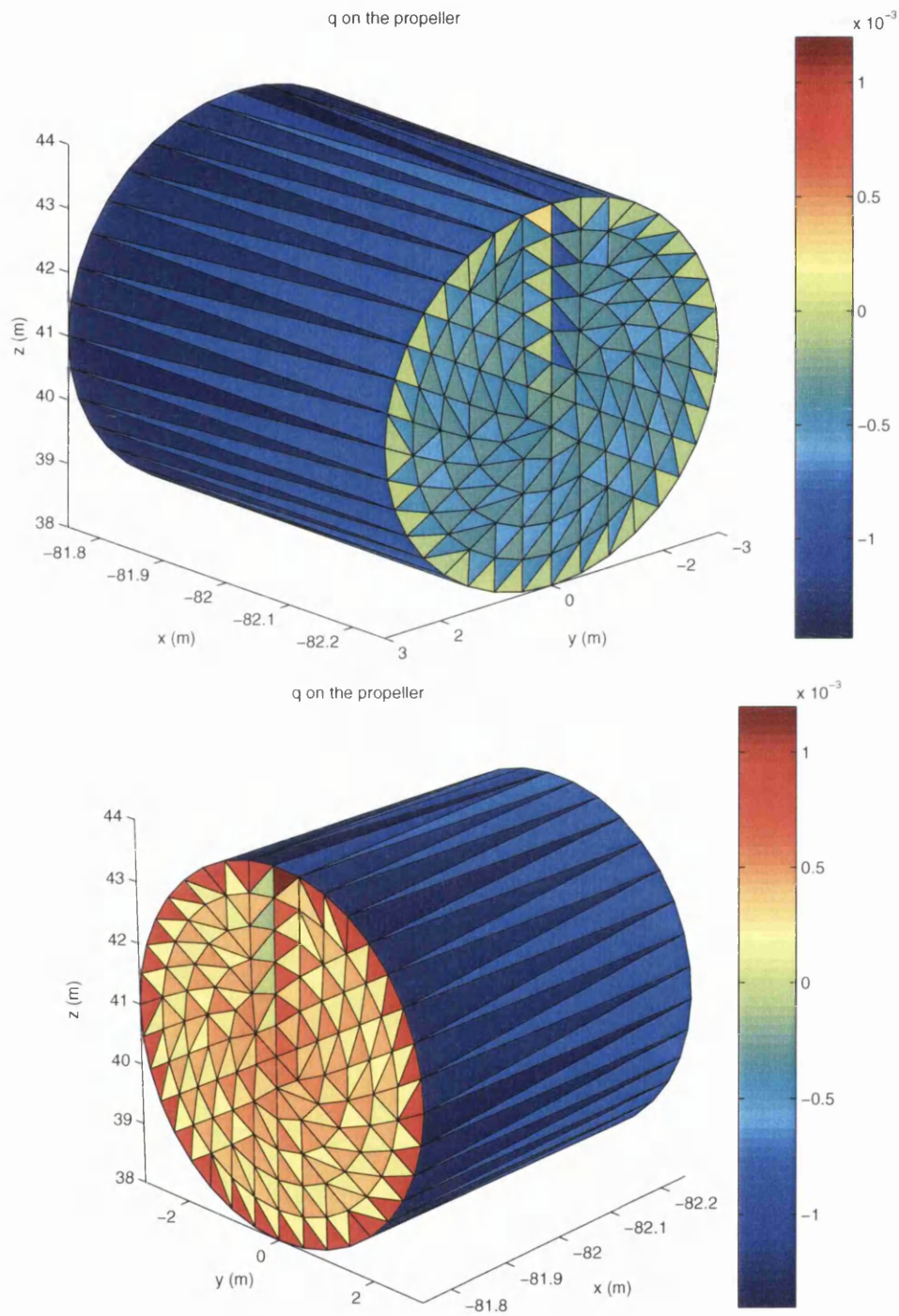
Figure 7.1: q on propeller, furthest face from hull (top) and nearest face to hull (bottom).
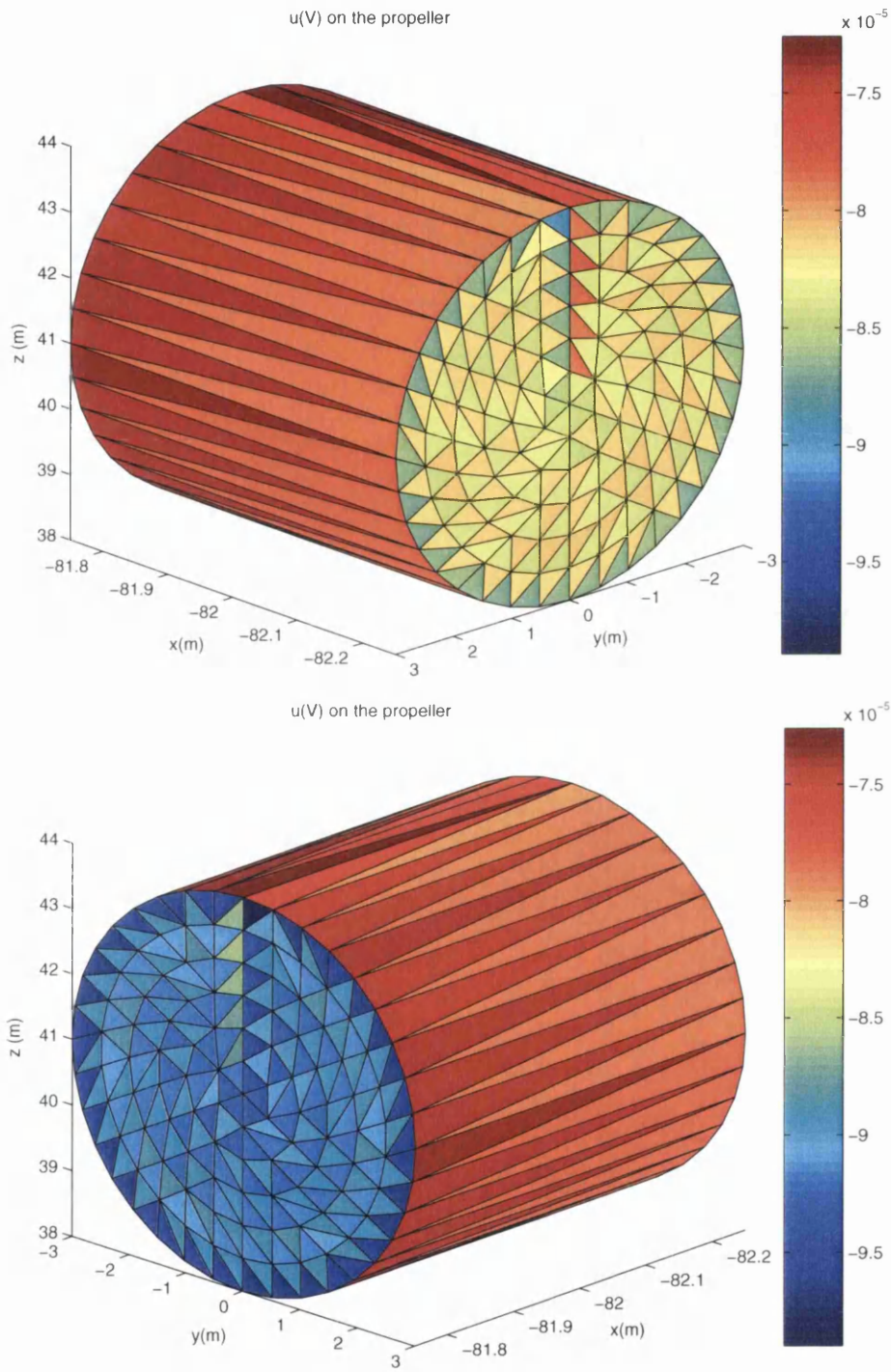
Figure 7.2: u on propeller, furthest face from hull (top) and nearest face to hull (bottom).
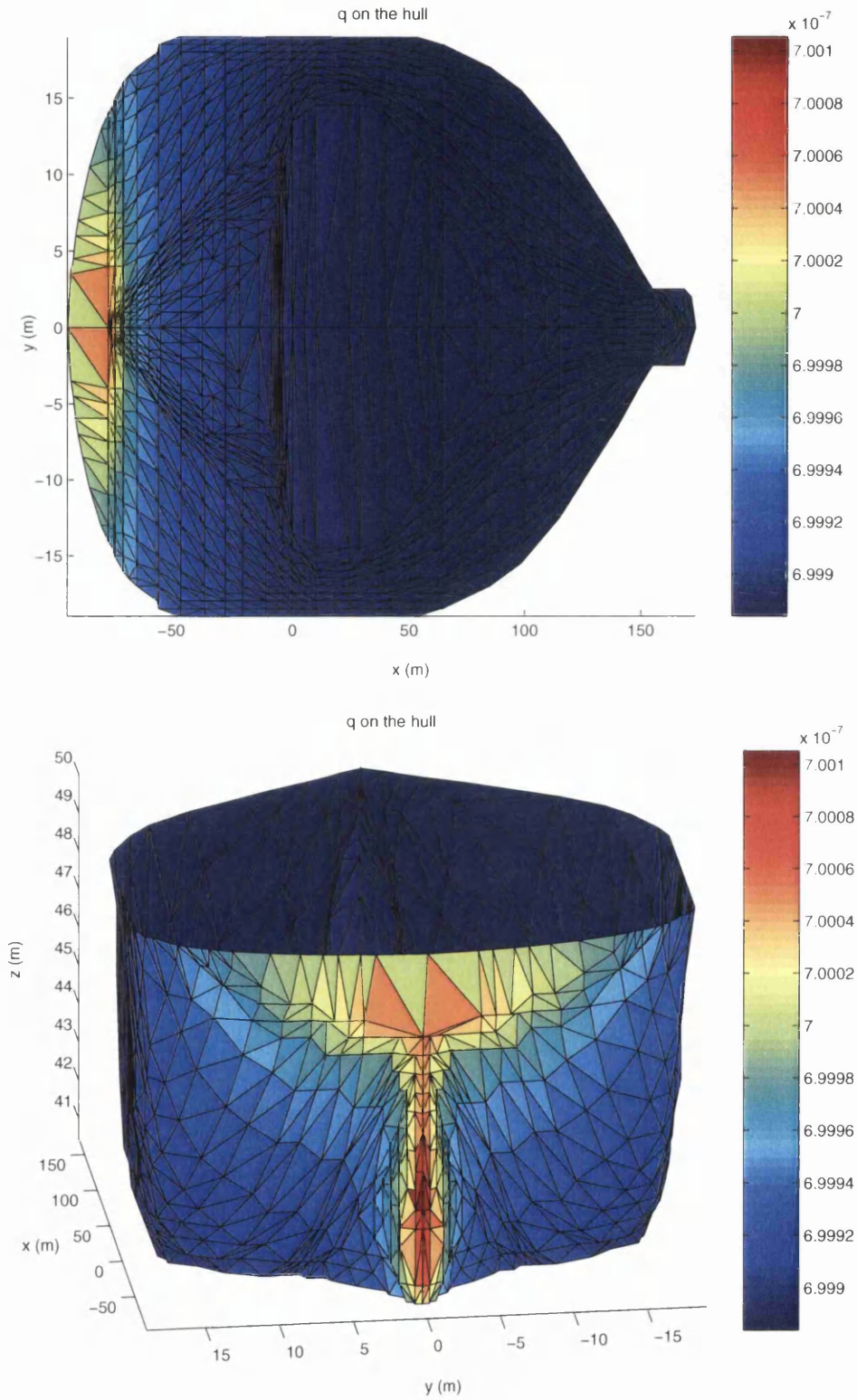
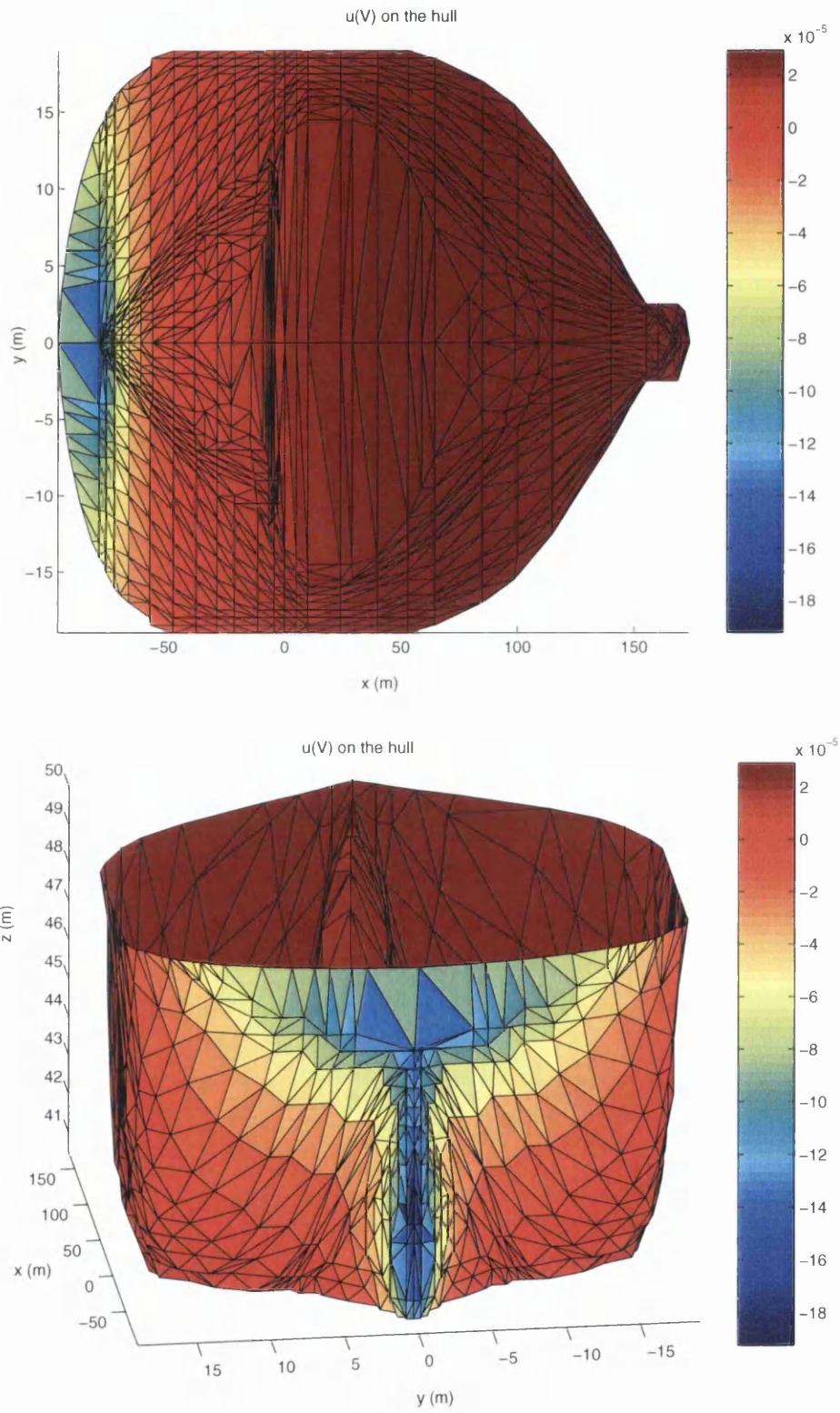Figure 7.3: q on the hull, aerial view (top) and stern view (bottom).

Figure 7.4: u on the hull, aerial view (top) and stern view (bottom).

With the solutions to the BEM equations for this model appearing valid, it is necessary to calculate the magnetic fields which result. The shape of the field and its magnitude are shown in figures 7.5 and 7.6 respectively.

Begin the analysis by considering the shape of the field, figure 7.5. The corrosion currents which flow in the sea are mainly focused about the propeller with emission from the side nearest the ship and absorption on the rim and furthest face. There is some current emitted by the hull but it is such a small amount that it has been neglected from this analysis. In common with standard engineering practise, the field is evaluated at points on a horizontal plane at a distance of 20m below the baseline of the hull, which in this model corresponds to a z coordinate of 20m.

With all the corrosion activity being centred around the propeller, it is expected that the magnetic field will be largest in the vicinity of this. Indeed this is what is shown in the xz cross-section shown in figure 7.5, and is clearly supported by the plot of the field's magnitude as shown in figure 7.6.

The direction of the field is dependent on two current paths. Firstly the corrosion currents flow in the negative x direction through the sea, while the return currents which flow from the region of absorption back through the ship to the element of the original emission. Consider the shape of the field from the sea currents. The field values for these were calculated using the proposed method of chapter 6 for which the direction depended on

$$-u d\mathbf{s} \times \mathbf{r} \tag{7.4.4}$$

where u is the potential of the element, $\mathbf{r}$ points from the source element to the field point and $d\mathbf{s}$ points out of the domain. It should be remembered that the field which is calculated using this formula has contributions from all the elements in the model, including those on the non-ship boundary and thus there will be both positive and negative potentials to be analysed. Hence it is better to consider the fields from the Biot-Savart point of view since then it is just a case of identifying the direction of current flow and using the right-hand rule to predict the field direction. Recall that the direction of the magnetic field from Biot-Savart Law for a current density $\mathbf{J}$ flowing through a volume dV is

$$\mathbf{J} \times \mathbf{R} dV \tag{7.4.5}$$

where $\mathbf{R}$ is the vector from the volume to the field point. Similarly for a current I flowing down a wire of vector component $\mathbf{dl}$

$$I\mathbf{dl} \times \mathbf{R} \tag{7.4.6}$$

Imagine looking at the model in the positive x direction, the sea currents will generally flow in the negative x direction. The sea currents spread out through the sea and do not follow one precise path. Therefore for every field point, there will be those volumes whose current densities result in the field flowing in a counter-clockwise direction in the yz plane i.e. at $z = 20m$

- $y > 0$, $B_y > 0$ and $B_z > 0$;

- $y < 0$, $B_y > 0$ and $B_z < 0$;

and those volumes whose contribution is in a clockwise direction

- $y > 0$, $B_y < 0$ and $B_z < 0$;

- $y < 0$, $B_y < 0$ and $B_z > 0$;

If the sea currents were allowed to spread out uniformly through the sea, then, as explained in chapter 2, the contributions to the field would cancel out at each field point resulting in no field. However, the sea surface prevents this uniform distribution and a field will be produced. Considering the contributions made from two source volumes, both a distance $|\mathbf{R}|$ from a field point but with one volume at negative the displacement of the other. For the volume closest to the ship, the current density $\mathbf{J}$ will be greater than the other volume further away from the ship, resulting in the field from the near volume dominating the other. Using eqn (7.4.5) this means that the field from the sea currents will be in a counter-clockwise direction. This argument holds no matter the size of $|\mathbf{R}|$ and since the source volume can be extremely close to the field point, it is possible for $|\mathbf{R}| \to 0$ which means that this field contribution can become relatively large compared to the others as all the contributions depend on a distance to the field point by an inverse square relation. Therefore, it follows that the field contribution from the sea currents should be in a counter-clockwise direction which agrees with the calculated result in figure 7.5 for the total field. However, the effect from the return current still needs to be considered which is one using the equation

derived for the dipole model in chapter 2, section 2.3.3. The field from the wire which represents the return path is calculated using the Biot-Savart Law with which the field drops off with a $\frac{1}{R^2}$ dependence.

The current down the return path will flow in the positive x direction and the right-hand rule shows that the magnetic field shall, at this depth, following a clockwise circular path in the yz plane. This is opposite to the sea currents contribution and hence the final shape of the field reduces to a direct contest between the two in terms of their respective magnitudes. As discussed above for the sea currents, the field magnitude at a field point depends on $\frac{|\mathbf{J}|}{R^2}$ where $\mathbf{J}$ is the current density at a point in the sea and $\mathbf{R}$ points from the source point to the field point. With the sea currents it is possible that $|\mathbf{R}|$ could be extremely close to zero and hence the sea currents could make a relatively large contribution to the total CRM field.

The return current focused at least 20m away from the field point, this means that although the return current will have a large magnitude than the densities in the sea, it will be significantly further from the field points than the closer sea currents. With the $\frac{1}{R^2}$ dependence of the contributions, it is reasonable to assume that the contribution to the CRM field from the return currents will be less that that from the sea currents, resulting in a total CRM field which has its direction in that of the contributions from the sea currents that are nearer the ship that itself, i.e. counter-clockwise. This is the direction shown in the plots.

To justify the magnitude of the field, consider the following rough approximation. Suppose that the hull is represented by a rectangle of length $300m$, breadth $40m$,and depth $10m$. The wetted surface area of such a model will be $A \approx 10^4 m^2$. From above it is known that the voltage across the interior metal work of the ship is $0.7V$. It will now be assumed that the propeller shares the same k value as the hull in the polarization relation eqn (7.2.1), then the resistance of the interior of the ship (including the paint coating) is approximated as

$$R = \frac{1}{kA} \approx \frac{1}{10^{-6}10^4} \approx 10^2 \Omega. \tag{7.4.7}$$

From the analysis above, it is known that although the sea currents are very small, the field which they produce dominates that from the return currents. However, the focusing of the sea currents into one concentrated return current means that the magnitudes of the two contributions should not be considerably different. By

approximating the magnitude of the contribution from the return currents, it should present a rough estimate at the magnitude of the actual CRM field. The magnitude of the concentrated return current can be shown from Ohm's Law to be approximately equal to $7 \times 10^{-3} A$. Therefore, if the magnetic field strength at $20m$ below this ship is approximated by assuming the ship to be an infinitely long wire in an uniform, infinite conducting sea, then

$$|\mathbf{B}| \approx \frac{\mu_0 I}{2\pi r} \approx 10^{-10} T. \tag{7.4.8}$$

This is smaller than what is calculated and displayed in figure 7.6 but this is expected. This is an approximation of the contribution from the return current which the previous analysis and shown to be smaller than the contribution from the dominant sea currents. Also this approximation has assumed that the currents have flowed along the entire length of the ship. In truth, it has been shown that the currents are emitted from the propeller and absorbed by other areas of the propeller so the factor of $200m$ for the length in the calculation of the wetted surface area could be neglected which would increase the size of the field by approximately 10^2 which would make the approximation $|\mathbf{B}| \approx 10^{-9} T$ which is consistent with the calculated values.
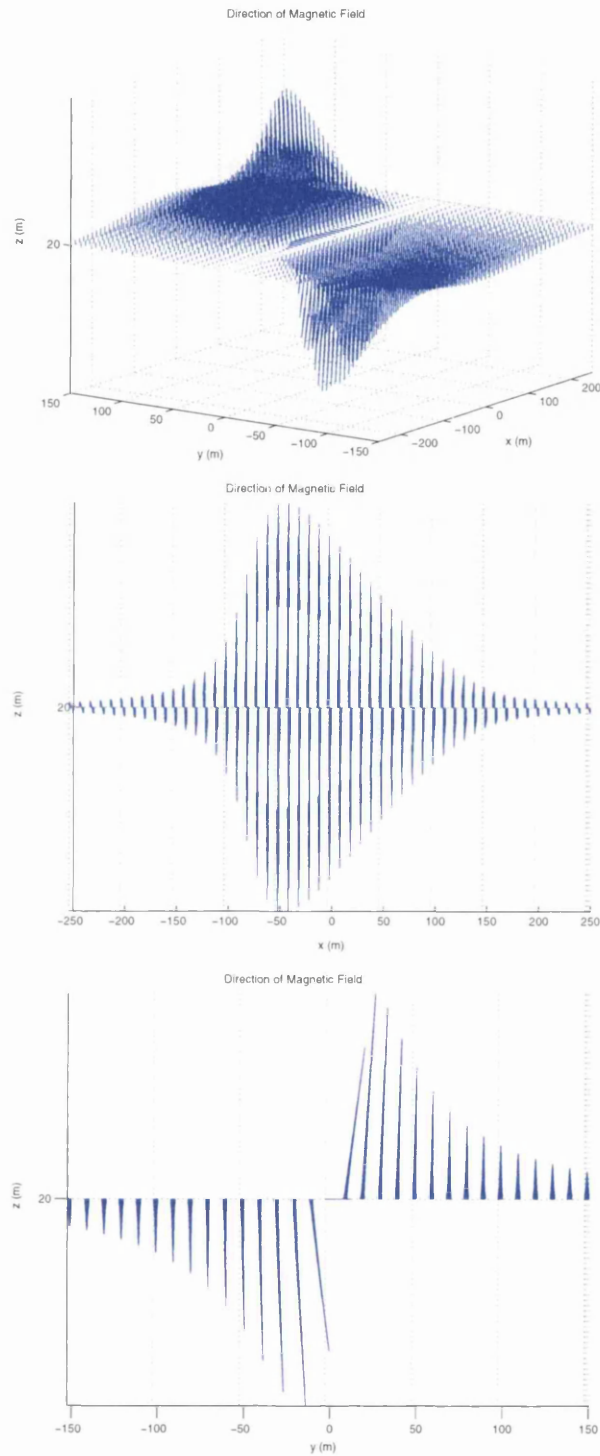
Figure 7.5: Magnetic field from corrosion currents, the three-dimensional view (top), xz cross-section (middle) with lines representing (B_x, B_y) and yz cross-section (bottom) with lines representing (B_y, B_z).

Figure 7.6: Magnitude of the magnetic field for perfect paint on the hull.

7.4.3 Verification by Dipole Approximation

As mentioned in chapter 2, the result from section 2.3.3, which provides an estimate of the magnetic field from a dipole model of a 'submarine', can be used to obtain an estimate of the CRM field from the ship.

This is done by taking each element on the hull which is emitting current and calculating the magnitude of this corrosion current. The location of the centroid of each emitting element is then averaged with that of the centre of the propeller so that they have the same x and z coordinate, with the difference in y coordinate being the length of the wire which connects them. At the emitting end of the wire it is assumed that there is a source while at the other end there is a sink. The aforementioned result is then applied to this configuration for the corrosion current from the original element, with the process being repeated for all other emitting elements. When the contributions from each individual element are summed, the result is an approximation at the CRM field. The approximation is shown in figures 7.7 and 7.8.

It is clear that this approximation of the field supports the CRM field which was calculated using the full method. Both the direction and the shape of the dipole approximated field shown in figure 7.7 are very similar to that produced by the full method. Any discrepancy in direction is due to the averaging of the locations of the propeller centre and the element centroids which will have altered the directions of the contributions to the total field. The magnitude of this approximated field is smaller than that calculated from the full method. There are two possible explanations for this. Firstly, while the full calculation was performed for a finite domain, the dipole approximation was based around calculations in a semi-infinite domain. This means that in the full calculation there is a non-conducting sea bed which will not allow the corrosion currents to flow past hence condensing them into the domain with the effect of increasing the magnitude of the CRM field. With this boundary neglected from the dipole approximation, the field should be smaller in magnitude as observed. This is a characteristic which should be present in all the dipole approximations. However, as mentioned earlier, in this model the corrosion currents are not terribly large and therefore they will not spread out far into the sea. This means that the effect of the non-conducting sea bed in the full calculation will not be terribly large. The second possible explanation is specific to this model. The dipole approximation
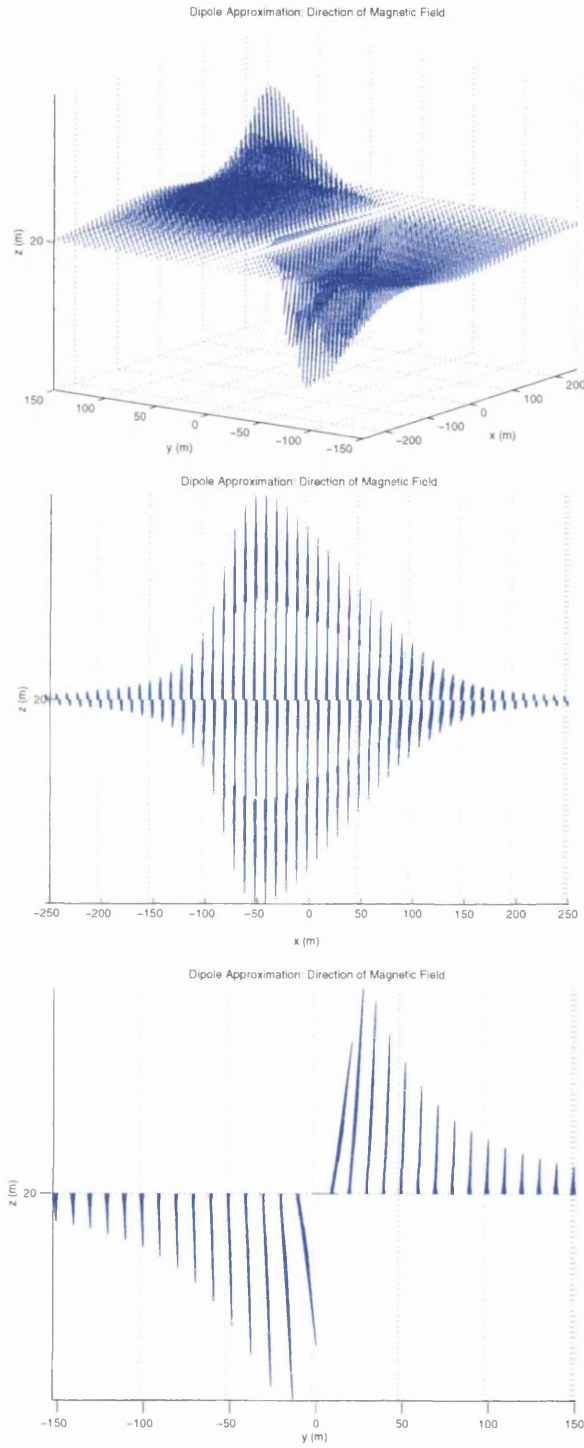
Figure 7.7: Dipole approximation of the magnetic field from corrosion currents, the three-dimensional view (top), xz cross-section (middle) with lines representing (B_x, B_y) and yz cross-section (bottom) with lines representing (B_y, B_z).
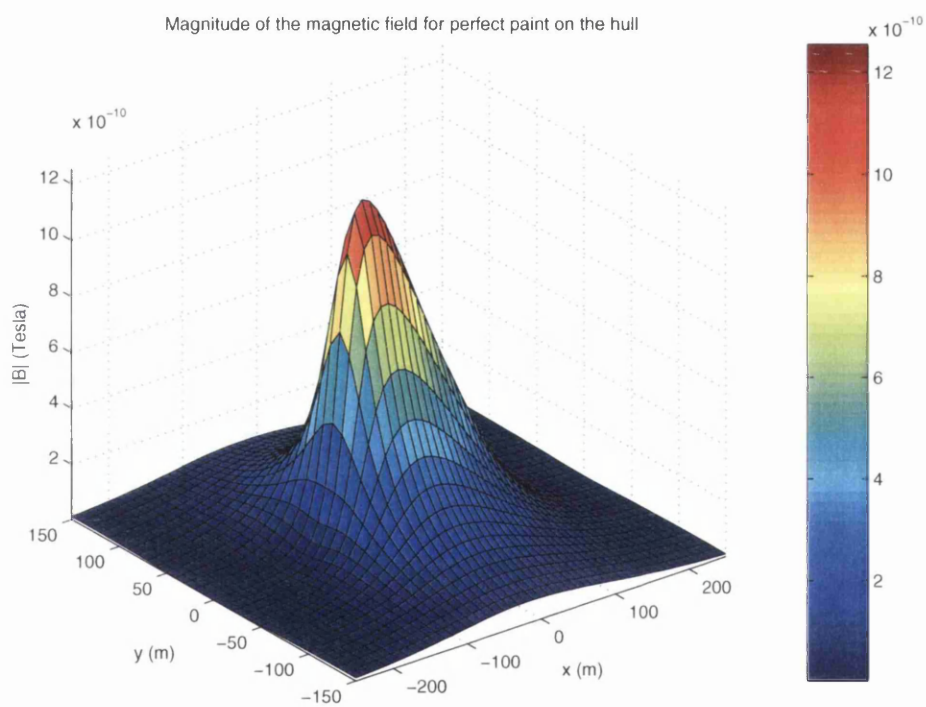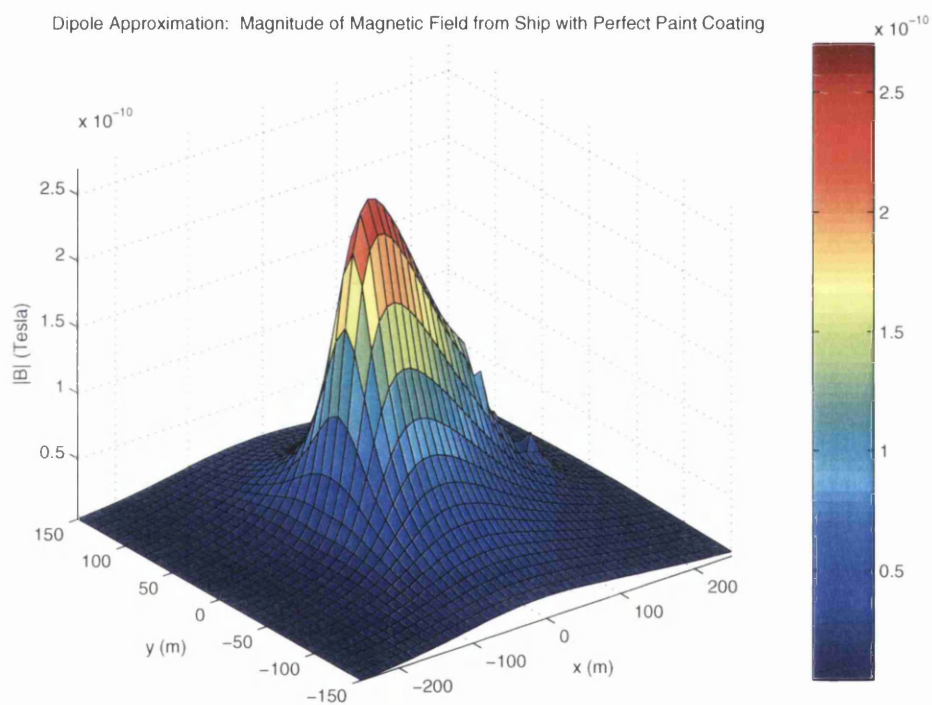
Figure 7.8: Dipole approximation of the magnitude of the magnetic field for perfect paint on the hull.

looks for elements on the hull which are emitting current, but it has been already shown that in this model the corrosion currents are mainly being emitted from the propeller face nearest the hull. With these currents not being included in the calculation, the magnitude of this field shall be less than for the field produced by the full method. The combined effect of these two discrepancies is the observed difference in the field magnitudes. Despite this the dipole approximated field is still of a similar order of magnitude to the field from the full method.

Therefore the magnetic field which the proposed method has calculated is of the correct order of magnitude and has the same shape and direction as that predicted for the situation of the hull being coated in a perfectly protective paint. Further support of these magnitudes, shapes and directions has been provided by a dipole approximation at the field. However this is a very idealised situation and the more physically realistic case of there being paint damage on the hull should now be considered.

7.5 Damaged Paint Coating - Analysis.

To model the situation of the paint on the hull being damaged, the model was amended as follows. The majority of the paint coating on the hull maintained its highly protective nature while an area toward the bow was deemed to have been damaged by increasing the value of k_i in eqn (7.2.1) by a factor of 1,000,000. This, as indicated by eqn (7.2.2), could correspond to either the conductivity of the surface layer having been increased by 1,000,000, or the paint thickness t being one million times thinner.

The elements for which the paint was damaged were those which lay with centroid in the range $133.8 \leq x \leq 153.8$. This encompassed some 149 elements of varying size and shape.

Using the results obtained for the perfect paint coating, it is again possible to make some predictions regarding the behaviour of the solution.

7.5.1 Predicted Behaviour.

In the analysis of the perfect paint coating, the hull was so well coated that only an extremely small, almost negligible amount, of the corrosion currents were emitted and this was at the stern which is extremely close to the propeller. The corrosion currents were caused by the propeller face closest to the hull corroding. In this case, there is now an area toward the bow which is able to corrode more freely than any other part of the hull.

The effect of this is that the corrosion currents will be emitted from this damaged area, and flow through the sea water to the propeller, where they will be absorbed. On the hull, it is expected that for the undamaged area the values of q should again be approximately zero while on the damaged area the q values should be positive. On the propeller, it is expected that the corrosion currents will be absorbed so the q values should be negative. However it still remains possible that there could be a small amount of current emission from the face of the propeller located nearest to the hull, as again the close proximity to the stern of this face could pull the potential of the face to a level where a small amount of corrosion can occur. With there now being an area which is relatively 'free' to corrode, it follows that in this model there will be more current in the sea, and the system as a whole. This will result in the magnitudes of the magnetic field

increasing to higher levels than calculated for the perfect paint coating. With the damaged area being located toward the bow, the currents will be flowing through the sea along the length of the ship which will stretch out the peak in the magnetic field obtained in the perfect paint case away from the vicinity of the propeller and along the hull. With the magnitudes of the currents in the sea and in the return current having increased by the same amount it is reasonable to assume that the direction of the field in the yz plane should be the same as in the perfect paint case.

As stated above, the potentials on the ship are hard to predict as their values are dependent on a complicated intertwined relation with V and q. However, with the current expected to flow from the damaged region on the hull to the propeller, it is expected that the potential on the damaged region should be greater than that on the propeller. The region of undamaged paint should have potentials which lie in between these two values. To avoid the occurrence of singularities in the potential the distribution over the ship should be continuous and of the form described previously. As was the case with the perfect paint case, the values of potentials will be verified using eqn (7.2.1).

7.5.2 Calculated Behaviour.

The calculated results of the BEM equations are shown in figures 7.9 - 7.12. Begin by considering the values of q on the propeller, figure 7.9. The first thing to note is the increase in the magnitudes of the q values compared to the perfect paint example which corresponds to an increase in the corrosion current in the model resulting from the potential difference between the hull and the propeller increasing [6].

On the rim of the propeller, the q values are negative and have a large magnitude compared with the faces of the propeller. This is consistent with the perfect paint scenario in indicating that the current is more easily absorbed by the outer rim due to the decrease in the distance that the current must travel through the sea to reach this area which reduces the resistance of the path. On the face furthest from the hull, the q values are negative as expected and have smaller magnitudes than the negative values on the rim. So, as with the perfect paint situation, the corrosion current is absorbed by the outer face of the propeller. Recall that in the perfect paint calculation the inner face of the propeller emitted

current indicating that it was corroding. In this calculation, the q values are negative and almost identical to the outer face. This shows that the damage to the paint on the hull has resulted in the corrosion currents originating solely from the damaged area, with the entire propeller acting as a receiver. The fact that the distribution of q over both faces is very nearly the same indicates that the the currents are just as easily absorbed at either face. The corrosion currents will always flow by the path of least resistance which in terms of distance would be to the inner face. However with the hull in close proximity to the inner face, the potentials on this face shall be slightly higher than on the outer face. This small difference in the potential seems to have meant that the resistance of the path to either face has become approximately the same. Especially since the damaged area of the hull is located toward the bow which means the currents have already travelled a large distance through the sea before reaching the propeller. The extra distance between the inner and outer face of the propeller is countered by the slightly higher potential on the inner face with the current struggling to distinguish a reduced resistance in the path to the the inner face rather than the outer one. Another reason for this could be that the corrosion currents emitted from the damaged region are so large that the amount of current trying to be absorbed by the propeller is massive and is approaching the propeller in an almost uniform distribution through the sea so that both faces are required to absorb as much as they can which would produce the same distribution on either face.

The effect of the hull on the propeller's levels of absorption is again noticeable on the upper area of the rim of the propeller which has q values which are slightly less absorbent that the other areas. This is best seen by the slightly greening of the elements on either face toward the upper area of the rim. This effect is consistent with what was observed in the perfect paint calculation.

Consider briefly the potential values on the propeller. The polarization relation between the u and the q values is again linear as shown by eqn (7.2.1). Also the values of k_i and e_i are the same for the propeller as in the perfect paint calculation, see eqn (7.4.2). In this calculation, the value of the potential of the internal metal structure of the vessel was -0.027883 V. Using these values in eqn (7.2.1), it is apparent that the values of u and q are consistent on the propeller, with again the influence of the hull over the potential on those elements toward the top of the propeller apparent.

Moving on to the hull, consider first the potential u, as shown in figure 7.12. Compare these figures with those for the perfect paint coating (figure 7.4) where the values of u were relatively small and uniform over the hull, the only small variation coming at the stern being due to the propeller. In this case, it is clear that the potential of the elements vary significantly over the entire surface of the hull, from approximately -0.3 V at the stern to +0.2 V at the bow. The values at the bow are larger due to the damaged paint in this section. This positive potential is a welcome aspect as it will attract the electrons emitted from ship, mainly from the propeller but also from the stern of the hull, and will thus be the region in which the corrosion current is emitted, i.e. positive q values. To check this consider figure 7.11.

It is clear that in the areas where the paint is still regarded as being perfect, the same behaviour as in the perfect paint case is observed with the q values being approximately zero. There is a difference around the stern where figure 7.3 shows that in the perfect paint case a small amount of current was emitted, i.e. positive q. In this case with the damaged paint, there is no such variation which is due to there being other areas on the ship which are able to provide the corrosion currents more readily. However, these details are small compared to the obvious area of interest on the hull, which are those elements which lie in the region of damage. As shown in figure 7.11 this is the area where the corrosion current is emitted from the hull. It also corresponds to the area of the hull with the highest potential values for reasons indicated above. By comparing the magnitudes of the q values on the hull and the propeller, the ones on the hull which are non-zero are, in general, approximately 10 times smaller than those on the propeller (which of course have different signs). This is due to the respective surface areas. The area on the hull is far greater than that of the propeller, and with the q values per element being related to the current density from/into that element, it follows that since all the current emitted from the hull must be absorbed by the propeller, each element on the propeller will have to absorb a higher density of current, and hence they will have a larger magnitude of q.

Again it is possible to check the potentials against the corresponding q values using eqn (7.2.1) where the values of e_i and k_i are the same on the undamaged areas of the hull as for the perfect paint case. In the damaged area, $k_i = 1$, which shows that the values of u and q correspond supporting the results from the BEM

calculation.

These figures for the damaged paint again display the pleasing extrapolation of the q and u values over neighbouring elements as observed above for the perfect paint case. This again provides reassurance that the method is operating correctly, so the next stage in the analysis is to consider the magnetic field.

Consider the calculated magnetic field shown in figures 7.13 and 7.14. It is clear that the spreading out of the field along the hull and its increase in magnitude that was predicted has been calculated. For the same reasons provided in the analysis of the perfect paint, it is expected the the shape of the CRM field would be governed by the field contribution from the sea currents closer to the ship than the field point, and again this is the case as shown in the three-dimensional view and the yz cross-section of figure 7.13. To verify this direction for the field it is again easier to think in terms of the Biot-Savart Law since it is clear what directions the currents should be flowing in.

Since the q values on the hull are virtually zero for non-damaged regions, it follows that the contribution to the field from the current related to these elements may be neglected. By considering the contribution from the current related to the damaged area only, an accurate portrayal of the field from the sea currents should be obtained.

The corrosion current from the damaged area flows to the propeller so from eqn (7.4.5), the direction of the field contributions from the sea currents is counter-clockwise for the same reasons as explained in the perfect paint case. Again the non-uniform distribution of the current through the sea means that the field contributions from the sea currents closer to the ship than the field points dominate the contributions from the sea currents further from the ship and also the return current. With there being this region of damaged paint, the elements in this region are able to corrode more readily so that there is a greater corrosion current forcing an increase in the total current flowing in the loop so that again the magnitude of the field should be greater. By comparing figures 7.14 and 7.6 it is clear that the sharp peak about the propeller for the perfect paint case has been stretched along the length of the hull for the damaged paint, and that the magnitude has also increased by a factor of approximately 10^3. The validity of this magnitude can be verified by a quantitative calculation. Although the dominant contributor to the field, ignore all the sea current contributions and
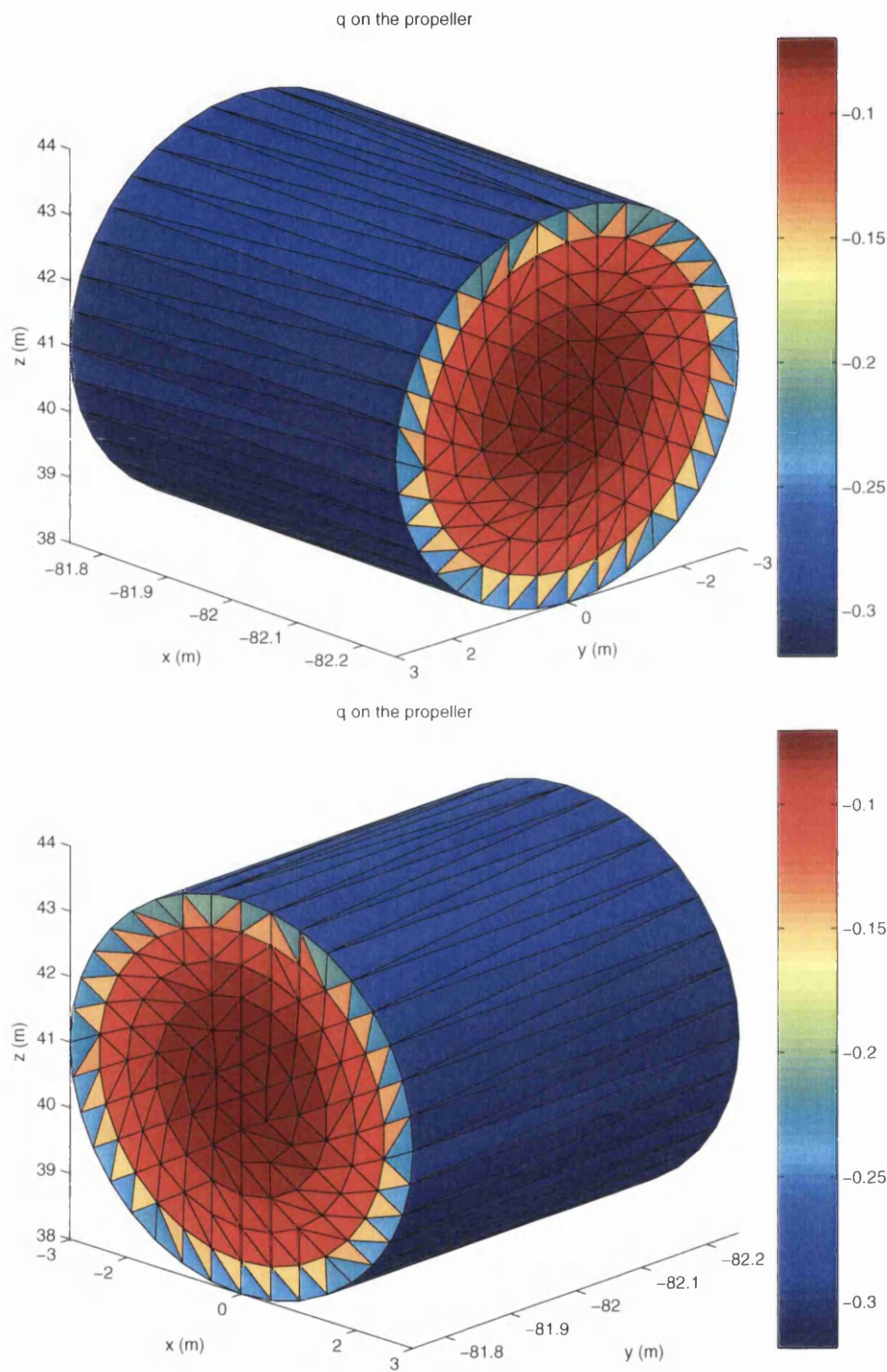
Figure 7.9: q on propeller, furthest face from hull (top) and nearest face to hull (bottom).
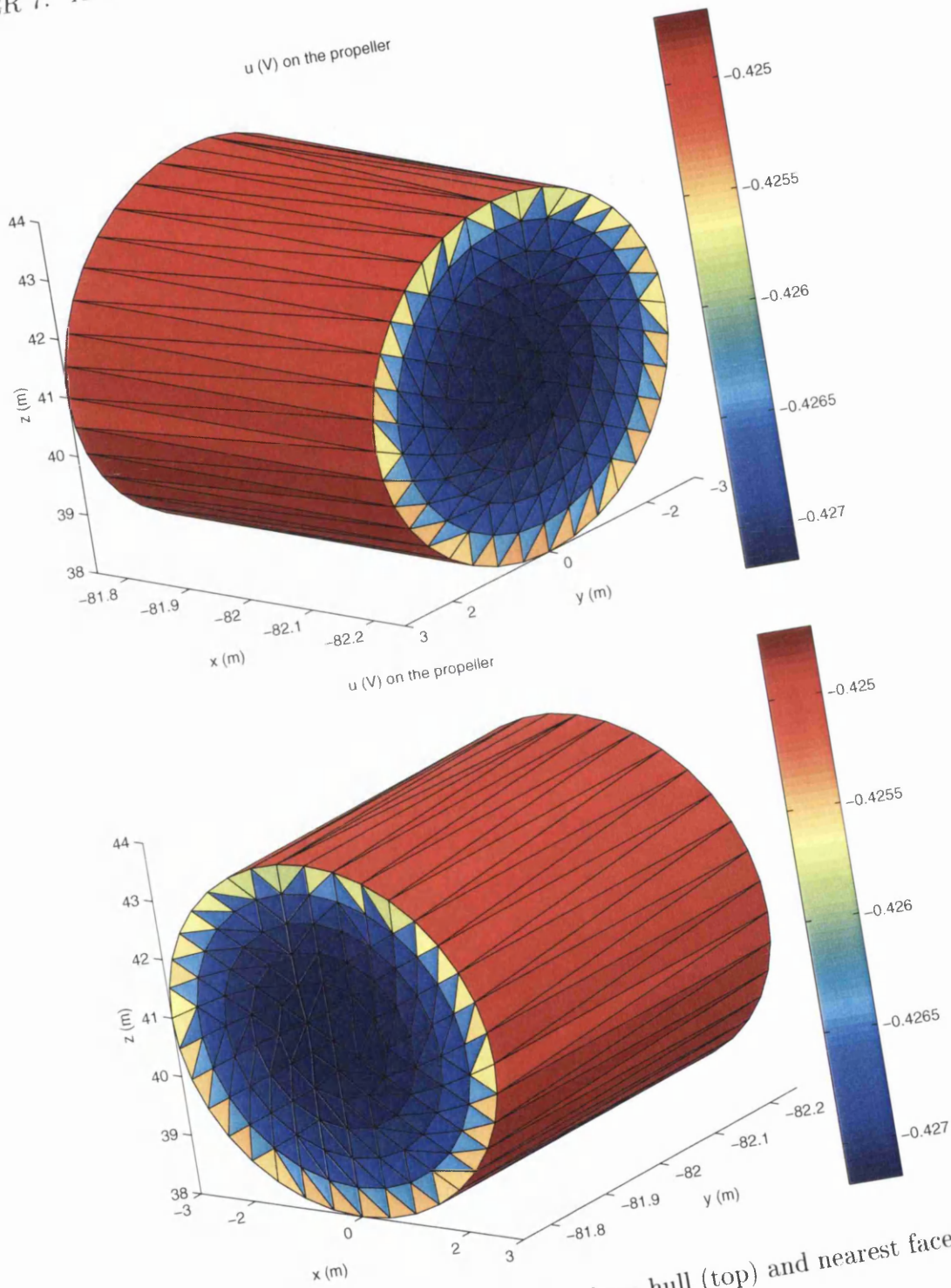
Figure 7.10: u on propeller, furthest face from hull (top) and nearest face to hull (bottom).
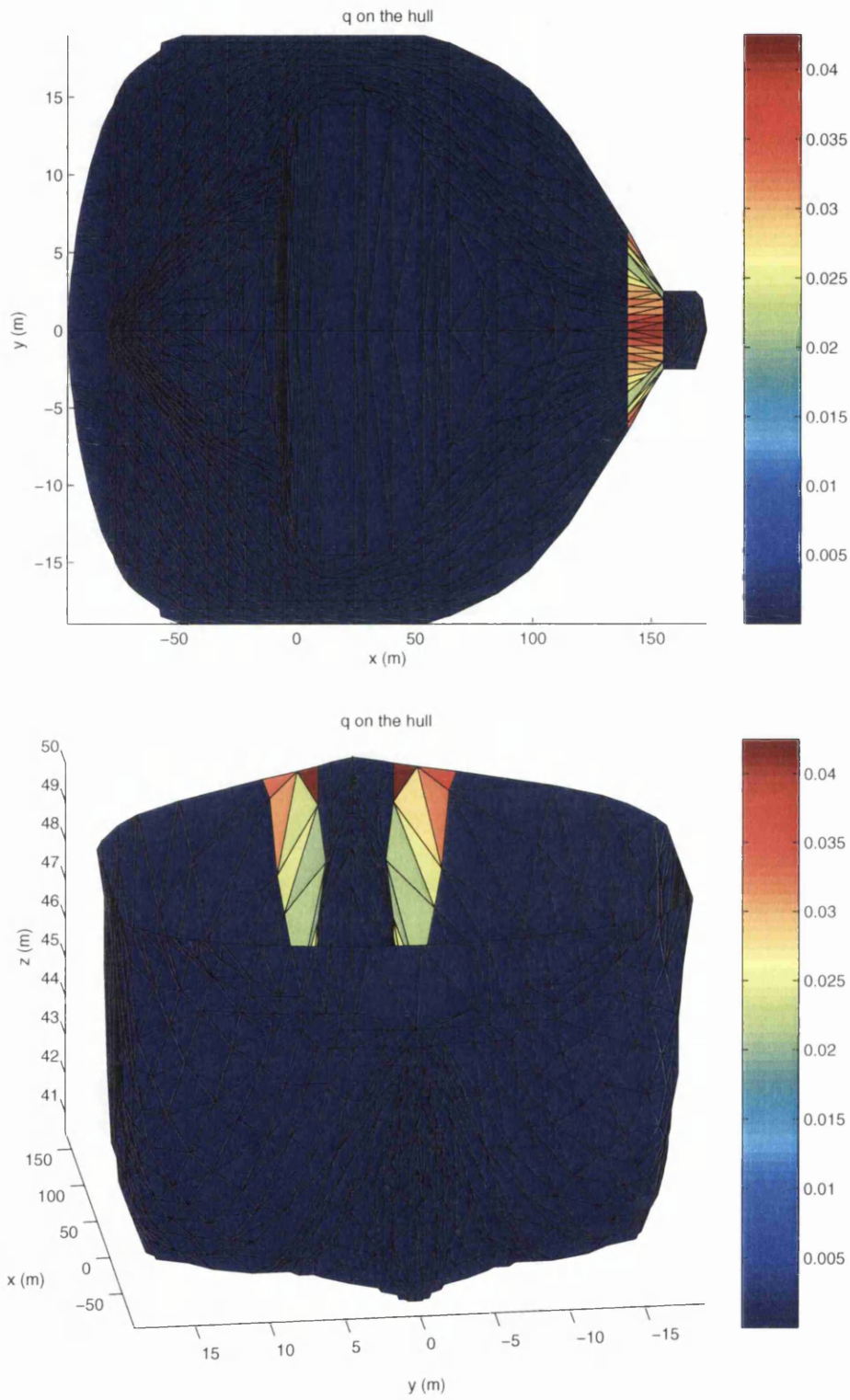
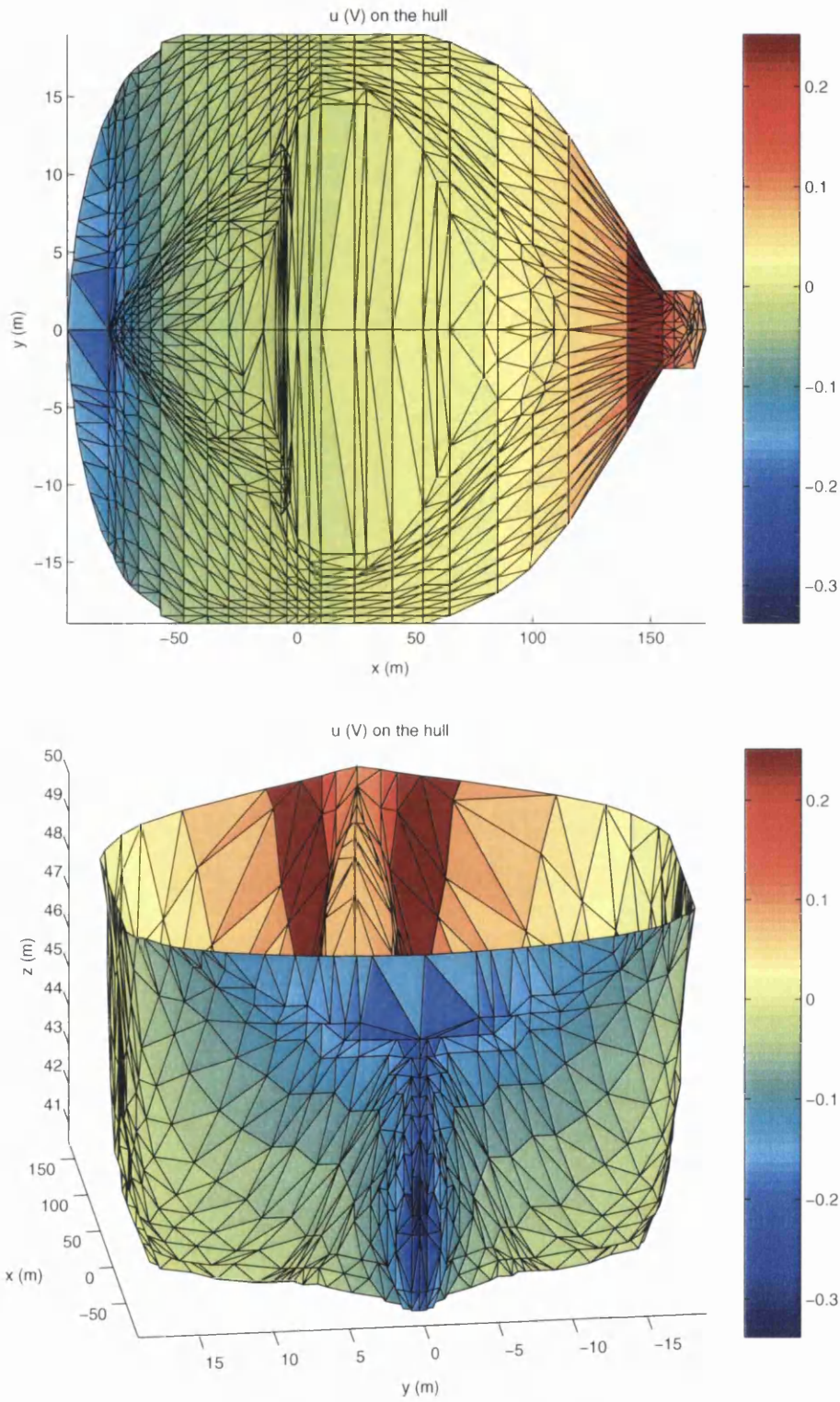Figure 7.11: q on the hull, aerial view (top) and view from stern (bottom).

Figure 7.12: u on the hull, aerial view (top) and view from stern (bottom).

concentrate on the return currents which should provide a decent approximation at the expected magnitude of the CRM field. There is a thin region of length $20m$ from which the currents are emitted to the sea, so using the previous rectangular approximation of the hull, this gives the wetted area of the hull emitting currents as

$$A \approx 20 \times (10 + 10 + 40) \approx 1200m^2. \tag{7.5.1}$$

From the polarization relation, it is known that in this damaged region $k = 1$, so the resistance of the return path through the ship to the outside of the hull is $R \approx 10^{-3}\Omega$. Also from above, the voltage across the metal work of the ship forming the return path is $V \approx 3 \times 10^{-2}V$ so that the return current can be approximated as $I \approx 3A$. Approximating the field at $20m$ below baseline as being that from an infinitely long straight wire in a uniform, infinite conducting medium, then $|\mathbf{B}| \approx 10^{-7}T$. This can be compared to the magnitude of $10^{-6}T$ which the calculation provided. It may be one order of magnitude smaller but, as mentioned, this approximation is of the return current contribution which is less than that from the dominant sea currents. Therefore it is reasonable to conclude that the field calculated has the correct orientation and a plausible magnitude.

It should be mentioned that the current passing along the shaft has been approximated to be approximately $3A$, where previously it was indicated that in real-life this currents should be of the order of a few hundred amps. The reason for this discrepancy is that in the polarization relation being used, the values of k have been made small to help with obtaining convergence of the PSOM method. By increasing these values, the currents could be increased to more realistic values but this would hinder the convergence of the method. This is situation would not be a problem if realistic polarization data had been available. However as mentioned previously, these test calculations are not supposed to be an in depth analysis of a real ship, rather an investigation as to whether the proposed method can model the characteristics of a ship which is corroding. Therefore, these smaller values for k will be persevered with as they aid the convergence of the process and still allow the various interesting corrosion characteristics to be modelled.
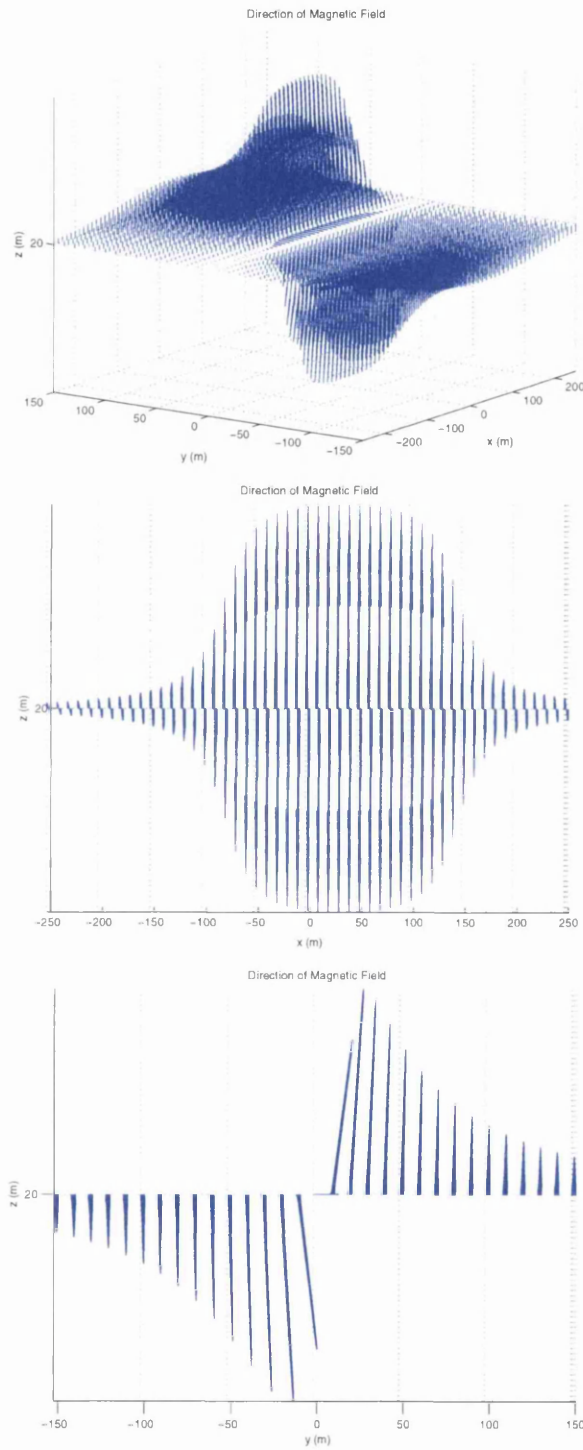
Figure 7.13: Magnetic field from corrosion currents, the three-dimensional view (top), xz cross-section (middle) and yz cross-section (bottom).

Figure 7.14: Magnitude of the magnetic field for a ship with damaged paint on the hull.

7.5.3 Verification by Dipole Approximation

As in section 7.4, it is possible to use the relation from section 2.3.3 to obtain a dipole approximation of the CRM field. The approximation is shown in figures 7.15 and 7.16.

Again the dipole approximation has provided a field which is in approximately the same direction and has the same shape as that calculated by the full method. When observed on figure 7.15, the shape of the field also looks similar. Again any discrepancy in the direction of the field, although small, will be the result of the approximation in the positions of the propeller and element centroid made by the dipole approximation. The magnitude of the field from the dipole approximation is smaller than that from the full method. Indeed in this case, the discrepancy seems to be slightly larger than for the previous case where the hull had a perfect paint coating. This is a result of this model producing higher levels of corrosion current which will be more spread out within the domain. This means that the non-conducting sea bed boundary in the full method will have a greater effect on the condensing of the currents within the domain, resulting in a larger field magnitude. Since this is the only major difference between the two fields, and it is expected and understood, this dipole approximated field has produced a field which supports the CRM field from the full method as being a reasonable representation of the actual CRM field.

The problem with this calculation is that although it may represent a more physically real situation, it is unlikely that the paint will be damaged to such an extent. A more realistic level of paint damage should also briefly be investigated.

Figure 7.15: Dipole approximation of the magnetic field from corrosion currents, the three-dimensional view (top), xz cross-section (middle) and yz cross-section (bottom).
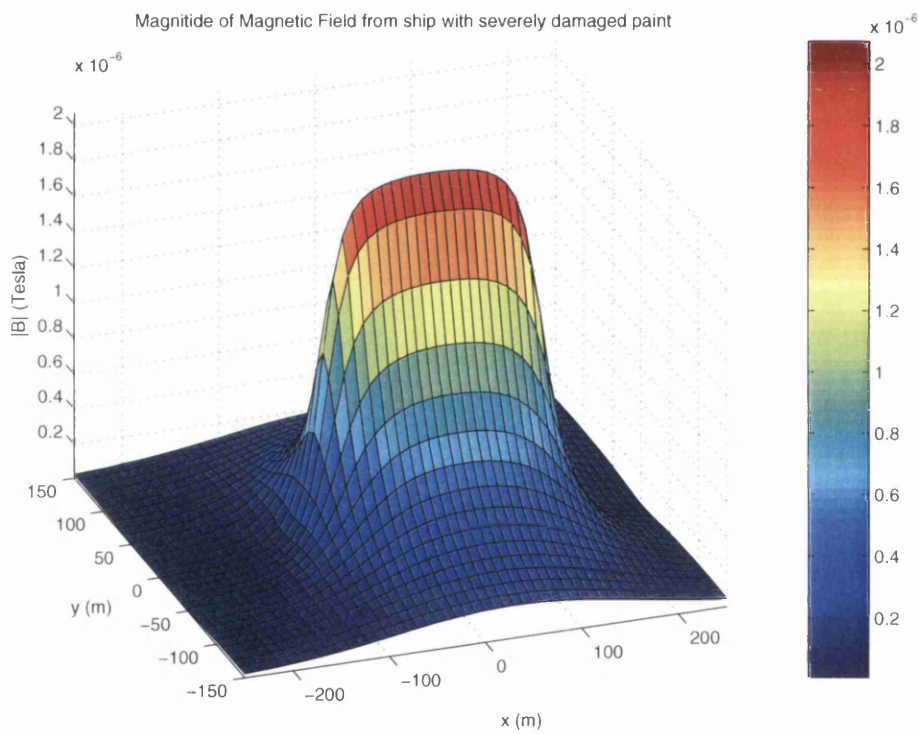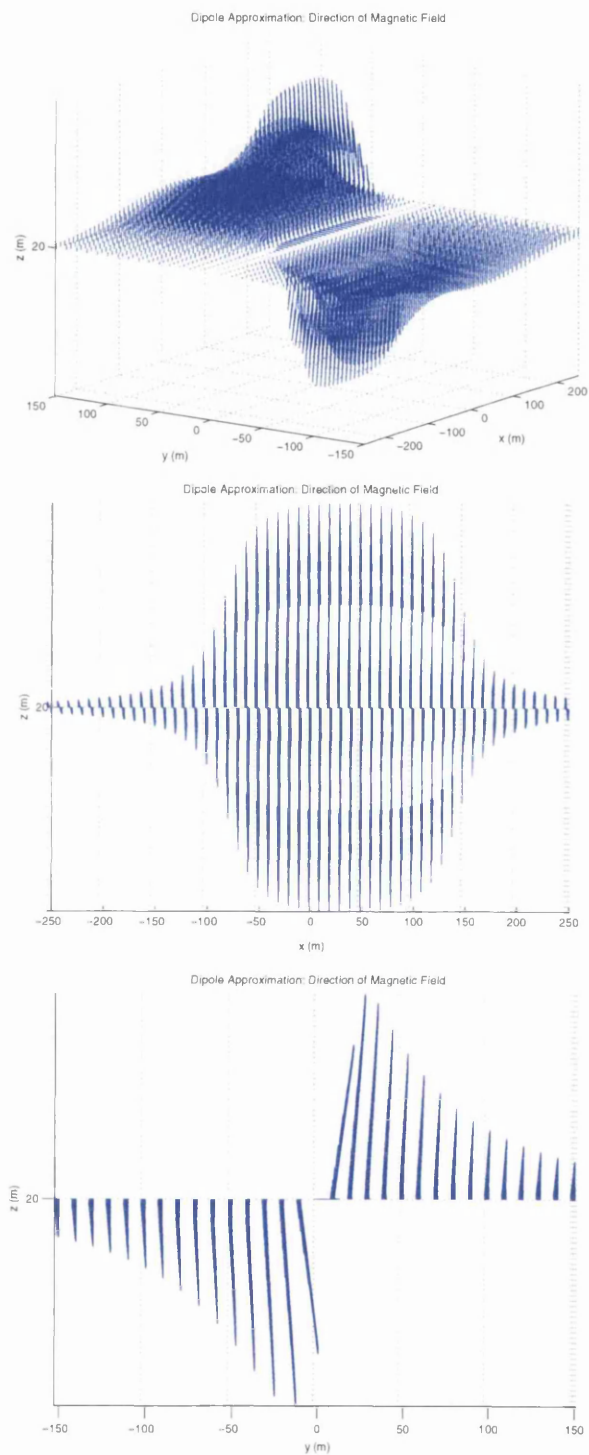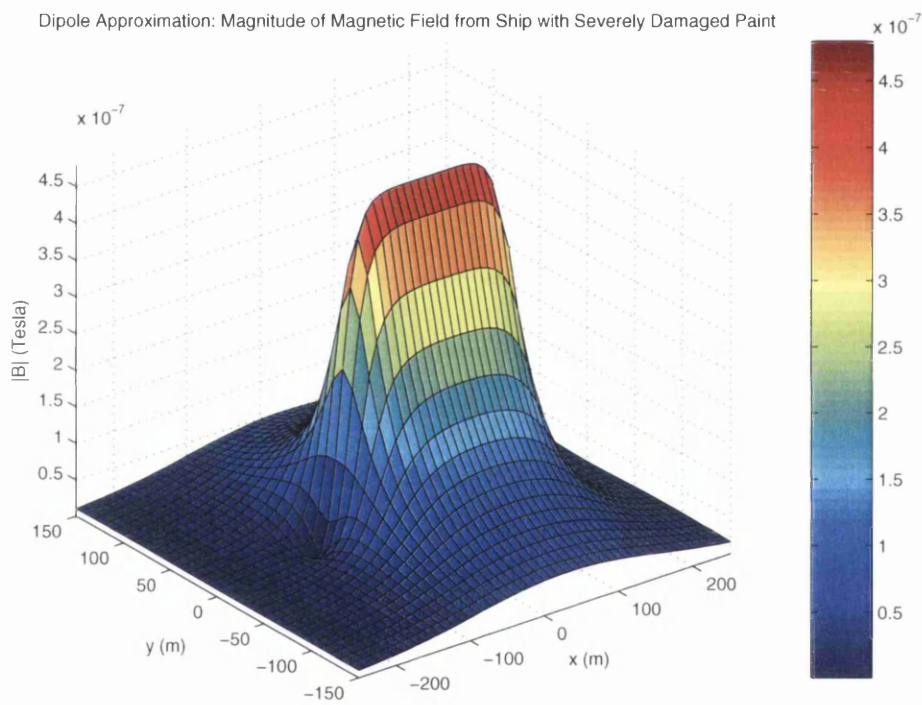
Figure 7.16: Dipole approximation of the magnitude of the magnetic field with damaged paint on the hull.

7.6   Less Severe Paint Damage - Analysis.

For the damaged area to be one million times more conductive than the perfect paint describes an extremely high level of paint damage. To provide reassurance that the characteristics observed for the damaged paint calculation were not just the consequence of this extreme paint damage, the calculation was repeated for the same region of the hull being damaged to a lesser extent. This time the damaged paint was only one thousand times more conductive than the perfect paint. Since there are no new concepts added to this calculation there will be no prediction of the behaviour of the solution to the BEM equation, only a comparison made to the case of the extreme paint damage and, where appropriate, the perfect paint case.

7.6.1   Comparison to the Extreme Paint Damage.

From the severely damaged calculation, the values of q on the propeller were all negative indicating that the corrosion current flowing through the sea was absorbed on the propeller. The values of q on either face were nearly identical with the inner face absorbing slightly less on the upper elements than the outer one due to the close proximity of the hull. This also effected the rim values although these were larger than on either face indicating a higher level of absorption. These features were also apparent from the potential plots as expected.

The results from this example are shown on figures 7.17 - 7.20. It is again obvious that the rim absorbs a higher density of the corrosion currents than either face, however the behaviour on the faces differ from each other. On the both faces, the q values are negative but those on the inner face are smaller in magnitude than those on the outer face which means that there is more of the corrosion current being absorbed at the outer face than the inner one. The reason for this is the same as for the similar behaviour that was observed in the previous calculations. The close proximity of the hull to the inner face directly effects the values of u and q on this face, forcing them to behave more like the hull in the sense that paint coating on the hull forces the potential to obtain values which restrict the corrosion currents from passing. On the propeller face this alters the potentials so as these element offer a slightly higher opposition to current absorption. The reason why this is not observed on the severely damaged

model is that the damage in the previous calculation resulted in an extremely large corrosion current being emitted. This meant that the potential difference between the damaged area and the propeller was so large that the small potential difference between either propeller face almost negligible in comparison. This coupled with the slightly higher resistance offered by the path to the outer face meant that approximately the same levels of current were absorbed at either face. In this calculation, the reduction in the level of paint damage has reduced the current emission and the potential difference between the damaged area and the propeller. As a consequence, the slightly higher potential on the inner face plays a more significant role in opposing current absorption there which forces the current to flow along the slightly longer path to the outer face. It should be emphasised that this is the *normal* situation. The situation which occurred in the perfect paint calculation, section 7.4, where differences could be seen over the propeller in terms of current emission on the inner face is the pathological non-realistic situation. This reduction in the current is highlighted by the different scales on the q figures of the two models. In this case, the paint damage is one thousand times less severe which has the effect of reducing the corrosion current in the system by around one thousand. As discussed above the values of q are directly related to the current size, and inversely related to the areas available for the currents to be absorbed. Since the same areas are absorbing in both models (i.e. the complete propeller) the q values in this case are around one thousand times smaller than in the extreme damage case.

On the hull, the values of u vary from being negative at the stern to being positive toward the bow. On this model, the magnitudes are approximately one hundred times smaller than in the severely damaged case. The actual values of u are not as significant as the value of $V - u$ which determines the value of q from the polarization relation. In this case, $V = 0.38966V$ which is approximately one hundred times larger than the extreme damage case so this balances out the increase in the u values. The key property though is that unlike the perfect paint case, figure 7.4, where the potential was approximately zero over the majority of the hull, this case displays similar behaviour to the severe damage case. So the corrosion currents in this case behave as in the severely damaged case in that they are emitted from the positive potential at the bow (see figure 7.19) and flow mainly to the propeller where they are absorbed primarily by the rim and the

outer face with the inner face absorbing less (due to the hull being close by). It appears at first glance that there is a constant emission of corrosion over the entire damaged region, but a closer examination has shown that this is incorrect. Figure 7.21 shows that there is a variation in the levels of corrosion over the damaged region which has been hidden by the contrasting values in q between the damaged and undamaged regions. The reason for this variation is not terribly clear but can be explained if the influence of the sea surface and the requirement for a continuous potential distribution over all the model is considered. This figure shows the variation in u across the damaged region because the argument which shows that current emission in this region is not constant is easier to understand by considering the variation of the potential.

In these calculations the sea surface has been specified to be non-conducting, so that it has $q = 0$ but may obtain non-zero potentials. The hull has positive potentials so it follows that the surrounding sea surface elements should also have positive potentials to ensure a continuous distribution. On the hull, the q values are determined from eqn (7.2.1) via the values of $V - u$. The key factor to the whole process of the corrosion of a ship is that the hull is *trying* to corrode. It is straining to have as large a q value as it can possibly have. For the undamaged areas, $k_i = 1 \times 10^{-6}$ which would mean that no matter what value of u an element had within the constrained range, the corresponding q value would be very small. In this solution, $V = 0.38966V$ which means that to obtain the most positive q value allowed within the constraints, the value for u on these undamaged areas should be as small as possible (from eqn (7.2.1)). The neighbouring sea surface elements to the undamaged hull regions shall then obtain similar size u values to ensure a continuous distribution. This distribution will spread to the sea elements which are in contact with the elements on damaged area of the hull. These upper most damaged elements will therefore have similar potentials again but with the increase in the conductivity of the paint ($k_i = 10^{-3}$) this will actually cause a large emission of corrosion currents. The method tries to match the current emission from this region to the current absorption on the propeller so the potentials over the rest of the elements will be varied. The potentials increase as the the depth of the ship increase, which relates to a decrease in current emission, and then begin to decrease as the base of the hull is approached, emitting larger corrosion currents.

Again it is not obvious why there is the increase in corrosion toward the base of the hull. It is most likely due to the paths available to the sea currents. The sea currents will always flow by the path of least resistance, but will also look to flow to the point of lowest potential, which on the propeller is the lower sections. Hence the most likely path for the corrosion currents to follow through the sea is that from the bottom of the hull to the lower regions of the propeller.

This is a feature which is also apparent on the figures for the case of the extreme paint damage of section 7.5.

The shape and magnitude of the resulting magnetic field are shown in figures 7.22 and 7.23. It is clear that the shape of the field is the same as for the severely damaged paint which would be expected due to the similarity in the current flow. The same situation has arisen with the potentials on the hull ranging from negative values at the stern to positive at the bow in the vicinity of the damage so it is again far easier to think of the field directions in terms of the Biot-Savart Law rather than the method proposed in chapter 6. The dominant field contributions will again be from the sea currents closer to the ship than the field point (the direction shown in figure 7.22 as counter-clockwise). The magnitude can again be verified by a similar quantitative calculation as performed for the severe paint damage. The area emitted the current to the sea is the same but with the decrease in level of damage to $k = 10^{-3}$, the resistance of the return path becomes $R = 1\Omega$. The potential across the ship's metal work is $V = 0.38966$ so the return current can be estimated to be $I \approx 0.4A$ which will result in a magnitude of the field of the order of $|\mathbf{B}| \approx 10^{-9}T$. Comparing this value to those shown on figure 7.23, the calculated magnitudes appear to be supported with the key aspect being that they have decreased from the severely damaged paint situation but are larger than for the perfect paint case. They may be a little larger than the approximated values but again this approximation was based on the return currents which were dominated by the larger sea current contributions so it is reasonable to conclude that the calculated field is perfectly valid.
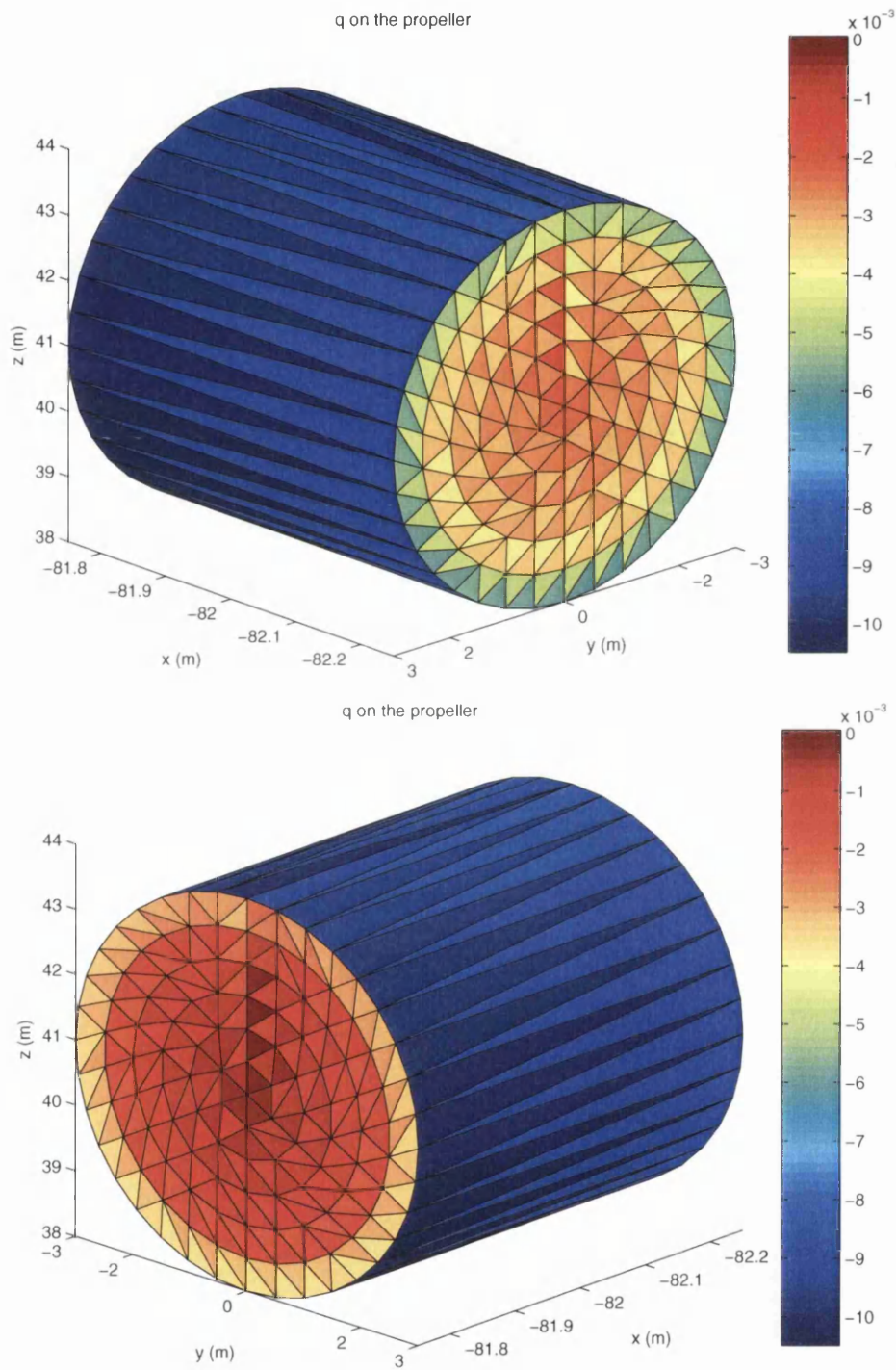
Figure 7.17: q on propeller, furthest face from hull (top) and nearest face to hull (bottom).
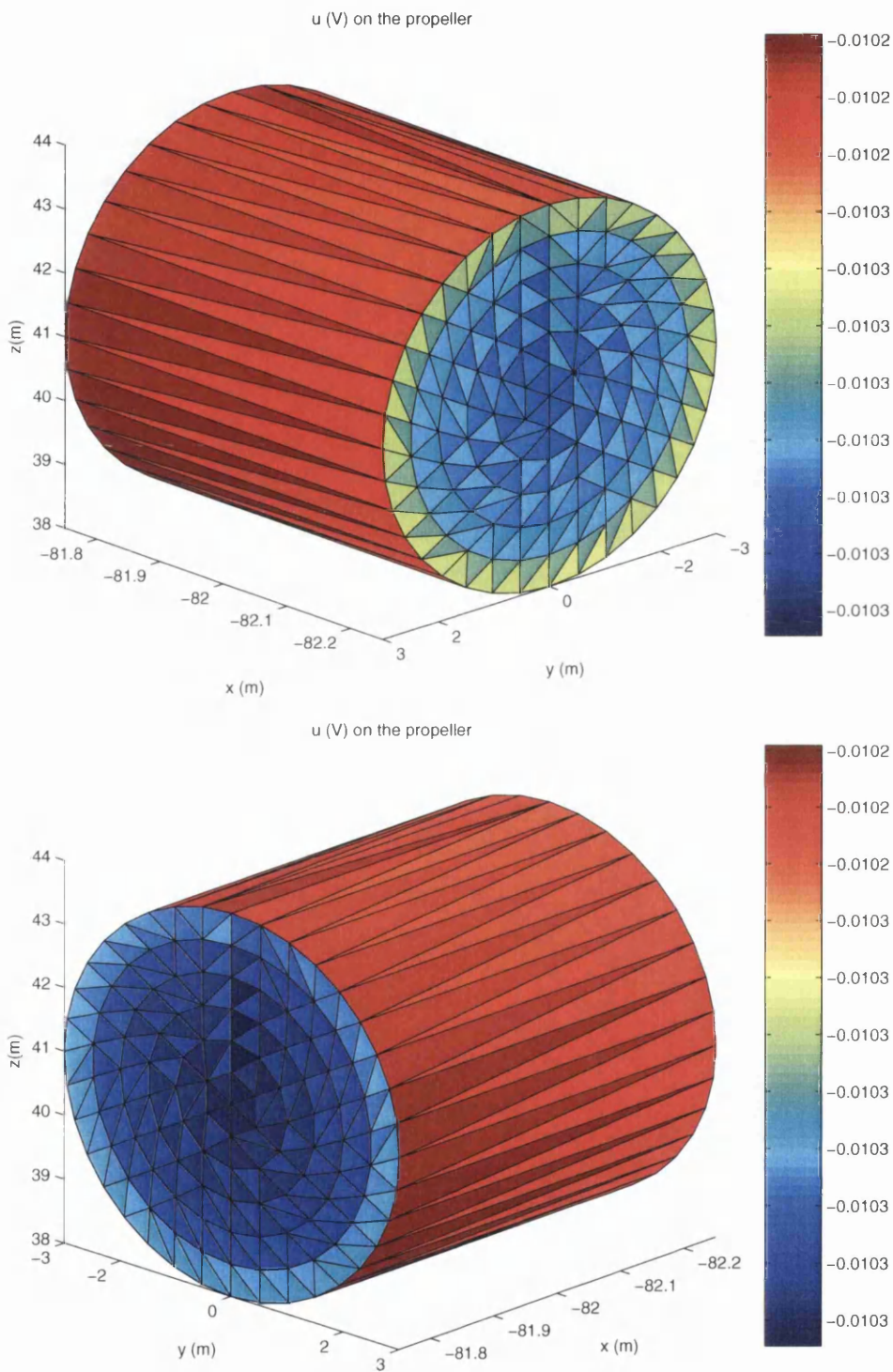
Figure 7.18: u on propeller, furthest face from hull (top) and nearest face to hull (bottom).
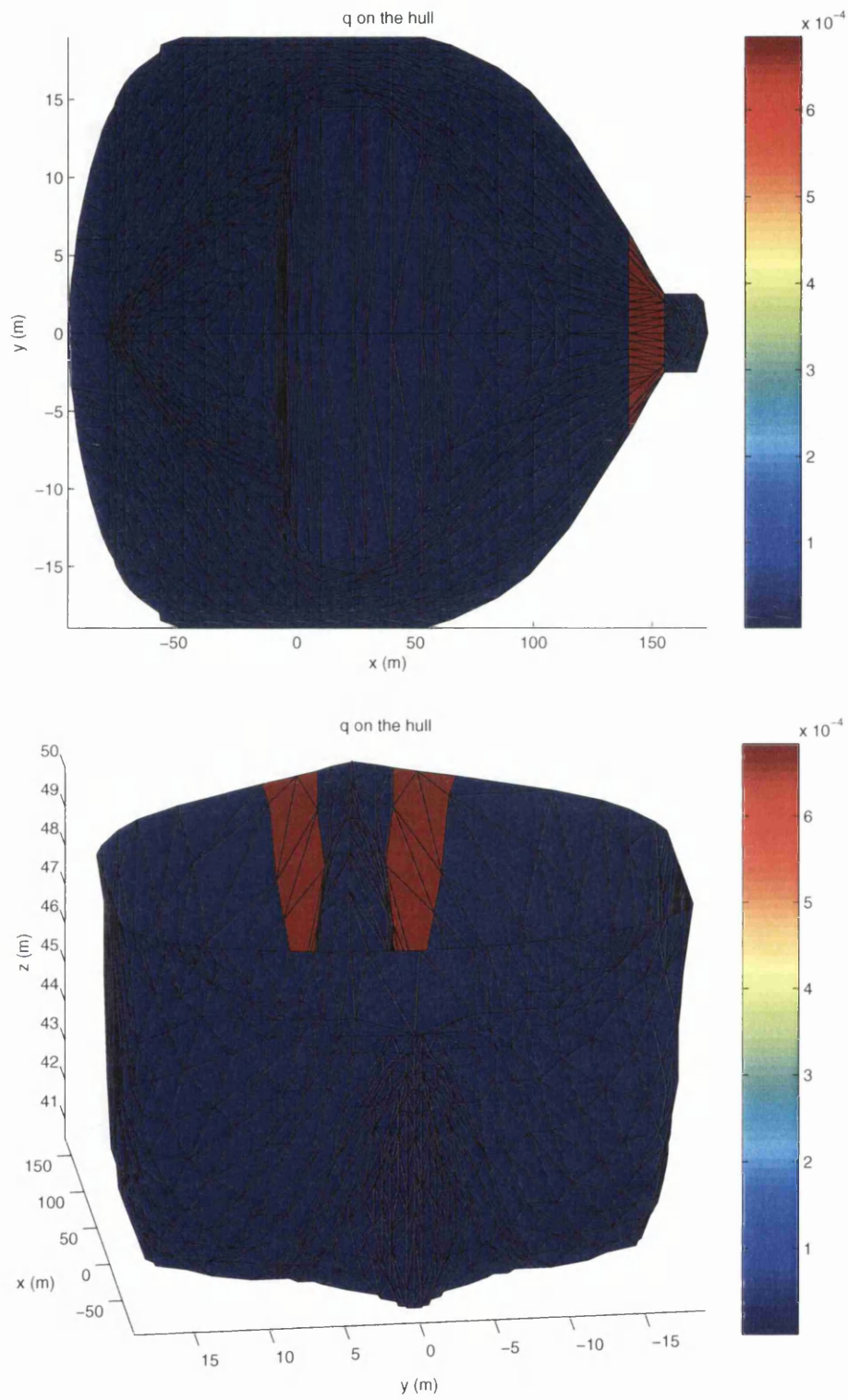
Figure 7.19: q on the hull, aerial view (top) and view from stern (bottom).
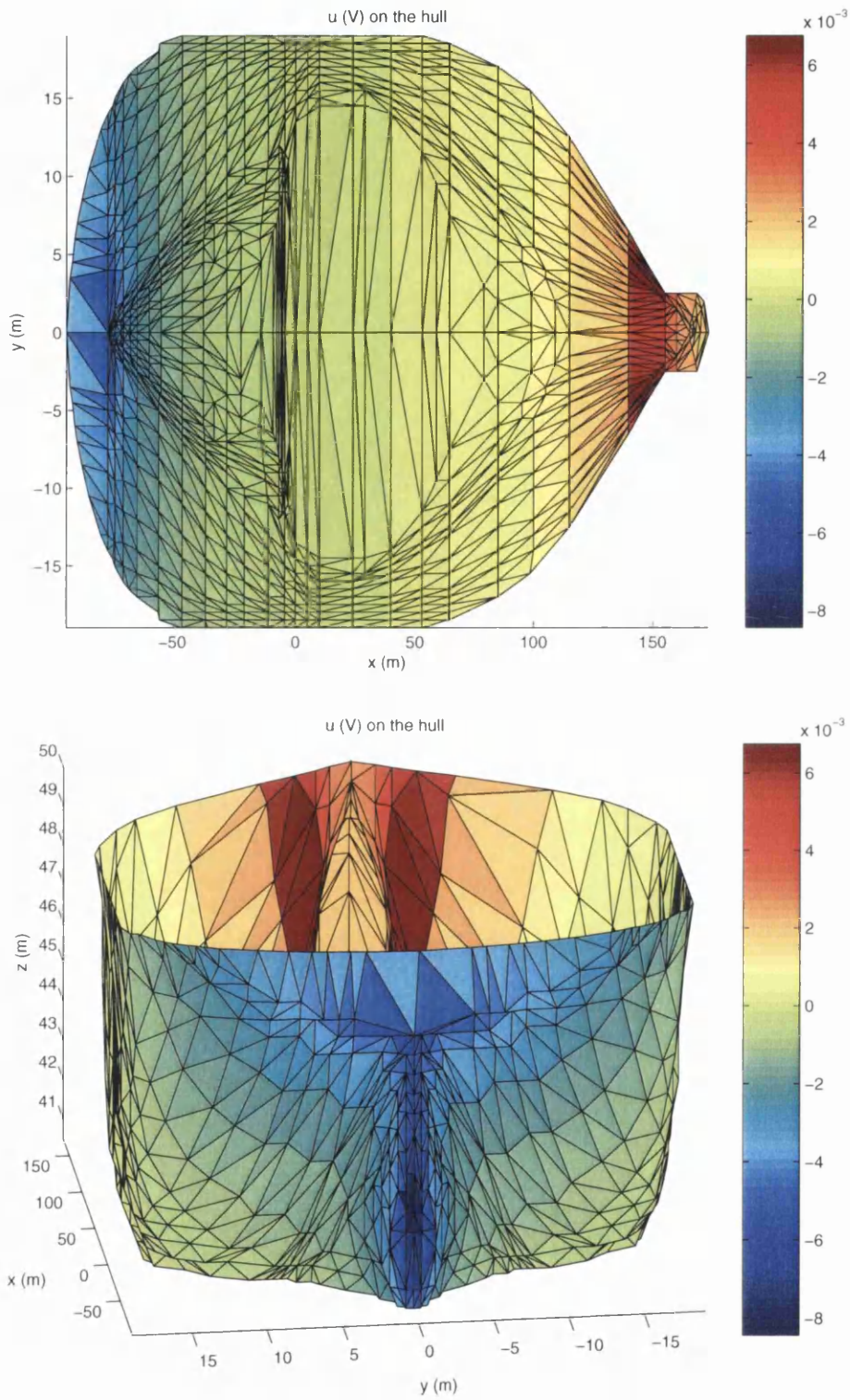
Figure 7.20: u on the hull, aerial view (top) and view from stern (bottom).
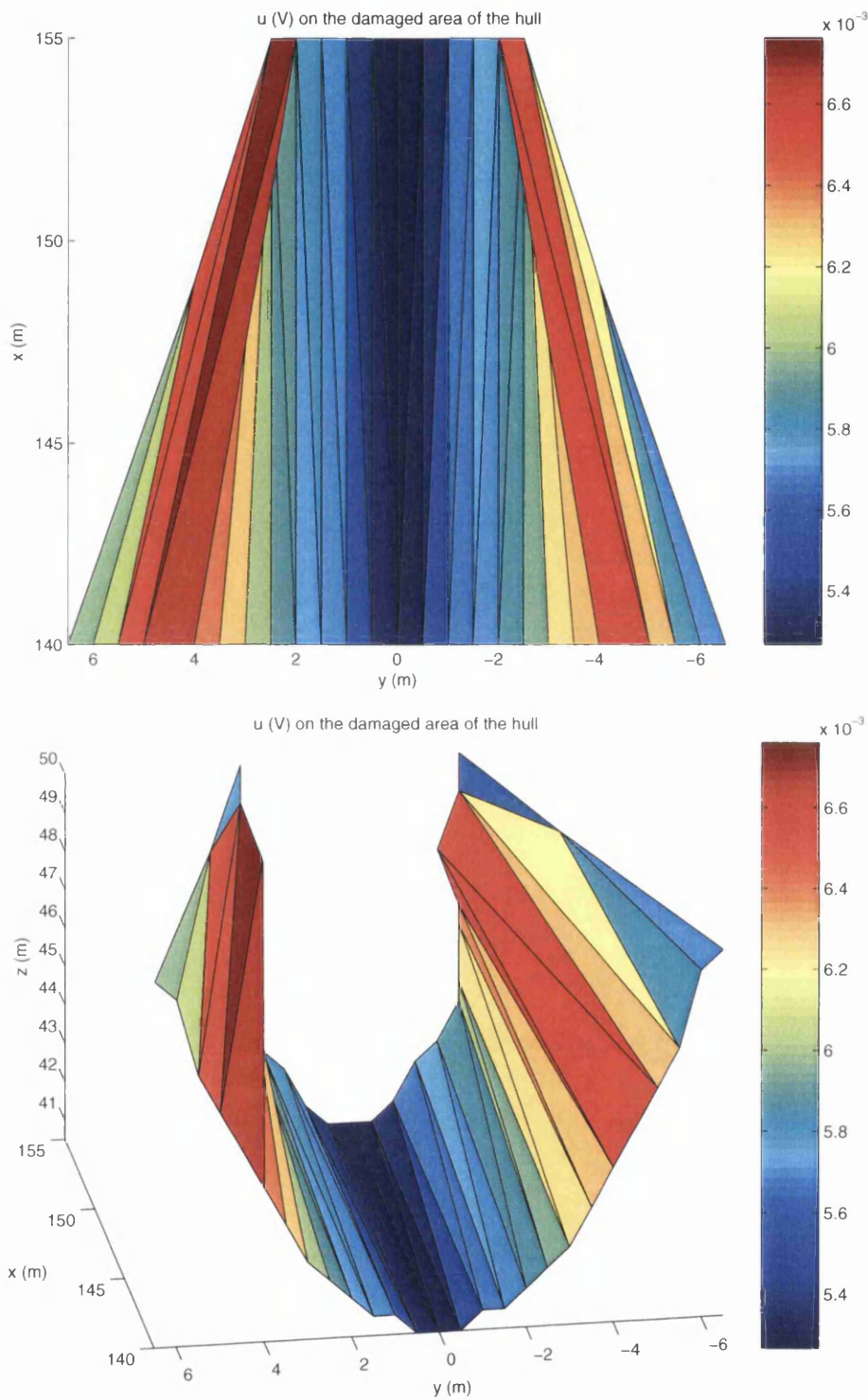
Figure 7.21: u on the damaged region, aerial view (top) and view from stern (bottom).
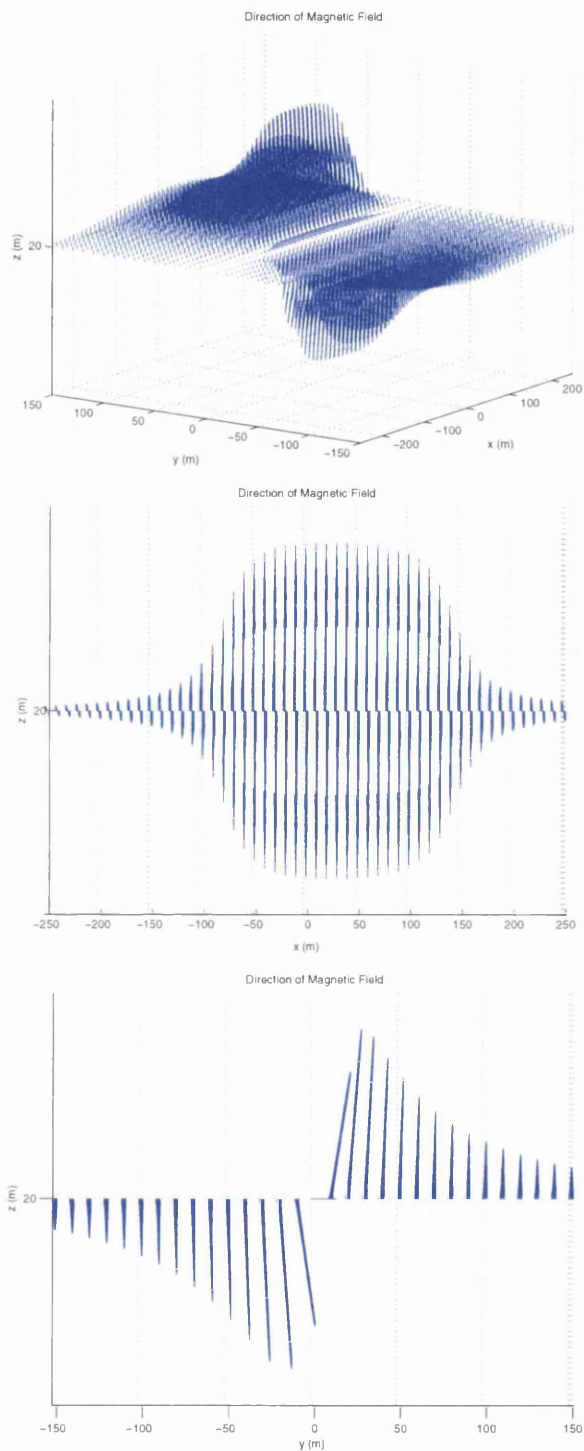
Figure 7.22: Magnetic field from corrosion currents, the three-dimensional view (top), xz cross-section (middle) and yz cross-section (bottom).
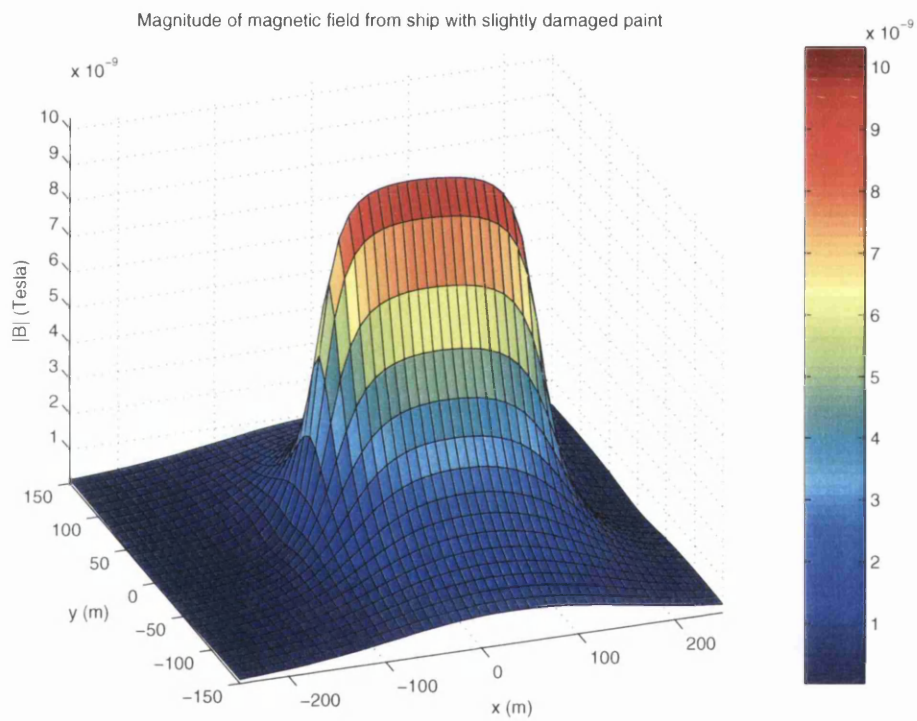
Figure 7.23: Magnitude of the magnetic field for a ship with less severely damaged paint on the hull.

7.6.2 Verification by Dipole Approximation

The dipole approximation of the CRM field is shown in figures 7.24 and 7.25.

As was the case in section 7.5, figure 7.24 indicates that the dipole approximated field is in agreement with that calculated from the full method in terms of shape and direction. The plot of the field magnitude, figure 7.25, is now larger than that for the field from the full method but in comparison to the field from the previous calculation in section 7.5 which was for severe paint damage, the field magnitude is less. As indicated in the previous sections this is due to there being less corrosion on this model, which reduces the corrosion currents in the sea and hence diminishes the effect of the non-conducting boundary in the full calculation. From this it can be concluded that in general the dipole approximation will over-estimate the CRM field from a model and would always predict a larger field magnitude if it were not for the non-conducting sea bed boundary which, for models with high levels of corrosion currents, will significantly increase the magnitude of the field so that it is larger than that approximated by the dipole model.

With the only noticeable discrepancy between the fields calculated by the full method and dipole approximation being in the magnitudes, and this being understood as a short coming in the formula used by the dipole approximation, this approximation adds further support to the CRM field calculated from the full method.

Figure 7.24: Dipole approximation of the magnetic field from corrosion currents, the three-dimensional view (top), xz cross-section (middle)and yz cross-section (bottom).
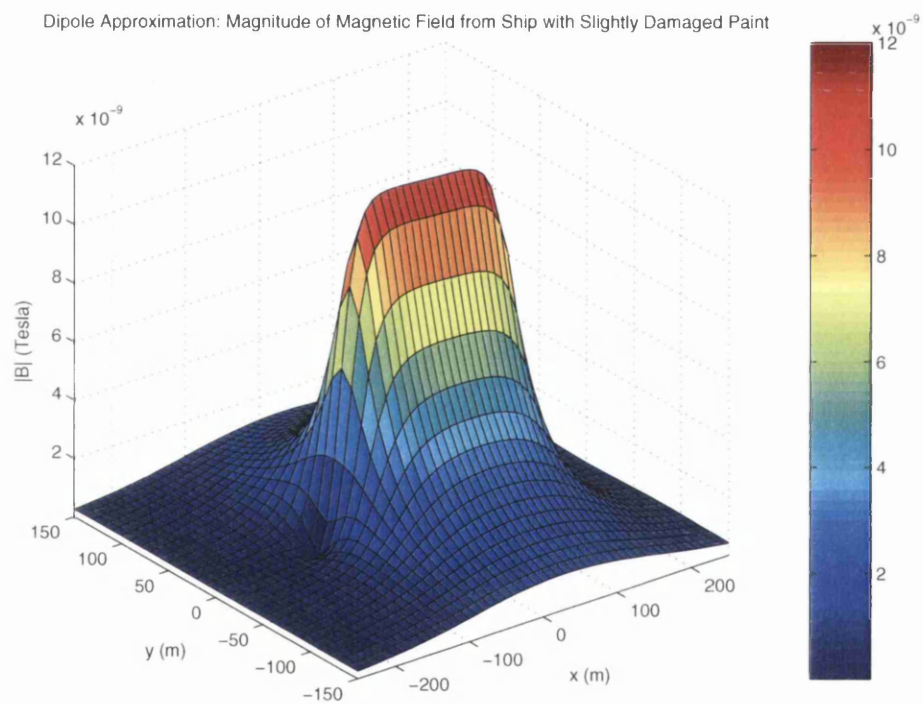
Figure 7.25: Dipole approximation of the magnitude of the magnetic field with less severely damaged paint on the hull.

7.7   ICCP Switched On - Analysis.

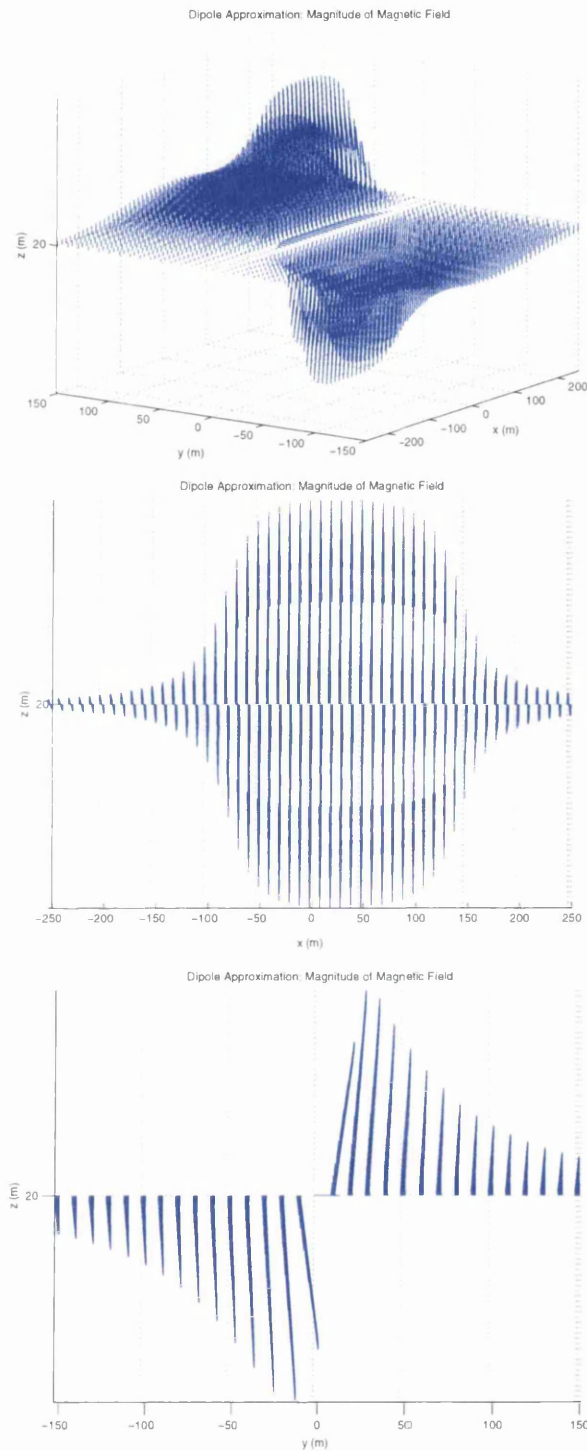In the previous two sections, two different levels of paint damage have been considered. Originally the damaged paint was deemed to be one million times more conductive than the perfect paint coating which covered the rest of the hull. This was felt to be an extreme case and therefore another situation was investigated where the damaged paint was reduced to be only one thousand times more conductive. In this section, an ICCP system is turned on which is intended to act to prevent corrosion of the hull, i.e. reduce the corrosion currents which are emanating from it.

To keep as close as possible to the real-life situations the hull was again covered with a perfect paint coating with damage in the region $133.8m \leq x \leq 153.8m$ and the conductivity of the paint increase by a factor of one thousand (i.e. the less severe damaged paint model). The ICCP system investigated involved two pairs of anodes, one pair located toward the bow of the ship and the other further toward the stern. To maintain the integrity of the mesh on the hull, existing elements were redefined to be anodes. This avoided altering the mesh to add in elements to act as the anodes, which would have increased the possibility of introducing overlapping elements or holes onto the hull mesh. The conditions required were that both elements in a pair had the same surface area, the same shape and orientation, and located symmetrically about the base line of the hull (i.e. had centroids with the same x and z coordinates, and one with the negative y coordinate of the other) [59, 62]. To model the element as an anode, the value of q could be set to a fixed value which represented the supplied current from the anode. Since the anodes have the same surface area, this meant that for each anode pair only one anode current was required to ensure that the anodes on either side of the baseline are outputting the same q values [17].

The common practise in industry is to split the hull into zones and have an anode configuration in each zone minimising the corrosion occurring [59]. On a large hull this can often require the hull being separated into somewhere in the region of two to six zones but is dependent on the requirements of the ship. There are many considerations which need to be taken into account when designing an ICCP system. These include the most likely location of the paint damage on the hull, the resultant magnetic field caused by the system when activated, the protection afforded to the hull, and the total amount of current required to operate

the system at which maximum protection is provided. It is possible to operate the anodes of the ICCP system separately and then perform an optimisation procedure to check whether the hull is satisfactorily protected [63], but this was felt to be too complex for initial calculations such as those performed here.

Most paint damage on a ship tends to be the result of two main factors. Firstly, the turbulent flow of water that occurs at the bow (where the hull breaks the water) and at the stern (where the propeller is rotating) acts to strip away the paint coating. Also when a hull is brought into contact with other objects such as the buffers on the sides of docks, the paint will be damaged. To counter the damage in these areas it is conventional for them to be given their own zone on the hull and hence their own ICCP anode configuration. With the damage considered in this calculation being located toward the bow only, it was deemed unnecessary to include other anode configurations in the other specific positions. Hence there were no anodes located in the immediate vicinity of the stern.

The anode pairs were located at $x = 60.67m$ and $x = -27.00m$, which is consistent with the positions used on smaller vessels such as generic warships [64]. In pursuit of pairs of elements that matched the conditions mentioned above, the elements that where actually selected at these x locations were almost predetermined and had centroids at locations $(60.67, \pm17.83, 46.33)$ and $(-27.00, \pm1.67, 40.50)$ respectively. This meant that the bow pair were located at realistic locations about midway up the sides of the hull. The anode pair toward the rear (the stern pair) were however located at slightly unrealistic positions close to the baseline.

The positioning of these anodes is not required to be concurrent to realistic systems since this research is investigating the ability of the proposed methods to evaluate the effects of the anodes, and is not concerned with any optimisation of the protection provided to the hull. To this end, the currents which were supplied to the anode pairs was $1A$ in both cases, which corresponded to q values of $8.419e - 02$ for the bow pair and $1.667e - 01$ for the stern pair. Notice that the stern anodes have a smaller area than the bow ones, a factor which will be emphasised by the figure showing q on the hull. Also the q values for the anodes are positive as required since this corresponds to current being emitted which results in electrons being supplied to the metal to prevent corrosion from occurring.

With this ICCP set up and hull damage as in section 7.6, it is possible to

predict the behaviour of the solution.

7.7.1 Predicted Behaviour.

To analyse the effect of the ICCP anodes, begin by considering the behaviour of the solution on the hull. The anodes of the ICCP system are pushing current into the sea water. This current must flow to other areas of the ship to avoid stray currents. As the analysis of the perfect paint coating situation indicated, the areas of the hull which are covered by perfect paint will not be willing to accept any of the current, so the only destinations for the current is the propeller and the section of damaged paint. At the damaged paint in the absence of the ICCP system, the hull will be corroding and trying to emit a corrosion current which requires the q values to be positive and the potentials u to be more positive than other areas of the ship, namely the propeller. However, with the ICCP anodes turned on, the potentials on these anodes will be greater than those on the damaged paint elements so some current will flow from the anodes to the damaged elements which will try to prevent them from emitting their own corrosion current.

However, there is no optimisation in this calculation which means the possibility of over-protection must not be dismissed. This occurs when the currents from the ICCP anodes are too large resulting in the current being absorbed at the damaged paint elements being so large that it not only prevents the emission of corrosion currents, it may actually reverse the flow so that these elements absorb a significant amount of current, which would be highlighted by these elements having negative q values. The physical effect of this is very significant as it will result in the blistering of the remaining paint on these elements and their neighbours. This seriously compromises the protective properties of these elements meaning that there are larger areas prone to corrosion. Hence more ICCP currents could be thought to be required to improve the protection provided, which again causes more damage and a vicious circle is completed. There is nothing that can be done about this possibility when there is no optimisation included in calculation but it is a scenario which must be considered. Ideally there will be no corrosion on the damaged elements [9], which would mean $q = 0$. However without optimisation this is improbable. The most likely situation though is that the damaged area will still emit corrosion currents but hopefully less than in the calculation for less severe paint damage with no ICCP system activated.

To summarise, it is expected that on the hull, the q values are positive for the anodes, approximately zero for all area of undamaged paint, and either positive, negative, or zero for the damaged region. It remains likely though that there will be a net flow of current out from the hull. The previous calculations have indicated that the propeller should have a lower potential than the hull, and consequently it is a likely destination of these emitted currents. This places a restriction on the potentials of the non-damaged elements of the hull which should not be more negative than the propeller (to prevent current absorption) nor should they be more positive than the anodes. To ensure that the potentials are continuous over the hull, this would require that in the vicinity of the anodes the potentials are largest whilst they decrease as the distance between the elements and the anodes increases. This should mean that at the stern and the bow, the potentials are at local minimum values. Recall, that the damaged area of the paint is located very close to the bow and in this area current will be getting absorbed or emitted depending on the level of protection provided by the anodes. This means that the potentials in this bow area will be different to those at the stern. When ICCP is switched off, it has been shown that the potentials will be positive in the damaged region, and hence it is reasonable to assume that with the ICCP anodes on, the potential in this area will be slightly larger than at other areas unless the corrosion is completely prevented by the ICCP system, or over-protection occurs.

Also at the stern, the hull is in close proximity to the propeller which is expected to be at a negative potential. This should have the effect of pulling down the potential in the stern of the hull. The combined effect of these actions on the hull is that there will be a continuous potential distribution across the hull with the areas of greatest magnitude being in the vicinity of the anodes while the stern will have the smallest potential (possibly even negative), and the bow will be at a slightly higher potential compared to other areas of the hull which are protect by perfect paint and are distant enough from the anodes to avoid being effected by any great amount.

This discussion also determines the expected behaviour on the propeller. Previous calculations have indicated that the propeller should be at a lower potential than the hull and hence will absorb any currents from the hull not dealt with as part of the protection process. Therefore the propeller should have negative q

values and u values smaller than anywhere else on the ship.

Since the ICCP system is supplying more current to the model it is expected the magnitudes of the magnetic field should increase, although the direction of the field should remain the same as in the previous calculations. However this is not definitely going to be the case because if the ICCP system manages to completely prevent corrosion, or at least significantly decrease it, there could be less current flowing in general. One definite consequence of this would be that there is less current flowing to the propeller and more to the damaged area of the hull. In this case, the main area of current activity will be between the anodes and the damaged paint and in this region there should be a peak in the magnetic field with the field over the rest of the ship being significantly diminished. However, as mentioned above, this is an unlikely scenario and hence most of the current is still expected to flow from the hull to the propeller. With this current being larger than in the previous calculation, the magnitude of the field should increase when compare to section 7.6, possibly with the most noticeable increase occurring between the stern anode pair and the propeller since the current from these anodes are less likely to be absorbed by the damaged region than those from the bow anodes. In either case the orientation of the field should be the same as the previous calculations since the same governing arguments still hold.

7.7.2 Calculated Behaviour.

The calculated behaviour of this model is shown in figures 7.28 -7.31. Begin by considering the solution on the propeller as depicted in figures 7.28 and 7.29. It was predicted that the majority of the current that is emitted by the ICCP system should be absorbed by the propeller, which would require negative q values, and indeed this is what is shown on figure 7.28. Similar with all the other calculations, the rim of the propeller seems to be accepting more of the current. The distributions of the q values on both faces are extremely similar, a characteristic which this model shares with the one for extreme paint damage in section 7.5. In that model it was hypothesised that this was due to there being a significantly larger potential difference between the source of the currents and the propeller than that which occurred between the two faces of the propeller due to the close proximity of the hull to the inner face. This meant that to the corrosion currents, the path to the outer propeller face offered similar resistance in

comparison to the path to the inner face despite the longer distance involved. This hypothesis is supported by this result since the anodes in this model should be at a far higher potential than the propeller creating the large potential difference. This has meant that there is a large current flowing to the propeller which is absorbed by each face almost equally.

The only difference between the two faces is at the top of the propeller, close to the hull. This feature is more prominent in the inside face as expected (figure 7.28(bottom)). This is the region which the hull is closest to and will hence have the greatest effect in pulling up the potentials to oppose current absorption.

The values of the potentials u on the propeller are shown in figure 7.29. These should all be less than the values of the potential on the ICCP anodes (which will most likely be positive) and this appears to be the case with these values being all negative. The key features of the q propeller plots are again evident here, with the rim being the most negative part of the propeller and the faces having similar potential distributions. Indeed the only real difference between the two faces occurs where the potentials have been compromised by the close proximity of the hull as expected.

The value of the potential on the metal work of the ship for this calculation is $V = 0.225191V$, so using the linear polarization relation, eqn (7.2.1), it is clear that the values for u and q on the propeller are consistent.

Again it is pleasing to see the extrapolation of the potentials over the faces follow the familiar pattern with the largest potential magnitudes occurring at the exterior of the face and then getting smaller as the centre is approached with those elements which share a side with an element further out having larger magnitudes that those which only share a point. This leads to the required continuous distribution.

Consider now the solution on the hull as shown in figures 7.30 and 7.31. Begin by considering the values of q depicted in figure 7.30. Firstly, the aerial view clearly indicates the locations of the anodes, with the bow pair located on the sides of the hull while the stern pair are located extremely close together about the base line, lying reasonably flat on the bottom of the hull. As stated previously, the values of q on each pair clearly indicate that the areas of the stern pair are smaller than for the bow pair. This figure appears to indicate that the majority of the hull is neither absorbing or emitting any currents. This was

predicted for those areas which had a undamaged paint coating, but for the area of damaged paint, $133.8m \leq x \leq 153.8m$, it was assumed that there would be some form of current flow, either in or out. Consider figure 7.26 shown below.
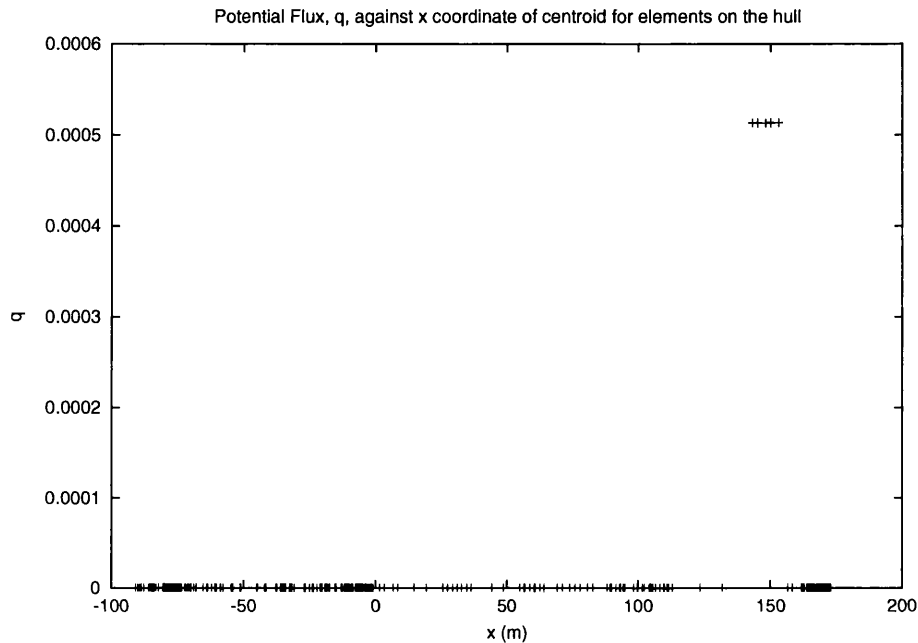
Figure 7.26: Plot of q against x-coordinate of the centroids of the elements on hull, excluding anodes.

This figure plots the values of q against the x coordinate of the centroid for every element on the hull except the anodes. Since this removes the large q values of the anodes from the plot, it highlights the small variations across the hull. It is clear that for all the areas where the paint is deemed perfect, the values for q are extremely close to zero as predicted. In the damaged region however, this plot indicates that the values for q are in fact non-zero and are small positive values of just over 0.0005, which are very much less that the values for the anodes, whose smallest value is approximately 0.08. Compare these values for the damaged region with the those for when the ICCP system is not operating (section 7.6) where the values are 0.0006. This indicates that the ICCP anodes do in fact supply current to the damaged area and impedes the corrosion currents that are produced, i.e. reduces the level of corrosion occurring. While the level of protection that is provided is not that great, and would not be acceptable in practise, it serves to indicate that the methods used here can successfully model

the effect an ICCP system may have on the corrosion of a hull.

Consider the potentials on the hull, figure 7.31. It is apparent that there are large positive potential values on the elements which represent the anodes of the ICCP system as expected. The neighbouring elements to these also have larger positive potentials than the rest of the hull, but these quickly drop back to the average potential for the hull due to the perfect paint which is forcing them to have zero q values. The majority of the hull away from the immediate vicinity of the anodes appears to be at an equal potential with the stern being slightly more negative than the rest which is due to the close proximity to the propeller. The q values on the hull apart from on the anodes were all zero except in the region of damaged paint where they were positive but significantly smaller than the magnitude on the anodes. This should correspond to a variation in the potential at this region, but it will be difficult to identify this due to the anode potentials spreading out the scale on the plot. However, if the area of damage is closely compared to the neighbouring elements, it is possible to see that there appears to be a small change in potential, i.e. the shade of green has darkened slightly. This is highlighted in the following plot, figure 7.27, which has not had the anode values removed since the potentials are extrapolated from the anodes to neighbouring elements which would also have to be removed. This was not a concern with the corresponding q plot since these values on the anodes are not extrapolate to the neighbouring elements.

Figure 7.27 clearly shows that there are peaks in the potentials surrounding the anodes and negative potentials at the stern as indicated by figure 7.31. In the region of the damaged paint it is possible to distinguish that the potentials do appear to increase slightly as expected.

As on the propeller the extrapolation of the potentials over the hull elements is encouraging as it shows the familiar pattern required to produce a continuous distribution. Once again eqn (7.2.1) can be used to show that the u and q values are consistent.

With the calculated solutions to the BEM equations making sense physically, the magnetic field will now be considered with particular attention paid to the comparison between this field and that produced for the less severely damaged paint in section 7.6. As with the previous calculations, the direction of the corrosion related magnetic field will be determined by the direction of the sea currents.
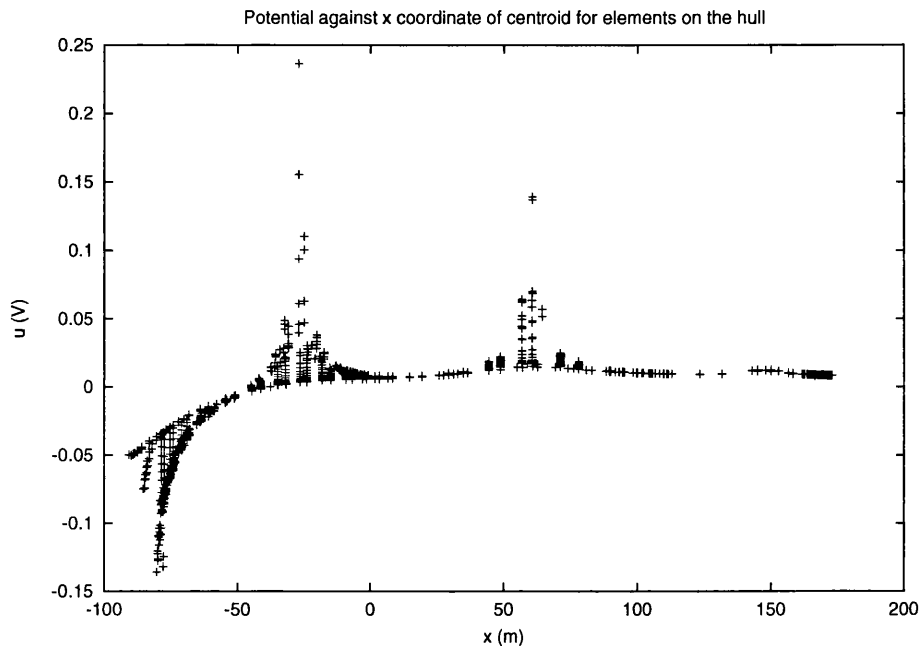
Figure 7.27: Plot of u against x-coordinate of the centroids of the elements on hull, including anodes.

For a field point, consider two volume elements an equal distance from the point but in opposite directions. The volume nearer the ship will have a higher current density than the volume further away which results in the counter-clockwise field direction as shown in figure 7.32.

All the ICCP anodes are supplying 1A to the model. In the region between the bow anode pair and the damaged paint, the current flowing to the propeller has been reduced in comparison to the less severe damaged paint calculation with the ICCP system deactivated. Hence the field in that region should be slightly less than in the previous calculation and this appears to be shown in figure 7.33. This protection has probably come from the bow anodes with the rest of the currents flowing to the propeller so in the region of these anodes ($x = 60.67m$) the field should increase in magnitude. Another increase should be apparent when the stern anodes are encountered ($x = -27m$) for similar reasons. After the propeller, the field should quickly reduce to zero. Both figures 7.32 and 7.33 support this behaviour. To confirm this is the case a quantitative calculation can provide good indications as to acceptable values of the field magnitude.

The conditions of the paint are the same as in section 7.6, only this time the

potential across the metal work of the hull is $V = 0.225191V$. Thus the return current flowing through the ship *from the sea currents only* is $I \approx 0.2A$ giving rise to the base magnetic field magnitude of approximately $|\mathbf{B}| \approx 10^{-9}T$ which is the approximate level predicted for the lesser paint damage case. However, except possibly at the extreme point of the bow, this magnitude is smaller that that calculated but this is to be expected since the effect of the anodes have not been included. Starting at the bow and moving toward the stern, the bow anode pair which supply $1A$ each to the system are encountered at $x = 60.67m$. So the return current from the propeller will have an extra $2A$ contribution which has not been included in the approximation up to this point, which increases the magnitude of the field to approximately $10^{-8}T$. Moving further toward the stern, at $x = -27m$ the stern anode pair is encountered which will add another $2A$ to the return current adding a further $10^{-8}T$ to the approximated magnetic field. Therefore it is thought that if the field is followed along the line $y = 0m$ from the bow, the field will increase at two points by significant amounts around the location of the anode pairs, and this is indeed what is depicted in figure 7.33 and also in the xz cross-section of the field shown in figure 7.32. However it appears that calculated field is still one order of magnitude larger that that justified by the preceding approximate calculation but this was expected for the reason explained in the analysis of previous cases.

A pleasing feature of these plots is that the overall the magnitude of the field is larger than in the case with lesser paint damage which is expected since the ICCP system has added current to the system which, although intended for the damaged area, has actually increased the current flow to the propeller significantly increasing the CRM field magnitude.
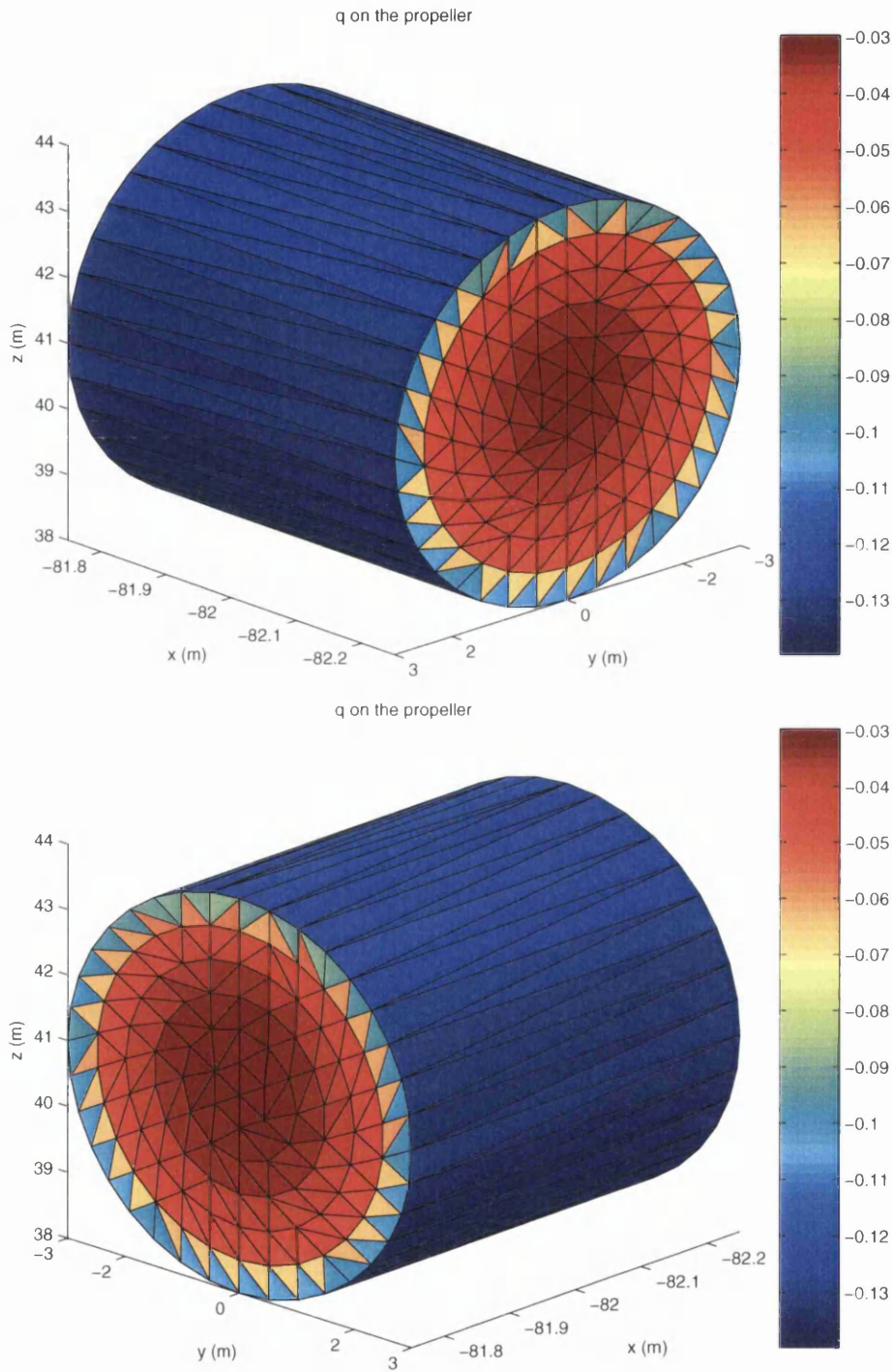
Figure 7.28: q on propeller, furthest face from hull (top) and nearest face to hull (bottom).
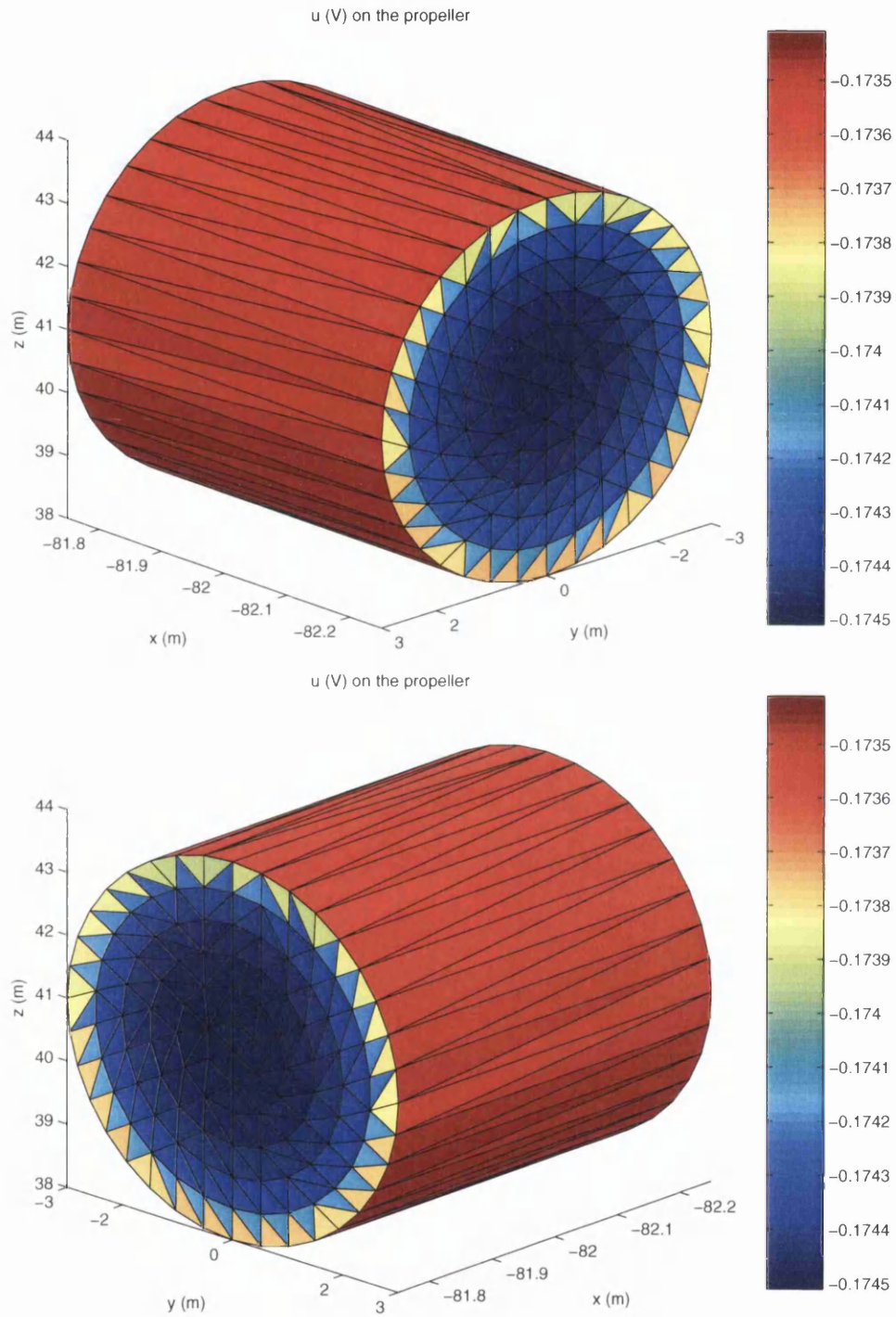
Figure 7.29: u on propeller, furthest face from hull (top) and nearest face to hull (bottom).
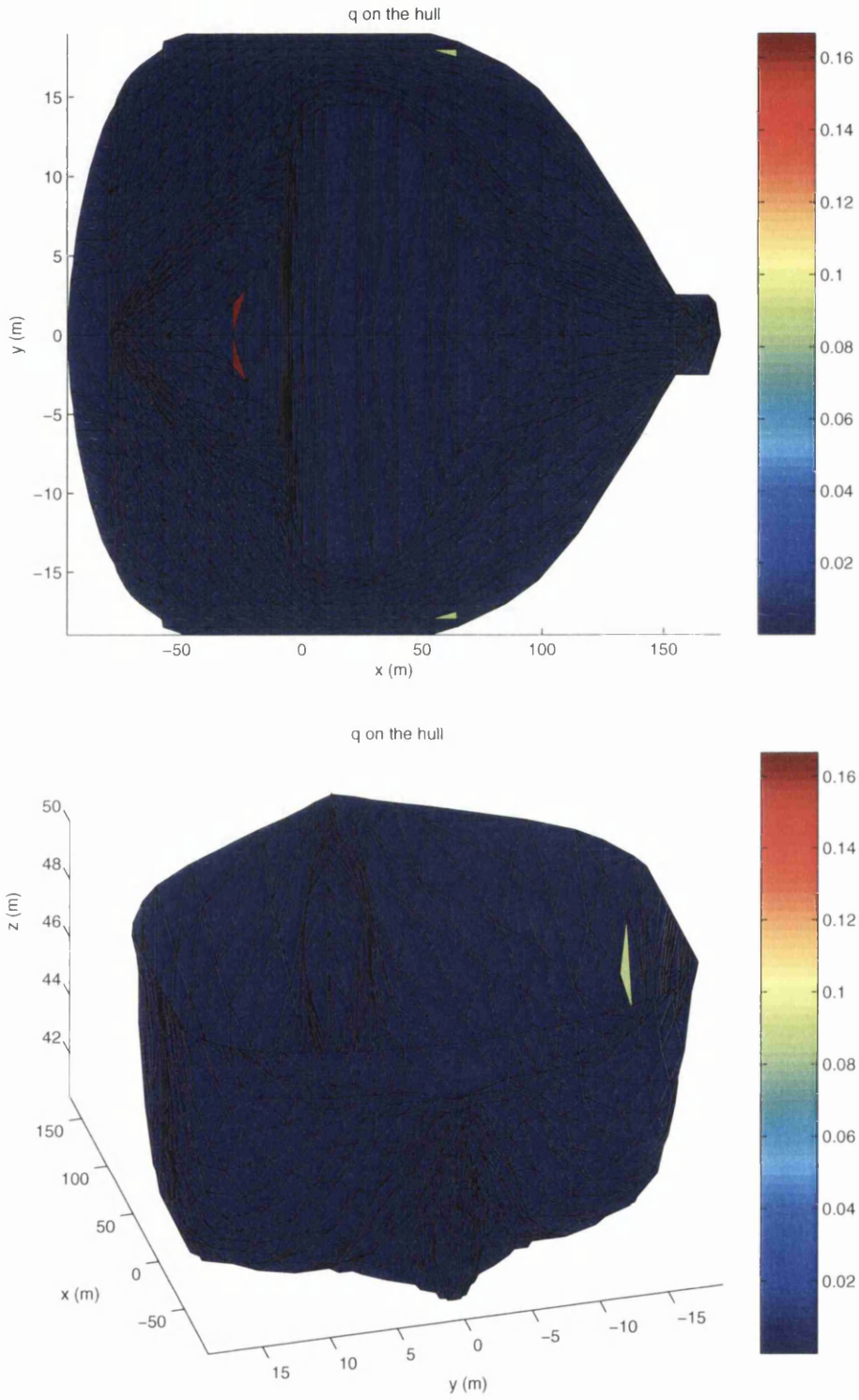
Figure 7.30: q on the hull, aerial view (top) and view from stern (bottom).

u (V) on the hull
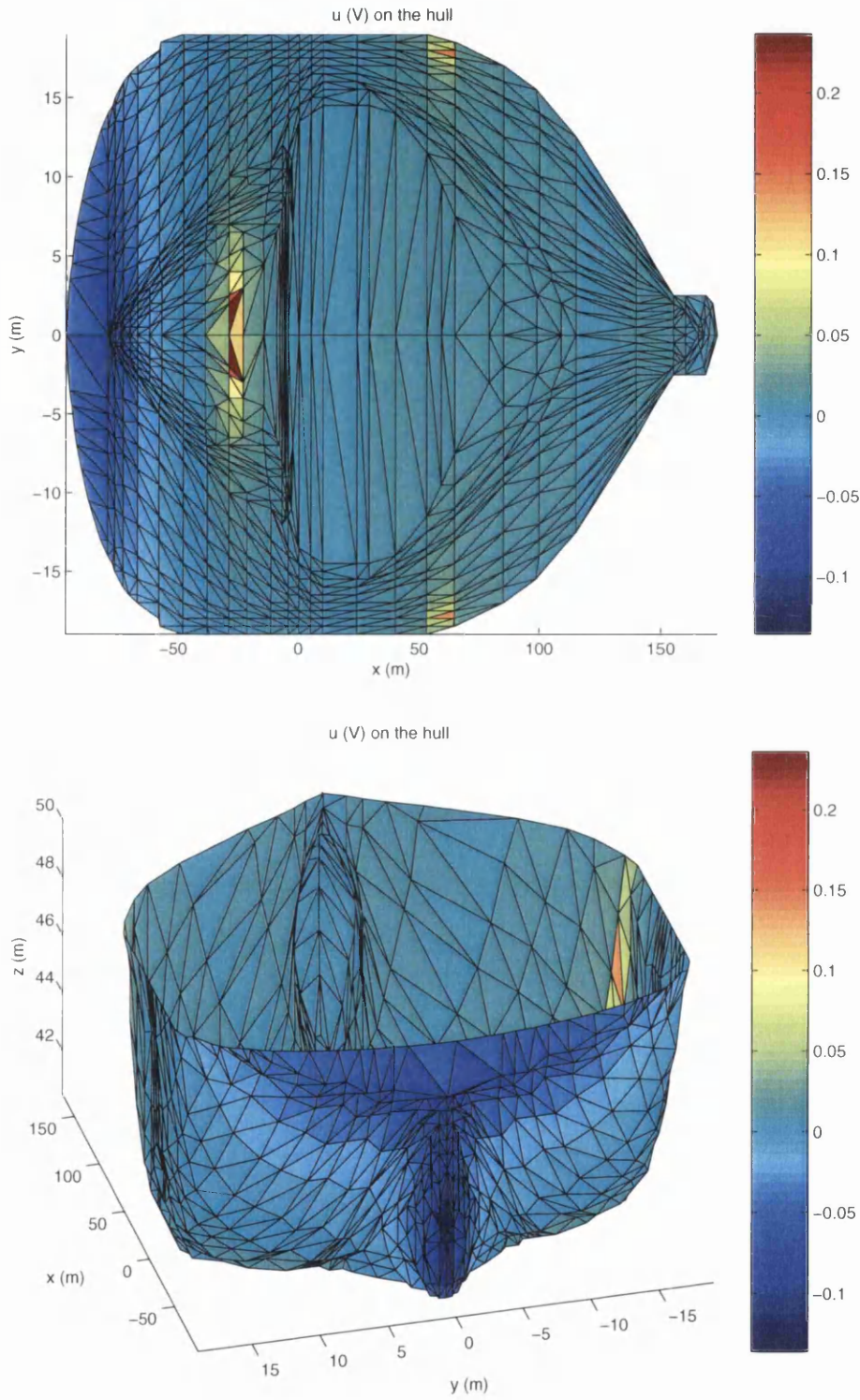
u (V) on the hull

Figure 7.31: u on the hull, aerial view (top) and view from stern (bottom).
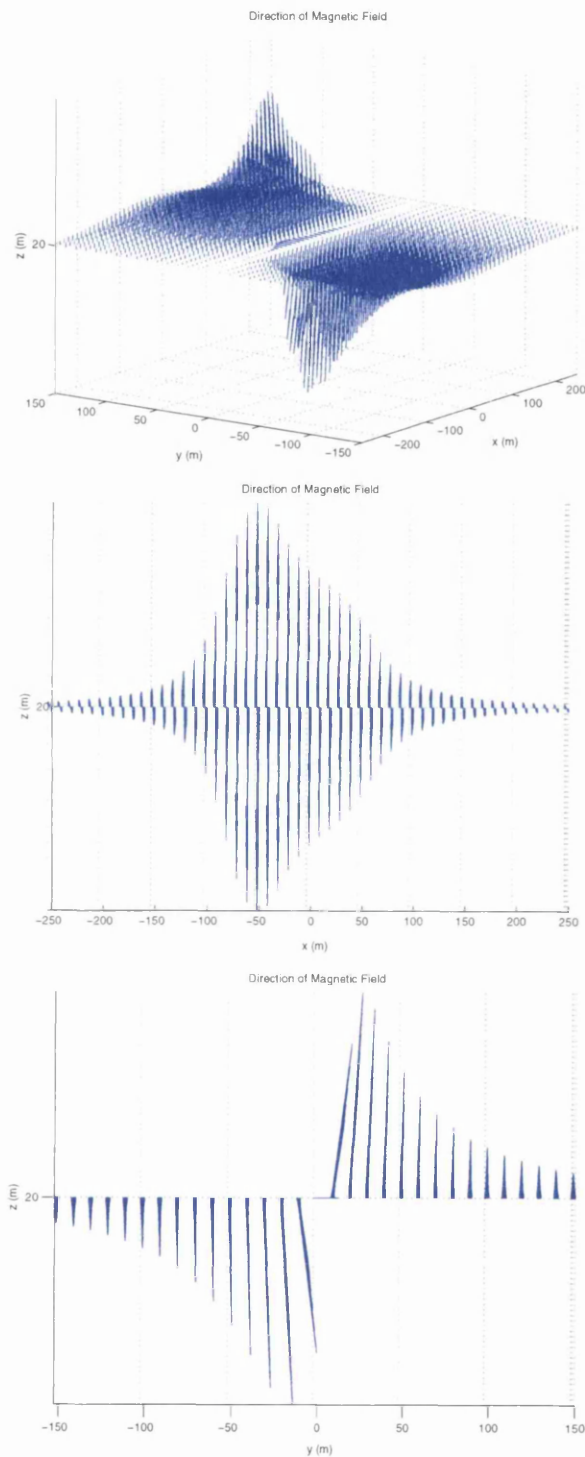
Figure 7.32: Magnetic field from corrosion currents, the three-dimensional view (top), xz cross-section (middle) and yz cross-section (bottom).
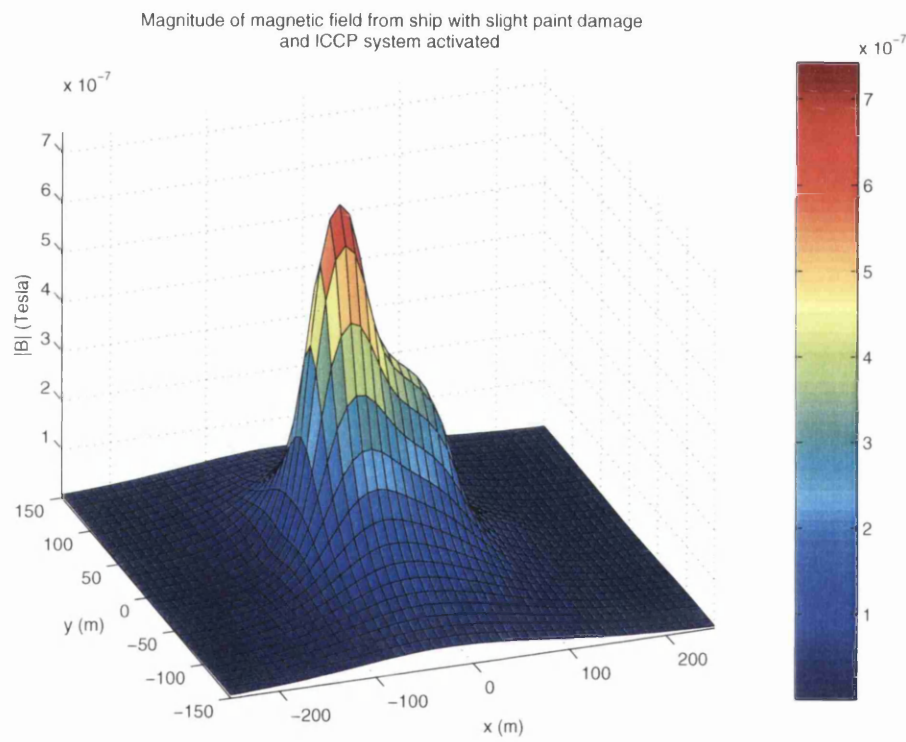
Figure 7.33: Magnitude of the magnetic field for a ship with damaged paint on the hull and an ICCP system activated.

7.7.3   Verification by Dipole Approximation

The dipole approximation of the CRM field is shown in figures 7.34 and 7.35.

Comparing the direction and shape of the fields calculated using the full method, figure 7.32, and the dipole approximation, figure 7.34, it appears that once again they both are in approximately the same direction and have similar shapes. As mentioned earlier, there is a higher level of corrosion currents flowing in this model than in the previous ones. As the comments made in section 7.6 regarding the under-approximation of the CRM field made by the dipole approximation when there are high levels of corrosion currents, it would be expected that the magnitude of the dipole approximated CRM field shall be less than that calculated from the full method. When the plots of the magnitudes of the two calculated fields are compared it is clear that this is indeed the case. In fact the magnitudes differ by a larger amount than in any of the previous calculations but this is again expected since this model has the highest level of corrosion currents flowing from the hull to the propeller. With the key features of the field from the full calculation being present in this dipole approximation (i.e. the increases in magnitude as the anodes are passed), the field produced by the full method is supported further.
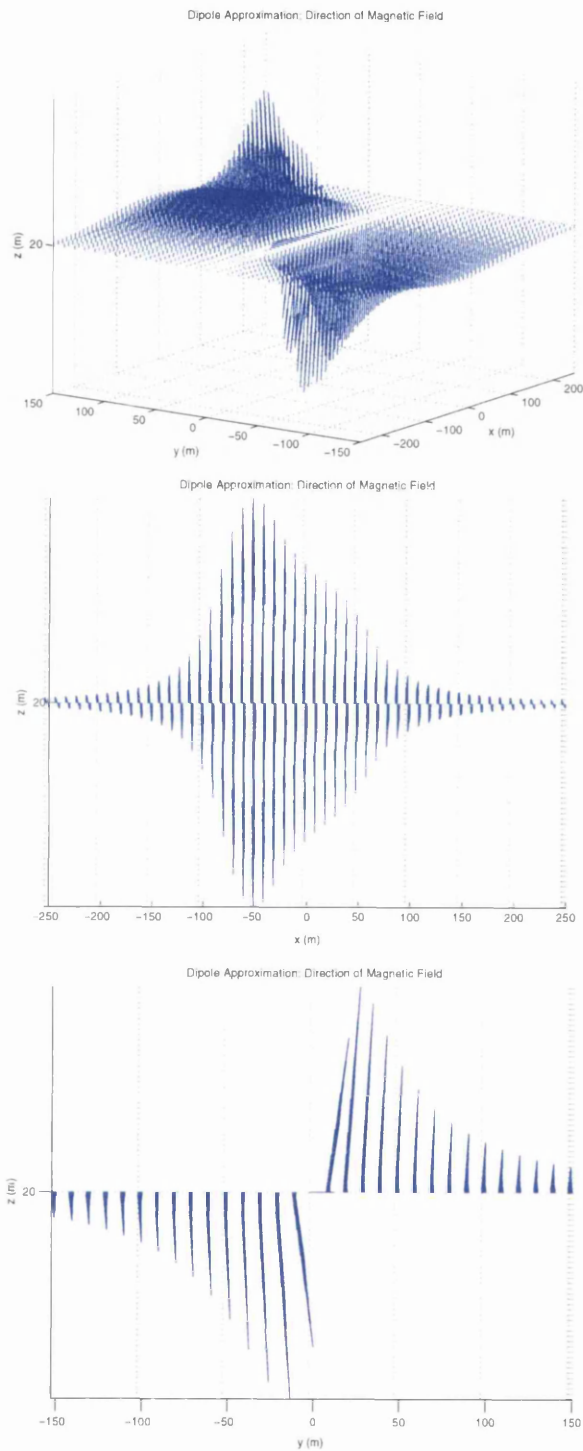
Figure 7.34: Dipole approximation of the magnetic field from corrosion currents, the three-dimensional view (top), xz cross-section (middle) and yz cross-section (bottom)
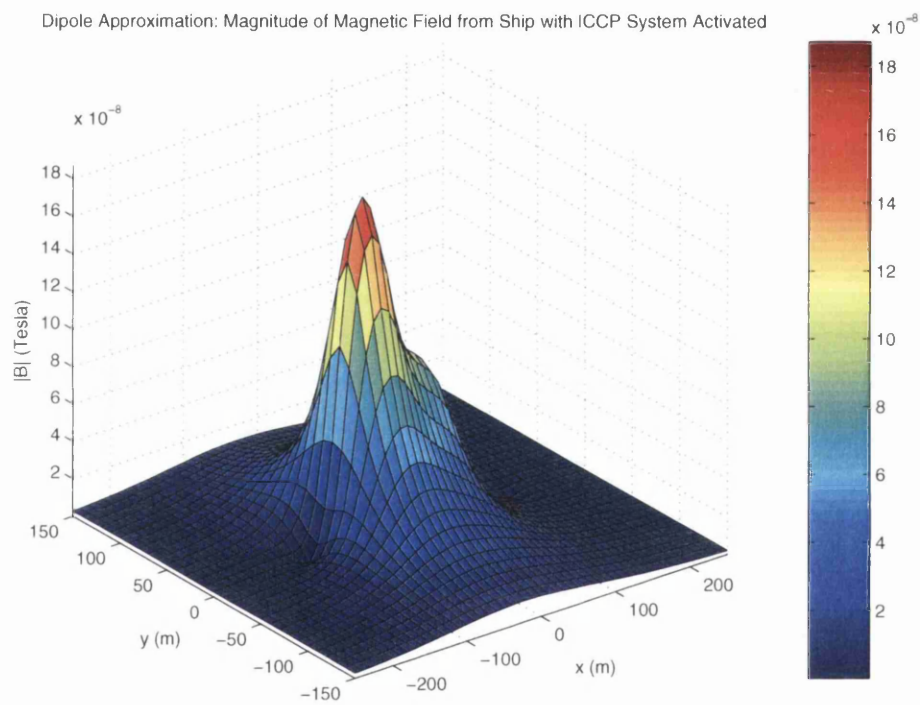
Figure 7.35: Dipole approximation of the magnitude of the magnetic field for a ship with damaged paint on the hull and an ICCP system activated.

Chapter 8

Analysis of Real Polarization Calculations

8.1 Introduction

As mentioned in chapter 7, the polarization relation between the potentials on the surface of metals in sea water and the related corrosion current densities are very complicated and depend on many factors. The previous chapter contained the analysis of some test calculations for a ship with various degrees of paint damage and ICCP settings for a simple linear polarization relation. This relation was able to model many of the significant characteristics of real-life corrosion. These calculations indicated that the modelling method developed in this research appears to be able to model the various features of such models. However it is essential that similar calculations were performed using a more realistic non-linear polarization relation. As stated previously, in real-life the polarization relation for metals in ships in highly non-linear [47], with many factors effecting the relation [6, 7]. Indeed the relations are so complicated that it is rare for a function to be fitted to gathered experimental data but instead vast tables of values are normally used in programs.

Unfortunately this polarization data was not available for this research as most companies involved in this area of research keep their data secret. However, the work of Sun & Liu [65] was used as a reference to provide a function which described a realistic non-linear polarization relation for the hull. The following discussions are based on their work.

190

It should also be noted that the physical structure of the model has remained unchanged from the previous linear calculations.

8.2 Non-linear Polarization Relation.

A polarization relationship for low carbon steel in sea water obtained from fitting the function to real data is

$$j_i = \exp\left(\frac{u_i + 693.91}{24}\right) + \frac{1}{\left(\frac{1}{86.06} + \exp\left(\frac{u_i + 521.6}{23.47}\right)\right)} - \exp\left(-\frac{u_i + 707.57}{55}\right) \quad (8.2.1)$$

For an element i, this relates the normal current density j_i emitted to the potential u_i. Here the potentials u_i are in mV and the current density is measured in $\frac{\mu A}{cm^2}$.

The polarization relation which is required to implement the method produced in this research requires the potential u_i to be related to its flux q_i so it necessary to modify this general relation. Using the following relations it was possible to relate the current density $\mathbf{j}$ to the outward normal derivative of the potential $\mathbf{q}$

$$\mathbf{j} = \sigma_{sea}\mathbf{E} \quad (8.2.2)$$
$$= -\sigma_{sea}\nabla\mathbf{u} \quad (8.2.3)$$
$$= -\sigma_{sea}\mathbf{q} \quad (8.2.4)$$
$$\Rightarrow \mathbf{q} = -\frac{\mathbf{j}}{\sigma_{sea}}. \quad (8.2.5)$$

This relation allows the necessary conversion of eqn (8.2.1) to obtain the polarization relation which related q_i to u_i as shown in eqn (8.2.6)

$$q_i = k_i\left(-\frac{1}{\sigma_{sea}}\right)\left(\exp\left(\frac{u_i + 693.91}{24}\right) + \frac{1}{\left(\frac{1}{86.06} + \exp\left(\frac{u_i + 521.6}{23.47}\right)\right)}\right.$$
$$\left. - \exp\left(-\frac{u_i + 707.57}{55}\right)\right). \quad (8.2.6)$$

One further modification which is evident in eqn (8.2.6) is the introduction of a scaling factor k_i with the same form as the one which was used in the linear relation enabling the paint coatings to be accounted in the model. Also it is necessary to somehow be able to modify the relation so that the potential of the internal structure of the ship, V, can be altered to remove any stray currents from

the model. Although V is not explicitly used by eqn (8.2.6), this was achieved by replacing the potentials u_i with an amended potential which indicated the potential difference between the potential on the internal structure, V, and that on the interface between the paint and the sea, u_i, i.e. in eqn (8.2.6), $u_i = V - u_i$.

As stated, this relation was based on experimental data and gave a close approximation to the true relation. Consider the exponential terms within the main parenthesis. In the general theory of polarization relations, the form of a relation to describe the corrosion of steel structures which accounts for the multiple electrochemical reactions and the mass transfer of oxygen is

$$j = j_1 - j_2 - j_3 \qquad (8.2.7)$$

where j_1, j_2, and j_3 represent the current density generated by iron oxidation, oxygen reduction, and hydrogen evolution respectively. These contributions can be described in general terms as

$$j_1 = \exp\left(\frac{u - u_1}{b_1}\right) \qquad (8.2.8)$$

$$j_2 = \left(\frac{1}{j_L} + \frac{1}{\exp\left(\frac{u - u_2}{b_2}\right)}\right)^{-1} \qquad (8.2.9)$$

$$j_3 = \exp\left(-\frac{u - u_3}{b_3}\right) \qquad (8.2.10)$$

where u_i, b_i $(i = 1, 2, 3)$, and j_L are all positive constants. From this it is clear that the relation used (eqn (8.2.6)) is of the correct form.

The non-linear nature of the polarization relation is shown in figure 8.1 for $k_i = 1$. The most crucial feature of eqn (8.2.6) is that there is a very limited range of potentials over which it is stable. Once the values of u_i exit this range, even if it is only for one single element, the solution becomes unstable and unrealistic values are obtained by the solution process. Another difficulty associated with this relation is that within the stable region, the values of q are almost constant. This will be even more so when the perfect paint coating is accounted for which will have a $|k| < 1$. The effect of this is that while the potentials may vary greatly the actual current emitted, represented by q, will stay constant. Therefore to get the proposed method to converge (to solution values which may be considered
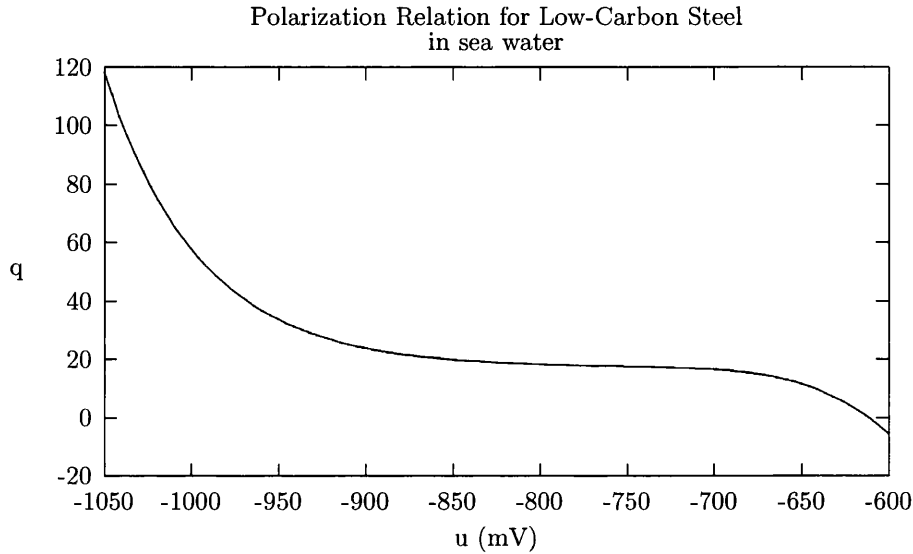
Figure 8.1: The non-linear polarization relationship (eqn (8.2.6)) used to model a more realistic situation.

as being realistic) is an extremely delicate process. The amended values for the potentials on the ship elements u_i must be strictly constrained, and since initially there is no known solution from similar calculations, the relaxation factor must be keep small to coax the approximate solution toward the correct one.

One problem applying this relation to the method is that it is specifically fitted to data for low-carbon steel. It will not apply to the Nickel-Aluminium-Bronze propeller. This means that another relation is required to represent the polarization relation here. For simplicity, the linear polarization relation (eqn (7.2.1)) was used again. The problem with this choice is highlighted by considering the situation when V is fixed, and positive. If u is positive and increasing on the hull, q emitted will increase. This will also increase the u values on the propeller. The linear calculations indicted that these will be negative so increasing them will reduce the q absorbed here. This conflict will make it more difficult to remove any stray currents. This was not ideal but it still allowed the method to be tested for non-linear polarization relations while also challenging its robustness.

8.3 Less Severe Paint Damage - Analysis.

The first case considered for the real polarization relation was that of less severe paint damage. To recap, this was the situation where the hull was coated with a perfect paint coating except in the region $133.8m < x < 153.8m$ where the paint had been damaged to be 1000 times more conductive than the perfect paint. The propeller was left uncoated. For these considerations the k_i values on the three different areas were

$$k_i = 10^{-3}, \quad \forall i \in \text{perfect paint,} \qquad (8.3.1)$$

$$k_i = 1, \quad \forall i \in \text{damaged paint,} \qquad (8.3.2)$$

$$k_i = 1, \quad \forall i \in \text{propeller.} \qquad (8.3.3)$$

These are not the same values that were used in the Less Severe Paint Damage case for the linear polarization relation. They had to be altered to obtain a convergent solution, and although this was not a desirable action to have to take, it is felt that it would not have been necessary if real polarization data was available. Therefore, the values calculated as the solutions to the BEM equations and the resultant magnetic fields are not comparable to the linear case but should show the same general behaviour, whilst also indicating whether this proposed method can model the fields when there is non-linear polarization data.

Using eqn (8.2.6), and the experience of the linear polarization calculations, it is possible to make some predictions on how the solutions to the system should behave.

8.3.1 Predicted Behaviour.

In the following discussion it should be reiterated that the constraining of the potentials u_i is actually the constraining of the potential difference between the potential on the internal structure and that on the interface between the paint and the water, i.e. $V - u_i$.

The key to trying to predict the behaviour of the solution is to recognise that when u_i is constrained to ensure that the polarization relation eqn (8.2.6) behaves in a stable fashion, the relation can be approximated as a shallow, linear relation. As mentioned above, for the undamaged paint regions of the hull where the basic

polarization shape is multiplied by the scaling factor $|k_i| < 1$, this linear trend on the stable region may be considered as being approximately constant. On the damaged paint area, this stable region will not be constant.

On the propeller the polarization relation used was the linear relation eqn (7.2.1) from the previous calculations. This means that on the propeller the behaviour is expected to be similar to that in the corresponding linear test case in section 7.6, namely it shall absorb the corrosion currents (q negative) with the rim absorbing at the highest density. The faces of the propeller will absorb less than the rim and the amount each face absorbs shall be determined by the level of corrosion on the hull, i.e. the potential difference between the hull and the propeller. It was shown in the corresponding linear polarization case that the outer face absorbed more current than the inner face. Other calculations for when there was a severely damaged region of paint (section 7.5) and when the ICCP anodes were turned on (section 7.7), showed that a large amount of corrosion related current and a resultant large potential difference between the region emitting the current and the propeller resulted in both faces absorbed roughly equal amounts. So although it is expected that the inner face should absorb less, the possibility that both faces absorb the same amounts should not be dismissed.

As mentioned, the behaviour of the propeller faces shall be governed by the level of corrosion which occurs on the hull, and this is not easy to predict due to eqn (8.2.6) being implemented for the first time. For the 'no-stray currents' condition to be satisfied while ensuring that only a reasonable amount of current was flowing through the sea, it was necessary to constrain the values of u and V on the hull so that $-1V \leq V - u \leq 0.7V$. For the majority of this region, the relation to q can be approximated to be linear and almost constant. Therefore the general behaviour of the corrosion on the hull should not completely differ from that in the linear calculation. Over the regions where the paint is undamaged, there should be approximately zero corrosion resulting in q values which are close to zero. The area of damaged paint is where the corrosion should take place, and hence should have positive q values. Since this is the first calculation using eqn (8.2.6) it is difficult to speculate as to the magnitude of the q values for the damaged region although taking into account the values from the unscaled relation in figure 8.1, and the value of k_i, it is reasonable to assume values with magnitude of order 0.01,

from which it follows that on the propeller, the magnitude of the q values should be larger, with the results from the linear polarization calculation suggesting that they should be larger by a factor of around 10.

Due to the almost constant nature of the polarization relation on the hull it is difficult to predict the potential distribution over the hull. It is expected that the values of u on the propeller should be more negative than those on the hull, which would mean that to ensure a continuous distribution of the potentials the stern should have potentials which are lower than on the rest of the hull. With there being no corrosion over the hull except on the damaged area, the potentials should not vary much but should instead slowly increase as the damaged area is approached. To be consistent with the distributions found from previous calculations, the potentials should be at their largest over the damaged area, but the values taken should still ensure that $V - u$ remains within the constrained limits. As the damaged area is passed and the bow approached the potentials should decrease smoothly.

The effect of this on the CRM field should be that it displays the same shape and direction as in the linear case. It is also expected that the magnitude increases since comparison to the q values obtained for the linear polarization relation show that the expect values here are significantly larger.

8.3.2 Calculated Behaviour.

The calculate results for the potential and its flux over the ship are shown in figures 8.2 - 8.5.

Begin by considering the q values on the propeller, figure 8.2. As predicted, the q values are negative indicating the absorption of the corrosion currents, while the rim absorbs the highest density. Also it appears that both faces absorb equal amounts suggesting that there is a large potential difference between the propeller and the damaged region of paint in comparison with the linear case. This corresponds to a comparatively large amount of corrosion currents flowing through the sea. One unexpected development is that when the upper section of the propeller, which is close to the hull, is compared to the lower section, it appears that the upper section is absorbing a higher density than the lower section. This is opposite to the pattern observed for the linear cases and is probably due to the conflicting behaviour of the different polarization relations

mention earlier. Since the distance between the hull and the propeller is the same for both sets of calculations, the effect of the hull on this section of the propeller must be the same. The polarization relation in the propeller is eqn (7.2.1) and the q values are negative. To obtain the largest amount of absorption at the upper elements would mean that these elements must have values for $V - u$ which are more negative than on the other elements. In this calculation, a satisfactory solution was obtained when $V = 0.1735810$ and from figure 8.3, the values of u are negative. This indicates that the potentials on the upper elements must be less negative than on the lower elements, and this is what has been calculated as shown in figure 8.3. A quick check using eqn (7.2.1) shows that the u and q values correspond as required, and the figure also shows a smooth distribution of the potentials of the hull as required. This rules out the possibility that there is some rogue behaviour in the calculation, so there must be some physical reason for this change in the behaviour in comparison to the linear case. To determine this reason, consider the behaviour of the solution on the hull.

When the q values for the hull are considered, figure 8.4, it is apparent that the non-linear polarization relation has allowed features which were initially hidden in the linear calculation to become more apparent. In both cases, there is approximately no current emission from the perfectly painted regions. In the linear case, figure 7.19, the area of damaged paint initially showed constant emission whilst this calculation clearly shows the level of corrosion varies. The difference is that in this calculation the further into the water the area goes, the level of corrosion reduces (i.e. as z goes down, q decreases). This results in less current flowing from the bottom of the hull. Current will always follow the path of least resistance, so for the majority of the corrosion current, which is emitted from higher up the hull, this corresponds to it following a path through the water to the nearest part of the propeller which is its upper section. While this observation is consistent with that of the propeller, it does not explain it.

It is difficult to understand why this variation on the hull has occurred, but it again seems likely that the sea surface plays a significant role in the behaviour as it did in the linear case. The sea surface has been specified to be non-conducting, so that it has $q = 0$ but may obtain non-zero potentials. The hull has positive potentials so it follows that the surrounding sea surface elements should also have positive potentials to ensure a continuous distribution. On the hull, the q values

are determined from eqn (8.2.6) and the values of $V - u$. As with the previous calculations, the hull is trying to corrode so it is straining to have as large a q value as it can possibly have. For the undamaged areas, $k_i = 0.001$ which would mean that no matter what value of u an element had within the constrained range, the corresponding q value would be very small. With the solution having $V = 0.1735810V$, this means that to get the highest level of corrosion possible from the undamaged regions of paint, the potentials u will have to be as positive as allowed by the constraints. Since a continuous distribution of u is required over all elements, this will result in the neighbouring sea surface elements having large potentials. When the damaged elements in contact with the sea surface are considered, the continuous nature of the distribution of potentials will force these elements to have large potentials, which corresponds to large current emission. To this point the process is the same as in the linear calculation.

Return to considering the propeller. With the potentials straining to be as large as possible on the hull, this means that the propeller elements closest to the hull shall have relatively high potential values. With the linear polarization relation being implemented here, this results in large current absorption, as indicated by the results. The method is still going to try and remove any stray currents, which results in it regulating the emission from the other damaged elements. With the upper elements in the damaged region emitting a large amount that is readily absorbed by the upper elements of the propeller, this will require the lower sections of the damaged paint to emit less which results in smaller positive potential values. This is the pattern shown in figures 8.4 and 8.5. Hence the behaviour of the corrosion current which has been calculated is reasonable.

Another noticeable feature on figure 8.5 is the values obtained for the potential at the bow and stern. At the stern, the close proximity to the propeller meant that the potentials were expected to be small, as they are. At the bow it was expected that the potentials would reduce slightly from the values on the damaged paint. This figure shows that while they have reduced, they have done so quite drastically. At the bow, the upper elements which are in contact with the sea surface have similar potentials as other regions of undamaged paint on the hull. The lower elements, which cover the surface of a section of the hull which is a short bulge sticking out at bow, have extremely small potentials, almost as low as those at the stern. As stated above, these elements should be trying to corrode

but their low potentials suggest otherwise. This is probably a direct consequence of the method trying to remove the stray currents. The closer to the base line of the hull the damaged region got, the lower the potentials became. This reduction reduced the q values from eqn (8.2.6). With the method reducing the potentials of the elements in the vicinity of these bow elements to reduce the q values, it is likely that their potentials were also reduced. With them not being directly linked to elements higher up the hull, or close to the sea surface, it would appear that their potentials were able to be reduced to quite small values. This coupled to the near constant polarization relation on the undamaged elements would mean that no matter how far the method reduced these potentials, it would have been unable to reduce their q values. As a result of the optimisation process used by the method, the potentials have been reduced to extremely low values for these bow elements as shown.

Checking the values of q obtained from eqn (8.2.6) with the potentials shows that the calculation is consistent on the hull. Although the calculated behaviour was slightly different from that which was predicted, the unexpected observations have been explained and the result is self-consistent. Overall the flow of the corrosion currents are still roughly what was expected so the behaviour of the CRM field should be as predicted. This is indeed what is observed in figure 8.6 and 8.7 with the direction of the field and its spread out nature along the hull being the same as in the linear calculation, but with the magnitude having increased.
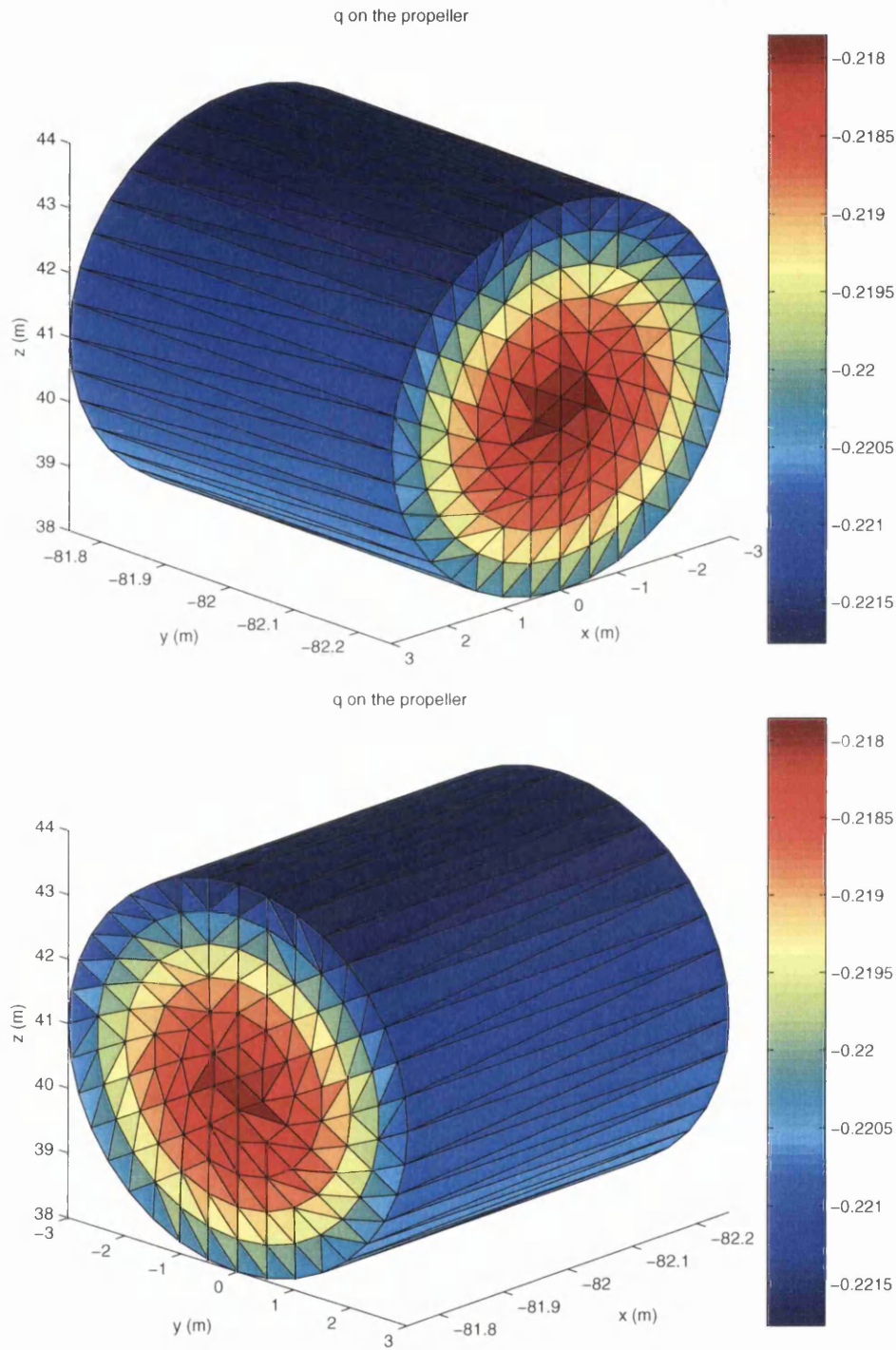
Figure 8.2: q on propeller, furthest face from hull (top) and nearest face to hull (bottom).
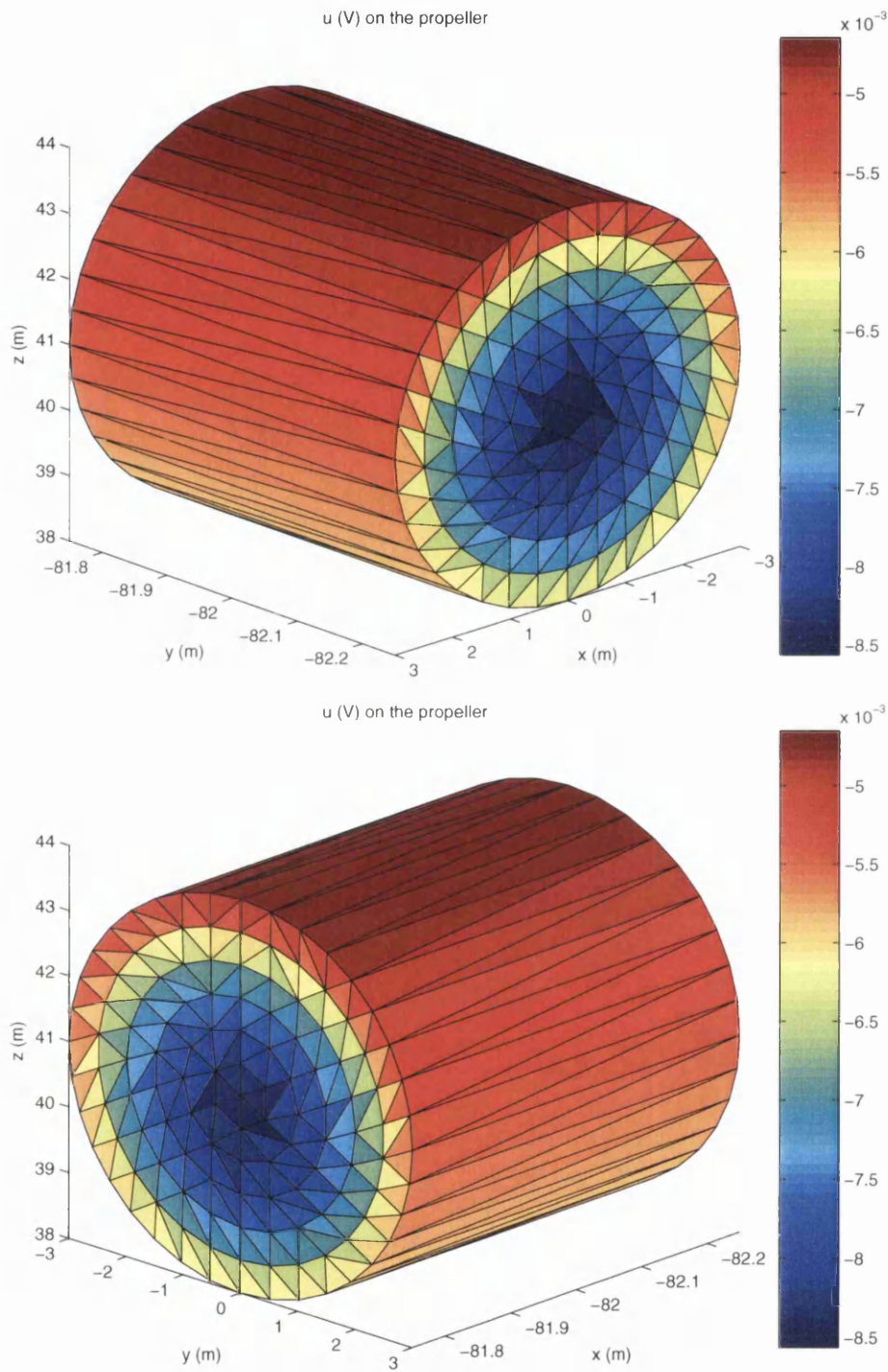
Figure 8.3: u on propeller, furthest face from hull (top) and nearest face to hull (bottom).
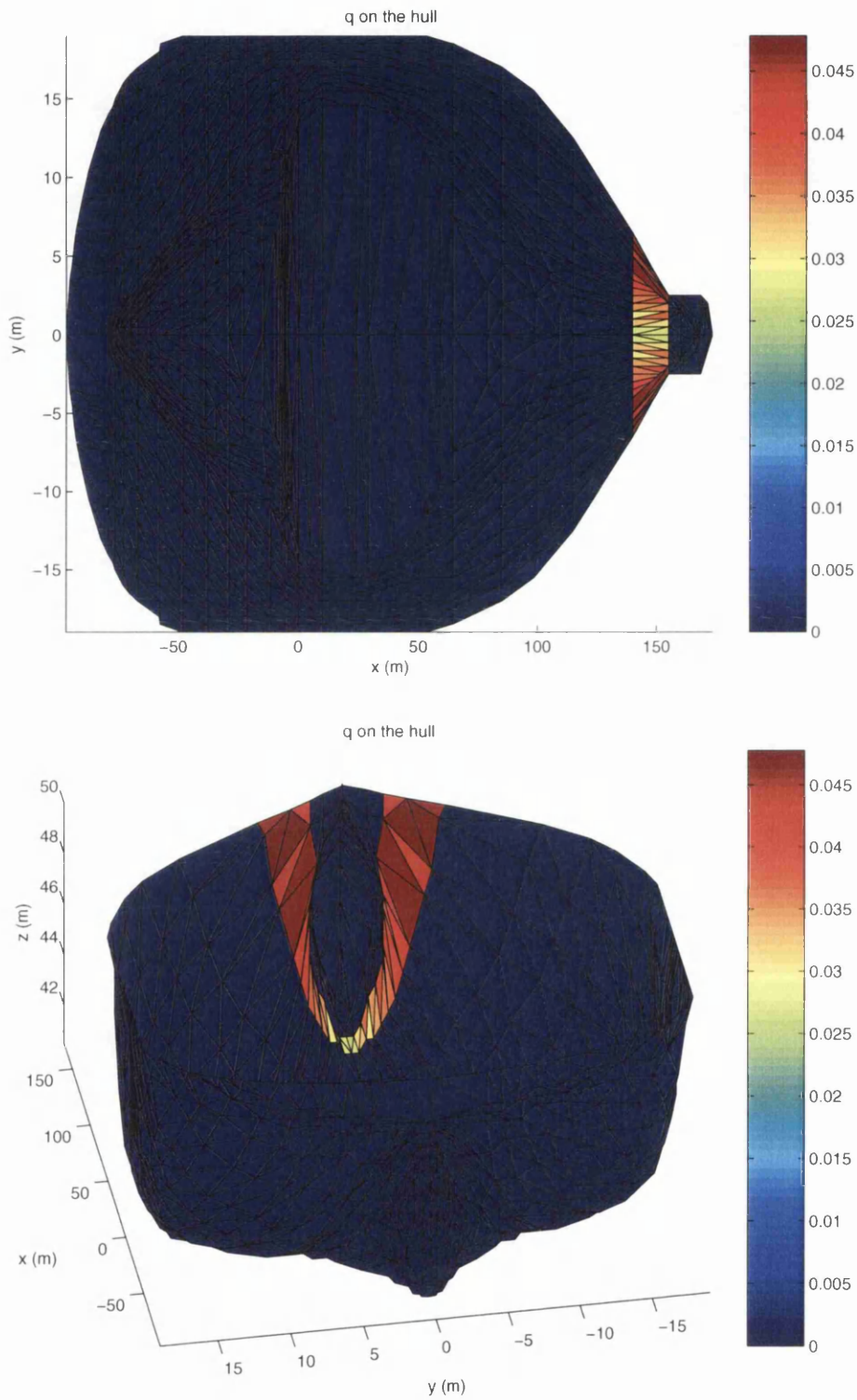
Figure 8.4: q on the hull, aerial view (top) and view from stern (bottom).
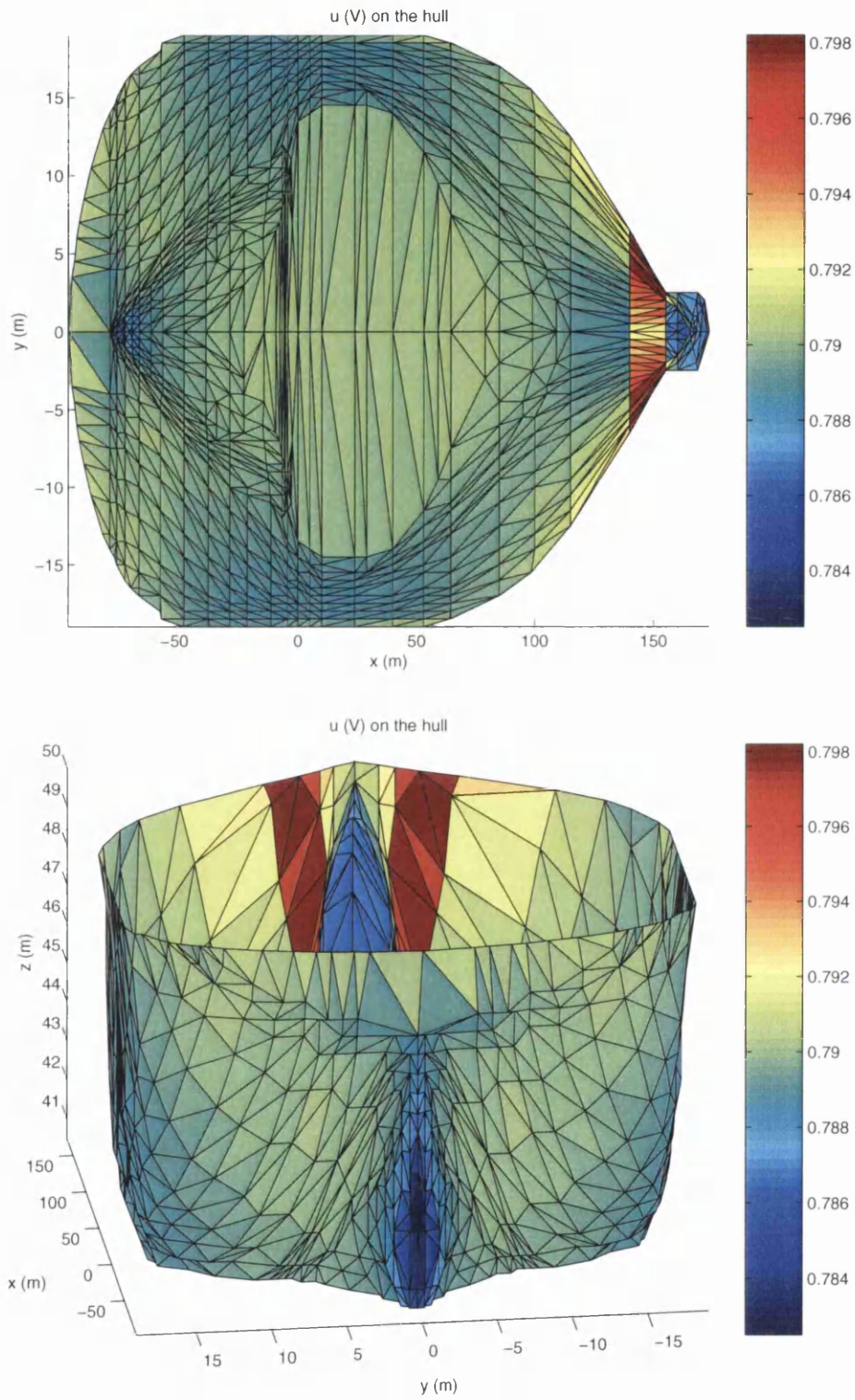
Figure 8.5: u on the hull, aerial view (top) and view from stern (bottom).

Figure 8.6: Magnetic field from corrosion currents, the three-dimensional view (top), xz cross-section (middle) and yz cross-section (bottom).

Figure 8.7: Magnitude of the magnetic field from a ship with slightly damaged paint on the hull with realistic polarization relation.

8.3.3 Verification by Dipole Approximation

The dipole approximation of the CRM field is shown in figures 8.8 and 8.9.

As the analysis of the calculations for a linear polarization relation have shown, the field calculated by the dipole approximation should have the same general direction and shape as the CRM field produced by the full calculation. This is indeed the case as can be seen by comparing figures 8.6 and 8.8.

For the similar calculation for linear polarization (section 7.6), it was observed that due to the reduced level of corrosion, which resulted in a relatively small amount of corrosion current flowing, the effect of the non-conducting sea bed in the full calculation was not enough to increase the magnitude of the CRM field to a great extent. This resulted in the magnitude of the field calculated by the dipole approximation being greater than that of the field from the full calculation. Despite the change in the polarization relation, it would be expected that the same effect should be observed here. Indeed, by comparing figures 8.7 and 8.9 it is clear that this is the case. Hence the dipole approximation has produced a field which fully supports the CRM field produced by the full method.

These results indicate that the procedure proposed in this research is able to respond to non-linear polarization relations on the hull. To further support this claim, the ICCP system from the linear calculation was switched on with this paint damage and the result investigated.
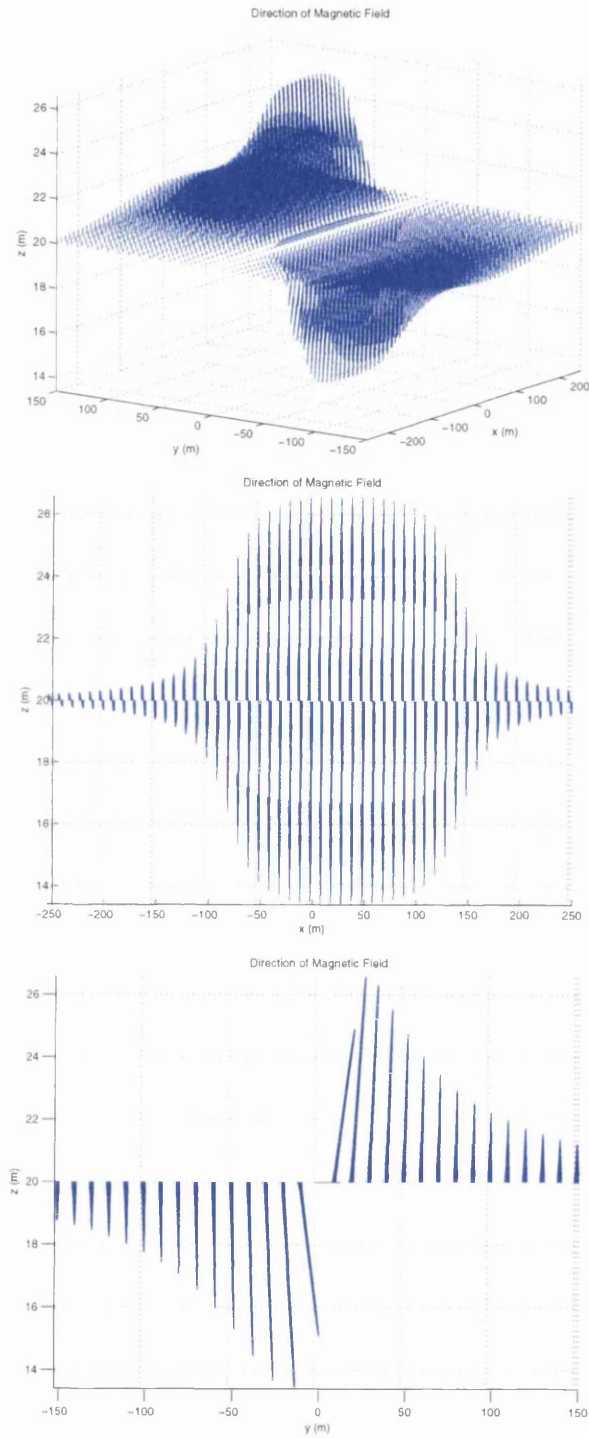
Figure 8.8: Dipole Approximation of the magnetic field from corrosion currents, the three-dimensional view (top), xz cross-section (middle) and yz cross-section (bottom).
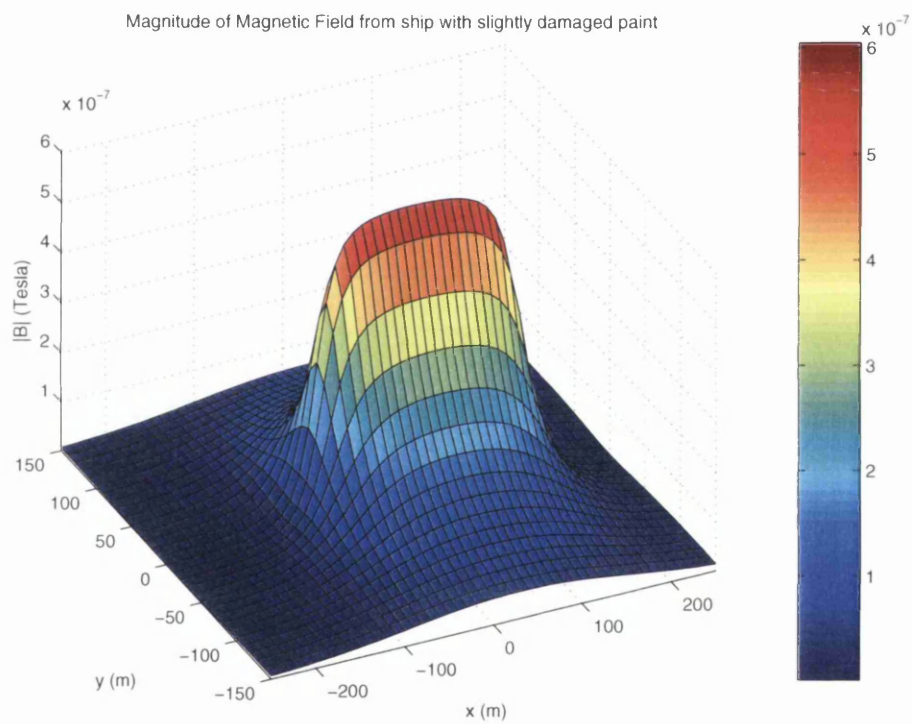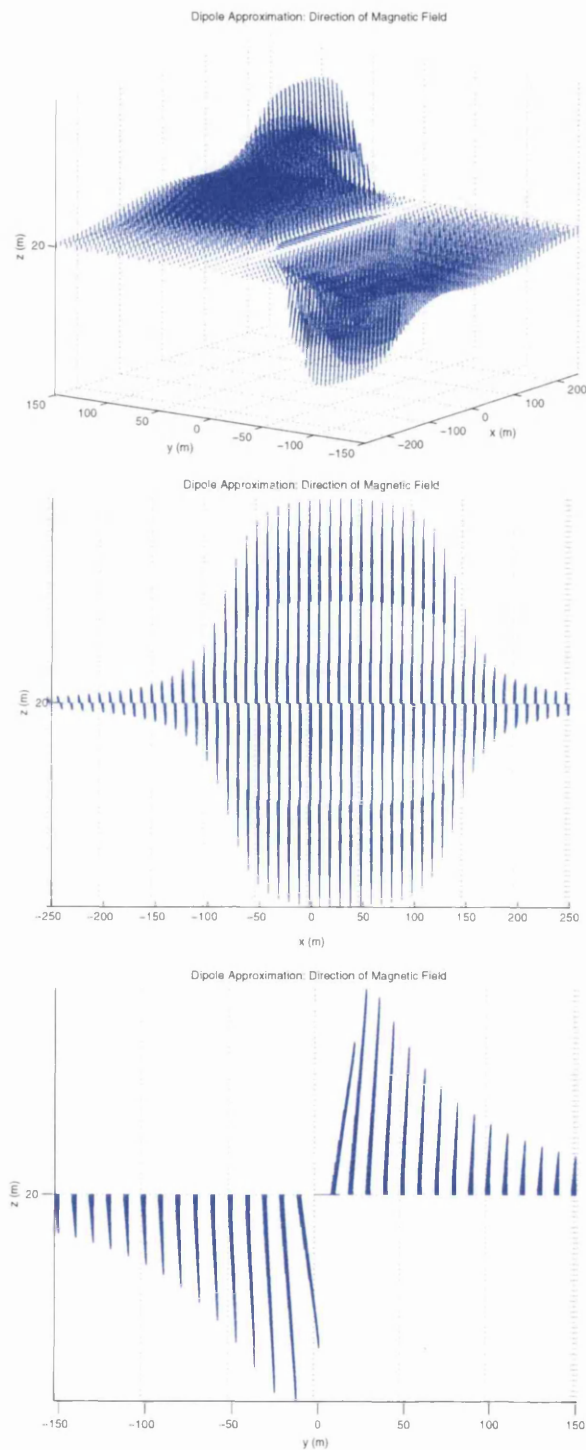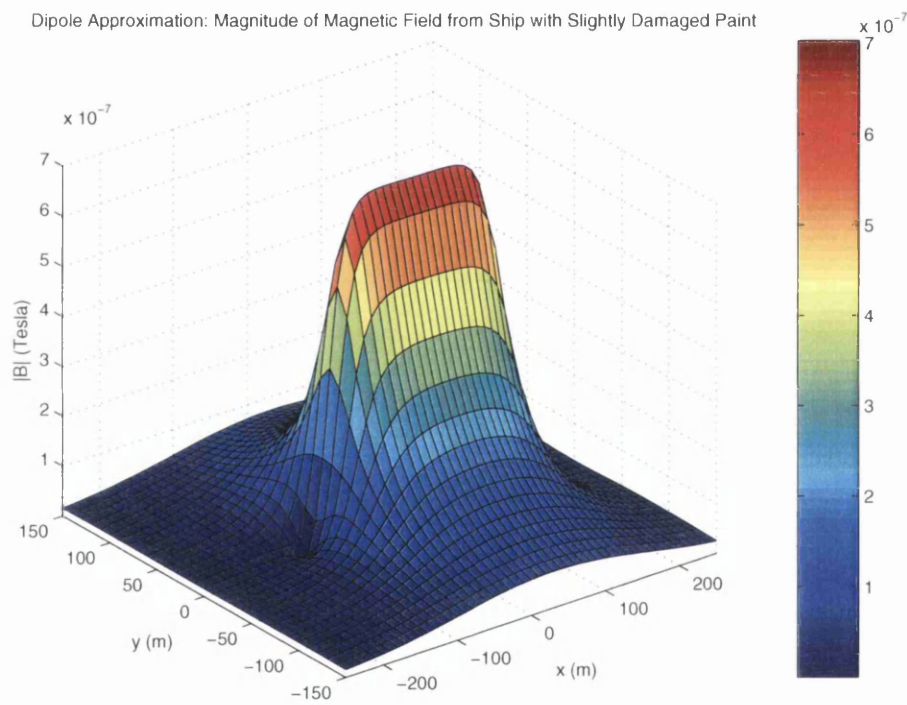
Figure 8.9: Dipole Approximation of the magnitude of the magnetic field from a ship with slightly damaged paint on the hull with realistic polarization relation.

8.4   ICCP Switch On - Analysis.

As with the linear polarization test calculations, the most complex case to consider is when there is paint damage on the hull and an ICCP system is used to try and prevent any corrosion from occurring.

This situation is now considered for the model with non-linear polarization on the hull. In terms of the location of the damaged paint, the locations of the anodes and the current supplied by them ($1A$ from each anode), the model considered is the same as in the linear polarization calculation of section 7.7. The polarization relations used were the same as in the ICCP off case considered above in section 8.3.

8.4.1   Predicted Behaviour

Recall that in section 7.7, activating the ICCP system could lead to a solution which was the superposition of two extreme possibilities. The first extreme was that not enough current could be provided to significantly prevent corrosion from the damaged paint region. This was what was calculated for the linear case and resulted in the majority of the anode currents flowing to the propeller which left the damaged region relatively free to corrode and produced a CRM field whose magnitude significantly increased as each electrode was encountered as a detector passed under the stationary ship from bow to stern. The second extreme outcome was that the ICCP anodes supplied too much current to the damaged region which would completely reverse the corrosion currents and, on a real ship, would do further damage to the paint. An ideal ICCP system configuration would strike a medium between these two situations and provide precisely enough current so that there was no corrosion at the damaged region while there was no remaining current flowing to the propeller. This would result in an extremely small CRM field. This outcome is unlikely however since there was no optimization procedure implemented in these calculations.

Before considering the likely behaviour on the propeller, it is first necessary to consider the effect of the non-linear polarization relation on the hull as this will determine the level of corrosion which occurs. With the linear calculation, it was observed that this ICCP configuration provided a small amount of protection to the damaged region. This was essentially due to the potential difference between

the anodes and the damaged region being less attractive to the anode currents than the potential difference between the anodes and the propeller. So far, the polarization relation is generally thought as indicating the amount of current which may be emitted from the hull, but the previous calculations have shown that it also indicates how easily the hull will absorb currents. With the non-linear polarization relation within the constrained region, there is range of values for the potential $V - u$ for which the hull will be able to absorb significant amounts of current in the damaged region. In comparison with the linear calculation, this would suggest that there is a greater likelihood of the potential values on the damaged region being such that the anode's currents could be absorbed. However, as stated before, the complex relation between the values of V, u, and q means that no definitive prediction can be made but it is expected that more protection will be given to the damaged region.

The undamaged paint shall again be unable to absorb any currents so any of the ICCP currents which do not flow to the damaged region will again flow to the propeller. On the propeller, this calculation should show that, like all the previous calculations, the rim should absorb the highest density of current. The levels of absorption on the faces depend on the potential differences between each and the emitting elements. As with the case when the ICCP system was not activated, it is expected that the non-damaged hull areas should have large positive potentials which will mean that the elements on the propeller close to the hull should also have large potentials. This means that the upper elements on the faces should absorb more than the other elements. Another effect of this is that it should increase the potentials of all the elements on the propeller so that they are much closer to the potentials on the damaged areas of the hull. To the ICCP anode currents, this will make them less attractive so that less current flows to the propeller, and the current that does will most likely flow to the upper elements.

The calculation of the previous section which did not have the ICCP system activated showed that the deeper into the water the damaged region went, the greater the reduction in the potentials. Since the anode currents will be looking to flow to regions of less potential, this suggests that most of the anode current which is absorbed by the damaged paint shall flow to the lower sections of the damaged area. This will certainly be the case of the bow pair of anodes which

are close to the damaged region and located midway up the sides. For the stern pair, the linear calculation seemed to indicate that they did not have that great an effect of the corrosion of the damaged region, with the majority of its currents flowing to the propeller. This may well be the case again, but if any of its currents flow to the damaged region the positioning of the pair on the very bottom of the hull would suggest that again the lower sections of the damaged area would be the destination. This all tends to suggest that the lower section of the damaged area shall be provided with the most protection and hence will corrode less than the higher regions. Again this supports the prediction that the upper elements on the propeller will absorb more than the lower elements since this current from the upper damaged elements will look to flow along the path of least resistance which will be to the upper sections of the propeller. The fact that the lower damaged elements seem to be more attractive to the anode currents increases the possibility that there may be some over-protection on these elements. This would result in negative q values.

The potential on the hull should follow a similar pattern to that for the linear calculation. The proximity of the propeller to the stern should result in the stern being at a lower potential compared to the rest of the hull. Moving along the hull, the potential should increase to localised peaks as the anodes are passed, although the potential must still have a continuous distribution. After the bow pair of anodes, the potential should drop off until the damaged region is encountered at which point it should change drastically, obtaining values which will signify emission/absorption of current. As previously discussed, the values can not be predicted as they will be dependent on the value of V but should become less positive the further into the water the element is located.

As the damaged area is passed, the potentials should return toward their values which indicate no corrosion taking place. As seen with the calculation for the non-linear polarization with ICCP off, the effect on the elements at the very front of the hull which are not in contact with the sea surface of the nearest face could see these elements have potentials very close to those at the stern.

The effect of the CRM field is not very clear as the field depends on the flow of the corrosion currents which, as indicated above, are not easy to predict. From the previous discussions, there appears to be two likely fields which are associated with the levels of protection provided by the ICCP system. Firstly, consider the

situation where the anodes are supplying the majority of their currents to the propellers. This situation shall be very similar to the linear case of section 7.7. As mentioned above, it is expected that the damaged region shall be receive more protection in this case which will be provided by more of the anode currents being absorbed by this region. Hence when the plane of evaluation (at $20m$ below the ship's base line) is traversed from the bow to the stern, the field shall be very similar to that for the linear case. The only real difference should be that the increases in the magnitude which occur when each anode pair of passed should be less in comparison to the rest of the field (as less current from each pair is flowing to the propeller than in the linear case). The direction of the field should be unaltered and still orientated in the counter-clockwise direction.

The second possible scenario is that which would occur if the majority of the anode currents flowed to the damaged area. In this case it would seem unlikely that the CRM field will have two distinct increases in magnitude as seen for the linear calculation. If enough of the anode currents flow to the damaged area through the sea, it is possible that the direction of the field may be opposite to that which has been calculate previously i.e. the field will be clockwise, however this remains unlikely. For this to occur it would require a complete reversal in the corrosion on the damaged regions. The lower section of the damaged area was speculated as being the most likely destination of the anode currents so while this area may be over-protected, the upper elements should still be corroding contributing to a field in the counter-clockwise direction. Also any currents from the anodes not absorbed by the damaged area, most likely from the stern anodes, will also flow to the propeller giving rise to a field in the usual direction. These arguments lead to the conclusion that the field is likely to be in the counter-clockwise direction. In this scenario, most of the activity would be focused around the region from the bow anodes to the damaged paint. The magnitude of the field again depends on the flow of the current from the anodes. With the majority of the currents flowing to the damaged region to inhibit corrosion, there would be less currents emitted from here. The current which is emitted is expected to be from the upper elements, and shall flow to the propeller. Any currents which are emitted from the anodes and are not absorbed by the damaged elements shall also flow to the propeller. Therefore it is expected that there shall be a current flow along the length of the ship which shall give rise to a field along

the length of the ship. The consequence of there being less corrosion and more absorption of the ICCP currents in the damaged region is that there shall be less current flowing in the sea between the anodes (particularly the bow pair) and the damaged region than in the ICCP off calculation. However, with the upper elements still corroding there will still be sea currents in this region. With over-protection on some of the lower elements in the damaged region expected, these currents will form a small current loop between the anodes and this region. These currents will flow close to the hull and will not effect any other region so the largest concentration of current should be between the damaged region and the anodes. This means that while the field shall spread along the entire ship, there will be a peak between the anodes and the damaged region. The magnitude of this peak is dependent in the level of protection which is being provided. As a consequence, as the propeller is approached the magnitude of the field would be less than that calculated from the case where the ICCP anode was de-activated.

However despite these two fields being the most probable, it still remains possible, although extremely unlikely, that the corrosion could be prevented completely with no anode currents left over, which would result in a CRM field which was small and constant over the entire ship.

8.4.2 Calculated Behaviour

The calculated behaviour on the ship is shown in figures 8.10 -8.13. Consider the q values on the propeller shown in figure 8.10. As expected the propeller has q values indicating the absorption of corrosion currents. Again the rim elements absorb the highest density of current with both faces displaying approximately the same pattern of q values. A close inspection of the upper elements on the faces indicate that the inner face is absorbing slightly more than the outer face as expected, but on both faces it is the upper elements which absorb more current than the lower elements. The similarity in q values on both faces is due to the current arriving at the propeller being unable to distinguish an easier path between the two, with the inner face having slightly higher potentials while the outer face requires a slightly longer path through the sea increasing the resistivity. For this calculation the value for the potential of the internal metal work of the ship was $V = 0.1129153V$. Using the linear polarization relation, eqn (7.2.1), along with $k_i = 1$ and $e_i = -0.4$, it is clear that the potentials shown in figure

8.11 match the values of q calculated.

The values of q on the propeller indicate the likely behaviour on the hull. The upper elements on the propeller absorb a higher density of current than the lower elements which, as mentioned in the previous subsection, indicates that the ICCP anodes will be supplying their protective currents to the lower elements in the damaged region rather than the higher elements. Comparing the magnitudes of q on the propeller with those which were obtained in the ICCP off calculation, figure 8.2, indicates that the sea current flowing in this model to the propeller is less than in the ICCP off case. This indicates that the lower elements in the damaged area are receiving a large portion of these protective currents resulting in them being well protected while the corrosion of the upper elements in the damaged region shall continue.

Figure 8.12 which shows the values of q on the hull. As expected the majority of the hull which is protected by the perfect paint coating is displaying very little or no corrosion ($q \approx 0$). Also the anode elements are clearly distinguished with the stern pair which have the smaller surface area outputting the highest current density (largest q values).

The main area of interest is the damaged region. In this region, the upper elements have positive q values which indicate that they are corroding but comparison with the values from the ICCP off calculation, figure 8.4, show that they are corroding less with the ICCP system on. This will mean that the magnitude of the CRM field should be smaller than in the ICCP off case. As the base of the hull in the damaged region is approached, the q values decrease and become negative which indicates current absorption. This corresponds to these elements being over-protected (which is undesirable for reasons mentioned previously). The predicted destination of the anode currents, other than the propeller, were the lower elements in the damaged region so this was behaviour comes as no surprise. With the current emission from the upper elements less than in the ICCP off case, it would appear that the current from the bow anodes are being distributed over whole damaged region. This would suggest that only a minority of these currents are flowing to the propeller. With the lower damaged elements absorbing such a high density of current, it seems likely that the stern anode pair, which is close to the base of the hull, are supplying the majority of their currents to these elements. This would again mean that a minority of the current from these anodes

would have the propeller as their destinations. Using the non-linear polarization relation, eqn (8.2.6), it is possible to verify that the potential values shown in figure 8.13 correspond to the q values. Again the continuous distribution of the potentials is evident, with the values increasing in the vicinity of the anodes, and the damaged paint region obtaining much higher values than the undamaged regions.

This shows that the results from the BEM calculation are valid and consistent with the predicted behaviour. The final part of the analysis is to check if the CRM field which was calculated is that which was predicted for these hull conditions.

With the ship conditions that are calculated, it appears that the situation which has arisen is more like the second of the two possibilities discussed above. It is clear that the region between the anodes and the damaged paint is where most of the current activity takes place. As mentioned the reduction in the q values on the damaged elements will result in the magnitude of the CRM field reducing. With the majority of the anode current flowing to the lower damaged elements, this should mean that on approach to the propeller down the ship, once the stern anodes are passed the main contribution to the CRM field shall be that from the corrosion currents from the upper damaged elements. The combination of all these factors is that the magnitude of the field should be greatest directly beneath the damaged region, and it should then drop off toward the propeller, which is the result shown in figure 8.15.

The direction of the field is still counter-clockwise over the entire plane of evaluation which may seem unexpected due to the anode currents flowing through the sea in the positive x direction which would lead to a clockwise field direction. However, there are also the return currents through the ship which would act to oppose this field. Combined with this is the corrosion current flowing from the upper elements to the propeller which will contribute to the counter-clockwise direction as previous calculations have shown. When the sea currents flow, they will follow the path of least resistance which means the shortest path through the sea water. The anodes are close to their currents destination so when their currents flow through the sea, they shall follow a path which is quite close to the hull, i.e. shall not spread out far into the sea. The corrosion currents from the upper damaged elements have a comparatively large distance to flow to the propeller. Hence they will spread out more into the sea which means that when the field
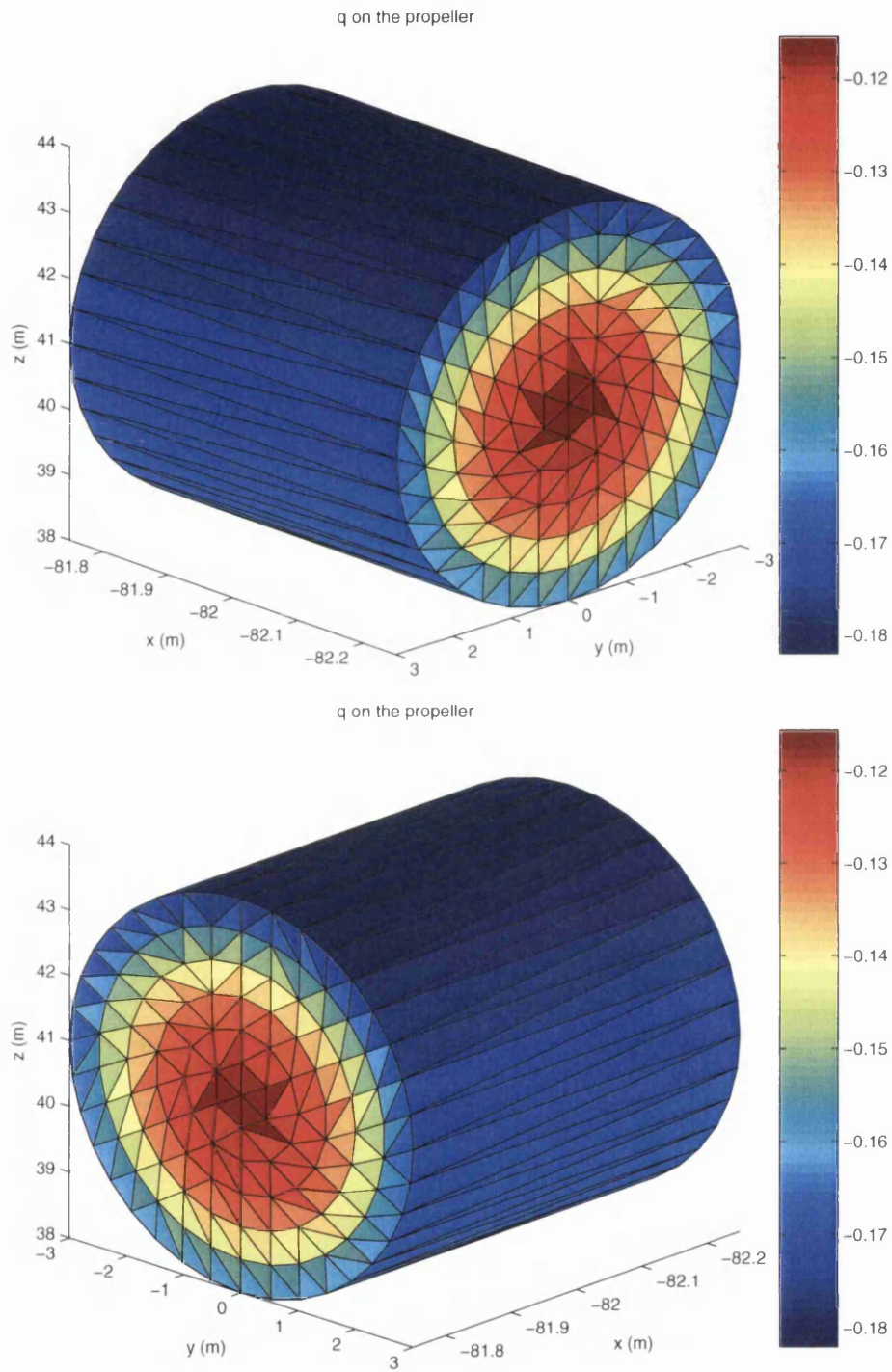
Figure 8.10: q on propeller, furthest face from hull (top) and nearest face to hull (bottom).
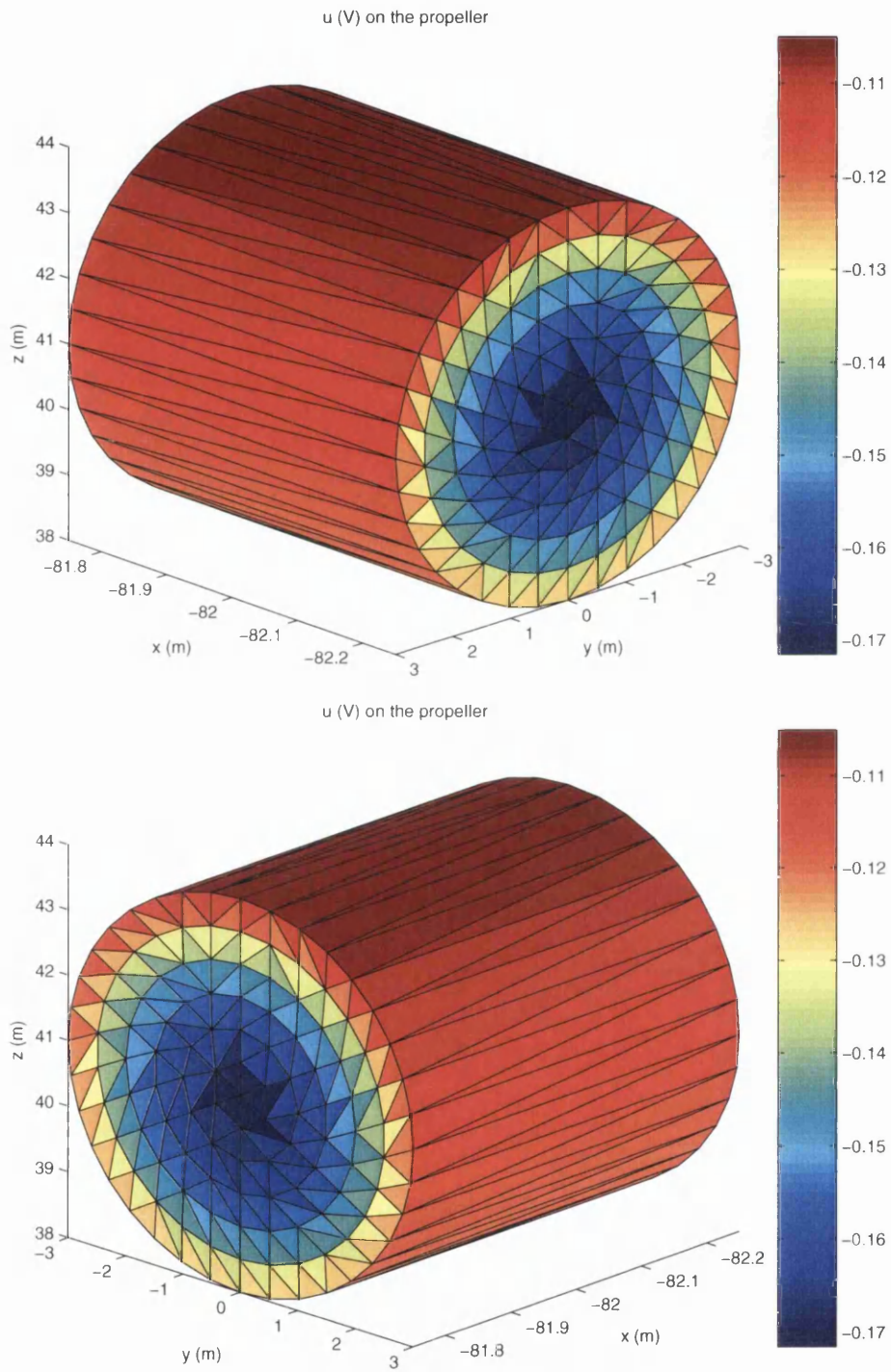
Figure 8.11: u on propeller, furthest face from hull (top) and nearest face to hull (bottom).
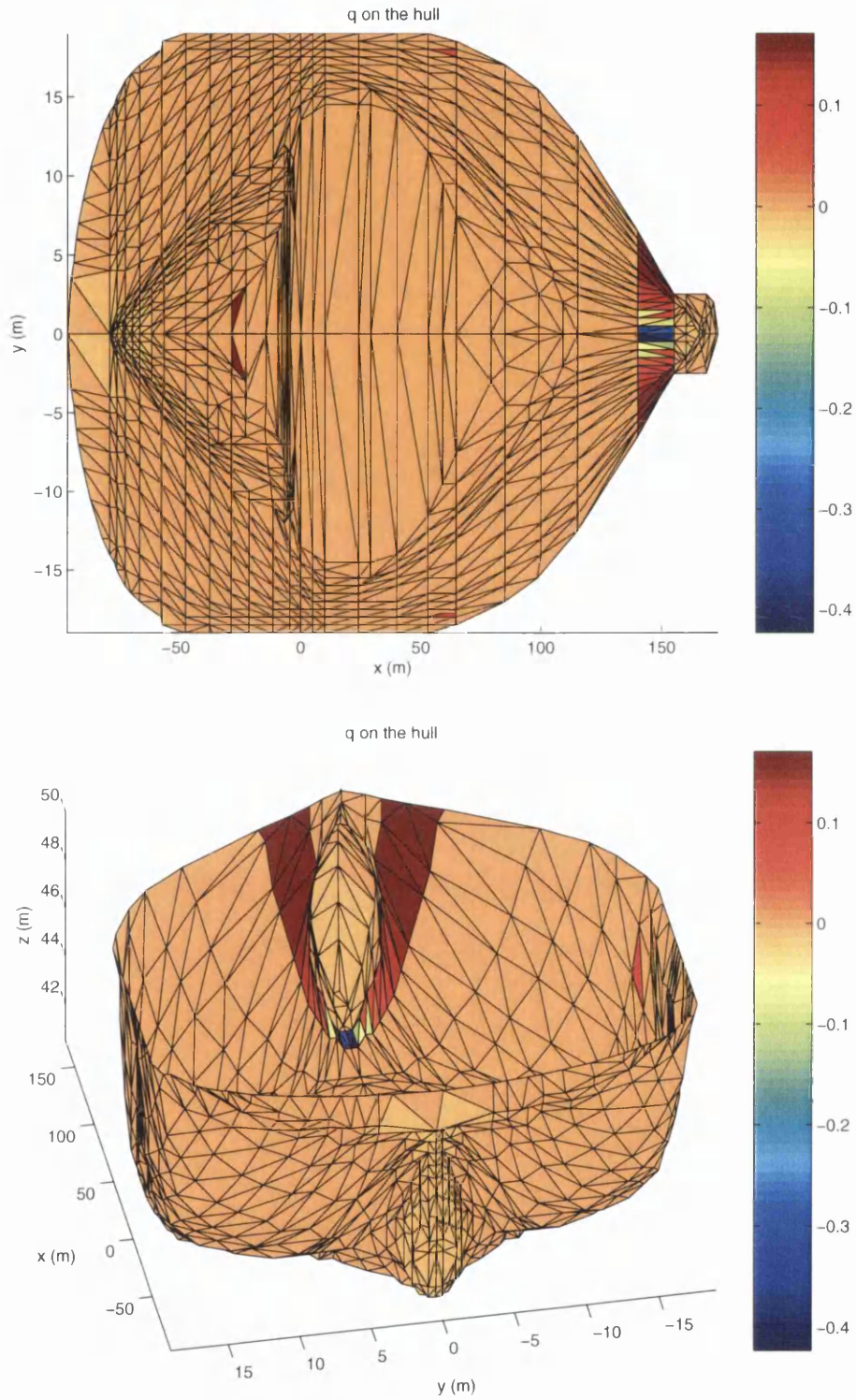
Figure 8.12: q on the hull, aerial view (top) and view from stern (bottom).
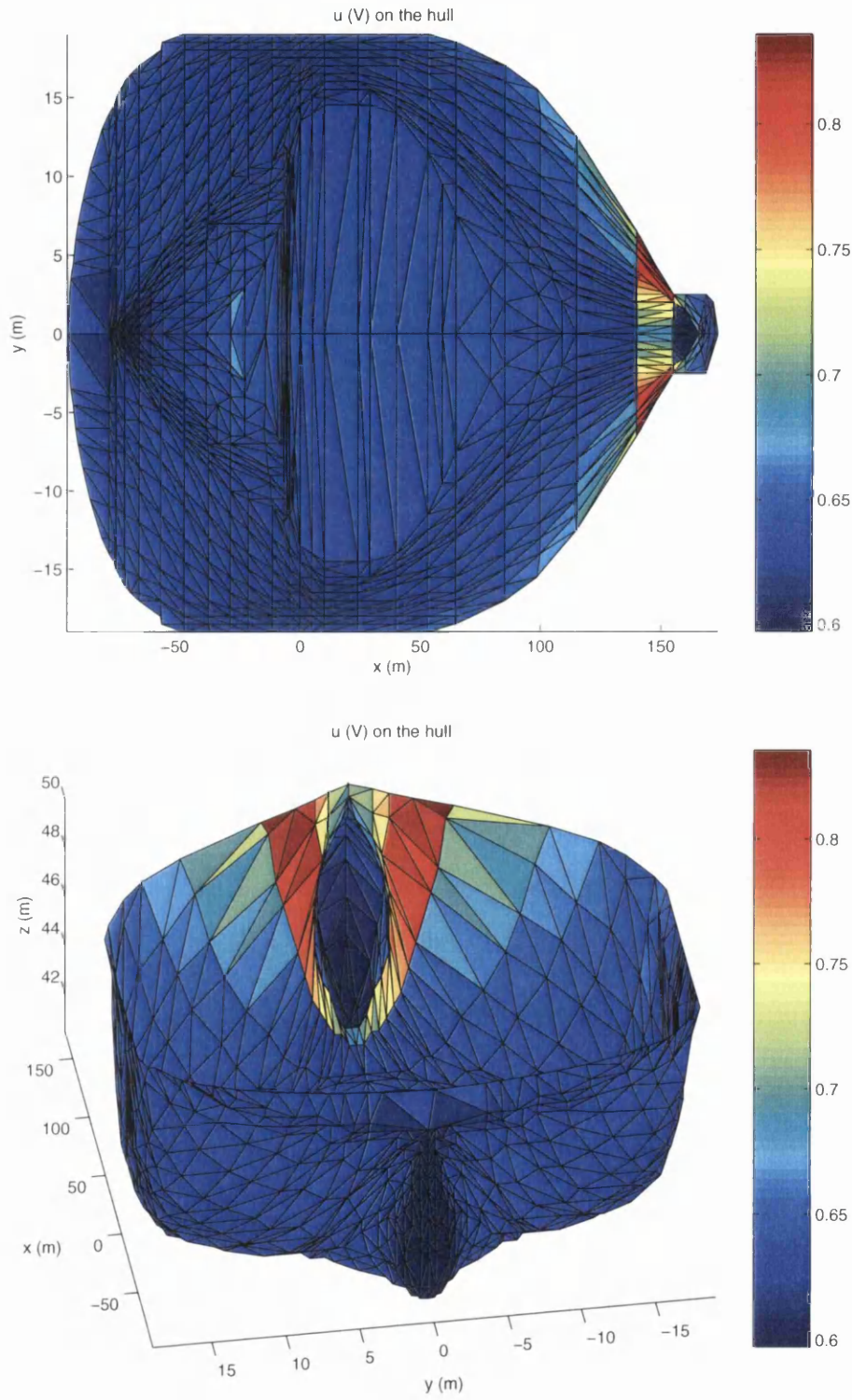
Figure 8.13: u on the hull, aerial view (top) and view from stern (bottom).

is evaluated at $20m$ below the base line of the hull, these currents will be most the influential and hence the field should be counter-clockwise as a consequence. This is shown in figure 8.14.

Figure 8.14: Magnetic field from corrosion currents, the three-dimensional view (top), xz cross-section (middle) and yz cross-section (bottom).

Figure 8.15: Magnitude of the magnetic field for a ship with slightly damaged paint on the hull with a realistic polarization relation, and the ICCP system activated.

8.4.3 Verification by Dipole Approximation

The dipole approximation of the CRM field is shown in figures 8.16 and 8.17.

The field produced by the dipole approximation again follows the same pattern as in the previous calculation. The shape of the field is very similar to that produced by the full calculation, and the direction is also the same. Any slight difference in the direction is due to the averaging of the source locations in the dipole approximation. As mentioned previously, for this model the currents supplied by the ICCP system flow mainly to the damaged region where for the majority of elements, their corrosion is inhibited. The other elements experience over-protection. This has the effect of reducing the corrosion related currents within the domain which will diminish the effect of the non-conducting sea bed in the full method. This is the opposite from the effect the ICCP system had for the corresponding calculation for linear polarization (section 7.7). In that calculation the magnitude of the CRM field produced by the full method was greater than for the field calculated by the dipole approximation. In this calculation it would be expected that the reduction in corrosion related currents would mean that the opposite would be true with the field from the dipole approximation having the greater magnitude. This is indeed the case which can be seen by comparing figures 8.15 and 8.17.

Therefore, this approximation seems to support the main characteristics of the CRM field calculated by the full method in terms of the magnitude, the direction, and the shape of the CRM field as well as the focusing of the current activity around the damaged region.
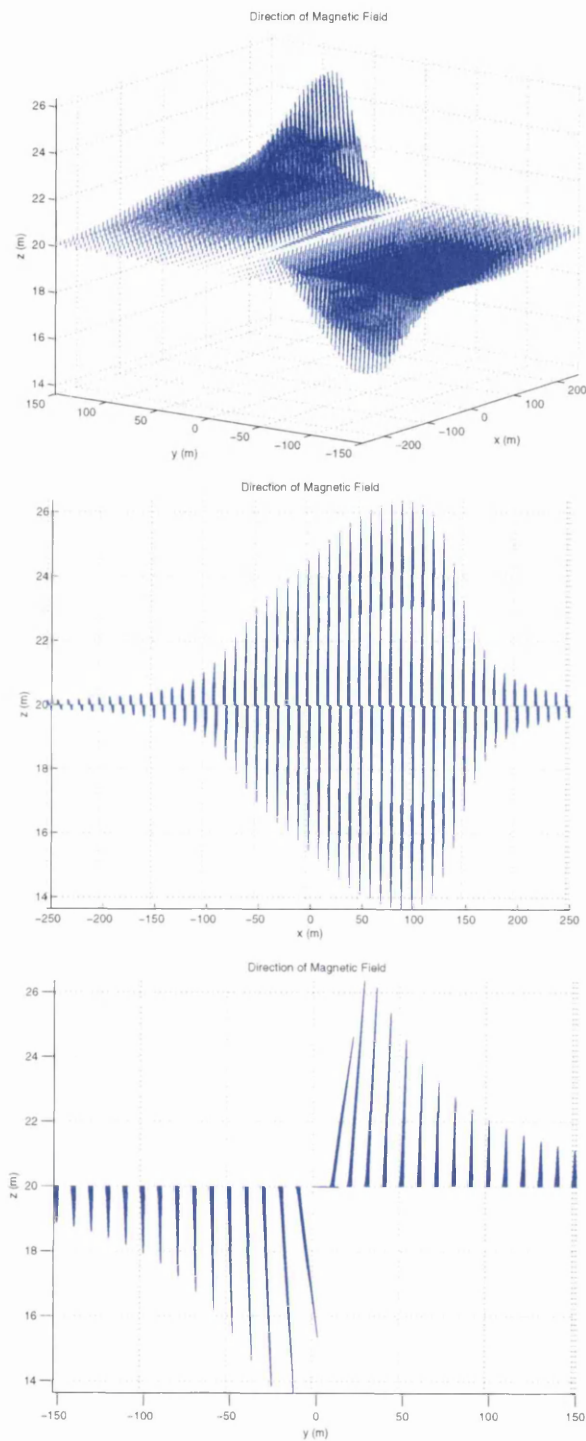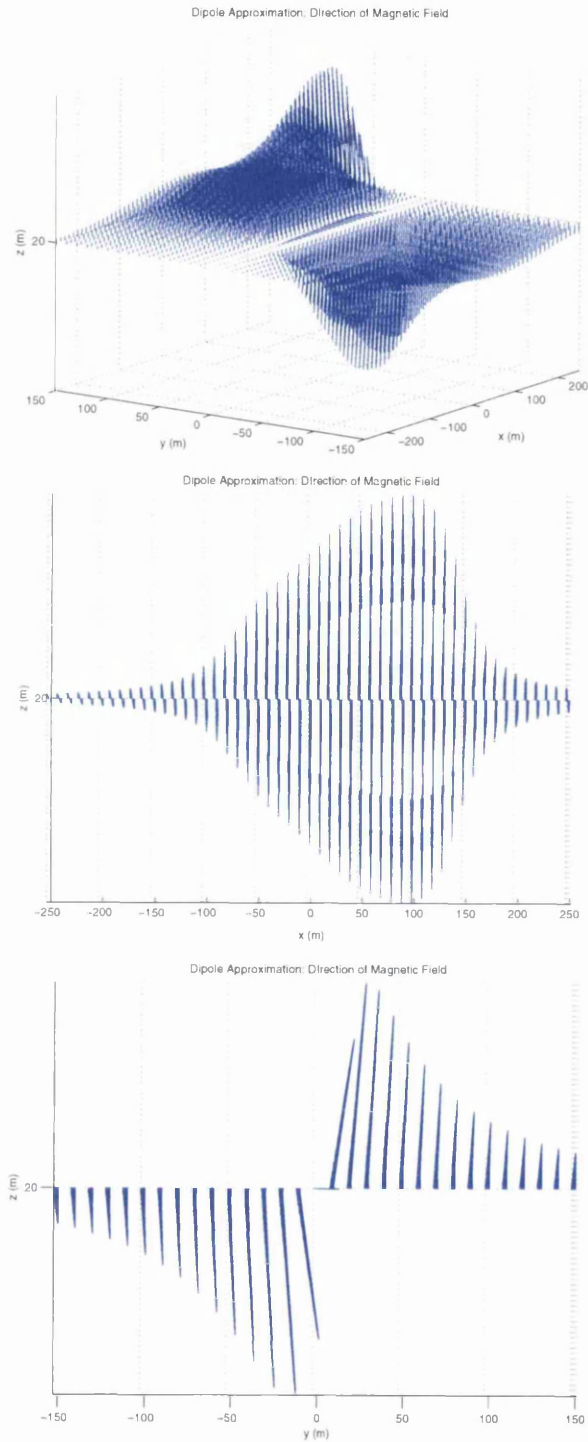
Figure 8.16: Dipole Approximation of the magnetic field from corrosion currents, the three-dimensional view (top), xz cross-section (middle) and yz cross-section (bottom).

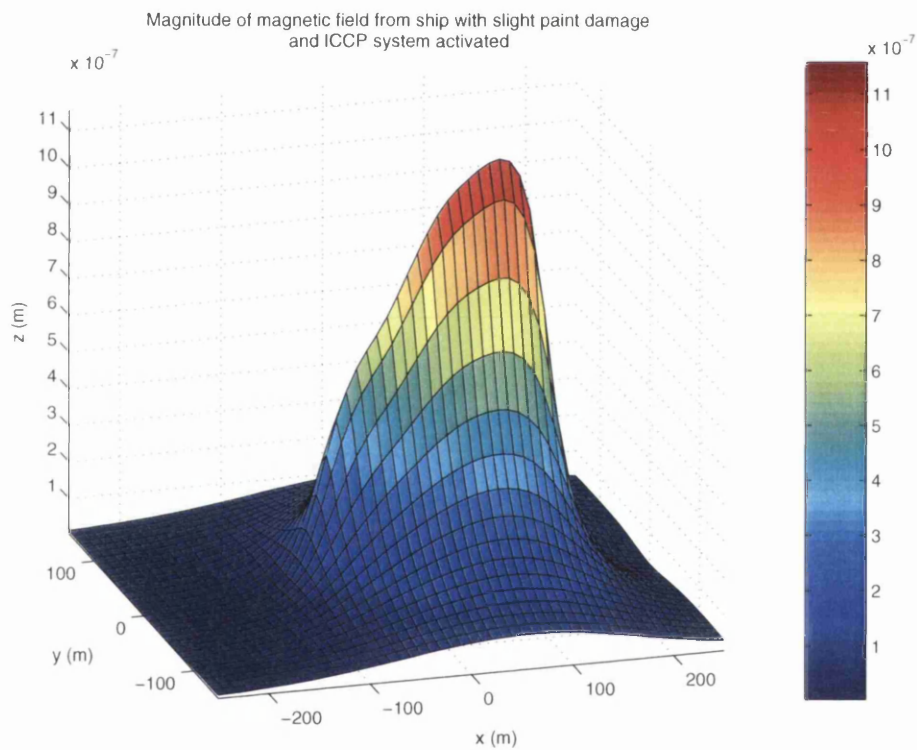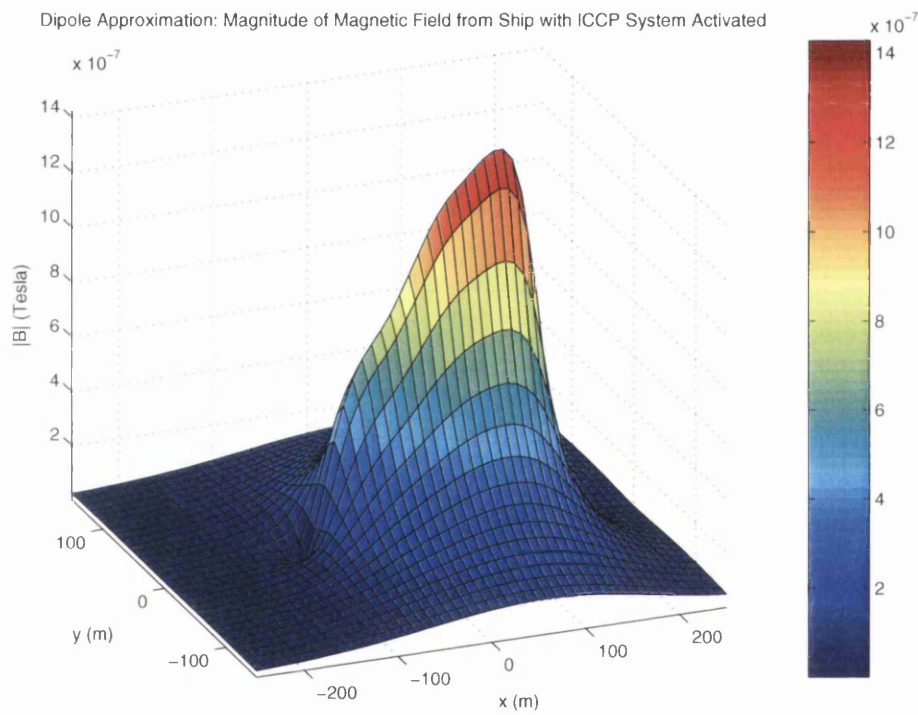Figure 8.17: Dipole Approximation of the magnitude of the magnetic field for a ship with slightly damaged paint on the hull with a realistic polarization relation, and the ICCP system activated

Chapter 9

Conclusions and Future Developments

There have been many areas covered by this research concerning the methods with which the corrosion related magnetic fields from ships in sea water are modelled. Each area has been covered in the preceding chapters, and were then combined to perform test calculations on a hull in a box of sea water. The individual methods were shown to work separately but it was only in these final test calculations that the validity of the combined method could be tested.

There are many key points to the results from the test calculations. The most important point to keep in mind is that the actual numerical values are not definitive for the ship which was modelled. To obtain definitive results would have required experimental polarization data specific for the metals used and the environment in which the ship was placed, i.e. specific to the sea environment. With this information not available it was necessary to form representative polarization relations, which were initially linear for the entire ship but were then developed to be non-linear over the hull.

Despite this, the capabilities of the procedure can still be assessed by considering the various situations which the ship could physically find herself in and determining whether the method could represent the situation mathematically.

The first situations considered used a linear polarization relation for the entire ship. Initially there was assumed to be a perfect paint coating on the hull which would prevent the corrosion of the metal. As expected [11] the corrosion activity was focused in the region of the propeller but was extremely low level. This

226

resulted in small corrosion currents and correspondingly CRM fields which were extremely small. One pleasing property of the solution was that the field did have a direction consistent with the flow of the currents in the model. The paint was then damaged to varying degrees over a specific region of the hull toward the bow which led to a varying amount of corrosion on the damaged region depending on the level of the damage. This agrees with physical observations since it produced different values for the potential difference between the propeller and the damaged region [6]. This resulted in the CRM field being spread out over the plane of evaluation below the ship. The magnitude of the field again varied proportionally to the level of damage. By then including an elementary ICCP system, the corrosion was to some extent inhibited as desired. Since the ICCP anode currents did not manage to flow completely to the damaged region (a consequence of the polarization function) the sea currents flowing to the propeller increased which, as expected, increased the CRM field magnitude.

To try and simulate more realistic situations, a non-linear polarization function based on experimental results was used on the hull. For this relation, a damaged paint calculation was performed which highlighted many of the features determined from the linear calculations, especially that the damage region did not corrode uniformly but instead corroded the most in the elements closer to the sea surface. This is consistent with what is observed on ships (the majority of corrosion tends to be located approximately at the water line of the hull). This calculation also indicated that the elements on the propeller closer to the hull would tend to absorb more current. This may not be a valid conclusion to apply in practise since the polarization relation applied on the propeller was still the simplistic linear one which had no experimental backing. By then implementing the same ICCP system as previously used, further properties of the model became highlighted which were previously disguised by the linear polarization.

Firstly the possibility that the ICCP system could supply too much current to protect the hull was observed. This leads to current being absorbed by damaged elements which was clearly indicated by the results. This is an extremely important situation to be able to highlight since in practise this situation can serious damaged the protective paint coating on the hull. Secondly, this calculation highlighted the importance of the ICCP anode location. On the damaged region, comparison to the ICCP off situation showed that the overall corrosion

was reduced but the lower elements were absorbing far more current from the ICCP anodes than the upper ones. The location of the bow pair of anodes half-way between the sea level and the base of the hull meant that their currents were opposing the corrosion of the entire damaged region. The stern anode pair were located on the base of the hull which resulted in their currents flowing to the lower elements resulting in these elements being over protected while the upper ones were still able to corrode. More logically positioned anodes could have distributed the ICCP currents to prevent the corrosion completely. Finally this calculation showed that when an ICCP system was activated, despite introducing more current to the model, it was possible to use the ICCP currents to reduce the overall magnitude of the CRM field. These are all key features which any modelling method of the CRM field from a ship must have as it enables an ICCP system to be designed so that it optimises protection provided to the hull and also minimises the magnitudes of the fields produced.

Therefore these final calculations have illustrated that the method produced by this research is capable of carrying out an analysis on real situations. Unfortunately, there were no published results available to which these results could be compared. There are many papers published which investigate the various aspects of modelling corroding ships with ICCP systems but since the primary objective of such a system is to protect the hull from corrosion, the majority of these publications focus on the electric potential distributions on the hull. Those publications which consider the signature produced focus mainly on the electric fields rather than the magnetic fields. Despite this, some of the findings in these publications support observations that can be made from the results of the test calculations presented here.

The calculation for an activated ICCP system with real polarization performed in section 8.4 indicated that with the ICCP anodes located closer to the bow than the stern, the protection was provided to the damaged region at the bow which is consistent with other studies [76]. This would mean that such an anode configuration would be unlikely to provide adequate protection to the hull area in the vicinity of the propeller (which as mentioned before is another likely area of paint damage). This is in complete agreement with studies [62] which included comparison to physical scale modelling results, and consistent with the standard design rules for ICCP systems [52, 64]. Due to the lack of detailed results from

other studies on the shape and direction of the CRM field, it is difficult to say for certain whether other published studies support the fields produced here although the indications are that they are valid [52], while other sources have also endorsed them [11].

These agreements with published results further support the methods presented as being valid for modelling the CRM fields from ships. Whether the combined method is superior to existing methods remains unclear. To determine this, calculations would have to be performed using this method in direct contest with existing commercial packages on a real situation which had physical values for the CRM fields measured for comparisons to be made in terms of efficiency, speed and accuracy. However, a great deal of work would be required before these comparisons could be made.

As it stands, this 'method' can not be considered a rival to existing commercial packages. It still consists of lots of separate programs and procedures which need to be run manually in a specific order to produce solutions. The mesh of the ship and the sea water domain were produced using a commercial package called 'FEMAP' [66] which although not specifically designed to produce surface meshes, could produce adequate meshes of the surfaces which could then be manually manipulated into a mesh which meet the needs of these methods. This original mesh was produced for our research by BAE Systems [67]. This meant that the methods were only tested on this one model. To make these methods useful in the industry, a meshing tool would need to be developed which could mesh up any geometry required. To then make the method commercial, all the various individual methods used would then need to be pulled together into one continuous program with a user interface which allowed all the control exhibited by the individual programs. For example, the conductivity of the sea water would have to be variable to allow models to be analysed in different environments. Only once this had been done could the result of this research be considered as a rival commercial tool and comparisons be made.

Aside from the user-interface improvements which could be made to the method, the actual modelling could be improved in various ways which would hopefully lead to improved accuracy.

The propeller was modelled using only a simple cylinder. This is common practise of the industry [62] with the only requirement that the surface area of the

cylinder is the same as that of an actual propeller [68]. The historical reason for this was that the simple cylinder shape was easily modelled using few elements and nodes which do not place excessive strain on the memory capacity of the computers at that time. Although this has provided sufficient approximations of the potential and its flux over the hull, and hence the CRM fields, recent research has shown that this rather naive approach hides some important shadowing effects of real propellers which can be included by using more elaborate shapes, such as a torus, to represent the propeller [68]. As the memory capacity of modern computers increase, there is no reason why these shapes should not be included in current models.

An obvious area of improvement which has been mentioned several times in this work is the polarization data. For any analysis of a system where numerical values rather than trends were required, it would be critical that there was real polarization data available which had been obtained from experiment. The different behaviour shown by the ICCP system calculations as the linear polarization relation on the hull was replaced by a non-linear one indicates exactly how critical this is. Even for simple qualitative analysis like that presented here, it would be necessary to get a representative relation to apply to the propeller to replace the linear relation currently applied here. Also there are indications that paint coatings on the propellers are going to become a common anti-corrosion measure and this should also be included [16].

The calculations in this research were all carried out for static considerations. This means that the results, qualitative though they are, can only truly be considered valid of a stationary ship. Since the domain contained no dockside or structure to which the ship could be tethered, this is an extremely simplified case. To improve the validity of the research it would be necessary to perform calculations for a ship in motion. This may be achieved by altering two features of the model. Firstly, since this would require the propeller to be rotating the shape used to model the propeller would need to be altered. Secondly, the motion of a ship through the water alters the interaction of the ship with the sea water, which in turns alters the polarization relation for the various metals [62]. Hence new polarization data would be required yet again.

When analysing proposed ICCP systems for a ship, it will be necessary to perform calculations for a range of anode locations and configurations. As shown

in the test calculations, poorly positioned anodes may do more harm than good. However, as mentioned, the location of the anodes were governed by requirement for elements which formed the pair having the same area. By incorporating a meshing tool into the method, specific anode elements could be located where required and the mesh altered around them. This would require the mesh to be checked after every new anode location had been added, but the mesh checking devices are already developed so this should cause no problem.

Also if this was developed it would then be possible to perform optimisation analysis for the ship to ensure that the ICCP system was configured so that the protection levels was maximised and the CRM fields minimised. To achieve this it would be necessary to develop some form of optimisation function which would be minimised when the best configuration has been found [52, 61]. To model the optimisation procedure, it would be necessary to be able to modify the the model to account for fundamental properties of any system such as

- anode material,

- anode location,

- anode current,

- anode shape.

With the model set up to deal with these variables, it is then necessary to specify exactly the properties that require to be optimised which could include

- minimal total anode current,

- maximal protection to surfaces,

- target CRM signature.

The levels at which the maximal protection to the hull surfaces is obtained may be judged by using target potential ranges in which the surface material is considered protected [9]. At the present the levels used by the industry are that on the hull the potential should be in the range $-950mV < u < -800mV$ (vs. Ag/AgCl electrode) [52]. The final optimisation target is that of the CRM signature. A ship operator may for some reason wish the ICCP system to provide his ship with

a specific CRM signature rather than a minimal one. In this case the optimisation is obviously concerned with how well this target signature is satisfied.

These future developments all arise from inadequacies in the methods developed but they are mostly caused by shortcomings in the data available for the calculations. They are also all concerned with the application of the combined method to the evaluation of the CRM fields from a ship. It should not be forgotten that the combined method is formed from individual methods each of which are based on solid physics.

The initial investigations of dipole models have provided a series of formulae in section 2.3.3 which can be used to produce an approximation of the CRM signature. When compared to the CRM signature produced by the full method, it was shown that while the dipole approximation would provide a field in approximately the same direction with the same shape, the magnitude of the field could be different. Depending on the level of corrosion that occurred on the ship, the approximated field could either over-estimate the magnitude (when there was a relatively low level of corrosion) or under-estimate it (when there was a high level of corrosion). The reason for this was that the dipole model was developed for a semi-infinite domain which excluded the effect of the non-conducting sea bed. With this deficiency recognised, it should be possible be develop the dipole model further so that it is removed. When this has been done the dipole model should the provided a quick and accurate tool for analysing proposed ICCP systems for ships. If the full calculation had been completed for a ship without an ICCP system activated, this CRM field could be used as a base field, on top of which the field from proposed ICCP anodes could be superimposed using this formula. This would allow a rough estimate of the effect of an ICCP system for that particular configuration. Many impractical configurations could hence be dismissed leaving only ones which looked promising. The full method could be applied to these remaining configurations. As it stands, the present dipole approximation could be used to provide an estimate but it would be unknown as to whether the field magnitude was an over or under estimate which, for reasons mentioned earlier, could prove catastrophic.

The new integral method based on the moments of triangular elements also could prove useful. For surface meshes, triangular elements can be used to cover all shapes, something which is not possible with other geometries. This means

that any calculation which requires the numerical integration over a surface, could use this method. Admittedly, when the integrals are over only a few elements other, more conventional, methods may be quicker but when there are many integrations required, the fact that this method can use calculated values means that a 'warm' start is available for every integral which could reduce the computation time to provide solutions of comparable accuracy to more conventional methods.

While the PSOM method of solving equations may not be the most efficient available, this research has hopefully highlighted that in certain situations the control that it will allow over the solution which is obtained can help solve systems that have many unknowns which are all intertwined and have to satisfy various constraints.

Perhaps the most pleasing development in this research was the new method for calculating the magnetic fields with in a domain of constant conductivity from the potentials on the boundary. This may prove extremely beneficial to those whose work concerns similar calculations to those considered in this research where the potentials are obtained using the BEM. It may also prove extremely useful to other areas where the magnetic field needs to be require from boundary values.

To conclude, using the methods developed in this research to perform actual calculations only a quantitative analysis of a ship corroding with protection provided by a paint coating and an ICCP system was possible. This analysis showed that the methods could demonstrate the required features of a system for such models. However, there is plenty of work that needs to be done before the combined method can be considered as a reliable tool for evaluating the CRM fields produced to an accurate level. Despite this, the research has produced new techniques, and highlighted old ones, which should hopefully prove useful to, specifically, the naval industry (both merchant and military) and more widely the community of mathematical modellers and applied physicists.

Appendix A

Black-Box Algorithms

This appendix includes algorithms which used in the methods described Chapter 5 and can be found in most texts concerning numerical recipes (see [45, 46],[48]-[51]). The purpose of this appendix is to provide a quick reminder of what the algorithms entail.

A.1 Forward Substitution

The following is the forward substitution algorithm used for solving the lower triangular system $L\mathbf{x} = \mathbf{b}$.

for $j = 1$ to n	(looping over the columns)
if $l_{jj} = 0$ then stop	(stop if matrix singular)
$x_j = \frac{b_j}{l_{jj}}$	(compute solution component)
for $i = j + 1$ to n	
$b_i = b_i - l_{ij}x_j$	(update the right hand side)
end	
end	
end	

Table A.1: Forward Substitution for Lower Triangular Systems

A.2 Backward Substitution

The backward substitution algorithm used for solving the upper triangular system $U\mathbf{x} = \mathbf{b}$.

```
for j = n to 1                    (looping backward over the columns)
    if u_jj = 0 then stop                    (stop if matrix singular)
        x_j = b_j/u_jj                       (compute solution component)
    for i = 1 to j - 1
        b_i = b_i - u_ij x_j                 (update the right hand side)
    end
  end
end
```

Table A.2: Backward Substitution for Upper Triangular Systems

A.3 Householder Reduction to Bidiagonal Form

The algorithm for a Householder reduction to bidiagonal form.

Given $A \in \Re^{m \times n}(m \geq n)$, the following algorithm overwrites A with $U_B^T A V_B = B$ where B is upper bidiagonal and U_B and V_B are orthogonal.

for $k = 1$ to n

    Determine a Householder matrix $\tilde{U}_k$ of order $m - k + 1$ such that

$$\tilde{U}_k \begin{bmatrix} a_{kk} \\ a_{kk+1} \\ \vdots \\ a_{mk} \end{bmatrix} = \begin{bmatrix} x \\ 0 \\ \vdots \\ 0 \end{bmatrix}$$

    $A = diag(I_{k-1}, \tilde{U}_k)A$

if $k \leq n - 2$ then

    Determine a Householder matrix $\tilde{V}_k$ of order $n - k + 1$ such that

    $[a_{k,k+1}, \ldots, a_{kn}]\tilde{V}_k = (x, 0, \ldots, 0)$

    $A = A\ diag(I_k, \tilde{V}_k)$

Table A.3: Householder Reduction to Bidiagonal Form.

A.4   Householder QR Factorization

The algorithm for the Householder QR Factorization

Let $A \in \Re^{m \times n}$ and denote the jth column of A by $\mathbf{a}_j$, the following forms the Householder transformations whose products form an orthogonal matrix Q such that $A = Q \begin{bmatrix} R \\ 0 \end{bmatrix}$ where R is an upper triangular matrix.

Loop over all the columns of A.
Compute the Householder vector $\mathbf{v}$ for the current column
$$\alpha_k = -sign(a_{kk})\sqrt{a_{kk}^2 + \ldots + A_{mk}^2}$$
$$\mathbf{v}_k = [0 \ldots 0 \ a_{kk} \ldots a_{mk}]^T - \alpha_k \mathbf{e}_k$$
if current column is already zero, then move onto the next column.
form Householder transformation matrix $H = I - 2\frac{\mathbf{v}_k \mathbf{v}_k^T}{\mathbf{v}_k^T \mathbf{v}_k}$
else apply the transform to the remaining sub-matrix
  for $j = k$ to n
    $\gamma_j = \mathbf{v}_k^T \mathbf{a}_j$
    $\mathbf{r}_j = \mathbf{a_j} - \frac{2\gamma_j}{\mathbf{v}_k^T \mathbf{v}_k}\mathbf{v}_k$
  end
end.

Table A.4: Householder QR Factorization.

A.5   QR Iteration

Algorithm for the QR iteration

Given $A \in \Re^{n \times n}$ matrix, this iteration will calculate approximations to all the eigenvectors which shall be stored in the columns of an A_k.

for $k = 1, 2, \ldots$
  Compute the QR Factorization using the Householder method
    (ensures matrices are normalised)
    $Q_k R_k = A_{k-1}$
  Generate the next matrix
    $A_k = R + kQ_k$
end

Table A.5: The QR Iteration.

Appendix B

Weighting Functions

This appendix briefly justifies the choice of weighting function used in the derivation of the boundary element method in chapter 3.

The easiest way to obtain a suitable weighting function for a problem is to use published tables of such functions which can be found in many texts [40, 43]. However, it is possible to derive a suitable function and in the following this is done using Green's Functions to solve a simple inhomogeneous partial differential equation.

Consider the weighting function $w(\mathbf{R})$. This function must provide each error term in eqn (3.5.1) with the correct significance. One function which will do this is the fundamental solution to a fundamental problem which has the same behaviour within the domain and on the boundary as the main, more complicated problem. In this case, the actual problem involves the electric potential on the boundary of the domain due to a source (corroding ship) within the domain. This can be reduced back to the fundamental problem where there is a charge density $\rho(\mathbf{R}_i)$ in the domain giving rise to the potential on the boundary. In this fundamental problem, if the potential function over the domain is u, then the governing equation is Poisson's Equation

$$\nabla^2 u = 4\pi\rho. \tag{B.0.1}$$

To solve this equation, and find the required weighting function, it is necessary to use Greens' functions [69, 70]. For those not familiar in using Green's Functions for this task, the basic principle is that when solving inhomogeneous, differential

237

equations, convolving with a Green's Function will provide the required solutions. If $G(\mathbf{R}, \mathbf{R}_i)$ is the Green's Function of some differential operator L, then the solution of the equation $Lf = h$ is the convolution of G with h,

$$f(\mathbf{R}) = \int h(\mathbf{R}_i) G(\mathbf{R}, \mathbf{R}_i) dV \qquad (\text{B.0.2})$$

This description of a Green's Function shows how useful they can be but it does not provide a true definition of one. There are various ways of considering Green's Functions, but in this case an informative description of one would be that a Green's Function of a linear operator L acting on distributions over a manifold M (which in this case may simply be regarded as $\Re^3$), at a point $\mathbf{R}_i$, is any solution of $Lf(\mathbf{R}) = \delta(\mathbf{R} - \mathbf{R}_i)$ where δ is the Dirac Delta function [70]. In theory, the Green's Function need not be unique but by introducing externally imposed criteria such as boundary conditions, a unique function may be obtained. Despite their name, it is best to regard Green's Functions as distributions rather than actual functions. Bearing this in mind the solution for f in eqn (B.0.2) can be thought of as an expansion of the solution using Dirac Delta Functions as the basis.

Before solving Poisson's Equation eqn (B.0.1), a small side calculation shall be provided which will prove crucial to the later analysis.

Let $R = |\mathbf{R} - \mathbf{R}_i|$. Consider the effect of integrating the Laplacian of the inverse distance function $\frac{1}{R}$ over a volume Ω, i.e.

$$\int_\Omega \nabla^2 \left(\frac{1}{|\mathbf{R} - \mathbf{R}_i|} \right) d^3\mathbf{R}. \qquad (\text{B.0.3})$$

To perform this integration, the divergence theorem is used and the domain of

the integration is a small sphere of radius R' which gives

$$
\begin{aligned}
\int_\Omega \nabla^2 \frac{1}{R} d^3 \mathbf{R} &= \int_\Omega \nabla \cdot \left(\nabla \frac{1}{R} \right) d^3 \mathbf{R} \\
&= \int_s \nabla \left(\frac{1}{R} \right) \cdot d\mathbf{s} \text{ by the divergence theorem} \\
&= \int_s \frac{\partial}{\partial R} \left(\frac{1}{R} \right) \hat{\mathbf{R}} \cdot d\mathbf{s} \\
&= \int_s -\frac{1}{R^2} \hat{\mathbf{R}} \cdot d\mathbf{s} \\
&= -4\pi \frac{R'^2}{R^2}.
\end{aligned}
\tag{B.0.4}
$$

If the distance R is positive but the volume of integration tends to zero ($R' \rightarrow 0$), then this integral will tend to zero. However, if the distance R is fixed to be the whole radius of the volume of integration so that $R = R'$, and then the volume of integration is reduced to zero, the value for the integral tends to -4π, or equivalently

$$
\nabla^2 \left(\frac{1}{|\mathbf{R} - \mathbf{R}_i|} \right) = -4\pi \delta^3 (\mathbf{R} - \mathbf{R}_i).
\tag{B.0.5}
$$

Keeping this result in mind, return now to solving eqn (B.0.1) and consider how to solve it using a Green's Function. What is required is a Green's Function which will expand the solution potential over the domain using the Dirac Delta functions as a basis. In other words, a distribution of the potential in the domain that satisfies the governing equation which is precisely what the weighting function should do in the more complicated problem. Therefore by finding the Green's Function, the weighting function is automatically found as well.

With Poisson's Equation, the linear differential operator is the Laplacian. From the previous discussion, this means that the Green's Function should satisfy

$$
\nabla^2 G(\mathbf{R}, \mathbf{R}_i) = \delta^3 (\mathbf{R} - \mathbf{R}_i).
\tag{B.0.6}
$$

From the result shown in eqn (B.0.5), this means that the desired Green's Function is

$$
G(\mathbf{R}, \mathbf{R}_i) = -\frac{1}{4\pi |\mathbf{R} - \mathbf{R}_i|}.
\tag{B.0.7}
$$

Since the require weighting function must only provide the same distributive

properties as this, it may be taken to be [44]

$$w(R) = \frac{1}{4\pi R}.$$

(B.0.8)

Appendix C

Numerical Calculation of Magnetic Field
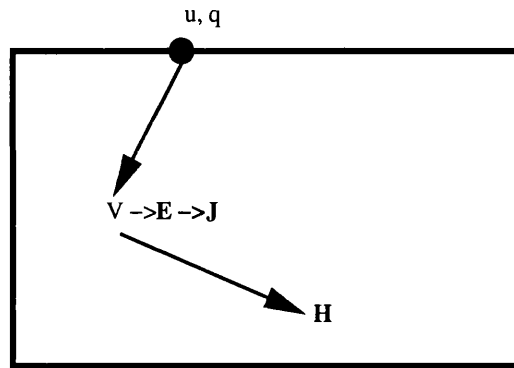
Figure C.1: Outline of Basic BEM Problem

The following arguments mirror those which lead to the discovery of the postulated theorem for calculating the magnetic field within a domain from the potentials on the boundary in chapter 6.

Assume that the boundary element calculation has been carried out, with u and q known at all points p on the boundary of a fictitious domain which is taken to be a box. It follows from the theory of the boundary element method that the potential $u_{i,j,k}$ at all interior points (i, j, k) can be calculated from eqn (6.2.1)

$$u_{i,j,k} = \sum_p q_p G_{i,j,k,p} - \sum_p u_p \hat{H}_{i,j,k,p}.$$

241

From now on, it shall be assumed that the values of potential $u_{i,j,k}$ at the interior points are known.

To apply finite differences, the domain needs to be discretized. For generality, the step length of the discretisation in the x direction is α, in the y direction is β, and is γ in the z direction. With the entire domain discretized, there are different sections for which the contribution from the interior points to **B** must be calculated in different fashions. There are those points completely inside the domain, those on a face of the domain, those on the edge between two faces of the domain, and those that are located at the corners of the domain where three faces meet. Contributions from points in each of these situations will be investigated in turn.

Begin by considering a point completely on the interior. The required second order central differences formulae are following [71]:

$$\frac{\partial u}{\partial x} = \frac{u_{i+1,j,k} - u_{i-1,j,k}}{2\alpha} \tag{C.0.1}$$

$$\frac{\partial u}{\partial y} = \frac{u_{i,j+1,k} - u_{i,j-1,k}}{2\beta} \tag{C.0.2}$$

$$\frac{\partial u}{\partial z} = \frac{u_{i,j,k+1} - u_{i,j,k-1}}{2\gamma} \tag{C.0.3}$$

To calculate the contribution to the magnetic field **B** from one of these interior points, begin by calculating the electric field at a point within the domain from the potentials at discrete points within the domain

$$\mathbf{E} = -\nabla u \tag{C.0.4}$$

$$= -\left(\frac{\partial u}{\partial x}, \frac{\partial u}{\partial y}, \frac{\partial u}{\partial z} \right) \tag{C.0.5}$$

$$= \left(\frac{u_{i-1,j,k} - u_{i+1,j,k}}{2\alpha}, \frac{u_{i,j-1,k} - u_{i,j+1,k}}{2\beta}, \frac{u_{ijk-1} - u_{i,j,k+1}}{2\gamma} \right).$$

This shall be non-zero unless there is some specific symmetry to the problem which leads to cancellation.

The next step is to calculate the current density at the point within the domain where **E** is known from

$$\mathbf{J} = \sigma \mathbf{E} \tag{C.0.6}$$

where σ is the conductivity of sea water.

The final step is to calculate the contribution to the magnetic field from this current density and this is done using a discretized version of the Biot-Savart Law. $\mathbf{B}$ will be evaluated at a point I with coordinates (X, Y, Z). Note that the source points are $x = i\alpha$, $y = j\beta$, and $z = k\gamma$ where i, j and k sum over all interior points of the domain. So

$$\mathbf{B} = \frac{\mu_0}{4\pi} \int_{u'} \frac{\mathbf{J} \times \mathbf{R}}{R^3} du' \text{ where } \mathbf{R} = ((X - i\alpha), (Y - j\beta), (Z - k\gamma))$$

or writing as a sum

$$\mathbf{B} = \frac{\mu_0 \alpha \beta \gamma}{4\pi} \sum_{i,j,k} \frac{\mathbf{E}_{i,j,k} \times \mathbf{R}_{i,j,k}}{R^3}. \tag{C.0.7}$$

To proceed, consider each component individually, beginning with the x-

component:

$$
\begin{aligned}
B_x &= \frac{\mu_0}{4\pi} \int_{u'} \frac{(J_y R_z - J_z R_y)\, du'}{R^3} \\
&= \frac{\mu_0 \sigma}{4\pi} \int_{u'} \frac{E_y R_z - E_z R_y}{R^3} du' \quad \text{where } du' = \alpha\beta\gamma \text{ is a volume element.} \\
&= \frac{\mu_0 \alpha\beta\gamma\sigma}{4\pi} \sum_{i,j,k} \frac{E_{y,i,j,k} R_{z,i,j,k} - E_{z,i,j,k} R_{y,i,j,k}}{R_{i,j,k}^3} \\
&= \frac{\mu_0 \alpha\beta\gamma\sigma}{4\pi} \sum_{i,j,k} \left\{ \frac{[u_{i,j-1,k} - u_{i,j+1,k}](Z - k\gamma)}{2\beta R_{i,j,k}^3} - \frac{[u_{i,j,k-1} - u_{i,j,k+1}](Y - j\beta)}{2\gamma R_{i,j,k}^3} \right\} \\
&= \frac{\mu_0 \alpha\beta\gamma\sigma}{4\pi} \sum_{i,j,k} \left\{ \frac{u_{i,j-1,k}(Z - k\gamma)}{2\beta R_{i,j,k}^3} - \frac{u_{i,j+1,k}(Z - k\gamma)}{2\beta R_{i,j,k}^3} - \frac{u_{i,j,k-1}(Y - j\beta)}{2\gamma R_{i,j,k}^3} \right. \\
&\qquad\qquad\qquad\qquad\qquad\qquad\qquad\qquad \left. + \frac{u_{i,j,k+1}(Y - j\beta)}{2\gamma R_{i,j,k}^3} \right\} \\
&= \frac{\mu_0 \alpha\beta\gamma\sigma}{4\pi} \sum_{i,j,k} \left\{ \frac{(Z - k\gamma)}{2\beta} \left(\frac{1}{R_{i,j+1,k}^3} - \frac{1}{R_{i,j-1,k}^3} \right) \right. \\
&\qquad\qquad\qquad\qquad\qquad \left. - \frac{(Y - j\beta)}{2\gamma} \left(\frac{1}{R_{i,j,k+1}^3} - \frac{1}{R_{i,j,k-1}} \right) \right\} u_{i,j,k} \\
&= \frac{\mu_0 \alpha\beta\gamma\sigma}{4\pi} \sum_{i,j,k} \left\{ (Z - k\gamma)\frac{\partial}{\partial y}\left(\frac{1}{R_{i,j,k}^3}\right) - (Y - j\beta)\frac{\partial}{\partial z}\left(\frac{1}{R_{i,j,k}^3}\right) \right\} u_{i,j,k} \\
&= \frac{\mu_0 \alpha\beta\gamma\sigma}{4\pi} \sum_{i,j,k} \left\{ \frac{-3(Z - k\gamma)(Y - j\beta)}{R_{i,j,k}^5} + \frac{3(Y - j\beta)(Z - k\gamma)}{R_{i,j,k}^5} \right\} u_{i,j,k} \\
&= 0.
\end{aligned}
$$

Results for the components B_y and B_z can be derived in the same way, and can be shown to be zero.

Hence

$$
\mathbf{B} = B_x \hat{\mathbf{u}}_x + B_y \hat{\mathbf{u}}_y + B_z \hat{\mathbf{u}}_z = 0\hat{\mathbf{u}}_x + 0\hat{\mathbf{u}}_y + 0\hat{\mathbf{u}}_z = \mathbf{0}
$$

for all interior points inside the domain. This clearly indicates that any magnetic field generated within the domain from the potentials located on the boundary depend only on these boundary values. The values of the potentials, and hence $\mathbf{E}$ and $\mathbf{J}$, at the interior points do not effect the magnetic field, as would be expected since these values are derived from the boundary values. However it is

necessary to investigate whether these boundary values provide a magnetic field as expected.

Consider a point on a face of the domain such that if the point is at location i, j, k then there exists points $i \pm 1, j \pm 1, k + 1, k + 2$ as shown in figure C.2.
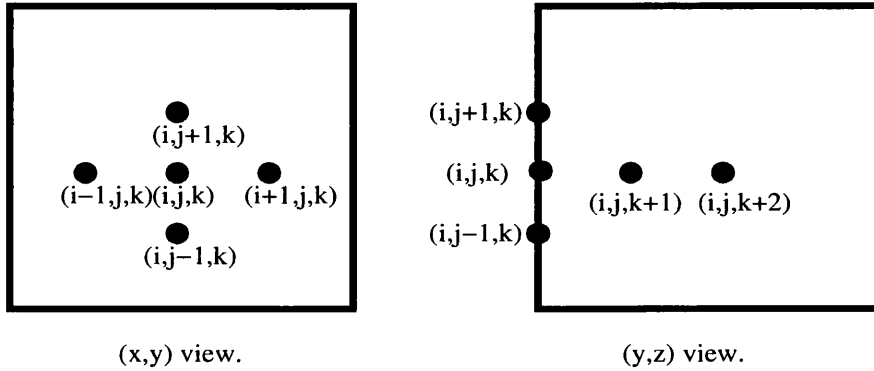

(x,y) view.   (y,z) view.

Figure C.2: Shows node location for the calculation of contribution to **B** from a node on a face of the fictitious domain.

This will allow the use of the following second order central difference formulae:-

$$\frac{\partial u}{\partial x} = \frac{u_{i+1,j,k} - u_{i-1,j,k}}{2\alpha} \tag{C.0.8}$$

$$\frac{\partial u}{\partial y} = \frac{u_{i,j+1,k} - u_{i,j-1,k}}{2\beta} \tag{C.0.9}$$

$$\frac{\partial u}{\partial z} = \frac{u_{i,j,k+2} - 4u_{i,j,k+1} + 3u_{i,j,k}}{2\gamma}. \tag{C.0.10}$$

Hence with the potential known at all points on the boundary, the electric field at any one of these points can be shown to be

$$\begin{aligned}
\mathbf{E} &= -\nabla u \\
&= \left(\frac{u_{i-1,j,k} - u_{i+1,j,k}}{2\alpha}, \frac{u_{i,j-1,k} - u_{i,j+1,k}}{2\beta}, \frac{-u_{i,j,k+2} + 4u_{i,j,k+1} - 3u_{i,j,k}}{2\gamma} \right)
\end{aligned}$$

and this in turn provides the current density **J** at this point using equation C.0.6, i.e.

$$\begin{aligned}
\mathbf{J} &= \sigma\mathbf{E} \\
&= \sigma \left(\frac{u_{i-1,j,k} - u_{i+1,j,k}}{2\alpha}, \frac{u_{i,j-1,k} - u_{i,j+1,k}}{2\beta}, \frac{-u_{i,j,k+2} + 4u_{i,j,k+1} - 3u_{i,j,k}}{2\gamma} \right).
\end{aligned}$$

To calculate the magnetic field at any point within the domain, the Biot-Savart Law is applied (in discretized format), i.e. eqn (C.0.7), with $\mathbf{E}$ and $\mathbf{R}$ evaluated at node (i, j, k), and $\mathbf{B}$ at (X, Y, Z).

For the x-component:

$$
\begin{aligned}
B_x &= \frac{\mu_0 \alpha \beta \gamma \sigma}{4\pi} \sum_{i,j,k} \frac{E_y R_z - E_z R_y}{R_{i,j,k}^3} \\
&= \frac{\mu_0 \alpha \beta \gamma \sigma}{4\pi} \sum_{i,j,k} \frac{1}{R_{i,j,k}^3} \left(\frac{(u_{i,j-1,k} - u_{i,j+1,k})}{2\beta} (Z - k\gamma) \right. \\
&\qquad\qquad\qquad\qquad \left. - \frac{(-u_{i,j,k+2} + 4u_{i,j,k+1} - 3u_{i,j,k})}{2\gamma} (Y - j\beta) \right) \\
&= \frac{\mu_0 \alpha \beta \gamma \sigma}{4\pi} \sum_{i,j,k} \left\{ \frac{(Z - k\gamma)}{2\beta} \left[\frac{1}{R_{i,j+1,k}^3} - \frac{1}{R_{i,j-1,k}^3} \right] \right. \\
&\qquad\qquad\qquad\qquad \left. + \frac{(Y - j\beta)}{2\gamma} \left[\frac{1}{R_{i,j,k-2}^3} - \frac{4}{R_{i,j,k-1}^3} + \frac{3}{R_{i,j,k}^3} \right] \right\} u_{i,j,k} \\
&= \frac{\mu_0 \alpha \beta \gamma \sigma}{4\pi} \sum_{i,j,k} \left\{ (Z - k\gamma) \frac{\partial}{\partial y} \left(\frac{1}{R_{i,j,k}^3} \right) + (Y - j\beta) \frac{\partial}{\partial z} \left(\frac{1}{R_{i,j,k}^3} \right) \right\} u_{i,j,k} \\
&= \frac{\mu_0 \alpha \beta \gamma \sigma}{4\pi} \sum_{i,j,k} \left\{ \frac{-3 (Z - k\gamma)(Y - j\beta)}{R_{i,j,k}^5} - \frac{3 (Y - j\beta)(Z - k\gamma)}{R_{i,j,k}^5} \right\} u_{i,j,k} \\
&= \frac{\mu_0 \alpha \beta \gamma \sigma}{4\pi} \sum_{i,j,k} \frac{-6 (Y - j\beta)(Z - k\gamma)}{R_{i,j,k}^5} u_{i,j,k} \\
&\neq 0
\end{aligned}
$$

Similar calculations for the y provide a non-zero contribution, while the z contribution turns out to be zero for this face.

Therefore a generalisation of this argument to the other faces leads to the conclusion that the contribution to $\mathbf{B}$ from points on the faces (i.e. on the boundary) are non-zero.

To continue investigating the effects on the $\mathbf{B}$ field from potentials on the boundary of the domain, consider a point (i, j, k) on one of the edges of the domain such that the points $i \pm 1, j + 1, j + 2, k + 1, k + 2$ all exist as shown in
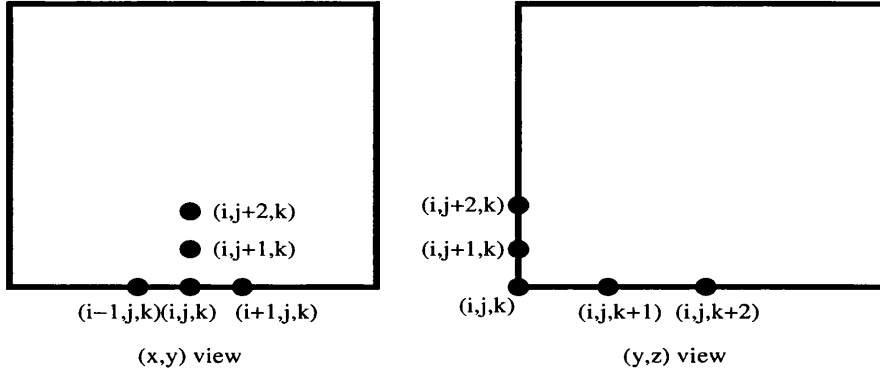
Figure C.3: Shows the node location for the calculation of the contribution to **B** from a node on an edge of the fictitious domain.

figure C.3. The second order difference formulae used in this case are

$$\frac{\partial u}{\partial x} = \frac{u_{i+1,j,k} - u_{i-1,j,k}}{2\alpha}, \tag{C.0.11}$$

$$\frac{\partial u}{\partial y} = \frac{u_{i,j+2,k} - 4u_{i,j+1,k} + 3u_{i,j,k}}{2\beta}, \tag{C.0.12}$$

$$\frac{\partial u}{\partial z} = \frac{u_{i,j,k+2} - 4u_{i,j,k+1} + 3u_{i,j,k}}{2\gamma}. \tag{C.0.13}$$

Proceeding in a similar fashion to that used above, it can be shown that from this edge, the x and y components makes zero contribution while the z component makes a non-zero contribution.

Again, a generalisation of this argument to the other edges leads to the conclusion that the contribution to **B** from a potential on an edge formed at the junction between two faces on the boundary of the domain is non-zero.

The final case to consider is that of the contribution made from the potential on a corner of the domain, i.e. where three boundary faces meet (see figure C.4).

Consider the corner i, j, k such that the nodes $i+1, i+2, j+1, j+2, k+1, k+2$
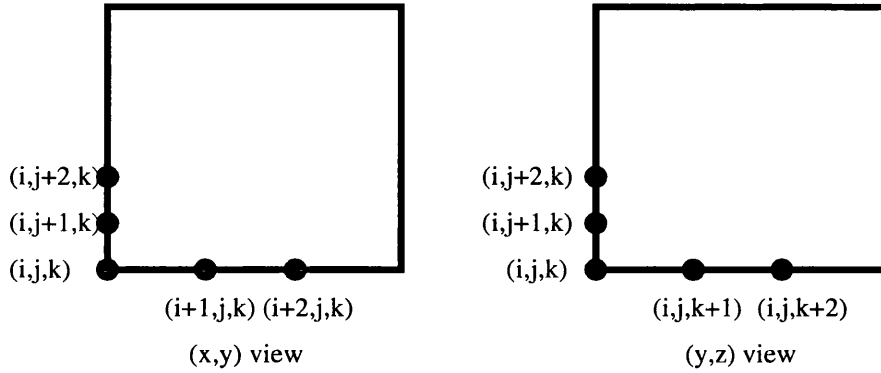
Figure C.4: Shows node location for the calculation of the contribution to **B** from a node on a corner of our fictitious domain.

all exist. The second order difference formulae are now

$$\frac{\partial u}{\partial x} = \frac{u_{i+2,j,k} - 4u_{i+1,j,k} + 3u_{i,j,k}}{2\alpha} \tag{C.0.14}$$

$$\frac{\partial u}{\partial y} = \frac{u_{i,j+2,k} - 4u_{i,j+1,k} + 3u_{i,j,k}}{2\beta} \tag{C.0.15}$$

$$\frac{\partial u}{\partial z} = \frac{u_{i,j,k+2} - 4u_{i,j,k+1} + 3u_{i,j,k}}{2\gamma} \tag{C.0.16}$$

Using the same arguments as before with this formulae shows that there is zero contribution from all three elements. This seems to suggest that the contribution to the magnetic field from the potentials located at corners of domain are zero, which is not what is expected as it does not match the analytic analysis.

The analytic analysis says that the contribution to the magnetic field from a potential at a corner node of the fictitious domain should, in general be non-zero, i.e.

$$\mathbf{B} = -\frac{\mu_0 \sigma}{4\pi} \int \frac{u'_c}{R^3} d\mathbf{s}' \times \mathbf{R} \neq 0$$

where u_c refers to the potential at the corner.

For this statement to hold true, $ds \neq 0$, which implies that the boundary must extend in some spatial context about the corner. This in turn enforces the conclusion that the corner node can *not* be located exactly in the corner. This being the case, the situation returns to that of a potential on an edge which has been shown to give a non-zero contribution to **B**.

Appendix D

Step size in summations

The work presented in this appendix provides evidence for the summations in eqn (4.2.6) of chapter 4 increasing the terms in their sequence by increments of 2.

The expression for $\frac{1}{R}$ may be written as

$$\frac{1}{R} = \frac{1}{\sqrt{(X-x)^2 + (Y-y)^2 + (Z-z)^2}} \tag{D.0.1}$$

As indicated in section 4.2, it is beneficial to perform the required differentiation with respect to the coordinates of the source point rather than the field element. Begin by considering the effect of differentiation with respect to X,

$$\frac{\partial}{\partial X}\frac{1}{R} = -\frac{(X-x)}{R^3} \tag{D.0.2}$$

$$\frac{\partial^2}{\partial X^2}\frac{1}{R} = -\frac{1}{R^3} + \frac{3(X-x)^2}{R^5} \tag{D.0.3}$$

$$\frac{\partial^3}{\partial X^3}\frac{1}{R} = \frac{9(X-x)}{R^5} - \frac{15(X-x)^3}{R^7}. \tag{D.0.4}$$

$$\tag{D.0.5}$$

Hence, when differentiation is performed with respect to X, the leading term may be expressed in general terms as

$$\frac{\partial^n}{\partial X^n}\frac{1}{R} = \frac{(-1)^n (X-x)^n}{R^{2n+1}} (2n-1)(2n-3)\ldots 5.3.1 \tag{D.0.6}$$

with a similar expression existing for differentiation with respect to Y.

Consider now the effect of cross differentiation, such as

$$\frac{\partial^3}{\partial Y \partial X^2} \frac{1}{R} = \frac{3(Y-y)}{R^5} - \frac{5.3.(X-x)(Y-y)}{R^7}. \tag{D.0.7}$$

So the expression for the cross derivative may be expressed as (omitting coefficients)

$$\frac{\partial^m}{\partial X^m} \frac{\partial^n}{\partial Y^n} \frac{1}{R} = \frac{(Y-y)^n (X-x)^m}{R^{2m+2n+1}} + \frac{(Y-y)^{n-2}(X-x)^m}{R^{2m+n+(n-2)+1}} + \cdots$$
$$+ \frac{(Y-y)^{1,0}(X-x)^{1,0}}{R}. \tag{D.0.8}$$

Applying this knowledge to eqn (4.2.6), it can be seen that p and q are powers due to the differentiation shown above which go from 0 or 1 to m for X or n for Y where m and n increase to infinity, i.e. for each $m($ or $n)$, $p($ or $q)$ goes from 0 or 1 (depending on $m mod 2$ or $n mod 2$) to m (or n) in steps of 2. The factors of

$$X^m Y^n \left(\frac{X}{R}\right)^p \left(\frac{Y}{R}\right)^q \text{ and } \frac{1}{R^{m+n+1}}$$

ensure that the dimensions are correct. All the negative factors and coefficients are included in the number A_{pq}^{mn}, which is calculated at the start of the computation and then referred to as and when required.

Appendix E

Normalised moment M_{01}

In chapter 4, it was stated that $M_{01}(\alpha) = 0$. The proof of this is provided here and makes full use of eqn (4.6.8) as shown:

$$
\begin{aligned}
M_{01}(\alpha) &= J_{11}\left(\alpha - \frac{4}{3}\right) + J_{11}(-\alpha) && \text{(E.0.1)} \\
&= \left(\alpha - \frac{4}{3}\right) J_{02}\left(\alpha - \frac{4}{3}\right) + \frac{2}{3} J_{01}\left(\alpha - \frac{4}{3}\right) + (-\alpha) J_{02}(-\alpha) \\
&\qquad\qquad + \frac{2}{3} J_{01}(-\alpha) && \text{(E.0.2)} \\
&= \left(\alpha - \frac{4}{3}\right) \frac{1}{3}\left[1 - \left(-\frac{1}{2}\right)^3\right] + \frac{2}{3}\frac{1}{2}\left[1 - \left(-\frac{1}{2}\right)^2\right] \\
&\qquad - \alpha\frac{1}{3}\left[1 - \left(-\frac{1}{2}\right)^3\right] + \frac{2}{3}\frac{1}{2}\left[1 - \left(-\frac{1}{2}\right)^2\right] && \text{(E.0.3)} \\
&= \frac{\alpha}{3}\frac{9}{8} - \frac{4}{9}\frac{9}{8} + \frac{1}{3}\frac{3}{4} - \frac{\alpha}{3}\frac{9}{8} + \frac{1}{3}\frac{3}{4} && \text{(E.0.4)} \\
&= 0. && \text{(E.0.5)}
\end{aligned}
$$

A similar proof exists for $M_{10}(\alpha) = 0$. These results can also be verified from eqn (4.6.4) with direct calculations of the integrals.

A physical interpretation of the direct consequence of the centroid of the triangular element being chosen as the origin shows that these values are valid. The centroid is another name for the centre of mass of an object, and if the triangle is supported under its centroid, or by a line passing under its centroid it

will be balanced. The moments discussed here refer to the integrals

$$M_{10}(\alpha) = \int_\Gamma x d\Gamma \qquad \text{(E.0.6)}$$

$$M_{01}(\alpha) = \int_\Gamma y d\Gamma \qquad \text{(E.0.7)}$$

which can be though of as being the normal physical moments of the weight about two such supporting lines. Since there will be equal amounts of the element above and below these lines, the integration will see these amounts cancelling leaving the normalised moments to be zero.

Bibliography

[1] Terrific Scientific,
http://www.terrific-scientific.co.uk

[2] National Physical Laboratory,
http://www.npl.co.uk

[3] Marine Corrosion Forum,
http://www.marinecorrosionforum.org

[4] BBC News Website,
http://news.bbc.co.uk/1/hi/world/europe/574746.stm

[5] A. V. Kildishev, J. A. Nyenhuis, A. V. Hetman. Zonal Magnetic Signatures
in Spherical and Prolate Spheroidal Analysis.
Proceedings of Marelec Conference 1999, 1999.

[6] R. A. Adey, C. A. Brebbia, S. M. Niku. Beasy-CP - A System for Analysis
of Galvanic Corrosion and Cathodic Protection using Boundary Elements.
*Betech26: Proceedings of the Second Boundary Element Technology Confer-
ence*, pages 85-107
Computational Mechanics Publications, 1986.

[7] M. G. Fontana. *Corrosion Engineering: Third Edition*,
McGraw-Hill Book Company, 1986.

[8] T. H. Rogers. *Marine Corrosion*,
George Newnes Ltd, 1968.

[9] F. L. Laque. *Marine Corrosion: Causes and Prevention*,
John Wiley & Sons, 1975.

[10] D. A. Jones. *Principles & Prevention of Corrosion (Second Edition)*,
Prentice Halls, 1996.

[11] BAE Systems, *Private Discussions - Confidential.*

[12] K. A. Chandler. *Marine & Offshore Corrosion*,
Butterworth & Co, 1985.

[13] J. H. Morgan. *Cathodic Protection: Its Theory and Practice in the Prevention of Corrosion.*
Leonard Hill [Books] Limited, 1959.

[14] J. Thompson, D. Vaitekunas, B. Brooking. Lowering Warship Signatures: Electromagnetic and Infrared.
Signature Management - The Pursuit of Stealth Conference 2000, 2000.

[15] E. Santana Diaz, R. Adey. *Predicting the Hull State from Information of Potential Measurements of the Hull.*
Computational Mechanics BEASY, www.beasy.com

[16] M. Atlar, E. J. Glover, C. D. Anderson, R. J. Mutton. Effect of New Generation Coatings on High Speed Propeller Performance.
Warship Cathodic Protection 2003 Symposium, 2003.

[17] N. G. Zamani, J. F. Porter. Boundary Element Simulation of the Cathodic Protection System in the Destroyer Class 280. *Boundary Element Techniques: Applications in Fluid Flow and Computational Aspects*, pages 123-137.
Computational Mechanics Publications, 1987.

[18] G. J. C. Aird. *Modelling the Induced Magnetic Signature of Naval Vessels.*
Department Of Physics and Astronomy, Univeristy Of Glasgow, 2000.

[19] P. G. Rawlins, S. J. Davidson. Modelling of AC Vesel Signatures Using Time Dependent Dipoles.
Proceedings of Marelec Conference 1999, 1999.

[20] G. Aird, A. Watt. Numerical Models to Study the Induced Magnetic Field Generated by the Internal Structure of Ships.
Proceedings of Marelec Conference 1999, 1999.

[21] V. G. DeGiorgi. *Finite Resistivity and Shipboard Corrosion Prevention System Performance.*
Mechanics of Materials Branch, Naval Research Laboratory, Washington, USA.

[22] S. Ramo, J. R. Whinnery, T. Van Duzer. *Fields and Waves in Communication Electronics (Third Edition).*
John Wiley & Sons, Inc., 1994.

[23] Dr. R. L. Crawford. *Private Communications.*

[24] W. R. Smythe. *Static and Dynamic Electricity (First Edition).*
McGraw-Hill Book Company, 1939.

[25] W. K. H. Panosky, M. Phillips. *Classical Electricity and Magnetism (Second Edition).*
Addison-Wesley Publishing Company, Inc., 1962.

[26] P. Lorrain, D. R. Corson, F. Lorrain. *Electromagnetic Fields and Waves (Third Edition).*
W.H. Freeman and Company, 1996.

[27] P. K. Banerjee, R. Butterfield. *Boundary Element Methods in Engineering Science.*
McGraw-Hill Book Company (UK) Limited, 1981.

[28] D. S. Burnet. *Finite Element Analysis from Concepts to Applications.*
Addison-Wesley Publishing Company, 1987.

[29] P. Tony, J. N. Rossettos. *Finite-Element Method, Basic Techniques and Implementation.*
The WIT Press, 1977.

[30] R. Courant. Variational Methods for the Solution of Problems of Equilibrium and Vibration.
Bull. Am. Math. Soc. **49:1-2**, 1943.

[31] I. J. Schoenberg. Contributions to the Problem of Approximation of Equidistant Data by Analytic Functions. Part A. On the Problem of Smoothing or

Graduation. A First Class of Analytic Approximation Formulae.
Quart Appl Math, **4:**45-99, 1946.

[32] J. Greenstadt. On the Reduction of Continuous Problems to Discrete Form.
IBM J Res Div, **3:**355-363, 1959.

[33] G. N. White. *Difference Equations for Plane Thermal Elasticity.*
LAMS-2745, Los Alamos Scientific Laboratories, Los Alamos, N. M., 1962.

[34] K. O. Friedrichs. *A Finite Difference Scheme for the Neumann and Dirichlet Problem.*
NYO-9760, Courant Institute of Mathematical Science, New York University, New York, 1962.

[35] J. McMahon. Lower Bounds for the Electrostatic Capacity of a Cube.
Proc. Roy. Irish Acad. **55***(A):*133-167, 1953.

[36] M. J. Turner, R. W. Clough, H. C. Martin, L. J. Topp. Stiffness and Deflection Analysis of Complex Structures.
J Aeron Sci, **23***(9):*805-823, 854, 1956.

[37] R. W. Clough. The Finite Element Method in Plane Stress Analysis.
Proc. Am. Soc. Civil Engineers. **87:**345-378, 1960.

[38] A. S. Cakmak, J. F. Botha, W. G. Gray. *Computational and Applied Mathematics for Engineering Analysis.*
Computational Mechanics Publications, 1987.

[39] C. A. Brebbia. *The Boundary Element Method for Engineers.*
Pentach Press, 1978.

[40] C. A. Brebbia. Fundamentals of Boundary Elements. *New Developments in Boundary Element Methods,* pages 3-33.
CML Publications, 1980.

[41] C. A. Brebbia. The Role of Boundary Elements in CIM. *Betech26: Proceedings of the Second Boundary Element Technology Conference,* pages 3-21.
Computational Mechanics Publications, 1986.

[42] W. J. Mansur, L. C. Wrobel, J. C. F. Telles, J. P. S. Azevado, J. A. F. Santiago. The PROCAT System for Cathodic Protection Design. *Boundary Element Techniques: Applications in Fluid Flow and Computational Aspects*, pages 139-159.
Computational Mechanics Publications, 1987.

[43] C. A. Brebbia, S. Walker *Boundary Element Techniques in Engineering.*
Newnes-Butterworths, 1980.

[44] L. C. Wrobel, C. A. Brebbia. Axisymmetric Potential Problems. *New Developments in Boundary Element Methods*, pages 77-89.
CML Publications, 1980.

[45] W. H. Press, B. P. Flannery, S. A. Teubolsky, W. T. Vetterling. *Numerical Recipes in C: The Art of Scientific Computing.*
Cambridge University Press, 1988.

[46] Mathematics Help Centre.
http://www.mathematicshelpcentral.com

[47] BEASY Software,
http://www.beasy.co.uk

[48] M. T. Heath. *Scientific Computing - An Introductory Survey (Second Edition).*
McGraw-Hill Higher Education, 2002.

[49] G. H. Golub, C. F. Van Loan. *Matrix Computations.*
The Johns Hopkins University Press, 1985.

[50] J. R. Shewchuk. *An Introduction to the Conjugate Gradient Method Without the Agonizing Pain.*
School of Computer Sience, Carnegie Mellon University, Pittsburgh, 1994.

[51] P. A. Jansson. *Deconvolution of Images and Spectra (Second Edition).*
Academic Press, 1997.

[52] S. Santana Diaz, R. Adey, J. Baynham, Y. H. Pei, Y. *Optimisation of ICCP systems to minimise electric signatures.*
Computational Mechanics BEASY, www.beasy.com

[53] H. D. Young, N. A. Freedman. *University Physics (Extended version with modern physics) (9th Edition)*, pp.913-914.
Addison-Wesley Publishing Company, Inc., 1996.

[54] H. D. Young, N. A. Freedman. *University Physics (Extended version with modern physics)(9th Edition)*, pp.908-909.
Addison-Wesley Publishing Company, Inc., 1996.

[55] S. Ramo, J. R. Whinnery, T. Van Duzer. *Fields and Waves in Communiction Electronics (Third Edition)*, pp.76.
John Wiley and Sons, Inc., 1994.

[56] D. J. Griffiths. *Introduction to Electrodynamics*, pp.186.
Prentice-Hall, Inc., 1981.

[57] Corrosion Source
www.corrosionsource.com

[58] Davis Engineering.
http://www.davis-eng.on.ca/emss.htm

[59] V. G. DeGiorgi, E. Hogan, K. Lucas, S. Wimmer. Computational and Experimental Methods in Modelling Electrochemical Corrosion Systems. *Second International Warship Cathodic Protection Symposium and Equipment Exhibition*,
Shrivenham, 2003.

[60] W. R. Jacob, C. P. Ganderton. Signature Mitigation by Potential Control of Sacrificial Anode Cathodic Protection. *Second International Warship Cathodic Protection Symposium and Equipment Exhibition*,
Shrivenham, 2003.

[61] P. G. Rawlins, C. P. Ganderton. Optimisation of Vessel ICCP Systems for Corrosion Protection and Signature. *Second International Warship Cathodic Protection Symposium and Equipment Exhibition*,
Shrivenham, 2003.

[62] Y. Wang, D. P. Brennan, J. F. Porter, K. J. KarisAllen. Evaluation of a Shipboard ICCP System using a Boundary Element Code. *Second International Warship Cathodic Protection Symposium and Equipment Exhibition*, Shrivenham, 2003.

[63] E. Santana Diaz, R. Adey, J. Baynham, Y. H. Pei. *Optimisation of ICCP Systems to Minimise Electric Signatures.*
Computational Mechanics BEASY, www.beasy.com

[64] A. S. Christopoulos. *Advancing Computational Prediction Techniques of Warship Corrosion Control and Electromagnetic Signatures.*
Maritime Operations Division, DSTO, Australia.

[65] W. Sun, K. M. Liu. Numerical Solution of Cathodic Protection Systems with Nonlinear Polarization Curves.
Journal of the Electrochemical Society, 147 (10): 3687-3690 OCT 2000,IDS Number:359GJ, ISSN:0013-4651.

[66] FEMAP,
http://www.femap.co.uk

[67] BAE SYSTEMS Customer Solutions & Support Land & Sea COC East, South Street, Scotstoun, Glasgow G14 OXN, United Kingdom.

[68] V. G. DeGiorgi, S. A. Wimmer. Influence of Geometric Detail in Component Modeling. *Twenty Sixth World Conference on Boundary Elements and Other Mesh Reduction Methods*,
WIT Press, 2004.

[69] MathWorld. The Web's Most Extensive Mathematics Resource.
http://mathworld.wolfram.com

[70] Wikipedia - Free Encyclopedia.
http://en.wikipedia.org

[71] A. W. Al-Khafaji, J. R. Tooley. *Numerical Methods in Engineering Practice*, Harcourt Brace Jovanovich College Publishers, 1986.

[72] D. Birkholz. Preservation of Iron Ships in the Marine Enviroment.
Third International Conference on the Technical Aspects of the Preservation of Historic Vessels, 1997.

[73] The Corrosion Doctors
www.corrosion-doctors.org

[74] G. N. Vanderplauts. *Numerical Optimization Techniques for Engineering Design with Applications.*
McGraw-Hill Book Company, 1984.

[75] V. Ashworth. *Boundary Element Techniques: Application in Fluid Flow and Computational Aspects.*
Pergamon Press, 1984.

[76] R. J. Holt. The Sources of Electric Fields in Sea Water, and their Measurement.
Warship CP, 2001, 2001.